SQUAT CIRCULAR BRIDGE PIERS UNDER MULTI-DIRECTIONAL SEISMIC ATTACK

A thesis submitted in partial fulfilment
of the requirements for the degree of
Doctor of Philosophy in Civil Engineering
at the
University of Canterbury
by

WONG, Yuk Lung

University of Canterbury,
Christchurch, New Zealand.

1990

ABSTRACT

This thesis presents an experimental investigation of seismic shear behaviour of spirally reinforced concrete circular columns. Sixteen cantilever column specimens, with an aspect ratio of two, were tested under quasi-static multi-directional lateral loading conditions. The main variables studied were the amount of spiral steel content, axial compression load intensity, and displacement history.

It was observed that the maximum measured strength, in terms of applied lateral force, appeared to develop at larger ductilities, as axial compression intensity increased. Unless premature shear failure occurred, the ratio of the maximum measured strength of a test column to its ideal flexural strength, computed by the ACI method, was always greater than unity. This strength ratio tended to increase with increasing axial compression load intensity, and decreasing severity of displacement history. For test columns exhibiting moderately ductile or ductile behaviour, the amount of spiral steel content appeared to have no influence on this strength ratio.

The onset of strength degradation was delayed as the spiral steel content increased, or when the severity of displacement pattern was reduced. Axial compression increased strength delay.

The displacement ductility capacity of test columns was distinctly improved with an increase of spiral steel content. Axial compression tended to increase ductility, whereas, the severity of the imposed regular displacement histories appeared to have minor adverse effects on ductility.

Finally, design recommendations on (1) an approach to calculate elastic deformations in reinforced concrete circular cantilever columns, and (2) a seismic shear design proposal taking into account selected levels of displacement ductility demands while also considering effects of imposed inelastic displacement histories, are presented. Good agreement with experimental values was achieved.

ACKNOWLEDGEMENTS

The research presented in this thesis was carried out in the Department of Civil Engineering, University of Canterbury, under the overall guidance of its head, Professor R. Park.

Firstly, I would like to express my genuine thanks to Professor T. Paulay, the main supervisor for this project, for his advice, constructive guidance, and particularly for his support and encouragement.

My sincere gratitude is due to Professor M.J.N. Priestley, the former main supervisor for this project, for all his invaluable advice and guidance.

I am also very thankful to Dr. A.J. Carr for his helpful advice given on numerous occasions.

I wish to take this opportunity to express my appreciation for the assistance given by the technical staff of the Civil Engineering Department, headed by the Senior Technical Officer, Mr. G.E. Hill. In particular, my special thanks are due to Messrs. P.F. Coursey, G.H. Clarke, P. Murphy, and S.L.K. Pasa for their contribution towards the construction and testing of column specimens. Thanks are also due to Mr. L.H. Gardner for the photographic processing, and Mr. H.H. Crowther for arranging the purchase of materials and equipment.

The financial assistance provided by the National Roads Board (Transit NZ) is very gratefully acknowledged.

Finally, a special thanks to my parents, and my fiancée, Florence, for their constant support and encouragement.

TABLE OF CONTENTS

NOTATION

Unless stated otherwise in the text, definitions of the notations used in the thesis are as follows:

A_c = area of concrete core of section measured to outside of peripheral spiral or hoop

A_e = effective shear area

A_g = gross concrete area

A_q = area contributed to shear stiffness

A_{sl} = cross-sectional area of longitudinal bar

A_{sp} = cross-sectional area of spiral reinforcement or circular hoop

A_v = area of the web reinforcement with spacing s

a = shear span

b_w = web width

C_c = flexural compression on concrete

C_d = compression force in diagonal concrete strut

C_{2c} = compression force in the horizontal compression chord at Section 2 due to V_c

C_{2s} = compression force in the horizontal compression chord at Section 2 due to V_s

c_s = distance from the centre of the column bar at the extreme tension fibre to the neutral axis

D = diameter of a circular column

D_r = damage ratio

$D_{r,n}$ = damage ratio at n^{th} cycle of load

$D_{r,o}$ = damage ratio under monotonic loading at displacement Δ_o

D_{rx} = damage ratio in the X direction

D_{ry} = damage ratio in the Y direction

d = effective depth of a section

d_b = bar diameter

d_{bl} = diameter of flexural bar

d_n = depth of concrete layer n

d_o = gross section depth

d_s = diameter of spiral or circular hoop, or diameter of circular concrete core measured to the centres of spirals

E = energy dissipation during a displacement path measured from force - displacement hysteretic curves

E_c = modulus of elasticity of concrete

E_{st} = modulus of elasticity of spiral

E_I = energy dissipation computed for an idealized system

F_{sp} = spiral force

F_{c1} = resultant concrete force at Section 1

F_{c2} = resultant concrete force at Section 2

f = form factor to allow for the nonuniform distribution of shear stress

f_c = concrete stress computed from stress - strain relation

f'_c = compressive (cylinder) strength of concrete

f_{cd} = compressive stress in diagonal concrete strut

f_{cr} = concrete stress at cracking

f_{c1} = principal tensile stress in concrete

f_{c2} = principal compressive stress in concrete

f_{lc} = longitudinal concrete stress

f_t = splitting tensile strength

f_{tc} = transverse concrete stress

f'_p = peak compressive strength of biaxially stressed concrete

f_{sl} = stress of longitudinal reinforcement

f_{st} = stress of spiral or transverse reinforcement

f_y = specified yield strength of flexural reinforcement

f_{yl} = yield strength of longitudinal reinforcement

f_{yt} = yield strength of transverse reinforcement

h = distance from column base to the level where tip deflection of the column is measured

jd = internal lever arm

K_v = shear stiffness

K_1, K_2 = column stiffnesses at different load levels

k = effectiveness coefficient for the 45° analogous truss

k_c = effective strength factor

L = distance from the point of counterflexure to the section of maximum moment, or shear span of a cantilever column

L_{be} = equivalent length for bar elongation within column support

L_c = clear height of fixed end column

L_g = gauge length of curvature measurements

L_p = plastic hinge length

l_d = development length of longitudinal (flexural) bar

M = bending moment

M^o = experimentally obtained maximum flexural capacity

M_x = bending moment at section x due to lateral load V

M_i = ideal flexural capacity calculated using an ultimate concrete strain of 0.003, measured material strengths, and a strength reduction factor of unity

M_1, M_2 = bending moments at Sections 1 and 2 respectively

M_y = idealized yield moment

m = flexural strength enhancement factor

N = applied axial load

n_E = E_{st}/E_c

n,m = spiral strain gauge

P = axial force

P_i = axial force computed using measured material strengths

P_o = concentric compressive axial load capacity of the section

r_d = strength reduction factor account for loading history

r_f = Δ_f/Δ

s = spacing of transverse reinforcement

s' = effective depth of diagonal concrete strut

T = period of the pier system

T_t = torque

T_s = tension force in web reinforcement

T_x = tension force in flexural reinforcement at distance x from support

T_1 = tension force in flexural reinforcement at Section 1

T_{1c} = tension force in flexural reinforcement at Section 1 due to V_c

T_{1s} = tension force in flexural reinforcement at Section 1 due to V_s

V = shear force or lateral load on a cantilever column

V_a = inclined shear transmitted across the inclined crack by aggregate interlock

V_{acc} = shear force transferable across the inclined cracks

V_c = shear force carried by concrete shear resisting mechanism

V_c' = shear force resisted across the flexural compression zone

V_{cf} = residual shear strength due to the concrete shear resisting mechanisms

V_{ci} = initial shear strength due to the concrete shear resisting mechanisms

V_{co} = achievable shear assigned to the "concrete mechanism" at μ_o

V_{cr} = strength at occurrence of inclined cracks

V_d = dowel force transmitted across the crack by flexural reinforcement

V_f = residual shear strength

V_{fl} = strength at first occurrence of horizontal flexural cracks

V_i = shear strength before degradation

V_{iv} = shear strength derived from non-seismic provisions of NZS 3101

V_{max} = maximum measured strength

V_{mo} = monotonic shear strength at the displacement Δ_o

V_{if} = ideal flexural strength, shear force corresponding to the development of ideal flexural capacity

V^{o}_{if} = flexural overstrength

V_{mo} = monotonic shear strength at the displacement Δ_o

V_n = peak shear strength at n^{th} load cycle

V_s = shear force carried by the analogous truss

V_s' = shear force carried by spirals in the radiating cracks region

V_{sf} = residual shear strength due to transverse reinforcement

V_{si} = shear force assigned to the spiral reinforcement crossing a 45° potential diagonal failure plane

V_{so} = achievable shear carried by spirals at μ_o

V_x = component of shear in East - West direction

V_y = component of shear in North - South direction

$V_{\mu o}$ = achievable strength at the dependable displacement ductility capacity

v = shear stress

v_{av} = average shear stress

v_b = basic shear stress

v_c = shear stress carried by concrete shear resisting mechanisms

v_{co} = V_{co}/A_e

v_{cr} = V_{cr}/A_e

v_i = V_i/A_e

v_n = shear stress at layer n

$v_{\mu o}$ = $V_{\mu o}/A_e$

v_{max} = V_{max}/A_e

v_{so} = V_{so}/A_e

v_u = ultimate shear stress

w_i = increment of damage occurring during i^{th} cycle of load

Z = gradient of confined concrete stress - strain curve

Z_n = confinement index

'b' = bi-directional 'b' type displacement pattern

'r' = bi-directional 'r' type displacement pattern

's' = bi-directional 's' type displacement pattern

'u' = uni-directional 'u' type displacement pattern

α = confinement ratio

α_V = direction of force vector V measured from North

α_δ = direction of displacement vector Δ measured from North

β = inclination of web reinforcement to the longitudinal axis of a beam

D = top end deflection of a cantilever column

ΔF_c = $F_{c1} - F_{c2}$

Δ_b = deflection due to bar elongation within the column support

Δ_f = deflection calculated from the experimentally obtained curvature profile

Δ_{fl} = deflection due to flexure

Δ_{gauge} = changes in gauge length

Δ_s = deflection due to core distortions caused by shear

Δ_{ts} = deflection due to the effects of diagonal tension cracks

Δx = distance between Sections 1 and 2

$\Delta_{x'}$ = displacement component in East - West direction

Δ_y = yield displacement

$\Delta_{y'}$ = displacement component in North - South direction

Δ_α = $\alpha_\delta - \alpha_v$

Δ_1 = shortening of the diagonal concrete strut of an analogous truss unit

Δ_3 = elongation of spirals of an analogous truss unit

Δ_4 = web distortion per length d_s

δ = slip of the column steel bar at the extreme tension fibre due tension stress penetration in the foundation

ε_{av} = average concrete strain

ε_c = concrete strain

ε_{cav} = average concrete strain at local crushing of cover concrete

ε_{cr} = concrete strain at cracking

ε_{cm} = concrete strain at the extreme compression fibre

ε_{lc} = longitudinal strain

ε_{ls} = strain of column steel bar at the extreme tension fibre

ε_{pav} = average concrete strain at first application of axial compression load

ε_s = strain of spirals

ε_{tc} = transverse strain

ε_0 = concrete strain at the development of the concrete compressive strength, f'_c

ε_1 = principal tensile strain

ε_2 = principal compressive strain

θ = average inclination of inclined cracks to the longitudinal axis of a beam or column element, or inclination of diagonal concrete strut to the longitudinal axis of a beam or column element

θ_g = rotation of the column at the first potentiometer level

θ_t = torsional rotation relative to the column base

θ_δ = rotation of the column at the column base due to slip δ

μ = imposed displacement ductility factor

μ_c = available ductility capacity

μ_f = ductility capacity when shear failure does not occur

μ_i = ductility capacity before significant plasticity is developed

μ_o = dependable displacement ductility capacity

μ_ϕ = curvature ductility factor

$\mu_{\phi I}$ = curvature ductility factor for an idealized system

ρ_{cc} = volumetric spiral content for concrete confinement requirements

ρ_l = longitudinal reinforcement content

ρ_s = $4\ A_{sp}/(d_s\ s)$, volumetric spiral or circular hoop content

ρ_{sNZ} = volumetric spiral or circular hoop content for confinement required by NZS 3101 Clause 6.5.4.3, taking a strength reduction factor of unity

ρ_t = transverse reinforcement ratio

p_w = tensile reinforcement content

ρ_{45} = volumetric spiral content required to resist ideal flexural strength by spirals using the 45° truss model

$\Sigma\mu$ = cumulative displacement ductility factor

σ_{av} = average spiral stress

σ_{cc} = confining stress at zero lateral load

τ_R = concrete shear stress specified in the CEB-FIP Model Code

Φ = curvature

Φ_{max} = maximum curvature measured at the first potentiometer level near the column base

Φ'_{max} = maximum curvature measured at the first potentiometer level near the column base, excluding effects of tension stress penetration along column bars in the foundation

Φ_u = curvature at displacement ductility factor μ

Φ_x = theoretical curvature corresponding to bending moment M_x

Φ_x' = theoretical curvature corresponding to internal moment $T_x(jd)$

Φ_y = yield curvature

Φ_1 = theoretical curvature corresponding to bending moment M_1

Ω = mechanical degree of shear reinforcement

CHAPTER A
INTRODUCTION

A.1 ASPECTS OF SEISMIC DESIGN PHILOSOPHIES

In seismic regions, design strategy for earthquake resistance [A.1] usually requires that under minor to moderate earthquakes, structures should resist the intensity of ground motions without structural damage, but with some nonstructural damage. Under severe earthquakes, some structural and nonstructural damage is accepted. However, collapse and loss of life must be avoided. Lifeline structures, such as bridges, should remain functional for post-earthquake rescue or economic recovery purposes. Consequently, better seismic performance is desired for bridge structures as compared with buildings.

Basically, three approaches have been used in design of earthquake-resistant structures. The first approach is to design the structure to remain elastic during seismic attacks. This approach usually ends up with uneconomical use of materials, and is not adopted in most cases.

The second approach is ductile design which allows the structure to undergo large but dependable inelastic deformation without significant strength degradation, through the formation of plastic hinges in the selected structural components. At the expense of ductility provided, the design inertia forces are somewhat smaller than the elastic response inertia forces induced by a severe earthquake. Moreover, the response of the structure to ground motions is generally reduced by increasing: (a) the natural period of the structure because of reduced overall stiffness, and (b) the damping of the structure as a result of seismic energy dissipation at plastic hinges.

The third approach is the use of base isolator for the seismic protection of structures. The structure or superstructure is supported on devices, which provide flexibility and energy absorbing capacity. The cyclic build-up of inertia forces is then retarded by extra damping from these energy dissipating devices. Due to the flexibility of these devices, the natural period of the overall structure can increase to a magnitude away from the period at which the ground motion has its greatest effect, so that lower levels of inertia forces will result. Thus, the damage to the isolated structure, if any, can be reduced.

Ductile design approach is by far the most commonly used method in earthquake-resistant reinforced concrete design. It is recognized that ductility of reinforced concrete structures can be achieved if sufficient transverse reinforcement is provided in potential plastic hinges to confine the concrete core, to prevent buckling of the longitudinal reinforcement, and to provide adequate shear reinforcement.

In assigning plastic hinges for collapse mechanisms of multistorey frames, the principle of strong column - weak beam is often followed. That is, formation of plastic hinges in columns is avoided, as a column failure may have more serious consequences than a beam failure. However, at some unavoidable localities, such as the first storey columns in buildings or bridge piers, the columns are required to exhibit ductile performance by developing plastic hinges. Hence, an understanding of the interaction of principal forces: axial load, bending moment, shear force, and possibly torsion, acting on such columns is needed. It is now realized [A.2, A.3] that when a column develops maximum feasible flexural strength at its plastic hinge(s), the shear force across the column should be determined from the equilibrium of forces, rather than from the design horizontal inertia force specified by code recommendations. In cases of short columns, large shear force will result, and shear design for these columns becomes critical. In some recent earthquakes, such as the 1967 Caracas Earthquake in Venezuela [A.4], the 1968 Tokachi-Oki Earthquake in Japan [A.5], the 1971 San Fernando Earthquake in California [A.6], and the 1987 Whittier Narrows Earthquake in California [A.7], serious non-ductile shear failures of building columns and bridge piers, of rectangular or circular cross-sections, were reported. Consequently, research relevant to the seismic shear behaviour of reinforced concrete columns has been very active in recent years.

A.2 A REVIEW OF SOME SHEAR STUDIES

A.2.1 Introduction

In this section, a review of the seismic shear behaviour of reinforced concrete columns is presented in four sub-sections. Section A.2.2 outlines the development of shear studies of reinforced concrete members prior to the early seventies. Section A.2.3 lists the important findings on the behaviour of reinforced concrete columns subjected to slow uni-directional cyclic shear loading. Section A.2.4 reports research results on reinforced concrete columns subjected to slow bi-directional cyclic shear loading. Lastly, Section A.2.5 gives concluding remarks on this topic.

A.2.2 Developments in the Study of Shear Behaviour of Reinforced Concrete Members Prior to Early Seventies

Two schools of thought on the basic nature of shear failure mechanisms of reinforced concrete lineal members, namely horizontal shear and diagonal tension emerged before 1900. However, it was only in 1902 that the first laboratory tests on the shear strength of plain concrete beams were reported by Mörsch [A.8]. In the following year, Mörsch [A.9] reported tests on reinforced concrete beams with web reinforcement. He indicated that diagonal tension was the cause of shear failure in reinforced concrete beams. The "Truss Analogy", which was developed by Ritter in 1899, appeared to give a good prediction of the action of web reinforcement. The concept of shear stress, $v = V/(b_w\ jd)$, where V was the shear force, b_w was the web width, and jd was the internal moment arm, variables which were introduced to measure the shear effect. Some important findings, prior to 1950, were:

In 1909, Talbot [A.10] reported that for beams with web reinforcement, the shear capacity increased with cement content, age of concrete, amount of longitudinal reinforcement, and decreasing span of beam for the same cross-section. It was beneficial to use bent-up bars as web reinforcement. Stirrup stresses computed from the Ritter's "Truss Analogy" appeared to be too high. He recommended that the stirrups designed according to the "Truss Analogy" should carry two thirds of the external shear force, and that the remaining one third should be assigned to the concrete compression zone. Mörsch [A.11] recommended, however, that the total shear should be carried by stirrups and bent-up bars. Most of the European codes adopted Mörsch's proposition for shear design, whereas the American practice [A.12] considered that part of the external shear could be resisted by concrete in the flexural compression zone of beam sections.

In 1929, the first laboratory tests, to study combined shear, bending and axial load, was reported by Mörsch [A.13]. The specimen had no web reinforcement.

From 1950 to 1960, shear and diagonal tension became a major topic. The research work was devoted mainly to members without web reinforcement in order to get a better understanding of shear failure mechanisms. Tests showed that the percentage of longitudinal reinforcement, the shear span to depth ratio, and the square root of concrete compressive strength, f'_c, were the three main parameters governing the shear capacity of reinforced concrete members without web reinforcement. Semi-empirical formulae to calculate the ultimate concrete shear strength were suggested. A few tests on reinforced concrete beams with web reinforcement were also reported. Test results have shown that the "Truss Analogy" remained a valid tool for the design of shear reinforcement of reinforced concrete beams at the ultimate state. Limited investigations on reinforced concrete members subjected to shear, bending and axial load were published. These indicated that the axial compression would increase the diagonal tension strength while the axial tension would reduce it. A comprehensive report on the development till early Sixties of the shear strength of reinforced concrete was compiled by ACI-ASCE Committee 326 [A.14] in 1962.

In the Sixties, the mechanism of shear transfer was recognised to consist of : (a) shear stress in the uncracked concrete, (b) aggregate interlock along the cracks, (c) dowel shear carried by longitudinal reinforcement, (d) arch action, and (e) web reinforcement. Different modes of shear failure of reinforced concrete beams were also identified. A review of over 200 publications during this period was published by Joint ASCE-ACI Task Committee 426 [A.15]in 1973. Tests on beams subjected to reversal cyclic shear loading were also reported. It appeared that the shear transferred by the flexural compression zone and aggregate interlock decreased as the severity of loading cycles increased. Bresler [A.16] proposed that web reinforcement be provided for the full shear in beams subjected to full load reversals. In regard to tied columns, Yamada and Furui [A.17] showed that when the shear span ratio or amount of web reinforcement reduced, or the axial load increased, the magnitude of inelastic deformation, decreased significantly. Hirosawa and Goto [A.18] reviewed a number of Japanese tests and they concluded that the axial load could enhance the shear strength of columns.

A.2.3 Important Findings Relevant to the Behaviour of Reinforced Concrete Columns Subjected to Slow Uni-directional Cyclic Shear Loading

During several large earthquakes, such as the Tokachi-Oki Earthquake [A.5] in Japan, the Caracas Earthquake in Venezuela [A.4] and the San Fernando Earthquake in California [A.6], many reinforced concrete columns failed in shear. Fuelled by such failures, a large number of studies were undertaking and numerous reports on the seismic shear strength of reinforced concrete columns were published since 1970. Various patterns of slow uni-directional cyclic shear loading were used in these tests to simulate seismic effects. The important findings for the seismic shear strength of square or rectangular reinforced concrete columns or beams , transversely reinforced by stirrups or ties were:

a) Brown and Jirsa [A.19] investigated the behaviour of doubly-reinforced concrete cantilever beams subjected to load reversals at 5 to 10 times the yield deflection, Δ_y. The aspect ratio, L/d, where L was the distance from the point of counterflexure to the section of maximum moment, and d was the effective depth of the rectangular section of the specimens, varied from 3 to 6. Shear reinforcement in form of 9.5 mm diameter close stirrups were provided to satisfy the requirements of ACI 318-63 [A.20] for shear (100 or 125 mm spacing) or for the confinement requirements (50 mm spacing). The tests indicated that a loss in stiffness with cycling was due to a combination of the Bauschinger effect in the flexural reinforcement, shear deformation, closure of residual crack openings and anchorage slip. Failure of the specimens was initiated by large shear deformation along planes which were approximately parallel with the plane of stirrups. The ability of the specimens to maintain load and energy absorbing capacity was significantly improved by increasing the transverse reinforcement content. A reduction in the shear span or an increase in the shear force on the beams, however, reduced the number of cycles which could be applied before failure.

b) Wight and Sozen [A.21] tested 12 specimens, which represented the part of a column between the points of counterflexure above and below a floor of a multistorey frame, subjected to large shear load reversals. The variables were axial load (0 to $0.15f'_cA_g$, where A_g is the gross concrete area), transverse reinforcement ratio[1], ρ_t, (0.33 to 1.47%), and deflection level (maximum $4\Delta_y$). The aspect ratio of the specimens was about 3.5. It was found that the presence of an axial compression load slowed the decay in

[1]: $\rho_t = A_v/(b_w\ s)$, where A_v is the area of web reinforcement with spacing s

strength and stiffness with load cycling. Specimens with transverse reinforcement designed to carry the total shear sustained three to four cycles to $4\Delta_y$. However, those with transverse reinforcement satisfying ACI 318-71 [A.22] survived only one cycle to $4\Delta_y$.

c) Later Gosain, Brown, and Jirsa [A.23] reviewed six test reports on reinforced concrete members under shear reversals and developed a modified work index as a measure of the severity of loading for a member. They concluded that for the reasonable energy dissipating capacity and performance under inelastic deformation, defined as the ability of the member to sustain 5 cycles to $5\Delta_y$ with a loss in shear strength not greater than 25% of the shear at first yield, the shear stress on the concrete core (measured to outside diameter of hoops) should be limited to $0.5\sqrt{f'_c}$ (MPa) provided that the axial compression was less than 10 MPa. They recommended that the transverse reinforcement should be designed to carry the total shear imposed on the section. However, in 1984, Hwang and Scribner [A.24] concluded that the modified work index, developed by Gosain, could not predict consistently the behaviour of a flexural member subjected to an arbitrary displacement history. Instead, the strength and stiffness degradation of reinforced concrete members, subjected to inelastic load reversals, was found to depend on the magnitude of displacement peaks in each loading cycle and the maximum shear stress level experienced by the members, and that it was relatively independent of the sequence in which large and small deformations were applied.

d) Atalay and Penzien [A.25] tested 12 cantilever columns with an aspect ratio of 5. They were subjected to axial compression load (0.1 to $0.3f'_cA_g$) and cyclic incremental lateral loading. In their study, displacement ductility was defined as the ratio of measured deflection to yield deflection, Δ_y. Yield deflection corresponded to the deflection calculated at the first yielding of tensile flexural steel, using analytical moment-curvature relationships. Consequently, Δ_y increased with higher axial compression load. They found that shear strength degradation of their specimens started at lower displacement ductility levels for increasing applied axial load. This degradation accelerated with higher axial load and increased spacing of transverse reinforcement. The rate of loading had no significant effect on inelastic cyclic behaviour. It is noted that their finding of the effects of axial compression load on strength degradation, contradicts those of the present study (Section E.3). This is due to different definitions of yield deflection. In the present project, the magnitude of experimentally established yield deflection decreased with an increase of axial compression load intensity (Table D.I).

e) Saatcioglu [A.26] tested seven cantilever columns (aspect ratio of 2.9) under shear reversals. He showed that the ductility of the column could be improved by an increase of shear reinforcement. The test specimens, designed to satisfy the ACI 318-83 [A.27] requirements for regions of high seismic risk, performed poorly under constant axial compression (about 60% of the balanced section axial load). More than 30% loss in strength was observed at the end of 3 cycles to $2\Delta_y$. However, a test specimen subjected to the same axial compression but with 50% more shear reinforcement than that required by ACI 318-83 showed a ductile behaviour.

f) Zagajeski, Betero and Bouwkamp [A.28] studied 7 specimens under cyclic shear loading. Each specimen represented a one bay two storey subassemblage of a spandrel wall frame. The column in the subassemblage was deflected in a double curvature pattern (aspect ratio of 1.5), and subjected to axial compression load (0.21 to $0.3f'_cA_g$). Two of them were reinforced by spirals. The columns and their supporting beams were designed according to UBC 1973 [A.29] requirements, in which the design shear strength took into account the contribution from concrete and transverse reinforcement. Test results indicated that the maximum shear achieved under monotonic loading (one load cycle to the pre-determined displacement level) was slightly higher than that under cyclic incremental loading (five load reversals to each pre-determined displacement level). The observed maximum shear strength in terms of stress varied from 0.7 to $0.87\sqrt{f'_c}$ (MPa). Relative storey rotation ductilities greater than 6 were observed in specimens under monotonic loading, and greater than 4 in specimens under cyclic incremental loading before brittle shear failure or substantial shear degradation (50% loss of the original column shear resistance) occurred. In this study, relative storey rotation ductility was defined as the ratio of relative storey rotation to yield relative storey rotation. Relative storey rotation was the measured displacement of the upper end of the column relative to its lower end, divided by the clear height of the column. The relative storey rotation at first yielding of tensile flexural steel was considered to be the yield relative storey rotation. It was assumed that this first yielding occurred at the tip displacement of 25.4 mm, measured at the top of each subassemblage.

g) Based on the lower bound theorem of limit analysis, Minami, et al [A.30] proposed a shear design equation for a reinforced concrete member. The ultimate shear strength was obtained by summing the strength of two types of shear resisting mechanisms: the beam mechanism and the arch mechanism (Fig. A.1). The joint translation angle (identical to relative storey rotation) of a member could be estimated as a linear function of the ratio

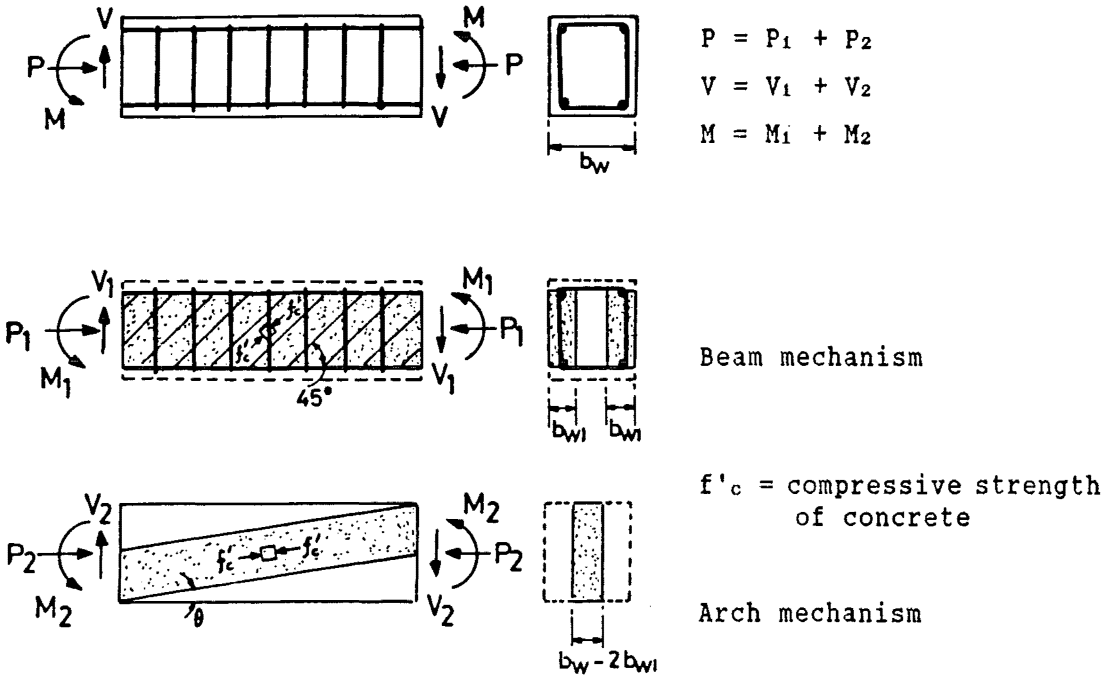

Fig. A.1 : Shear resistant mechanisms for reinforced concrete members [A.30]

of the transverse reinforcement content to its critical content. In this particular case, the critical transverse reinforcement content was the required quantity to secure flexural failure of the member. It was derived from the proposed shear design equation.

h) Watanabe and Muguruma [A.31] also suggested that the shear capacity was given by the superposition of the contributions due to the arch and the truss mechanisms. However, the resultant stress of concrete strut was taken to be the sum of the concrete stresses calculated from the arch and the truss mechanisms respectively. For the purpose of simplicity, the difference of strut angle in each mechanism was ignored. This resultant stress was found to be a good measure of ductility. Higher ductility could be attained by reducing the resultant stress level in concrete strut.

i) An extensive programme to study the performance of reinforced concrete bridge piers has been conducted at the University of Canterbury [A.32] since 1974. The effects of varying the aspect ratio (2 and 4), and the axial compression load (0.3 to $0.67f'_cA_g$) on the available ductility and on force - displacement hysteretic responses were carefully studied. For most of the specimens, the amount of transverse reinforcement in the potential plastic hinge region was governed by NZS 3101 [A.33] confinement rather than shear requirements. It was found that all test columns developed moments in excess of the theoretical flexural strength calculated with ACI methods [A.27], which assumed a maximum concrete compressive strain of 0.003.

Measured material strengths and a strength reduction factor of unity were used. This increase of resistance was found to be due to an enhancement in concrete strength brought about by confinement when axial load on the columns was significant. It was also due to strain hardening of longitudinal reinforcement at high strain levels. The force - displacement hysteretic response was maintained stable at displacement ductility even greater than 6. Tests also indicated that if the spacing of transverse reinforcement was greater than six times the longitudinal bar diameter, the failure of these specimens could involve premature buckling of longitudinal reinforcement. The emphasis of research at the University of Canterbury was on the flexural response of reinforced concrete columns rather than effects of shear. The typical aspect ratio of these specimens was 4 so that shear did not develop into a critical parameter.

Only limited research on the shear strength of reinforced concrete members with circular cross-section and with circular hoops or spirals as transverse reinforcement could also be identified in the technical literature. More important observations were:

a) Karlsson [A.34] tested 6 spirally reinforced concrete square columns with an aspect ratio of 3. These were subjected to cyclic lateral loading with different axial load intensity. The spiral reinforcement was proved to be very effective in acting as confining and shear reinforcement.

b) Khalifa and Collins [A.35] tested five circular columns with an aspect ratio of 1.4. All specimens were transversely reinforced with circular hoops. Four of them were subjected to monotonic lateral loading while only one was subjected to load reversals. It was found that the experimentally observed shear strength was generally 20% higher than those predicted by relevant ACI 318-77 [A.36] equations. The compression field theory [A.37] was able to predict the shear strength fairly accurately. However, the validity of these findings for the case with cyclic loading was uncertain.

c) Arakawa, et al [A.38] tested twelve spirally confined concrete columns. It was concluded that shear strength and ductility at ultimate improved with an increase in spiral reinforcement content. Axial compression load increased the ultimate shear strength but it resulted in strength degradation. Longitudinal reinforcement content appeared to have a little effect on ultimate shear strength. The ultimate shear strength of these specimens could be predicted fairly well using formulae proposed by Shibata [A.39] or Hirosawa [A.18].

d) Since 1978, a systemic study of shear strength of circular columns was carried out at the University of Canterbury. Five squat octagonal columns with an aspect ratio of 2, transversely reinforced by spirals, were tested [A.40] under cyclic shear loading with various axial compression load intensity (0.24 to $0.7f'_cA_g$). The amount of spiral reinforcement at the potential plastic hinge region in four specimens, which was originally designed according to an early draft of NZS 3101 [A.41] for confinement requirements, was about 85% of the amount required by current NZS 3101 [A.33] confinement requirements. The quantity of spiral reinforcement for the specimen with high axial compression load ($0.7f'_cA_g$) was 37% larger than required by NZS 3101. All specimens exhibited stable force - displacement hysteretic response up to the displacement ductility of 6 with little strength degradation. The experimentally observed strength was at least 20% greater than the theoretical flexural strength evaluated using ACI methods with a strength reduction factor of unity. Priestley and Park [A.32] studied the shear carried by concrete, V_c, for these specimens by subtracting the shear carried by the spiral reinforcement, V_s, from the total shear, V. The term V_s could be estimated from spiral strain measurements and the observed crack patterns, i.e. perceived failure plane. It was found that for higher axial compression load intensity, the experimentally observed values of shear carried by concrete, V_c, after extensive inelastic load cycling, were significantly less than the corresponding values given by NZS 3101 equations.

In order to obtain more information on the seismic shear strength of circular reinforced concrete columns, Ang [A.2] tested 25 circular columns subjected to slow incremental cyclic shear loading. The main variables were the aspect ratio (L/D = 1.5, 2.0 and 2.5), the axial compression load (0, 0.1 and $0.2f'_cA_g$), and the spiral reinforcement content. Four failure modes were identified, depending on the displacement ductility at which the stability of hysteretic response could no longer be maintained. The test results indicated that the strength of concrete shear resisting mechanism, expressed by V_c was a function of imposed displacement ductility level, and that it was increased by either reducing the aspect ratio lower than 2.0 or by increasing axial compression level or both. However, the application of high axial compression load accelerated the rate of strength degradation after the maximum shear force had been reached. An increase in spiral reinforcement content distinctly improved shear strength, ductile performance and energy dissipation capacity. Current design codes were found to be too conservative in the estimation of the shear force carried by the concrete mechanism. This project is intended to be a continuation and extension of the work undertaken by Ang.

A.2.4 Research on Reinforced Concrete Columns Subjected to Slow Bi-directional Cyclic Shear Loading

Although information found on the shear strength of reinforced concrete columns subjected to bi-directional cyclic shear loading is limited, there has been evidence that the shear performance depends also on the selected displacement path. Fig. A.2 shows some of the displacement paths used in previous research of this topic.

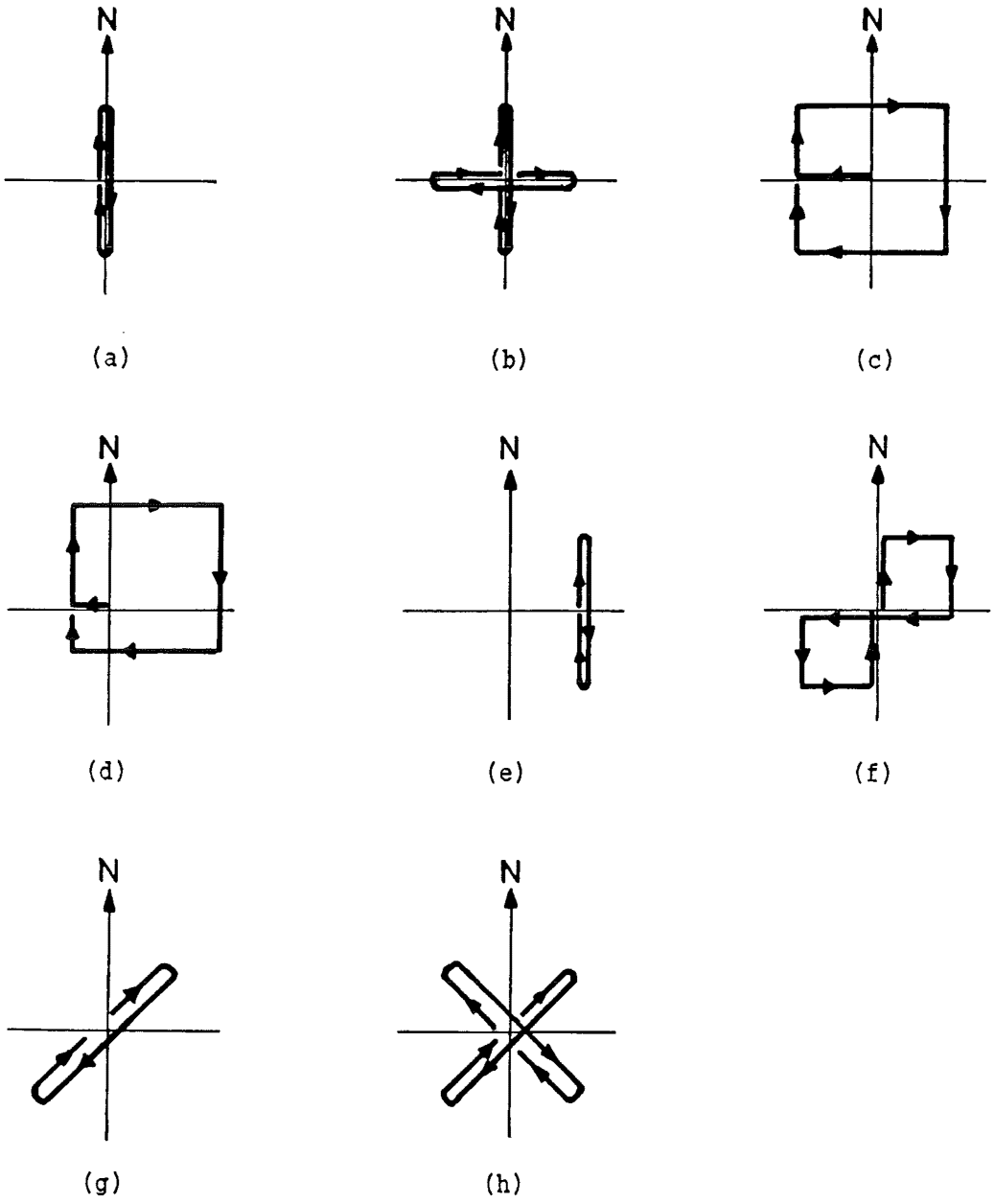

Fig. A.2 : Lateral displacement paths used in the study of the shear strength of columns

Otani [A.42] tested 8 reinforced concrete square columns with an aspect ratio of 4, subjected to various displacement paths (Figs. A.2a, b, c, d). The shear strength of specimens, as evaluated from ACI 318-77 [A.36] requirements, varied from 0.9 to 3.0 times the shear corresponding to the calculated flexural strength. It was concluded that the increase in shear reinforcement content significantly improved the ductility of the specimen. Also it concentrated the damage at the plastic hinge region. When the specimen was subjected to a cross-shaped displacement path (Fig. A.2b), the member stiffness in one direction was reduced as a result of damage inflicted during loading in the transverse direction. However, the hysteretic response and the load carrying capacity of the specimen subjected to this displacement path were very similar to the ones subjected to uni-directional load cycling (Fig. A.2a) provided that the same number and same magnitude of displacement cycles were applied in both cases. When subjected to bi-directional loading (Figs. A.2c and d), specimens started to yield, in the principal direction (NS or EW), at a significantly lower strength than that under uni-directional loading.

At the University of Texas [A.43, A.44, A.45], over 40 specimens with rectangular cross-sections, with both ends restrained against rotation to simulate short columns between stiff floors, were tested to study the effects of deformation paths (Figs. A.2a, b, c, e, f, g, h), axial load level, transverse reinforcement content, and geometry of specimen (square and rectangular) on the shear strength and on deterioration. It was observed that the previous displacement paths did not significantly affect the maximum shear strength as long as the displacement level was kept below that at the development of the maximum shear strength in the companion monotonic tests. The repeated square-shaped displacement path (Fig. A.2c) was found to be the most severe loading pattern. This caused rapid degradation of both strength and stiffness. Axial compression load increased shear strength and initial stiffness of the column but it also enhanced the strength degradation and stiffness reduction with cycling at a displacement equal to or greater than the displacement at the development of maximum shear strength. Axial tension load reduced the shear strength but also slowed strength degradation.

No information relevant to experimental work which addressed specifically the behaviour of the circular reinforced concrete columns, or columns reinforced with circular hoops or spirals subjected to bi-directional cyclic shear loading could be located.

A.2.5 Concluding Remarks on Literature Review

It has been shown that the influence on the shear behaviour of reinforced concrete members, and various shear resisting mechanisms of some key parameters, such as aspect ratio, axial load intensity, reinforcement content, and material properties, have been fairly well established from the past research. However, widely differing load, boundary, geometric and other conditions, employed in the projects which have been briefly reviewed here, did not permit a consistent correlation between findings of different authors to be established. It is not surprising to find that greater differences in approaches to the design of shear strength, embodied in various codes, exist than for other structural actions, such as flexure with and without axial load.

It appears that the general tendency in established codified design procedures for shear strength follows a concept whereby some of the shear resistance is assigned to the transverse (shear) reinforcement, and the remainder to the concrete, V_c. It is emphasized that the term V_c is only used for the convenience of designers. This quantity attempts to express the contribution to shear strength of all mechanisms other than the web reinforcement (truss mechanism). The term V_c includes contributions originating from the tensile strength of uncracked concrete, shear transfer in the flexural compression zone, and by aggregate interlock action across diagonal cracks, as well as by dowel action of reinforcement where the same is subjected to shear strains or shear displacement between crack faces.

The major difficulty in the assessment of the contribution of transverse reinforcement to the shear strength of columns comes from its multiple roles. Ties, hoops or spirals will also act as confining reinforcement while they also restrain the principal column bars against buckling, particularly at advanced stages of inelastic loading. Therefore, while making strain measurement, it is difficult to separate the two major causes of tensile strains i.e. confinement and shear transfer as part of the truss mechanism. When axial compression load on a column is negligibly small, the primary cause of tensile forces in the transverse reinforcement after the development of diagonal cracks, will be shear. On the other hand, when large axial compression load is applied to a column, confinement of the plastic hinge zone assumes great importance in sustaining load with significant ductility. It is at this stage when it is very difficult, if not impossible, to separate the influence of confining action and shear mechanism on the tensile strains developed in the transverse reinforcement. Moreover,

the mechanism of the confinement of the concrete in the plastic hinge region of columns will be significantly influenced by the presence or absence of diagonal cracks. These aspects, to be examined in other chapters, are considered to account partly for apparent conflicts in the interpretation of column test results, reviewed in this chapter.

A.3 SCOPE OF RESEARCH

The main objective of the research reported in this thesis was to experimentally investigate seismic shear behaviour, and to quantify important parameters affecting the overall performance of spirally reinforced concrete circular columns subjected to shear force, bending moment and axial load. A further objective was to develop a seismic shear design proposal taking into account the selected levels of displacement ductility demands, while also considering effects of imposed inelastic displacement patterns.

This research is the continuation of shear study of circular columns in the Civil Engineering Department of the University of Canterbury. Previous investigation reported by Ang [A.2] indicated that the existing design methods, based on simple monotonic tests of beam sections subjected to axial load, did not provide a realistic assessment of shear strength of circular columns. In his test program, twenty five column models were subjected to quasi-static uni-directional cyclic loading. The variables studied were amount of spiral steel content, aspect ratio, and axial compression load intensity.

It is evident that ground motions from earthquake are random in nature, and take place in variable directions. Some columns may be equally affected by displacements in any direction. Shear strength derived from uni-directional cyclic tests may not adequately represent the strength under multi-directional seismic attacks. There is limited evidence (Section A.2.4) that rectangular and square columns subjected to bi-directional cyclic loading exhibit a lower shear strength than equivalent columns subjected to uni-directional cyclic loading. This may be attributed to the development of two intersecting sets of flexure-shear cracks resulting in more damages to core concrete. Therefore, multi-directional displacement history is chosen as one of the main variables studied in this research.

Other main variables investigated are: the amount of spiral steel content, and axial compression load intensity. In this research, sixteen column models similar to those of Ang were constructed and tested under quasi-static conditions.

A.4 FORMAT OF THE THESIS

This thesis consists of seven chapters, namely Chapter A to Chapter G. Following Chapter G, the list of references, and five appendices (Appendix I to Appendix V) are included.

Chapter A covers some aspects of seismic design philosophies, and outlines some important studies on shear behaviour of reinforced concrete members. It also states scopes of this research.

A brief review of six shear models for reinforced concrete elements, and their applicability on predicting the seismic shear behaviour of reinforced concrete circular columns are presented in Chapter B.

Chapter C details design parameters, construction of test specimens, instrumentation, testing procedure, and measured material properties of test units.

Chapter D gives a record of general performance of test columns, and detailed description of individual test results.

Based on the experimental information from Chapter D, the performance of test columns, with respect to hysteretic response, yield displacement, components of deflections, spiral strain distribution, and energy dissipation, is compared in Chapter E. A discussion on shear carrying mechanisms is also offered.

Chapter F presents design recommendations on two topics, namely, an approach to evaluate elastic deformations in reinforced concrete circular cantilever columns, and a proposal of seismic shear design for reinforced concrete circular columns. A summary of these recommendations in form of flow charts is given at the end of this chapter.

Finally, Chapter G concludes the experimental findings, and analytical studies of this research. From which, suggestions for further research on seismic shear behaviour of circular column are outlined.

The appendices are supplementary information or calculations related to the previous chapters. They are: shear force assigned to the spiral reinforcement, dynamic analysis of circular reinforced concrete pier systems subjected to two dimensional earthquake motions, evaluation of lateral forces acting on a test column, the estimation of stresses induced in spirals and longitudinal bars by torsion, and moment - curvature relationships for reinforced concrete sections with flexure and axial load.

CHAPTER B
REVIEW OF THEORETICAL MODELS

B.1 INTRODUCTION

In this chapter, six theoretical models used to predict the shear behaviour of reinforced concrete members, are reviewed. They are: the truss analogy, limit analysis based on perfect plasticity, the diagonal compression field theory, Ang's shear design procedure for circular reinforced concrete columns [B.1], a conceptual model for shear behaviour under multi-directional loading [B.2], and a predictive guide for behaviour classification of reinforced concrete members [B.3]. The last two models, used in a study of fixed end square reinforced concrete columns under uni-directional and bi-directional cyclic loading, are extracted from the research reports of the University of Texas at Austin [B.2, B.3]. Subsequently, the applicability of these existing models to predict the shear behaviour of circular reinforced concrete columns under inelastic bi-directional loading histories are discussed.

B.2 THEORETICAL MODELS

B.2.1 The Truss Analogy

When a reinforced concrete member is subjected to flexural and shear loading, a biaxial stress state is generated. When in a region the principal tensile stress exceeds the tensile strength of concrete, cracks are created approximately perpendicular to this principal tensile stress direction. Usually, vertical flexural cracks at right angles to the longitudinal axis of the member are formed first at the extreme tensile fiber. These extend into inclined cracks (diagonal tension cracks) at region of higher shear.

For a member with no web reinforcement, the external shear force at the post-cracking state is resisted by vertical shear contributed by the concrete compression zone, the cracked concrete zone through aggregate interlock, and by dowel action of the flexural reinforcement. Such a shear resisting mechanism is illustrated in Fig. B.1,

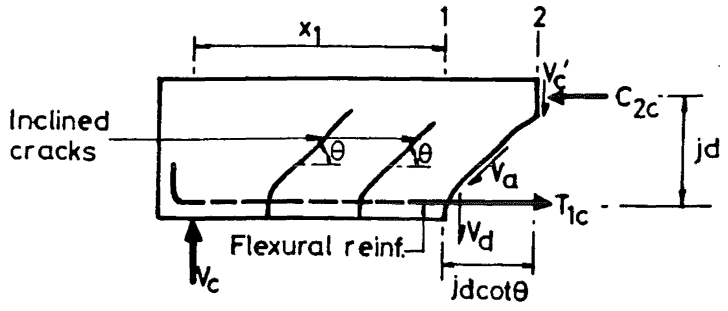

Fig. B.1 : Forces on the free body of a reinforced concrete beam element with no web reinforcement

where V_c = shear force carried by concrete shear resisting mechanism

V_c' = shear force resisted across the flexural compression zone

V_a = inclined shear transmitted across the inclined crack by aggregate interlock

V_d = dowel force transmitted across the crack by the flexural reinforcement

and θ = average inclination of inclined cracks to the longitudinal axis of a beam element

From the equilibrium of forces,

$$V_c = V_c' + V_a \sin\theta + V_d \qquad (B.1)$$

The tension force in flexural steel at Section 1 due to V_c is T_{1c} where

$$T_{1c} \approx (V_c\ (x_1 + jd\ \cot\theta) - V_d\ jd\ \cot\theta)/jd \qquad (B.2)$$

The compression force in horizontal compression chord at Section 2 due to V_c is C_{2c} where

$$C_{2c} = (V_c\ x_1 + V_c'\ jd\ \cot\theta)/jd$$

$$= T_{1c} - V_a \cos\theta \qquad (B.3)$$

By the introduction of web reinforcement, a post-cracking shear capacity, higher than V_c, is achieved. This increase can be modelled by an analogous plane truss consisting of the concrete compression zone, longitudinal tensile bars, diagonal concrete struts, and web reinforcement, serving as horizontal compression chord, horizontal tension chord, compression and tension web members respectively. Fig. B2 shows this familiar analogous truss resisting the external shear force, V_s.

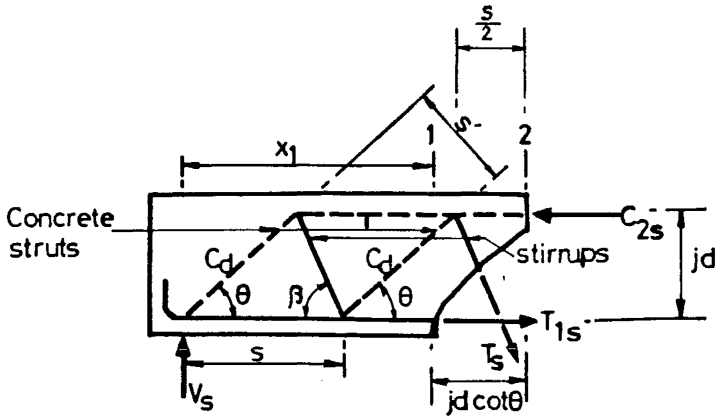

Fig. B.2 : Forces on the free body of an analogous truss

where V_s = shear force carried by the analogous truss

T_s = tension force in web reinforcement

C_{2s} = compression force in horizontal compression chord at Section 2 due to V_s

T_{1s} = tension force in flexural reinforcement at Section 1 due to V_s

C_d = compression force in diagonal concrete strut

ß = inclination of web reinforcement to the longitudinal axis of beam

θ = inclination of diagonal concrete strut to the longitudinal axis of beam, generally taken to be parallel with the diagonal cracks

s = horizontal spacing of web reinforcement

s' = effective depth of diagonal concrete strut

From the truss geometry,

$$s = jd\ (\cot\theta + \cot\beta) \qquad (B.4)$$

$$s' = s \sin\theta$$

$$= jd \sin\theta\ (\cot\theta + \cot\beta) \qquad (B.5)$$

and from equilibrium criterion for a "joint",

$$V_s = C_d \sin\theta$$

$$= T_s \sin\beta \qquad (B.6)$$

Combining Eqs. (B.4) and (B.6), the force in the web reinforcement per unit length can be expressed as

$$T_s/s = V_s/(jd \sin\beta\ (\cot\theta + \cot\beta))$$

$$= A_v f_{st}/s \qquad (B.7)$$

where A_v = area of the web reinforcement with spacing s

f_{st} = stress in web reinforcement

By combining Eqs. (B.5) and (B.6), the average compressive stress in diagonal concrete strut, f_{cd} can be approximated as

$$f_{cd} = C_d/(b_w\ s') = V_s/(b_w\ jd\ \sin^2\theta\ (\cot\theta + \cot\beta)) \quad (B.8)$$

where b_w = web width of the beam

The chord forces are

$$T_{1s} = V_s\ (x_1/jd + \cot\theta/2 - \cot\beta/2) \quad (B.9)$$

$$C_{2s} = T_{1s} + T_s \cos\beta = V_s\ (x_1/jd + \cot\theta/2 + \cot\beta/2) \quad (B.10)$$

It may then be assumed that the total external shear, V, is resisted partly by the truss mechanism, V_s, and partly by the concrete shear resisting mechanism, V_c. i.e.

$$V = V_s + V_c = A_v\ f_{st}\ jd\ \sin\beta\ (\cot\theta + \cot\beta)/s + V_c \quad (B.11)$$

or expressed in terms of nominal shear stress, v, we have

$$v = V/(b_w\ d) = A_v\ f_{st}\ jd\ \sin\beta\ (\cot\theta + \cot\beta)/(s\ b_w\ d) + V_c/(b_w\ d) \quad (B.12a)$$

By assuming that $jd \approx d$, then

$$v = \rho_t\ f_{st}\ \sin\beta\ (\cot\theta + \cot\beta) + v_c \quad (B.12b)$$

where $\rho_t = A_v/(s\ b_w)$ (B.12c)

and $v_c = V_c/(b_w\ d)$ (B.12d)

The ideal shear stress, v_i, is assumed to be reached when the web reinforcement develops its yield strength, f_{yt}. Hence

$$v_i = \rho_t\ f_{yt}\ \sin\beta\ (\cot\theta + \cot\beta) + v_c \quad (B.13)$$

Correspondingly, the flexural tensile reinforcement at Section 1 should be designed to resist the total tension force, T_1

$$T_1 = T_{1s} + T_{1c} = M_1/jd + V_c\ \cot\theta + 0.5\ V_s(\cot\theta - \cot\beta) - V_d\ \cot\theta \quad (B.14)$$

where M_1 = bending moment at Section 1

The term ($V_d\ \cot\theta$) estimating the dowel action, is usually neglected for the design purpose.

An upper limit of v_u is set to prevent compression failure of the diagonal concrete strut. Eq. (B.8) can be rewritten as

$$V_s/(b_w\ jd) = f_{cd}\ \sin^2\theta\ (\cot\theta + \cot\beta) \qquad (B.15)$$

The average strength of the diagonal concrete strut, f_{cd}, can be estimated as a function of the compressive cylinder strength of concrete, f'_c.

$$f_{cd} = k_c\ f'_c \qquad (B.16)$$

where k_c = effective strength factor.

Values of $0.6 < k_c < 0.9$ have been suggested [B.4, B.5]. Recent research [B.9] showed that this value, being affected by the tensile strains generated transversely in the diagonal struts, is considerably less than 0.6.

Eqs. (B.11) and (B.14) are the general forms of the shear and flexure design formulae for rectangular or tee-shaped reinforced concrete beams, suggested by most of design codes. Table B.I summarizes the shear design provisions of different codes using the analogous truss model. Each design code has its own recommendations on the inclination of diagonal concrete struts, θ, the dependable value of v_c, and the upper limit of v_u. In the traditional truss model, θ is assumed to be 45°. Leonhardt [B.10] tested several beams with vertical stirrups, i.e. $\beta = 90°$, under monotonic loading. He found that the shear strength could be satisfactorily expressed by Eq. (B.11) until yielding of the web reinforcement when the angle θ was assumed to be 45°. The value of V_c has traditionally been assumed to be equal to diagonal cracking load. Thus, it was assumed to be independent of the quantity of the web reinforcement. However, it has been established that the inclination of diagonal compression and shear cracks in beams may be more or less than 45° at the ultimate state. The shear strength predicted by the 45° truss model was often found to be conservative. A variable-angle truss model was suggested by Lampert and Thurlimann [B.11]. The ideal shear stress, v_i, is expressed by Eq. (B.13) with the angle θ varied within a certain range. The limitation on the variation of angle θ is used so as to control the crack width prior to yielding of both the web and flexural tension reinforcement. For example, CEB-FIP Code [B.5] limits the range of θ so that $3/5 \leq \tan\theta \leq 5/3$. At the ultimate state, the widening of shear cracks causes rapid deterioration of the aggregate interlock. Its dependable contribution will reduce. Therefore v_c is always assumed to be zero in the variable-angle truss model.

Table B.I : Comparison of non-seismic shear design provisions of different codes based on the truss analogy

	** ACI [B.6]		NZS [B.7]	CAN [B.8] (simplified method)	CEB-FIP [B.5]
	Approximate	More "exact"			
v_c (flexure only)	$0.17 \sqrt{f'_c}$	$0.16 \sqrt{f'_c} + 17.2 \rho_w V_u d/M_u$ $\leq 0.30 \sqrt{f'_c}$ $V_u d/M_u \leq 1.0$	$v_b = (0.07 + 10 \rho_w) \sqrt{f'_c}$ $0.08 \sqrt{f'_c} \leq v_b \leq 0.2 \sqrt{f'_c}$	$v_b = 0.12 \sqrt{f'_c}$ (for normal density concrete) $v_c = v_b$	$2.5 \tau_R$ $\tau_R = 0.054 f'^{0.67}_c$
v_c (with axial tension)	zero	$0.17 (1 + 0.30 P_u/A_g) \sqrt{f'_c}$ P_u is negative for tension	$(1 + 12 P_u/(f'_c A_g)) v_b$ P_u is negative for tension	$(1 - P_u/P_r) v_b$ P_u is positive for tension P_r is axial tensile resistance of member ignoring any contribution of concrete	$2.5\tau_R$ if the position of neutral axis is within the cross-section. Otherwise, v_c is taken equal to 0
v_c (with axial compression)	$0.17 (1 + 0.073 P_u/A_g) \sqrt{f'_c}$	$0.16 \sqrt{f'_c} + 17.2 \rho_w V_u d/M_m$ $M_m = M_u - P_u (4h - d)/8$ > 0 upper bound is $0.30 \sqrt{f'_c} (\sqrt{1 + 0.3 P_u/A_g})$	$(1 + 3 P_u/(f'_c A_g)) v_b$	$(1 - 3 P_u/(f'_c A_g)) v_b$	$2.5 \tau_R \beta_1$ $\beta_1 = 1 + M_o/M_u$ ≤ 2 M_o is decompression moment
Maximum allowable shear stress	$v_s \leq 0.67 \sqrt{f'_c}$	$v_s \leq 0.67 \sqrt{f'_c}$	$v_u \leq 0.2 f'_c$ ≤ 6 MPa	$v_u \leq 0.6 \sqrt{f'_c}$ (for normal density concrete)	$v_u \leq 0.3 f'_c$ (for vertical web reinforcement)
Inclination of concrete strut, θ	45°	45°	45°	45°	a) for standard method $\theta = 45°$ b) for variable-angle truss method $31° \leq \theta \leq 59°$ and $v_c = 0$ if shear stress $v \geq 2 v_c$

Note: All stresses in MPa

**: ACI 318-89 limits $\sqrt{f'_c}$ to 8 MPa except for beams with enough stirrups to allow post cracking capacity.

B.2.2 Limit Analysis Based on Perfect Plasticity

Lower bound and upper bound theorems of limit analysis, based on perfect plasticity, have also been used to determine the shear strength of reinforced concrete components. The lower bound theorem states that if a safe and statically admissible stress distribution can be found, the structure will not collapse or will just be at the point of collapse. On the other hand, the structure will collapse if the rate of external work done exceeds the rate of internal energy dissipation, both calculated with the use of an admissible displacement field (upper bound theorem). The following sections illustrate the application of these theorems to determine the shear strength of a simple beam with web reinforcement and subjected to symmetrical loads (Fig. B.3). The basic assumptions are:

a) The yield criterion for each, steel and concrete, is rigid-plastic, as shown in Fig. B.4.

b) Reinforcement resists axial forces only.

B.2.2.1 Lower bound solution

An admissible stress field of the beam is shown in Fig. B.5. The concrete in the web is subjected to uniaxial compression, and both compression and tension chords are stressed not exceeding yield. For convenience, the shear stress, v, and the equivalent transverse stress due to stirrups, $\rho_t f_{yt}$, are expressed as

$$v = V/(b_w d) \tag{B.17}$$

and $$\rho_t f_{yt} = A_v f_{yt}/(b_w s) \tag{B.18}$$

From equilibrium condition of the element "A", shown in Fig. B.5,

$$f'_c \sin^2\theta + \rho_t f_{yt} = 0 \tag{B.19}$$

and $$v = f'_c \sin\theta \cos\theta \tag{B.20}$$

By solving Eqs. (B.19) and (B.20), the lower bound solution is obtained. Thus

$$v/f'_c = \sqrt{\Omega\ (1-\Omega)} \leq 0.5 \tag{B.21}$$

where $$\Omega = \rho_t f_{yt}/f'_c \tag{B.22}$$

and $$\tan\theta = \sqrt{\Omega/(1-\Omega)} \tag{B.23}$$

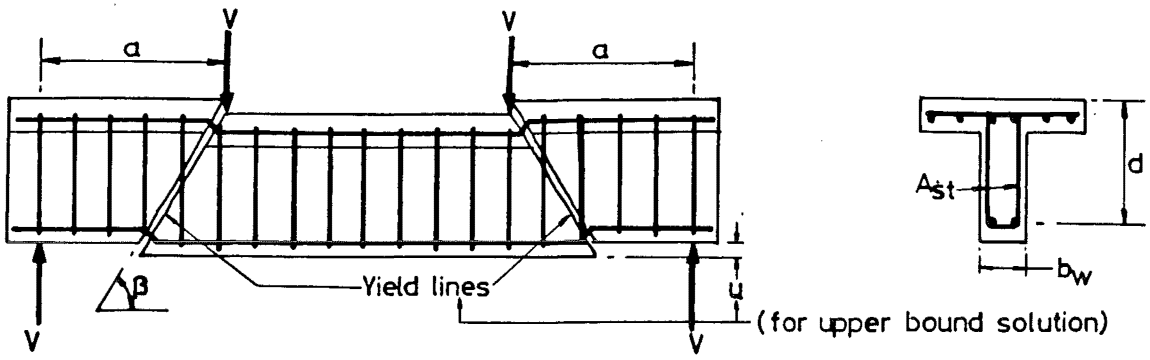

Fig. B.3 : General arrangement of a beam (Displacement field for upper bound solution included)

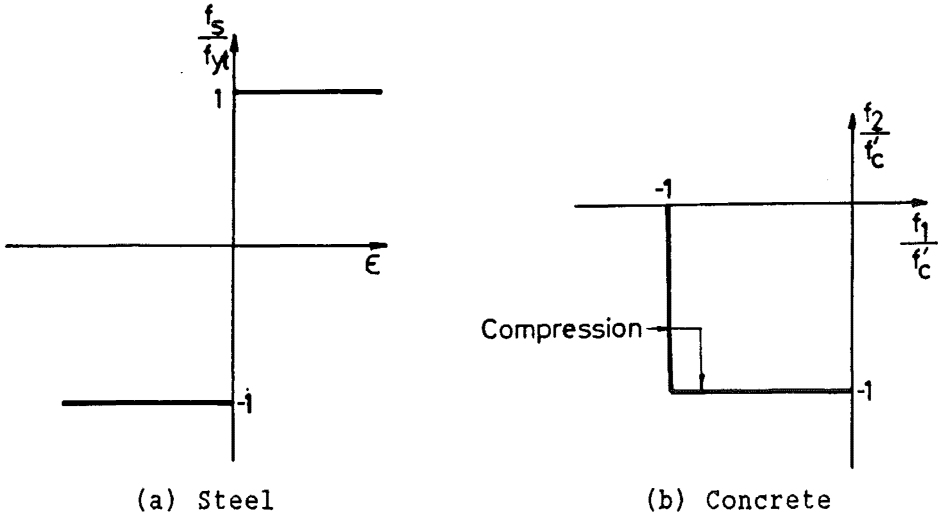

Fig. B.4 : Yield criteria

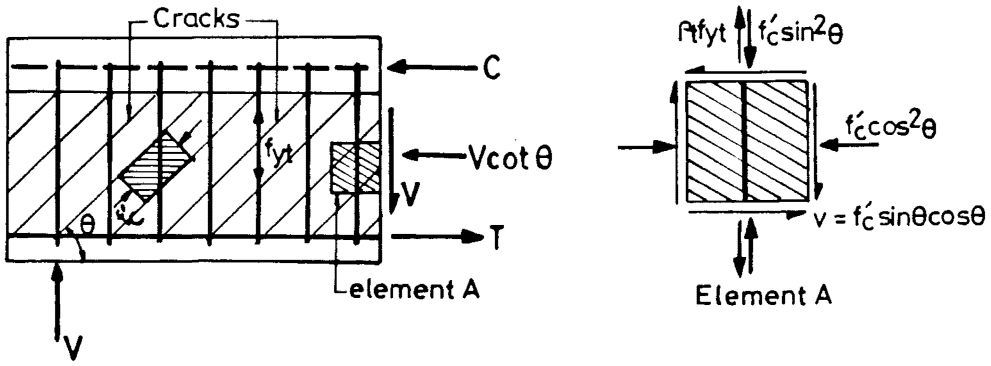

Fig. B.5 : Admissible stress field for lower bound solution

B.2.2.2 Upper bound solution

Fig. B.3 shows the kinematically admissible displacement field, where the central part between the two yield lines inclining at the angle ß is subjected to a vertical displacement u. It is further assumed that the flow rule at the yield line is valid, and that the contribution due to longitudinal reinforcement is negligible. Then the external work done and internal work [B.12] can be equated, thus

$$u\,V = u\,\rho_t\,f_{yt}\,b_w\,d\,\cot\beta + 0.5\,u\,f'_c\,b_w\,(1 - \cos\beta)\,d/\sin\beta \qquad (B.24)$$

It is then found that

$$v/f'_c = \Omega\,\cot\beta + 0.5\,(1 - \cos\beta)/\sin\beta \qquad (B.25)$$

The lowest upper bound is found from the condition that

$\partial V/\partial\beta = o$, and hence

$$\tan\beta = 2\,(\sqrt{\Omega\,(1 - \Omega)})/(1 - 2\,\Omega) \qquad (B.26)$$

Substituting Eq. (B.26) into Eq. (B.25), it is found that

$$v/f'_c = \sqrt{\Omega\,(1 - \Omega)} \qquad (B.27)$$

From the limitation of the geometrical boundary conditions,

$$d/a \leq \tan\beta \leq \infty \qquad (B.28)$$

where a and d are defined in Fig. B.3.

Hence, if ß, calculated from Eq. (B.26), does not satisfy Eq. (B.28), we may set $\tan\beta = d/a$, in which case the solution becomes

$$v/f'_c = 0.5\,((1 + (a/d)^2)^{0.5} - a/d) + \Omega\,a/d \qquad (B.29)$$

Finally, when the lower and upper bound theorems yield the same answer, the "exact" solution is said to have been achieved.

B.2.3 Diagonal Compression Field Theory

B.2.3.1 Constituent relationships

The diagonal compression field theory, developed largely by Collins et al [B.13, B.14] enables a prediction on the shear behaviour of a reinforced concrete member under monotonic loading to be made. The principles of this theory can best be illustrated by a reinforced concrete panel subjected to plane stresses. Such a panel may be considered to represent an element within the shear affected region of a reinforced concrete element. Fig. B.6 shows the stress - strain response of such panel. The basic assumptions used are:

a) Cracks are smeared out in a continuous fashion so that only average stresses and strains are considered.

b) Concrete and reinforcement are subjected to the same average strain.

c) The relationships of average stresses or strains within this panel can be represented by Mohr's circles.

The response of the reinforced concrete panel can be predicted by utilizing equilibrium conditions of stresses (Fig. B.6b), compatibility requirements of strains (Fig. B.6a), and lastly stress-strain relationships (Fig. B.6c). Two distinct features of this theory are to be noted:

1. The inclination of the principal compressive stress in concrete, θ_2, is equal to the inclination of the principal compressive strain, θ_1. Reinforcement bars carry only axial forces. This assumption of the diagonal compression field theory was verified by the test results obtained from 30 reinforced concrete panels, studied by Vecchio and Collins [B.9].

2. The magnitude of the principal compressive stress in concrete, f_{c2}, does not depend on the principal compressive strain, ε_2, only, but also on the principal tensile strain, ε_1. It can be expressed as

$$f_{c2} = f'_p \, (2\,\varepsilon_2/\varepsilon_0 - (\varepsilon_2/\varepsilon_0)^2) \qquad \text{(B.30a)}$$

$$f'_p = k_c \, f'_c \qquad \text{(B.30b)}$$

$$k_c = 1/(0.8 - 0.34\,\varepsilon_1/\varepsilon_0) \leq 1.0 \qquad \text{(B.30c)}$$

where f'_p = peak compressive strength of biaxially stressed concrete

f'_c = concrete cylinder compressive strength

and ε_0 = concrete strain at the development of the concrete compressive strength, f'_c

Both compressive stress and compressive strain are negative quantities.

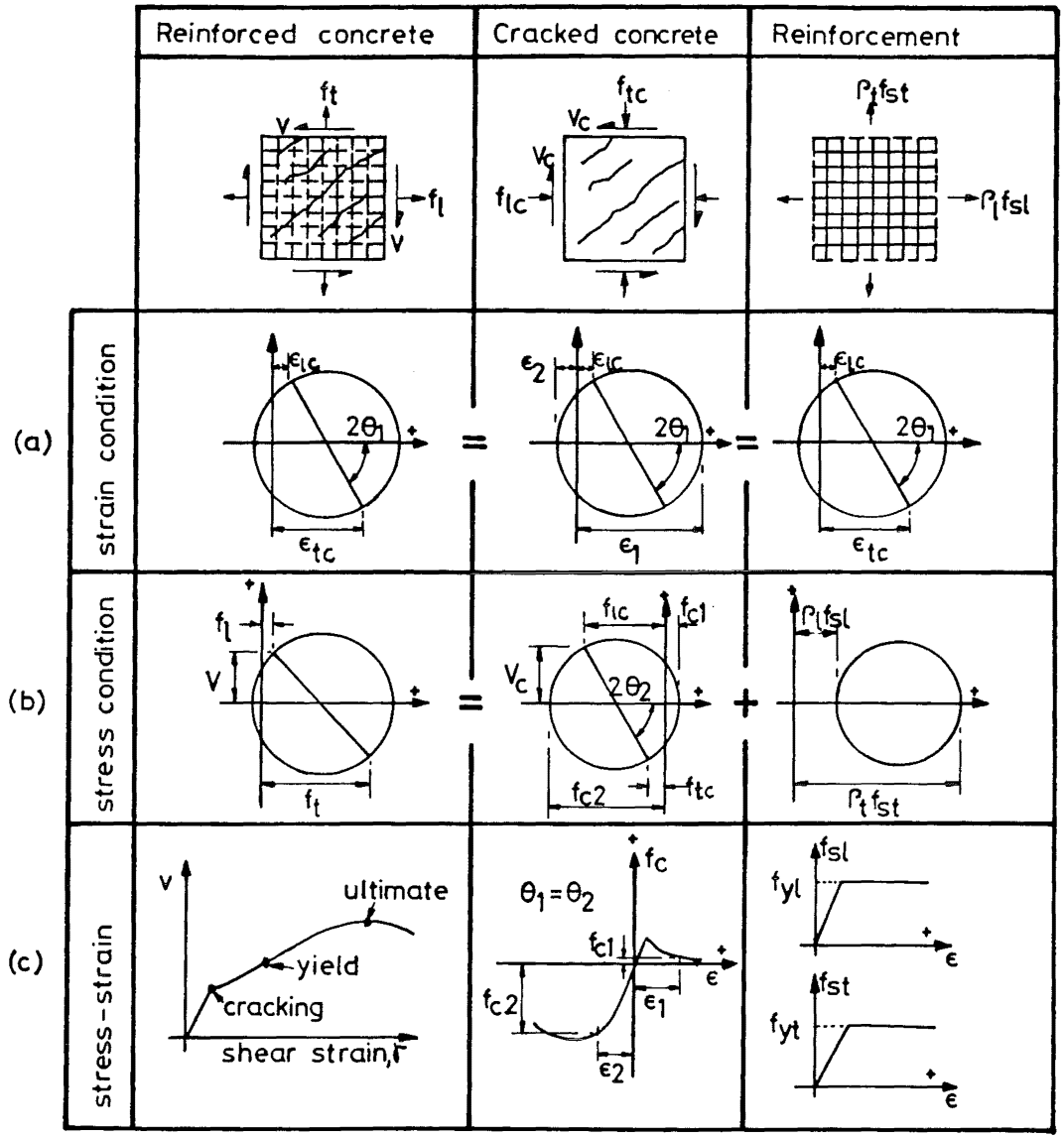

Fig. B.6 : Stress - strain response of a reinforced concrete panel

On the other hand, the average principal tensile stress in concrete, f_{c1}, can be expressed as

$$\text{when } \varepsilon_1 \leq \varepsilon_{cr}, \quad f_{c1} = E_c \, \varepsilon_1 \tag{B.31a}$$

$$\varepsilon_1 > \varepsilon_{cr}, \quad f_{c1} = f_{cr}/(1 + \sqrt{200 \, \varepsilon_1}) \tag{B.31b}$$

$$\text{where } \varepsilon_{cr} = f_{cr}/E_c \tag{B.31c}$$

$$E_c = 2 \, f'_c/\varepsilon_0 \tag{B.31d}$$

$$\text{and} \quad f_{cr} = 0.33 \sqrt{-f'_c} \tag{B.31e}$$

Eqs. (B.30 and B.31) were proposed by Vecchio and Collins in a recent version of the diagonal compression field theory [B.14].

The application of the diagonal compression field theory to predict the response of a section of a reinforced concrete column loaded in combined shear, flexure, and axial load can be carried out by performing sectional analyses. A cross-section, Section 1, shown in Figs. B.7a and B.7e, is subdivided into a number of horizontal layers. The analysis process also requires estimates of (a) longitudinal strain profiles, and (b) shear flow profiles. Each layer is solved individually, using these estimates and satisfying equilibrium, compatibility, and stress - strain relations (Section B.2.3.2). The distribution of longitudinal stresses is then obtained. These stresses should balance the applied axial load, N, and moment, M_1. In case of unbalance, it is necessary to adjust the assumed longitudinal strain profile until sectional equilibrium is achieved. The assumed shear flow profile is checked by analyzing Section 2 (Fig. B.7e), which is a short distance, Δx, away from Section 1. Both sections are analyzed for the same shear stress distribution. By considering the equilibrium of each layer as a free-body (Fig. B.7h), the calculated shear stress, v_n, at layer "n" is

$$v_n = \Delta F_c/(b_n \, \Delta x) \tag{B.32a}$$

$$\text{where } \Delta x = (M_1 - M_2)/V \tag{B.32b}$$

$$\text{and} \quad \Delta F_c = F_{c1} - F_{c2} \tag{B.32c}$$

If the shear flow profile so obtained does not agree with the estimated one, the shear flow profile has to be revised. The analysis is repeated till an acceptable convergence is attained.

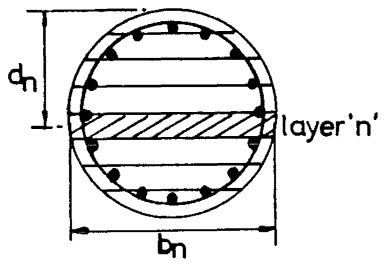

(a) Cross-section divided into layers

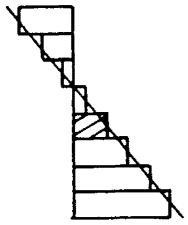

(b) Longitudinal strain, ε_{lc}

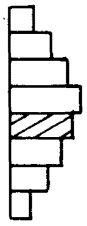

(c) shear stress, v

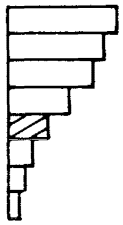

(d) Longitudinal concrete stress, f_{lc}

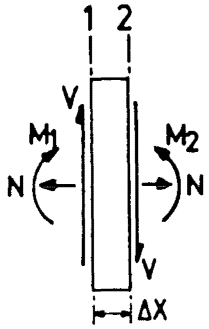

(e) Resultant forces

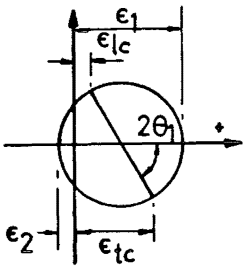

(f) Concrete strains in layer "n"

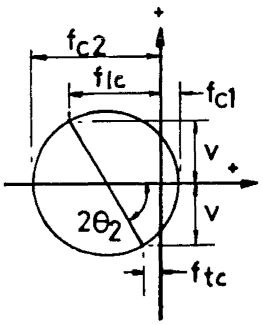

(g) Concrete stresses in layer "n"

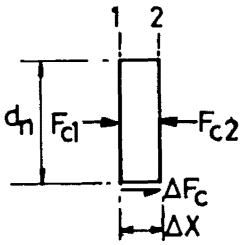

(h) Derivation of shear stress distribution

Fig. B.7 : Principles of the compression field theory as applied to a section subjected to shear, moment, and axial load

B.2.3.2 Analysis procedure for determining response of a concrete layer subjected to biaxial stresses

1. From the given longitudinal strain profile (Fig. B.7b), the longitudinal strain, ε_{lc}, is known.

2. From the assumed shear stress distribution (Fig. B.7c), the shear stress, v, is known. In the first trial, a parabolic distribution is suggested.

3. The principal tensile strain, ε_1, is estimated, noting that $\varepsilon_1 > \varepsilon_{lc}$.

4. From Eq. (B.31a or B.31b), the principal concrete tensile stress, f_{c1}, is determined.

5. The transverse concrete stress, f_{tc}, is found by considering equilibrium in the transverse direction, assuming yielding of the transverse reinforcement.

6. Knowing f_{tc}, v, and f_{c1}, the inclination of principal compressive stress, θ_2, is determined from the Mohr circle of stresses (Fig. B.7g).

7. According to the assumption stated earlier, the inclination of principal compressive strain, θ_1, is equal to θ_2.

8. With known values of ε_1, ε_{lc}, and θ_1, the concrete transverse strain, ε_{tc}, is obtained from the Mohr circle of strains (Fig. B.7f).

9. If ε_{tc} is greater than or equal to the yield strain of transverse reinforcement, the analysis continues with step 12. Otherwise, step 10 is followed.

10. A smaller value of ε_{tc} is estimated. The corresponding f_{tc} is again determined as in step 5.

11. Steps 6 to 8 are repeated to evaluate ε_{tc}. If the calculated value of ε_{tc} does not agree with the estimated one, obtained in step 10, step 10 is repeated.

12. The principal compressive strain, $\varepsilon_2 = \varepsilon_{lc} + \varepsilon_{tc} - \varepsilon_1$.

13. From Eq. (B.30a), the principal compressive stress, f_{c2}, is calculated.

14. From the Mohr circle of stresses, another value of f_{c2} is obtained (θ_2, v, and f_{tc} are already known).

15. Both values of f_{c2} are compared. If they do not agree with each other, ε_1 is revised and the analysis returns to step 3.

16. From the Mohr circle of stresses, the longitudinal concrete stress, f_{lc}, is also obtained.

B.2.4 Ang's Shear Design Procedure For Circular Reinforced Concrete Columns

B.2.4.1 Basic concepts

From experimental observations of circular reinforced concrete columns subjected to uni-directional cyclic loading [B.1], it was found that the shear carried by concrete was greatly underestimated by relevant requirements of most design codes. Before the occurrence of significant strength degradation, the ductility capacity of columns was found to depend on the ratio of shear strength to flexural overstrength. Flexural overstrength, V^o_{lf}, is defined as flexural strength with material strength enhancements taken into account. These strength enhancements were primarily due to confinement of concrete and strainhardening of steel.

Ang then proposed a practical shear design procedure. In this, the relation between strength, V, and available ductility capacity, μ_c, of circular reinforced concrete columns is expressed by two linear functions as shown in Fig. B.8. Available ductility capacity is defined as the displacement ductility factor at which the stability of hysteretic response can no longer be maintained. The control parameters are:

a) Shear strength before degradation, V_l. This can be achieved at moderate displacement ductility, μ_l, i.e., before significant plasticity is developed.

b) Residual shear strength, V_f, which is maintained at a ductility capacity, μ_f, when shear failure does not occur. The estimation of μ_f is shown in Section B.2.4.2c.

If the shear demand, V, at flexural overstrength, V°_{if} falls between V_i and V_f, the available ductility capacity, μ_c, can be obtained by linear interpolation, as shown by curve 2 in Fig. B.8. If V°_{if} is less than V_f, ductile flexural response, typically in this case $\mu_c > 6$, can be expected (curve 1 in Fig. B.8).

However, if V°_{if} is found to be greater than the shear strength before degradation, V_i, the available shear strength may be assumed to be V_i. The corresponding displacement capacity is μ_i. From test results, μ_i was found to be 2.0.

Finally, if V°_{if} is greater than V_i, a brittle shear failure ($\mu_c < 1.0$) is to be expected when V_i is reached (curve 3 in Fig. B.8).

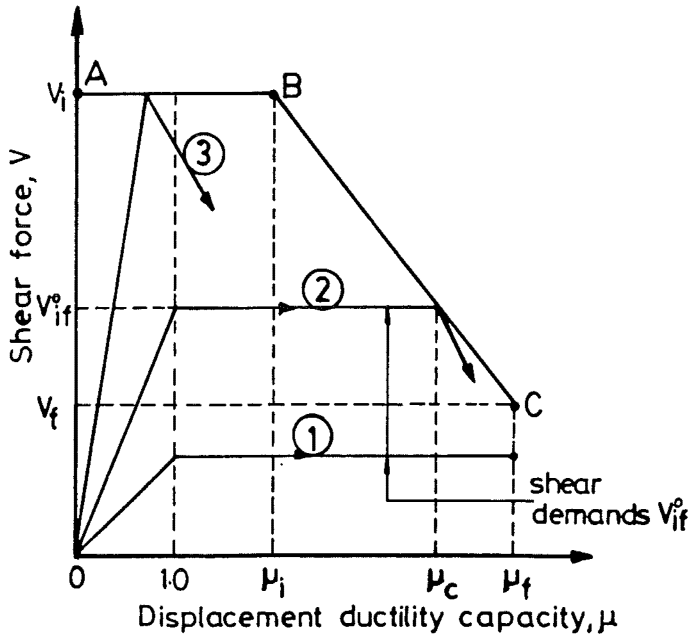

Fig. B.8 : Relationship between shear strength and displacement ductility capacity

B.2.4.2 The determination of shear strengths and ductilities [B.1]

a) Estimation of the shear strength before degradation, V_i

Adopting the traditional additive principle,

$$V_i = V_{si} + V_{ci} \quad \text{(B.33a)}$$

where V_{si} = shear force assigned to the spiral reinforcement crossing a 45° potential diagonal failure plane. The derivation of this expression is shown in Appendix I.

$$= 0.5\,\pi\,A_{sp}\,f_{yt}\,d_s/s \quad \text{(B.33b)}$$

V_{ci} = shear force assigned to "concrete mechanisms" only. It was derived empirically by subtracting V_{si} from the total applied shear force V_i.

$$= \alpha_i\,(1 + 3\,P_i/(f'_c\,A_g))\,v_b\,A_e \quad \text{(B.33c)}$$

where $\alpha_i = 2.0\,D/L \geq 1.0$ (B.33d)

$v_b = (0.056 + 24\,\rho_w)\,\sqrt{f'_c} \leq 0.37\,\sqrt{f'_c}$ (B.33e)

A_{sp} = cross-sectional area of spiral reinforcement or circular hoop

d_s = diameter of spiral or circular hoop

s = centre-to-centre spacing of spirals or circular hoops

P_i = Axial force computed using measured material strengths. P_i is positive for compression.

$A_g = \pi\,D^2/4$, gross concrete area

$A_e = 0.8\,A_g$, assumed effective shear area

D = overall diameter of a circular column

L = shear-span length of a cantilever column

ρ_w = tensile reinforcement content

= (area of flexural reinforcement in tension)/A_g

b) Estimation of the residual shear strength, V_f

The previous additive principle, Eq. (B.33a), is used, i.e.

$$V_f = V_{sf} + V_{cf} \leq V_i \quad \text{(B.34a)}$$

where $V_{sf} = 0.5\,k\,\pi\,A_{sp}\,f_{yt}\,d_s/s$ (B.34b)

V_{cf} = shear force assigned to the concrete alone

$$= v_{cf}\,A_e \quad \text{(B.34c)}$$

where $k = \cot\theta = \sqrt{(0.193 - \Omega)/\Omega} \leq L/D$ (B.34d)

with $45° \geq \theta \geq 25°$ (B.34e)

where θ = inclination of the potential shear failure plane, measured from the longitudinal axis of the column

$\Omega = \rho_s\,f_{yt}/(2\,f'_c)$ (B.34f)

and $v_{cf} = 0.185\,\sqrt{f'_c}$ when $\rho_s \geq 0.01$ (B.34g)

or $v_{cf} = 18.5\,\rho_s\,\sqrt{f'_c}$ when $\rho_s < 0.01$ (B.34h)

ρ_s = volumetric spiral or circular hoop content

$= 4\ A_{sp}/(d_s\ s)$ (B.34i)

The shear strength which is resisted by concrete within the flexural compression zone and by aggregate interlock, deteriorates at higher displacement ductility levels. Consequently, a larger contribution from spiral reinforcement, to take up the external shear, is needed. This may be achieved by decreasing the inclination angle θ of the analogous diagonal compression strut. This is recognized by the k factor, given by Eq. (B.34b). The evaluation of the k factor was based on the lower bound solution of the plastic theory, as outlined in Section B.2.2, and it was calibrated from the results of test units which failed in a ductile flexural mode.

The expression for shear carried by concrete, i.e. V_{cf}, was obtained experimentally from test units which exhibited a ductile flexural failure mode. It was determined by subtracting V_{sf} from the applied shear V_f at the displacement ductility capacity, μ_f.

c) Estimation of the ductility capacity when shear failure can be avoided, μ_f

The displacement ductility factor, μ_f, is expressed as:

$\mu_f = 1 + 3\ (1 + 5.4\ \alpha)\ (L_p/L)\ (2 - L_p/L)$ (B.35a)

where α = confinement ratio

$= \rho_s\,(\text{provided})/\rho_{sNZ}$ (B.35b)

ρ_{sNZ} = volumetric spiral or circular hoop reinforcement content for confinement required by NZS 3101 Clause 6.5.4.3, taking a strength reduction factor of unity.

$= 0.45(A_g/A_c - 1)(f'_c/f_{yt})(0.5 + 1.25\ P_l/(f'_c\ A_g))$ (B.35c)

or $= 0.12(f'_c/f_{yt})(0.5 + 1.25\ P_l/(f'_c\ A_g))$ (B.35d)

whichever is greater

A_c = area of concrete core of section measured to outside of peripheral spiral or hoop.

L_p = plastic hinge length

$= 0.08\ L + 6\ d_{bl}$ (B.35e)

d_{bl} = diameter of flexural bar

The derivation of Eq. (B.35a) is quite lengthy [B.15]. It is based on the following assumptions:

1. The equation is only suitable for a cantilever column subjected to constant shear.

2. Plastic deformation is solely due to flexural rotations within the plastic hinge. The value of plastic hinge length, L_p, was proposed by Priestley and Park [B.15].

3. A cantilever column with $L/D \geq 4$, and confinement to the requirement of NZS 3101 possesses a dependable ductility capacity of 6. This statement was derived from test results [B.16]. Such a column is used as a calibration unit.

4. The curvature ductility capacity is a linear function of the confinement ratio, α.

The development of Eq. (B.35a) is outlined as follows:

i) From assumptions "1" and "2", the available curvature ductility, μ_ϕ, for such a column can be shown to be

$$\mu_\phi = \Phi_u/\Phi_y = 1 + 0.67\,(\mu - 1)/((L_p/L)\,(2 - L_p/L)) \qquad (B.36)$$

where Φ_u = curvature at displacement ductility factor μ
Φ_y = yield curvature
μ = imposed displacement ductility

ii) Based on assumption "3", let a calibration unit have $L/D = 4$, $\mu = 6$, $D = 400$ mm, and $d_{b1} = 16$ mm. These values are then substituted into Eqs. (B.35c and B.36) and a curvature ductility, $\mu_\phi = 13.8$ is obtained.

iii) Assumption "4" is expressed as

$$\mu_\phi = c_1 + c_2\,\alpha \qquad (B.37)$$

where c_1 and c_2 are constants.
The physical meaning of c_1 is the curvature ductility of an unconfined concrete column. It is suggested that $c_1 = 3$.

iv) The values of $c_1 = 3$, $\mu_\phi = 13.8$, and $\alpha = 1$ are then substituted into Eq. (B.37), and thus c_2 is found to be 10.8.

v) Eq. (B.35a) is finally obtained by equating Eq. (B.36) with Eq. (B.37).

In order to investigate the influence of confinement ratio, α, on μ_f, a numerical example is offered. By assigning D = 400 mm, L = 800 mm, and d_{b1} = 16 mm to Eq. (B.35a), we have

μ_f = 7.9 when α = 1.0

and μ_f = 5.0 when α = 0.5

As illustrated in this example, μ_f is not overly sensitive to variations of α. Ductile failure response will be obtained when the shear demand at flexural overstrength, V^o_{if}, is not greater than the residual shear strength, V_f. Eqs. (B.35c and B.35d) show that the confining steel content, ρ_s, depends on the magnitude of the axial compressive stress. However, for the same value of α, μ_f is independent of axial load intensity.

d) Estimation of shear demand at the development of flexural overstrength, V^o_{if}

It is known that the experimentally obtained maximum flexural capacity, M^o, of a reinforced concrete member is often significantly greater than its ideal flexural capacity, M_i, calculated by ACI method, assuming a limiting concrete compressive strain of 0.003, measured material strength properties, and a strength reduction factor of unity. This is primarily a result of (a) strain-hardening of steel, and (b) enhancement in concrete strength due to confinement when axial compressive load is also present. As an example, Fig. B.9 shows the variation of flexural strength enhancement factor, m (= M^o/M_i), with axial compressive load intensity for columns using Grade 275 steel [B.1]. These columns were tested at the University of Canterbury. By regression analysis, m can be expressed as:

when $P_i/(f'_c A_g) > 0.1$, $m = 2.35 (P_i/(f'_c A_g) - 0.1)^2 + m_i$ (B.38a)

when $P_i/(f'_c A_g) \leq 0.1$ $m = m_i$ (B.38b)

where m_i = 1.13 for Grade 275 steel (B.38c)

As a result, all except one data [B.1] are within ± 15% of this value as seen in Fig. B.9a.

Fig. B.9b shows the variation of m with confinement ratio, α (see Eq. (B.35b) for the definition of α). It is noted that at a medium and low axial load intensity ($P_i/(f'_c A_g) < 0.4$), the values of m remain fairly constant. At a higher axial load intensity ($P_i/(f'_c A_g) \geq 0.4$), enhancement in concrete compressive strength can be readily developed by transverse confinement reinforcement so that the flexural strength enhancement factor, m, increases with confinement ratio.

In the case of a member reinforced for flexure with Grade 380 steel, it was assumed [B.1] that the flexural strength enhancement factor, m, was also predicted by the form of Eq. (B.38a). However, m_1 was taken to be 1.22, as implied in NZS 3101, to account for somewhat greater strain-hardening.

i.e. $m_1 = 1.22$ for Grade 380 steel (B.38d)

When designing for shear strength, the flexural overstrength should not be underestimated. Hence, values obtained by Eqs. (B.38a to B.38d) should be multiplied by a factor of 1.15 to obtain upper bound values. For example, the upper bound values of m become 1.40, 1.43, and 1.65 for $P_1/(f'_c A_g) = 0.0$, 0.2, and 0.4 respectively, when the measured properties of Grade 380 steel and concrete are used. NZS 3101 also suggests the ratio of probable (measured) strength to specified strength to be 1.15. Therefore, the flexural strength enhancement factor, m, should be further multiplied by the factor 1.15 if the specified material properties are used in the design calculations.

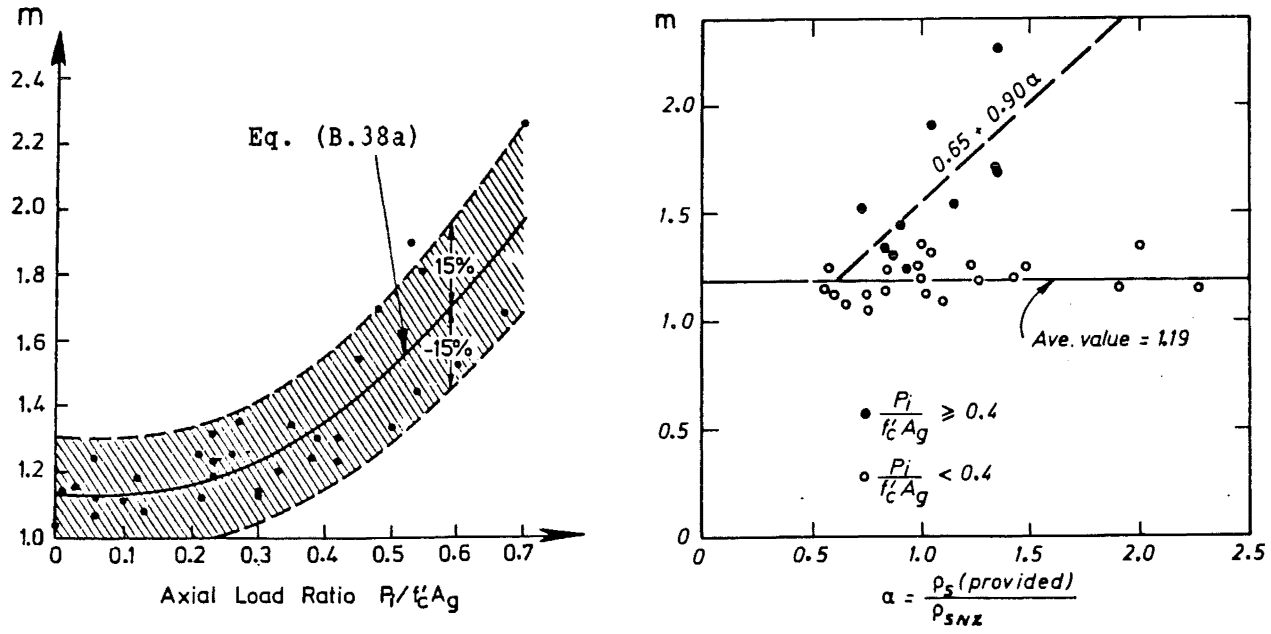

(a) Axial compression level (b) Confinement ratio

Fig. B.9 : Variation of flexural strength enhancement factor, m

B.2.5 A Conceptual Model for Shear Behaviour under Multi-directional Loading

Maruyama and Jirsa [B.2] tested 10 fixed end square reinforced concrete columns (Fig. B.10). The only variable was the loading history. A conceptual model to simulate the experimental shear force - displacement hysteretic curves was then formulated as follows:

1. Under monotonic loading, the shear force - displacement, V - Δ, relationship can be expressed as:

$$V = f_1(\Delta) \tag{B.39}$$

A term called damage ratio, D_r, which represents the magnitude or extent of damage on the column as a result of loading, is also expressed as a function of the displacement.

$$D_r = f_2(\Delta) \tag{B.40}$$

2. Subjected to uni-directional repeated cyclic loading to the same displacement peak, Δ_o, the damage ratio at the n^{th} cycle of load, $D_{r,n}$, is said to increase as:

$$D_{r,n} = D_{r,o} \sum_{1}^{n} w_i \tag{B.41}$$

where $D_{r,o}$ = damage ratio under monotonic loading at displacement Δ_o.

w_i = increment of damage occurring during i^{th} cycle of load, which is a function of n obtained by regression analysis of the test results.

n = number of load cycles

Under monotonic loading, the same damage ratio, $D_{r,n}$, would be reached when displacement is increased to Δ_n. Hence Δ_n can be calculated by inverting Eq. (B.40), i.e.

$$\Delta_n = f_2^{-1}(D_{r,n}) \tag{B.42}$$

Thus, the peak shear strength is assumed to reduce with each load cycle. Therefore, the peak shear strength at n^{th} load cycle, V_n, can be expressed as

$$V_n = V_{mo}\, f_3(\Delta_o/\Delta_n) \tag{B.43}$$

where V_{mo} = monotonic shear strength at the displacement Δ_o.

The shear force - displacement, V - Δ, hysteretic curve in the n^{th} load cycle can be expressed by a suitable shape function f_4.

$$V = f_4(\Delta, \Delta_o, V_n) \qquad (B.44)$$

3. Under bi-directional loading history, it is assumed that the damage ratio has directional properties. Loading in one, say X, direction, can produce a component of the damage ratio with respect to the orthogonal direction, Y direction. This relation is defined by

$$D_{ry} = f_5(D_{rx}) \qquad (B.45)$$

where D_{ry} = damage ratio in the Y direction

D_{rx} = damage ratio in the X direction

and f_5 = orthogonality function, which defines the influence of loading in the orthogonal direction.

The difficulty with this approach is the finding of the unknown functions (f_1 to f_5). It is also impossible to develop a general function f_5 which is able to take care of all arbitrary bi-directional loading histories. This means that, for each specified bi-directional loading pattern, a special function f_5 has to be determined individually for a particular specimen. Therefore, all these functions need to be generated from the experimentally obtained shear force - displacement hysteretic loops by curve fitting methods. These were illustrated in the Texas report [B.2]. At the present stage, this approach appears to be unsuitable for application to actual bridge pier design.

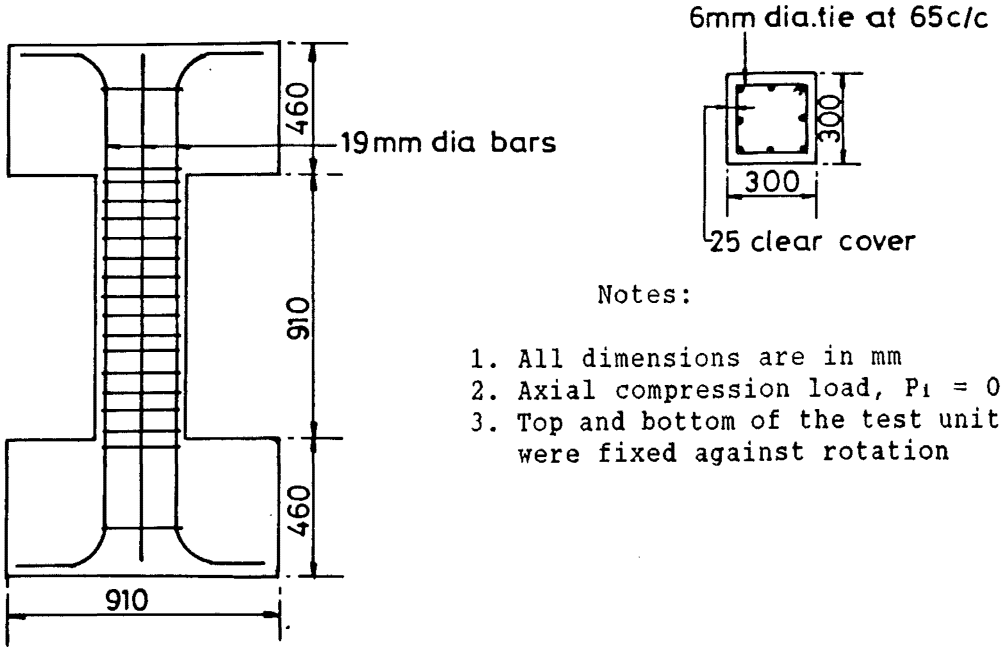

Fig. B.10 : Dimensions of test specimen [B.2]

B.2.6 A Predictive Guide for Behaviour Classification of Reinforced Concrete Members

Woodward and Jirsa [B.3] investigated the failure modes of their columns and those of numerous Japanese test columns. Using these studies, they suggested a predictive guide for behaviour classification of reinforced concrete members under uni-directional cyclic loading.

This predictive guide is reproduced in form of flow chart (Fig. B.11) to give indications of the effects and significance of various criteria on column behaviour. As shown in that figure, five criteria (comparison between flexural capacity and concrete shear capacity, comparison between flexural capacity and after cracking shear capacity, bond criterion, confinement criterion, and longitudinal bar buckling criterion) are allocated to Junctions A to F respectively. At each junction, the details of a column are then checked against the corresponding criterion. When the criterion is not satisfied, the probable feature of failure of the column is shown on the "NO" branch at the junction concerned.

As described in the guide, the flexural capacity is quantified as the shear at the development of flexural overstrength, V^{o}_{1f}. It is taken as the reference capacity for reinforced concrete members. The concrete shear capacity, V_c' is the shear force transferable across the flexural compression zone before the formation of inclined cracks. The value of 1.0 for the ratio of V_c'/V^{o}_{1f} represents the division between shear - dominated and flexure - dominated behaviours. After cracking capacity, V_{acc}, is the shear force transferable across the inclined cracks. It is directly proportional to the amount of transverse reinforcement. The effectiveness of confinement is determined by an index, $Z_u = Z/(1 - P/P_o)$, where Z is the gradient of the descending branch of confined concrete stress - strain curve (Fig. 6.14 in Woodward's thesis), P is the applied compressive axial load, and P_o is the concentric compressive axial load capacity of the section. Bond degradation and longitudinal bar buckling are controlled by the development length of longitudinal bar, l_d, and spacing of transverse reinforcement, s, respectively. Quantitative formulations of these criteria are given in the original research report [B.3]. Furthermore, as evidence obtained for bi-directional loading histories was inadequate at the time of preparation of the predictive guide, the quantitative criteria would need to be modified to account for loading history.

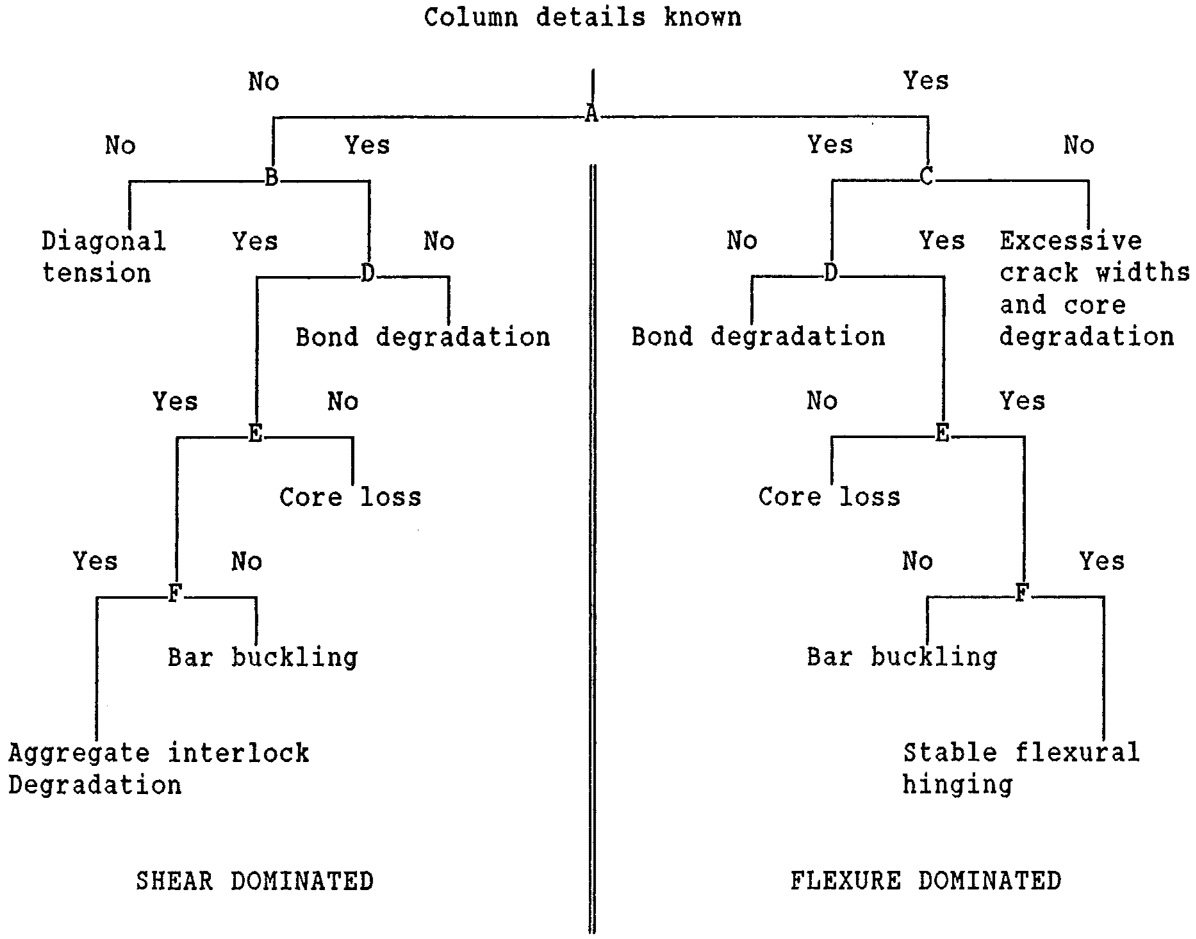

Junctions	Functions	Criteria
A	Separate shear dominated from flexure dominated columns	$V_c' \geq V°_{if}$
B	Restrain load induced inclined cracking	$V_{acc} \geq V°_{if}$
C	Restrain widening of flexure-shear cracks	$V_{acc} \geq 0.5V°_{if}$
D	Indicate likelihood of bond degradation	$l_d \leq d_o$, & $l_d \leq L_c/2$
E	Indicate likelihood of core loss	$Z_n < 15$
F	Indicate longitudinal bar buckling tendency	$s \leq 2\ d_{bl}$ at plastic hinge $s \leq 4\ d_{bl}$ outside plastic hinge

where d_o = gross section depth
L_c = clear height of fixed end column
d_{bl} = longitudinal bar diameter

Fig. B.11 Schematic of predictive guide [B.3]

B.3 APPLICABILITY OF EXISTING MODELS TO PREDICT SHEAR BEHAVIOUR OF CIRCULAR REINFORCED CONCRETE COLUMNS UNDER INELASTIC BI-DIRECTIONAL LOADING HISTORIES

The oldest shear transfer model, the truss analogy provides a simple and clear concept for shear transfer in reinforced concrete members. The accuracy of shear strength predicted by this model depends on assigning proper values for inclination, θ, and compressive strength, f_{cd}, of analogous concrete struts. If a 45° truss model is used, shear carried concrete, V_c, is introduced to account for any shear resistance in excess of that provided by the 45° truss. Although a lot of monotonic and uni-directional cyclic loading tests on square or rectangular members have been done to determine suitable values of θ, f_{cd}, and V_c, quantitative assessments of these values for circular members subjected to inelastic bi-directional loading histories have not been established. Previous researches have shown that reinforced concrete members exhibit shear strength degradation during inelastic monotonic or cyclic loading. Experimental results presented in Chapters D and F of this report further confirm that the shear resistance and the rate of strength degradation of circular reinforced concrete columns vary with loading histories. Since compatibility of deformation is not considered in the traditional truss analogy, it cannot relate shear strength with imposed ductility.

Limit analysis based on perfect plasticity provides straight forward means to evaluate the upper and lower bound solutions of shear strength. The reliability of the predicted strengths rests on appropriate assumptions of yield criteria. When simple yield criteria are applied, complicated characteristics of cracked concrete under multi-directional stresses are often overlooked. An experimentally obtained correction factor is then included in the formulation so that the predicted strengths will be consistent with the experimental findings. For instance, Ang has applied limit analyses to determine the residual shear strength of circular columns subjected to uni-directional cyclic loading (Section B.2.4.2). An empirical value, called shear force assigned to concrete alone, was required and was added to the shear predicted by the lower bound solution in order to obtain agreement with the experimental results. If a similar strategy is to be employed for the same columns, but subjected to bi-directional cyclic loading, that empirical value, which is likely to be different from the previous one, should be experimentally obtained.

Like the traditional truss analogy, limit analysis offers no information with respect to relationships between shear resistance and imposed ductility levels. As experiments indicated the dependence of shear strength on imposed inelastic deformations, such information is essential for the design of reinforced concrete members under seismic loading.

The diagonal compression field theory, which was developed from variable-angle truss models, is capable of predicting the force - deformation response of reinforced concrete element subjected to in plane shear and axial stresses, by considering equilibrium conditions, strain compatibility requirements, and stress - strain relationships. A remarkable feature of this theory is the identification of the softening effect on the concrete principal compressive stress as a function of its principal tensile strain. The "softened" stress - strain relations for concrete were then derived from tests on reinforced concrete membrane elements, the majority of which were subjected to monotonic pure shear load. A basic assumption of the theory is that for each strain state, there exists only one corresponding stress state. The influence of loading histories, which might alter the strain state while loading of an element remains unchanged, is not considered. Therefore, the theory appears to be suitable to deal with problems under monotonic loading. For cyclic loading or more complex loading histories, the theory can, at most, provide an upper bound solution, at which the structure might show unexpected strength deterioration if it is designed accordingly. Moreover, as the proposed concrete "softening factor" was determined from testing of reinforced concrete panels, the direct application of this factor to simulate the response of cracked concrete elements in circular columns under orthogonal cyclic loading would need to be verified. The softening effect on the concrete principal compressive stress may be aggravated by cracks formed during loading in orthogonal directions. Hence, unless further development of the diagonal compression field theory is reported, the application of existing material constitutive laws to predict force - deformation responses of circular reinforced concrete columns under inelastic bi-directional cyclic loading histories does not appear to be justified.

The unique feature of Ang's shear design procedure is its ability to evaluate the maximum obtainable strength, and the available displacement ductility level of a circular reinforced concrete column subjected to uni-directional cyclic loading. As a result, column failure modes can be predicted and a suitable design procedure adopted, depending on the likely ductility demand. However, results of the present tests with similar columns

but subjected to bi-directional loading histories revealed that Ang's proposal overestimates maximum obtainable strengths and available ductility levels for columns with low axial compression. Under bi-directional cyclic loading, the force - displacement hysteretic response was found to exhibit gradual strength degradation at each repeated load cycle to the same ductility level. The experimentally observed available displacement ductility level, μ_c, defined by Ang as the value at which the stability of the hysteretic response could no longer be maintained, was sometimes difficult to establish with certainty. Ang's shear design procedure gives no prediction of the magnitude of maximum strength at the available ductility level, μ_c. Without this information, the probable strength envelope curve of a column cannot be established. Based on the test results of the present project, certain assumptions made for calculating some parameters, such as yield displacements, curvature ductilities, and column displacements due to plastic hinge rotation, did not appear to be justified. Hence, the idea to modify Ang's prediction of available ductility level to cope with bi-directional loading histories, was abandoned.

The conceptual model of shear force - displacement hysteretic relations suggested by Maruyama and Jirsa indicates that the strength of a reinforced concrete member is very much deformation - path dependent. In their study, a few displacement patterns, taken as the only variable, were under investigation. For this reason, the validity of their proposed empirical shape functions to account for other possible displacement patterns is questionable. It was beyond the scope of this project to attempt to generalize this concept of shear modelling so as to include other important parameters, such as axial load intensity, reinforcement contents or geometric properties, without introducing excessive amounts of complex empirical formulations.

The predictive guide to behaviour classification of reinforced concrete members, developed by Woodward and Jirsa, highlights the criteria affecting the stability of force - displacement hysteretic response. This guide can serve as a step by step design procedure to examine the possible failure modes of a reinforced concrete member. However, it appears that the proposed longitudinal bar buckling criterion is unnecessarily severe for practical purposes. No known code requires $s \leq 2d_{bl}$ at a plastic hinge or $s \leq 4d_{bl}$ outside a plastic hinge. In this aspect, current NZS 3101 [B.7] requires $s \leq 6\ d_{bl}$ at potential plastic hinge regions. This requirement was obtained from experimental observation of column tests at the University of

Canterbury. Recent analytical study [B.17] also indicated that $s \leq 6\ d_{bl}$ was of the right order. Furthermore, the predictive guide does not consider the prediction of the available ductility achieved at the predicted strength level, the rate of strength degradation, and the effects of bi-directional loading histories.

It was considered that a direct application of the above-mentioned models could not give a satisfactory prediction of the shear behaviour of circular reinforced concrete columns subjected to inelastic bi-directional loading histories. It must be recognized that none of the studies, summarized above, intended to examine bi-directional displacement patterns and histories, as major parameters of seismic response. This was the motivation for the experimental research reported here. Therefore, the aim of this project is to provide (a) a better understanding of rather complex shear behaviour, and (b) useful data for the formulation of design recommendations on circular reinforced concrete columns, as shown in Chapter F.

CHAPTER C
THE PLANNING OF THE EXPERIMENTAL PROGRAM AND MATERIAL PROPERTIES OF COLUMN UNITS

C.1 INTRODUCTION

The experimental programme consisted of testing sixteen reinforced concrete circular cantilever columns subjected to quasi-static uni-directional and bi-directional shear loading histories simulating actual seismic forces. The main variables studied are the axial compression load intensity, the amount of transverse reinforcement (spirals), and the displacement pattern. In this chapter, aspects of the design, construction, instrumentation, testing procedures, and measured material properties of column units are described. Experimental observations, and the evaluation of test results are presented in the following chapter.

C.2 DESIGN PRINCIPLES

C.2.1 Design Parameters

An experimental and theoretical investigation based on static tests of twenty-five reinforced concrete circular cantilever columns under uni-directional cyclic lateral loading was reported by Ang [C.1] in 1985. In his study, the major variables were the aspect ratio, L/D (L/D = 1.5, 2.0, 2.5), the axial compression load intensity, $P_l/(f'_c A_g)$ ($P_l/(f'_c A_g)$ = 0, 0.1, 0.2), and the transverse reinforcement (spiral) content, ρ_s, as defined by Eq. (B.34i) (ρ_s = 0.38% to 2.46%). The outside diameter of all test columns was 400 mm. Most of the columns used 16 mm diameter Grade 380 deformed bars for longitudinal reinforcement, resulting in a relatively large longitudinal reinforcement content, ρ_l, of 3.2%. The compressive cylinder strength of concrete, f'_c, was aimed at 30 MPa. Based on Ang's test results, four failure modes in terms of the available displacement ductility, μ_c, were identified. They were ductile flexural failure (D-F), shear failure with moderate ductility (MD-S), shear failure with limited ductility (LD-S), and brittle shear failure (B-S) corresponding to $\mu_c > 6$, $4 < \mu_c \leq 6$, $2 < \mu_c \leq 4$, and $\mu_c \leq 2$ respectively. A design recommendation on the shear strength of reinforced concrete circular columns was then proposed, as outlined in Section B.2.4.

In order to verify the correlation between the behaviours of the circular columns under uni-directional and more realistic bi-directional cyclic lateral loading, and to evaluate the validity of Ang's proposal for shear design of columns subjected to bi-directional loading patterns, it was considered the column specimens of this project be designed so as to be similar to those of Ang. Therefore the parameters affecting properties of the units were the same as those used by Ang. Details of the test units and loading frames are described subsequently.

C.2.2 General Layout of Test Set-up

Fig. C.1 shows the general layouts of a test unit and the test set-up. The column unit was cast in situ on a massive 900 mm x 900 mm x 752 mm reinforced concrete base. Two L-shaped steel loading frames were used to introduce the lateral force. One such frame was bolted to each the east and south vertical sides of the column base. A steel shear connector was attached to the column head by friction grip bolts. Each loading frame accommodated a double acting hydraulic jack (1 MN capacity) with a load cell attached to it. These jacks were mounted horizontally between two universal joints which in turn had been connected to the loading frame and the shear connector of the specimen respectively.

The system consisted of a test unit and two loading frames. When no axial load was applied to the system (Fig. C.2a), the system was supported by a 100 mm diameter steel ball pin-connection at the centre of the bottom of the column base. In addition, timber supports were placed under the far ends of the loading frame to stabilize the system.

When axial compression load was applied to the test unit, the system was set up within a 10 MN capacity testing machine (Fig. C.2b). The required axial compression load was applied by the DARTEC Universal Testing Machine through the 100 mm diameter steel balls held within the shear connector at the top of the column and the centre of the base . Over-turning effects due to the eccentric weights from the loading frames were balanced by the horizontal friction couples induced at the two steel ball pin-connections. Shear forces acting on the column unit were introduced by activating the horizontal hydraulic jacks. Since these forces were internal within the test system, no additional lateral supports to the system were required.

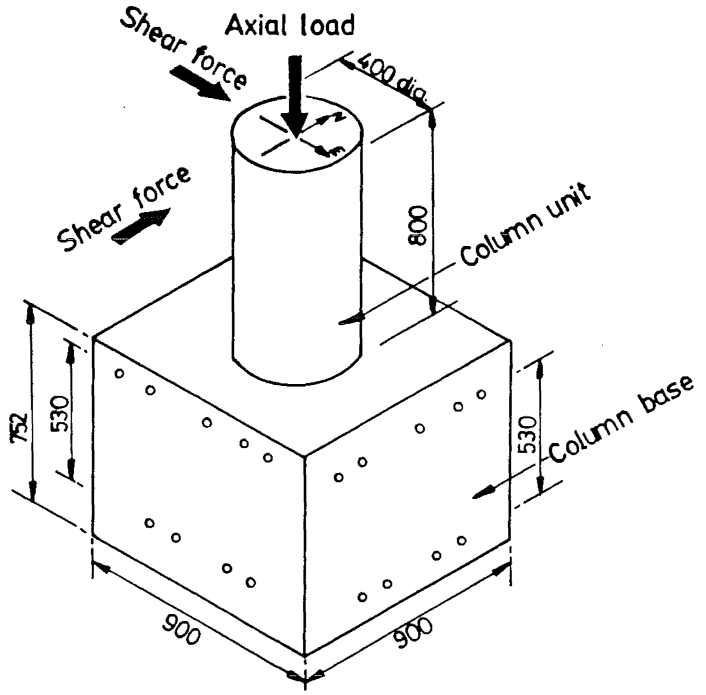

(a) Test unit

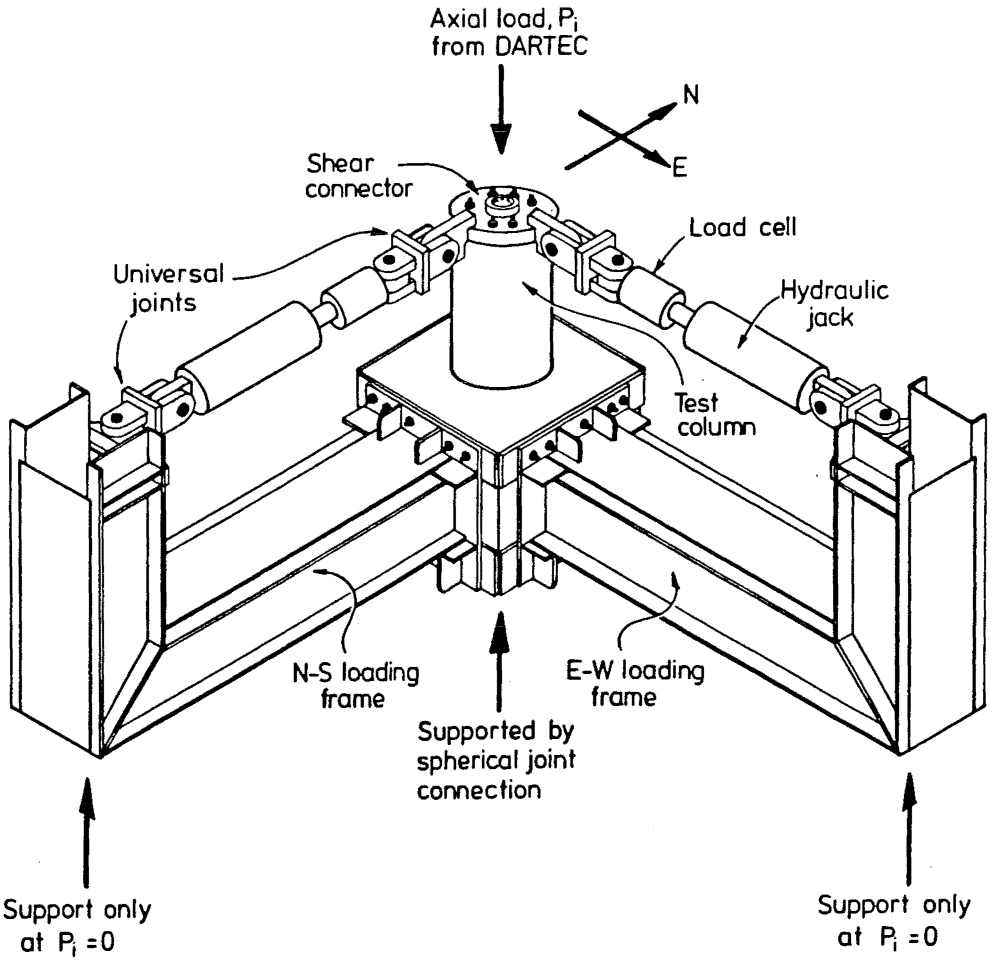

(b) Test set-up

Fig. C.1 : General layout of test unit and test set-up

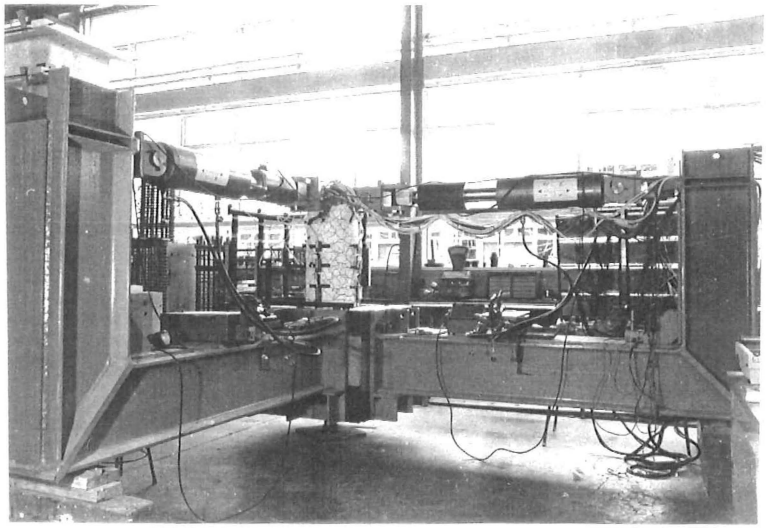

(a) Under no axial load condition

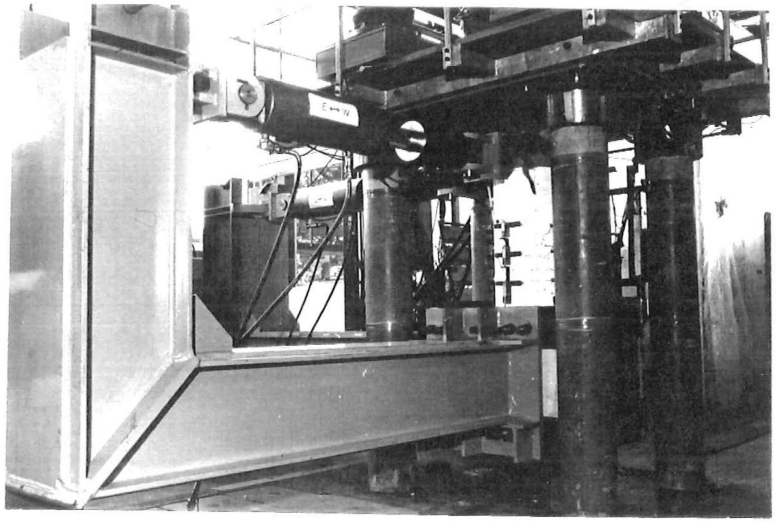

(b) Under axial load condition

Fig. C.2 : Overall view of column unit under testing

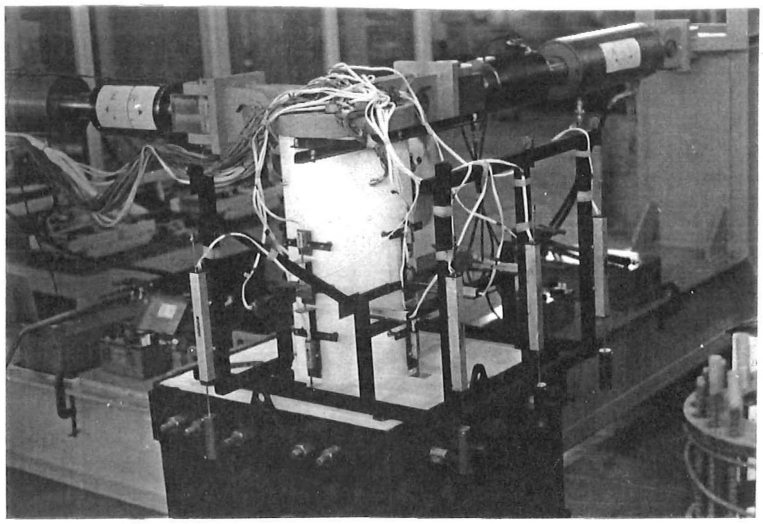

Fig. C.3 : Set-up of the instrumentation frame

C.2.3 Design of Column Units

a) Unit size

The diameter of all test columns, as shown in Fig. C.1a, was 400 mm. This was about 1/5 to 2/5 of a prototype size. The height of the column was 770 mm but the horizontal forces were applied at the level of 800 mm above the bottom of the column giving the constant aspect ratio, L/D, of 2.

b) Reinforcement

Twenty 16 mm diameter Grade 380 deformed steel bars were evenly distributed longitudinally around the inner circumference of the transverse reinforcement (spirals). The longitudinal reinforcement content, ρ_l, was 3.2%. With such a proportion of longitudinal reinforcement content and low aspect ratio, shear effect was expected to be critical because a large horizontal force was required to develop the full flexural capacity of a column.

6 mm or 10 mm diameter Grade 275 mild steel round bars, rolled in form of spirals, were used as the transverse reinforcement in the columns. The thickness of concrete cover to spirals was 15 mm, except in Unit 15, where it was 11 mm. This was the result of replacing the intended 6 mm diameter spirals by 10 mm diameter spirals. The influence of the amount of spiral steel content on the performance of a column under loading was studied by varying the spiral spacing, s, from 15 mm to 80 mm. To make the fabrication of the spiral cage as simple as possible, this spacing was kept uniform over the full height of the column. In most of the cases, the amount of spiral steel content of the test column did not meet the NZS 3101 Code [C.2] shear design requirements for seismic forces (Clause 7.5). However, the criterion that spiral spacing should not be greater than six times the diameter of a longitudinal bar [C.2] was satisfied. Therefore, the probability of premature failure of a column due to buckling of the longitudinal bars was considered to be minimal. In order to improve shear transfer at the top of the column, three turns of 10 mm diameter spiral at 15 mm pitch were provided immediately under the shear ring.

c) Axial load

Three levels of axial compression load, P_i = 0, $0.2f'_cA_g$, $0.4f'_cA_g$, on test units were intended. However, due to the arrangement of the axial load sensor of the DARTEC Universal Testing Machine, which was located under the test unit, the corresponding axial compression load intensities, $P_i/(f'_cA_g)$, on columns became 0, 0.19 and 0.39, after deducting the weights of the test unit and the loading frames. The relative load intensity, $P_i/(f'_cA_g)$ = 0.39 is considered to be the practical upper limit for the design of a bridge pier. Throughout testing, the specified axial load intensity on a column was maintained constant.

In Ang's project [C.1], fourteen column specimens, similar to the current units, were tested under uni-directional 'u' type displacement pattern (Section C.3.1), and zero axial load condition. Therefore, repetition of such tests were not included in the present programme.

d) Summary of column design

Table C.I lists the reinforcement details of 16 column units. In terms of Ang's proposal for shear design of circular reinforced concrete columns, this test program covers a wide range of column failure modes, from ductile flexural to brittle shear failure, when subjected to uni-directional cyclic shear loading. It was expected that the performance of these units under a bi-directional cyclic shear loading would not be better than that under uni-directional cyclic loading. Ang's proposal was considered to provide a good basis for this investigation.

Table C.I : Reinforcement details of column units

1	2	3	4	5	6	7	8	9
Unit		aspect ratio	$\frac{P_l}{f'_c A_g}$	spiral reinforcement			longitudinal reinforcement	
no.	notation	L/D	-	d_b	s	ρ_s	quantity	ρ_l
		-		mm	mm	%	-	%
1	2R10-60u		0.19	10	60	1.450		
2	4R6 -65u		0.39	6	65	0.476		
3	4R10-60u		0.39	10	60	1.450		
4	0R6 -80b		0.00	6	80	0.387		
5	0R6 -50b		0.00	6	50	0.619		
6	0R6 -30b		0.00	6	30	1.032		
7	2R6 -60b		0.19	6	60	0.516		
8	2R6 -30b	2.0	0.19	6	30	1.032	20-HD16	3.20
9	4R6 -40b		0.39	6	40	0.774		
10	4R10-65b		0.39	10	65	1.340		
11	0R6 -30s		0.00	6	30	1.032		
12	0R10-35s		0.00	10	35	2.460		
13	2R6 -30s		0.19	6	30	1.032		
14	2R10-60s		0.19	10	60	1.450		
15	4R10-60s		0.39	10	60	1.420		
16	2R6 -30r		0.19	6	30	1.032		

2 : Notation used with the test units
0R6 -80b

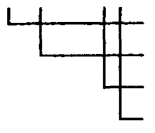

5 : Plain round bars were used

8 : 16 mm diameter Grade 380 deformed bars

C.3 DISPLACEMENT PATTERNS AND EXPERIMENTAL YIELD DISPLACEMENT

C.3.1 Displacement Patterns

Dynamic analyses of bridge pier models under different seismic excitations indicated that significant bi-directional deformation patterns may exist in many cases. Consequently, major flexural - shear cracks at different directions are to be expected to develop in such reinforced concrete columns. This may be accompanied by considerable reduction in strength as well as an increase in the rate of strength degradation, when compared with units which are subjected to uni-directional cyclic loading only. Therefore, the major aim of this project was to explore features of the behaviour of circular reinforced concrete columns subjected to bi-directional shear attacks. For convenience, the term bi-directional loading is used because horizontal forces were introduced to the test specimens by means of hydraulic jacks acting at right angles to each other. The vector sum of these two forces could also be considered to represent uni-directional loading of a circular column, where the direction and magnitude of this single horizontal force is being varied during the test.

Four types of displacement patterns were used in this project. They are described as follows:

a) Uni-directional 'u' type displacement pattern

The uni-directional 'u' type displacement pattern (Fig. C.4) is identical to that adopted by Ang when testing his 25 circular reinforced concrete columns (Section C.2.1). The purposes of testing three units in this project under this same displacement pattern, were to provide supplementary information to Ang's findings, and to verify Ang's shear design proposal for columns with axial compression load intensity, $P_l/(f'_c A_g)$ equal to 0.19 and 0.39 respectively.

The displacement path (Fig. C.4a) is cyclic along the East - West principal axis. The test column was initially subjected to five cycles of lateral force to 75% of its ideal flexural strength, V_{lf}, from which an experimental value of yield displacement, Δ_y, was determined from the first load cycle (Section C.3.2). Subsequently, five complete displacement cycles to a ductility factor, μ, of 1.5, 2, 4, 6, and possibly 8 were applied (Fig. C.4b).

In this project, the ideal flexural strength, V_{if}, is defined as the shear force at the development of ideal flexural capacity, M_i, calculated by the ACI method, assuming a limiting concrete compressive strain of 0.003, measured material strength properties, and a strength reduction factor of unity.

A displacement ductility factor, μ, is defined as the ratio of the distance 'Δ' (Figs. C.4a, C.5a, C.6a, and C.7), measured between a displacement peak and the zero displacement position, to the corresponding yield displacement, Δ_y.

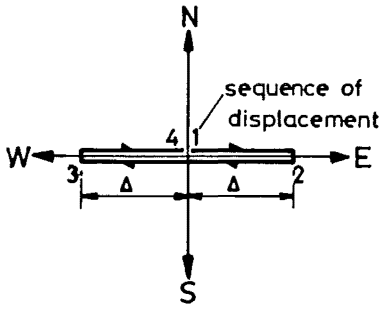

(a) Displacement orbit

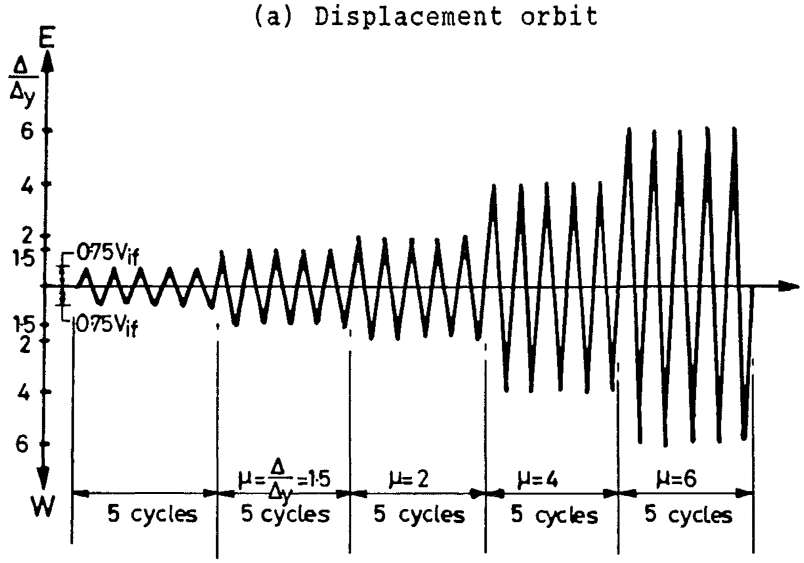

(b) Loading sequence

Fig. C.4 : Uni-directional 'u' type displacement pattern

b) Bi-directional 'b' type displacement pattern

Bi-directional 'b' type displacement pattern (Fig. C.5a) has been used by previous researchers [C.3, C.4] to study the influence of previous loading in an orthogonal direction on the behaviour of reinforced concrete columns. In Fig. C.5a, one load cycle consists of the completion of one displacement path along both the North - South and East - West principal axes respectively. The standard loading sequence (Fig. C.5b) started with one cycle of lateral force to $0.37V_{if}$. During the following cycle of lateral force to $0.75V_{if}$, the experimental yield displacement, Δ_y, was established (Fig. C.8). Afterwards, two load cycles to displacement ductility factor, μ, of 1.25, 2, 3, 4, 5, and possibly 6 were carried out in turn.

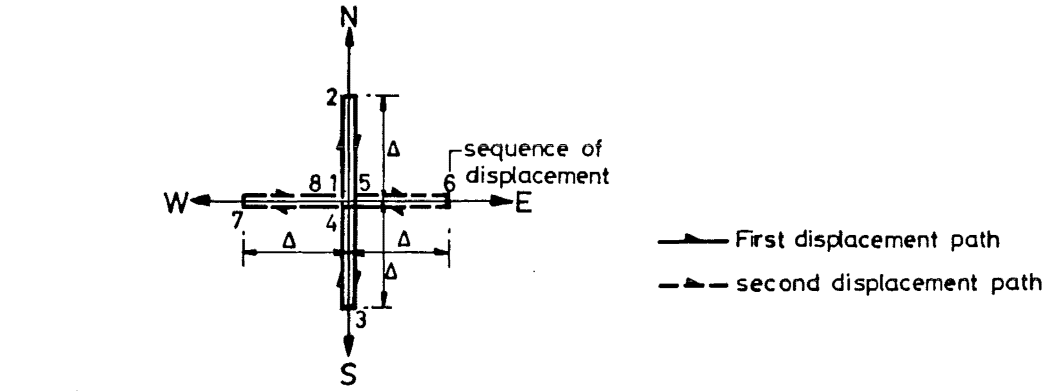

(a) Displacement orbit

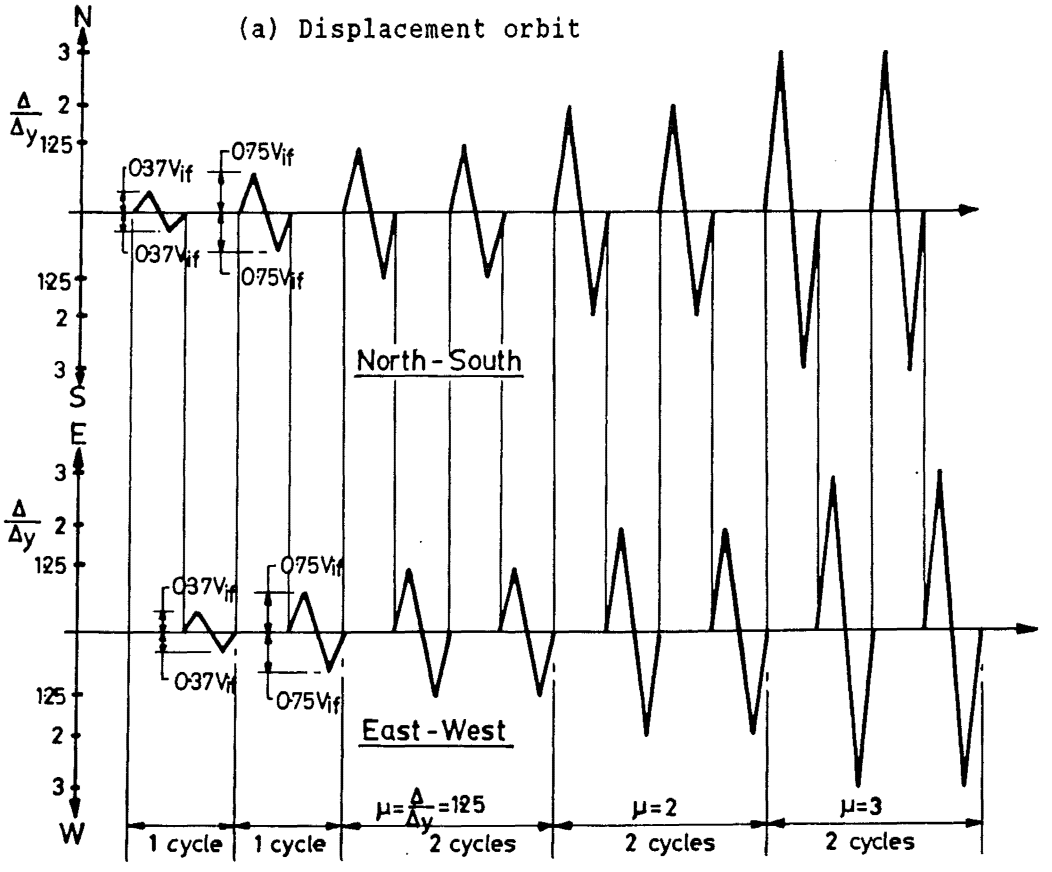

(b) Loading sequence

Fig. C.5 : Bi-directional 'b' type displacement pattern

c) Bi-directional 's' type displacement pattern

It has been reported [C.4] that reinforced concrete columns subjected to bi-directional displacement patterns, which were similar to the 's' type displacement pattern used in this project (Fig. C.6), resulted in more severe damage in columns than those formed by the 'b' type displacement pattern. In order to study the extent of the influence of a load path on the performance of circular reinforced concrete columns, five column units were tested under this 's' type displacement history. The experimental yield displacements of these five units were taken to be the same values as those observed with their corresponding companion units, tested under either the 'u' or 'b' type displacement patterns.

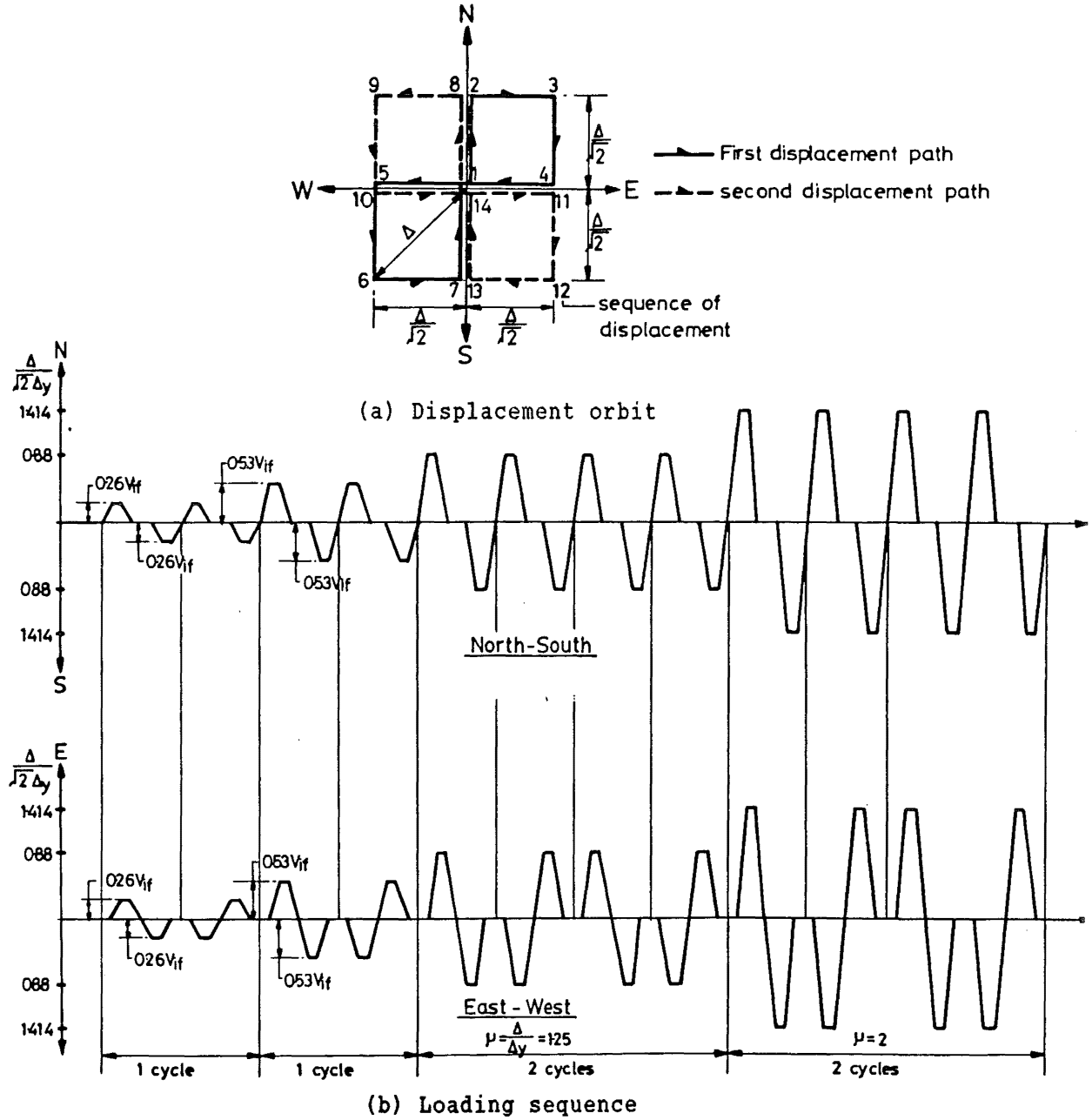

Fig. C.6 : Bi-directional 's' type displacement pattern

Referring to Fig. C.6a, one load cycle is defined as the completion of the NE - SW and the NW - SE displacement paths, whereas displacement peaks are lateral deflections in NE, SW, NW, and SE directions. The standard loading sequence (Fig. C.6b) started with one cycle to resultant lateral force of $0.37V_{if}$, and another cycle to $0.75V_{if}$. Subsequent loadings consisted of two complete cycles to displacement ductility factors, μ, in the order of 1.25, 2, 3, 4, 5, and possibly 6.

d) Bi-directional 'r' type displacement pattern

It must be appreciated that the displacement history of a reinforced concrete column under a seismic attack can never be as regular as the displacement patterns just described. A more realistic bi-directional 'r' type displacement pattern, which was derived from dynamic analysis of circular reinforced concrete pier systems subjected to two dimensional earthquake motions, was used in testing of Unit 16. By comparing the test results of Unit 16 with those of its companion units, an indication on the suitability of the chosen displacement patterns in simulating a severe seismic attack could be obtained.

The details and results of dynamic time - history analyses of pier systems with different initial periods of vibration, and subjected to different earthquake records, are given in Appendix II. With these information, the 'r' type displacement pattern (Fig. C.7), was formulated. This displacement pattern was composed of three displacement paths, denoted I, II, and III. Displacement path I (from control point 0 to control point 9) simulated the displacement pattern (Fig. II.4d in Appendix II) of the pier system with an initial period of 1.2 seconds, subjected to El-Centro 1979 NS/EW earthquake record with ground acceleration magnification factor of 1.5. This resulted in achieving the largest ductility demand in the time - history analyses. Displacement path II (from control point 9 to control point 17) simulated the displacement pattern of the pier system with an initial period of 0.6 second also subjected to the same earthquake excitation. The displacement path III (from control point 17 to control point 36), which was essentially a circular displacement path to ductility level of 4, was constructed arbitrarily. The value of yield displacement for this unit was taken to be that of its companion test specimen, Unit 8. The test column was initially subjected to displacement path I. If there were no signs of distress after completing the first load path, it would then be subjected to displacement path II. Subsequently, if the column still appeared to be in a reasonably good state, it would be subjected to the last displacement path III. In fact, the complete displacement path, shown in Fig. C.7, was imposed on this test unit.

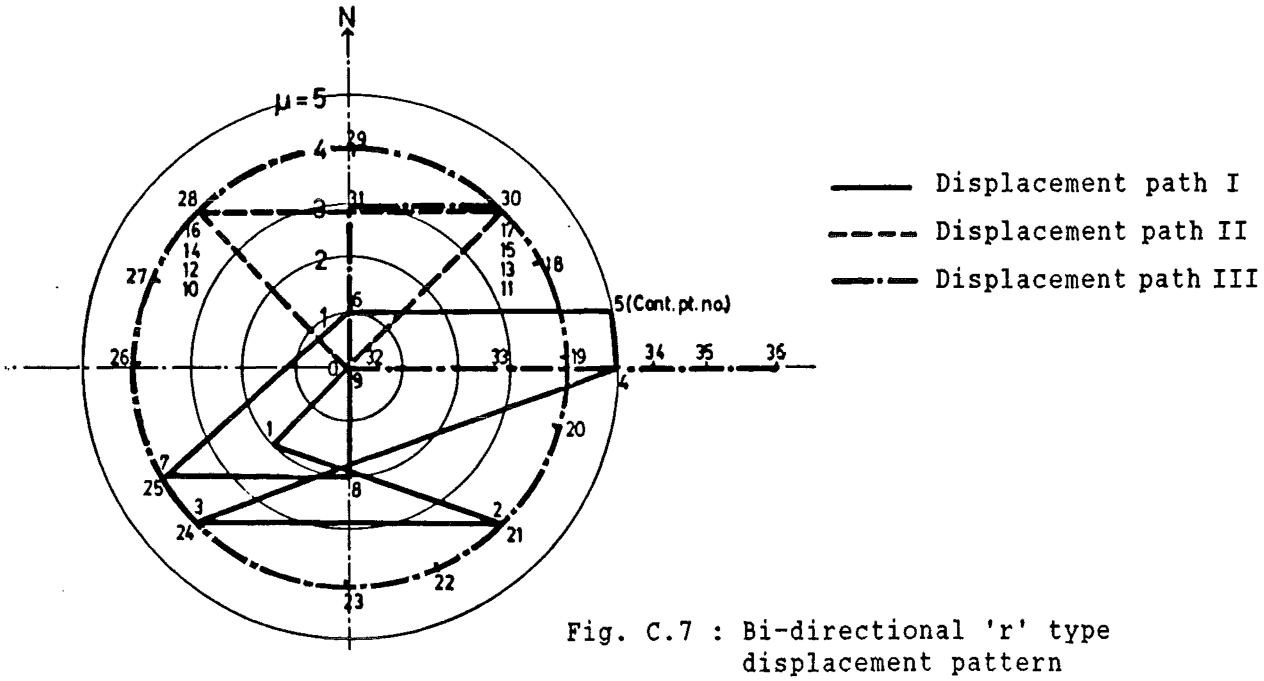

Fig. C.7 : Bi-directional 'r' type displacement pattern

C.3.2 Experimentally Established Yield Displacements

For both 'u' and 'b' type displacement patterns, the experimental yield displacement, Δ_y, of a test column was determined from the first cycle to lateral force, V equal to 75% of the column's ideal flexural strength, V_{if}. From the load displacement graph (Fig. C.8), it was defined by extrapolating a straight line from the origin through the coordinates at $0.75V_{if}$ to the level of V_{if}, The yield displacement, Δ_y, was the average of the values found at loading in east - west directions, and north - south directions for 'u' and 'b' type displacement patterns respectively.

In the case of a column subjected to either 's' or 'r' type displacement pattern, it was not possible to use this method to determine the experimental yield displacement. Therefore, the value of yield displacement obtained from a companion unit, tested under 'u' or 'b' type displacement pattern, was adopted.

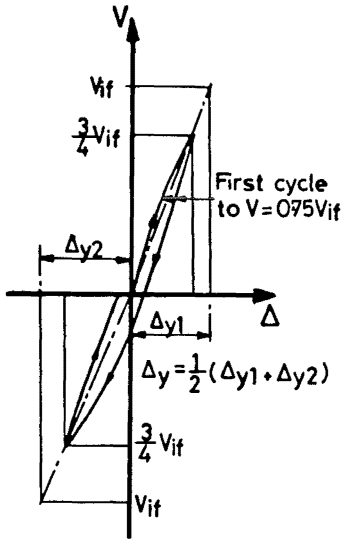

Fig. C.8 : Determination of the experimental value of the yield displacement, Δ_y

C.4 CONCRETE MIX FOR COLUMN UNITS

The target strength of concrete for the column units was 30 MPa at 28 days with a maximum size aggregate of 20 mm. In order to obtain better workability, the slump was specified to be 100 mm. Table C.II shows the proportion of each component of the design mix by weight. The concrete was a standard mix type which has been commonly used in the locality. It was supplied by a local commercial ready mix concrete company.

Table C.II : Concrete mix proportion for column units

Component	aggregate 19 mm	aggregate 13 mm	fine sand	coarse sand	cement	water
Weight in Kg	565	555	176	663	230	154

C.5 THE COLUMN BASE

The column base was to act as a rigid foundation for the column test unit while also supporting two steel loading frames. It was a reinforced concrete block to accommodate one layer of 28 mm diameter horizontal holes at the top and at the bottom, separately across the north - south and the east -west directions (Fig. C.9). For this purpose, 36 mm outside diameter PVC tubes were inserted and left in the concrete. The 25 mm diameter bolts were subsequently used for attaching the loading frames.

The base was reinforced with Grade 275 steel deformed bars to resist the maximum forces and bending moments developed from both the column unit and the two loading frames. Reinforcement details are shown in Fig. C.9. Unless otherwise indicated in this figure, 24 mm diameter deformed bars (D24) bent in form of rectangular loops, were used as main reinforcement for the base. The lap joints of these loops were connected by welding. The concrete strength aimed at in 28 days was 40 MPa.

In general, vertical column bars were designed to extend down to the bottom of the base block for anchorage purposes. When this detail could not be achieved, because of the obstruction caused by the bottom layers of PVC tubes, the column bar was terminated at the level of obstruction with a standard hook. Inside the base block, the column bars were tied by five turns of 6 mm diameter spirals in order to keep them in position during concreting the column base.

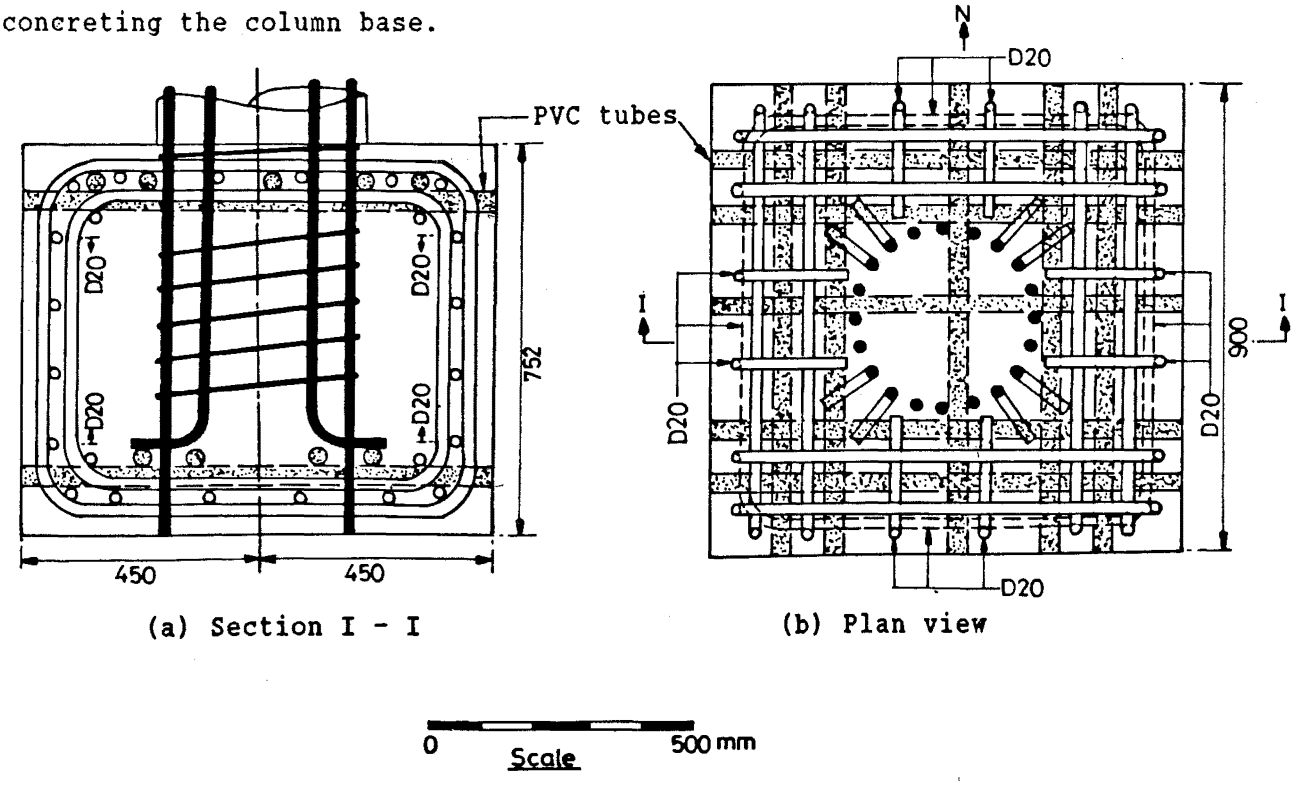

Fig. C.9 : Reinforcement details of the column base

C.6 THE STEEL LOADING FRAME AND ITS CONNECTIONS TO THE COLUMN

Fig. C.10 shows details of the steel loading frames and Fig. C.11 gives details of the universal joints. The horizontal and vertical members of the loading frame were made of two rolled steel Grade 250 channel sections, back to back and connected by 20 mm thick steel plates welded to the flanges. The two members were then welded to a 32 mm thick steel plate at the knee to form a L-shaped frame which was capable of resisting ± 800 kN horizontal force from the hydraulic jack. The expected maximum force was ± 500 kN. Two 360° freely rotating universal joints were provided between the loading frame and the shear connector at the column head (Fig. C.11). Their function was to transfer the horizontal load, while minimizing undesirable bending and torque on both the loading frame and the column unit during the bi-directional displacement of the column.

Details of shear transfer at the column head are shown in Fig. C.12. The force from the horizontal hydraulic jack was transferred to the shear connector through the universal joint. The shear connector in turn was connected to a shear ring which was constructed with column, by 8 - 24 mm H.S. friction grip bolts. When the column was also subjected to an axial compression load, a large portion of this shear load would have been transferred by friction directly from the shear ring connector to the concrete surface at the column head.

C.7 CONSTRUCTION OF THE TEST UNITS

Each test unit was built in two stages. The first stage was the construction of the column base, and the second stage was the construction of the remaining parts, the column unit. Two sets of plywood moulds for the column bases and six sets of cylindrical sheet metal moulds for column units were prepared. Details of the construction work are described as follows.

C.7.1 Construction of Column Bases

In order to facilitate speedy construction work, reinforcement details of the column base and those of the column unit were designed in such a way that the two components could be fabricated independently.

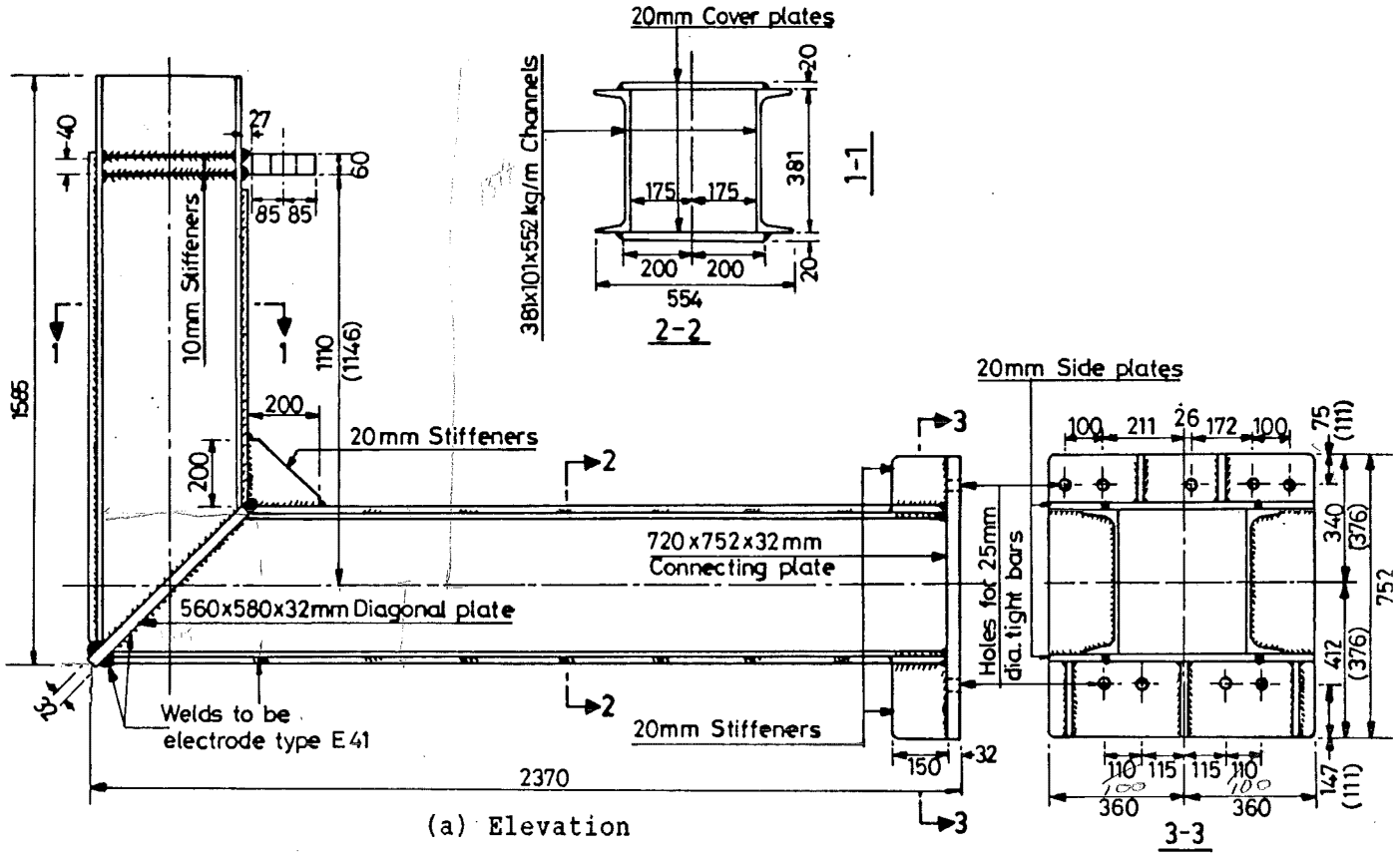

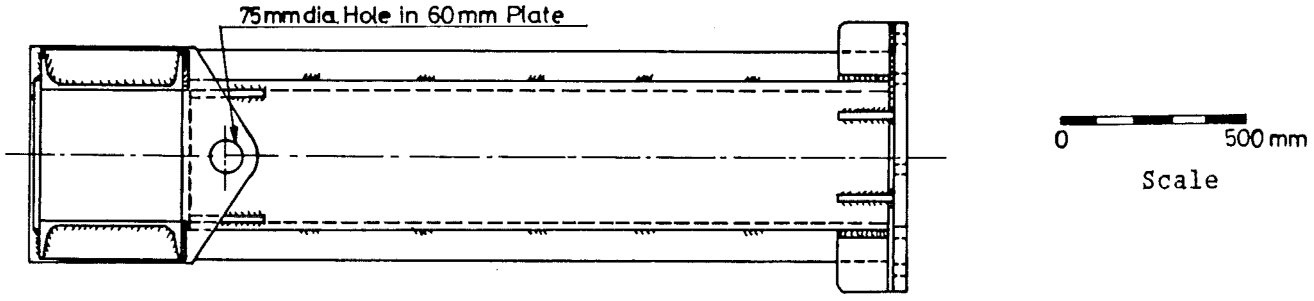

Fig. C.10 : Loading frame details

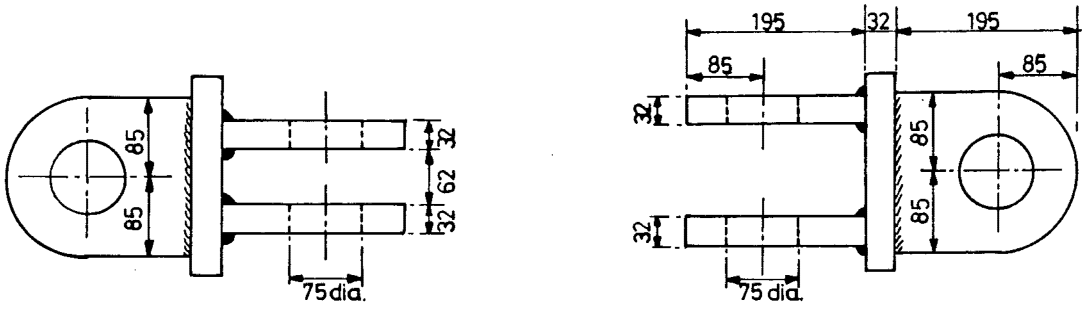

All dimensions in mm

Fig. C.11 : Details of universal joint

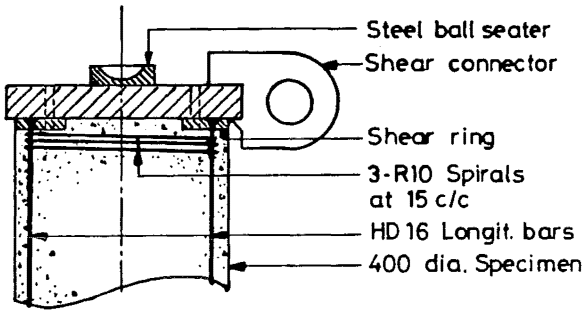

(a) Set-up of shear transfer

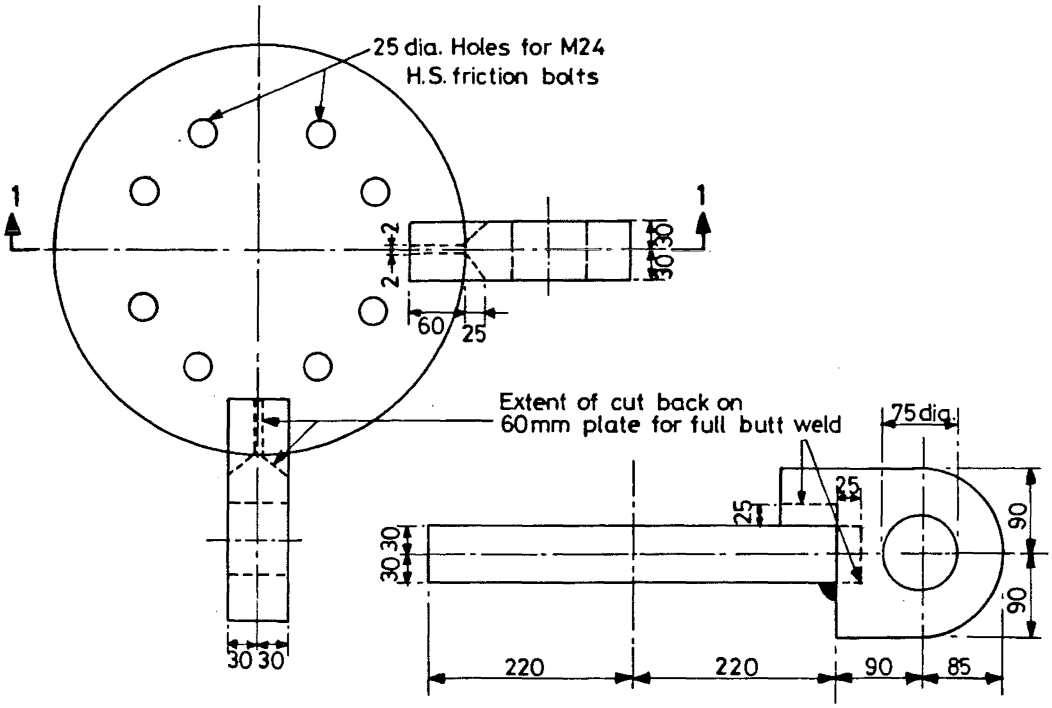

(b) Plan view of shear connector

Section 1 - 1

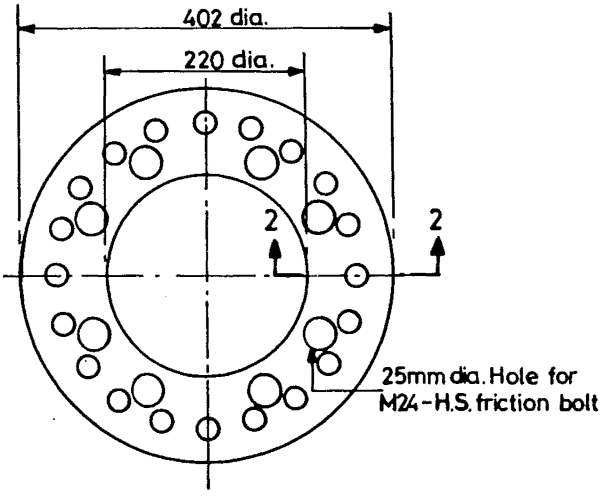

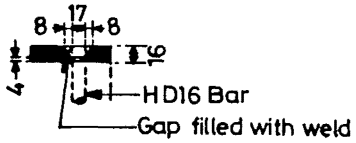

Section 2 - 2

All dimensions in mm

(c) Details of shear ring

Fig. C.12 : Details of shear transfer at column head

When the reinforcement cage for the column base was completed, it was placed on metal studs and supported at the correct level. The reinforcement cage of the column unit, with correct spiral spacing, was then inserted vertically into the reinforcement cage of the column base. Since some of the vertical column bars extended down to the bottom of the column base, as seen in Fig. C.9a, the column reinforcement cage was also vertically self-supported. A quantity of 18, 36 mm outside diameter PVC tubes, each of 900 mm length were installed at the specified locations between the column base reinforcement bars (Fig. C.9). The four sides of the plywood moulds were assembled around the column base reinforcement and were held in position by bolting the 25 mm diameter steel tie bars passing through pre-formed holes in the mould and the corresponding PVC tubes in the reinforcement cage (Fig. C.13). The alignment of the column reinforcement cage was adjusted by temporary tie wires linking the column reinforcement and the plywood mould.

In order to improve the rigidity of the column reinforcement cage, a 16 mm thick steel shear ring was attached to the top of the tied column bars so that each vertical bar could be welded within the corresponding hole of the ring. All joints around the mould were sealed with joint sealant compound.

Two column bases were cast at a time. During construction, the concrete was poured into the mould in four layers which were adequately compacted by internal vibrators. Nine 200 x 100 mm concrete test cylinders were prepared for each concreting operation. After initial set of the concrete, the surface was covered with moist sacks. The following day, the construction joint for the column unit was prepared by wire-brushing of the surface to expose the coarse aggregate (Fig. C.14b). After two days, the plywood sides were removed and the concrete was covered with moist sacks and plastic sheeting for at least one week.

C.7.2 Construction of Column Units

After the column base had been cured for seven days, preparatory work for concreting the column unit could be started. The shear ring was located at the correct level and the vertical column bars were welded to the shear ring for anchorage purposes. Splices of spirals were also made with a single V flare weld over a lap length of 90 mm. Strain gauges and rods for potentiometers were installed as shown in Fig. C.14. A cylindrical 2 mm thick sheet metal mould was slid over the column reinforcement cage through

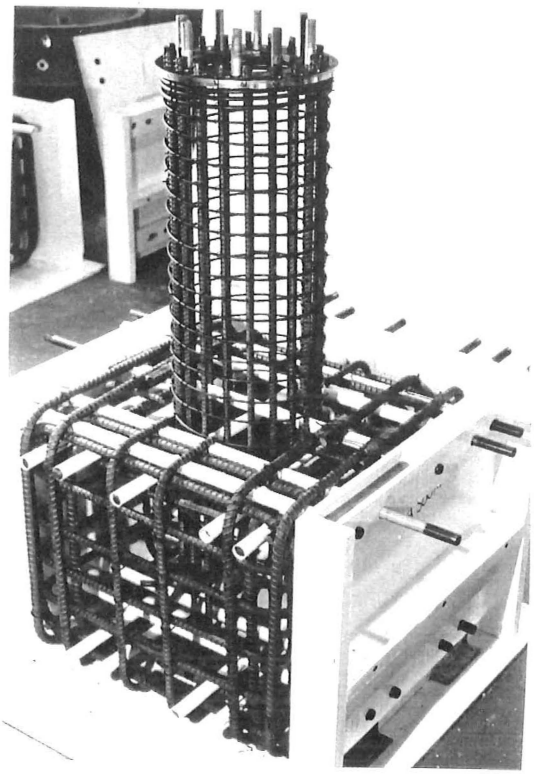

Fig. C.13 : Typical reinforcement cage of test unit

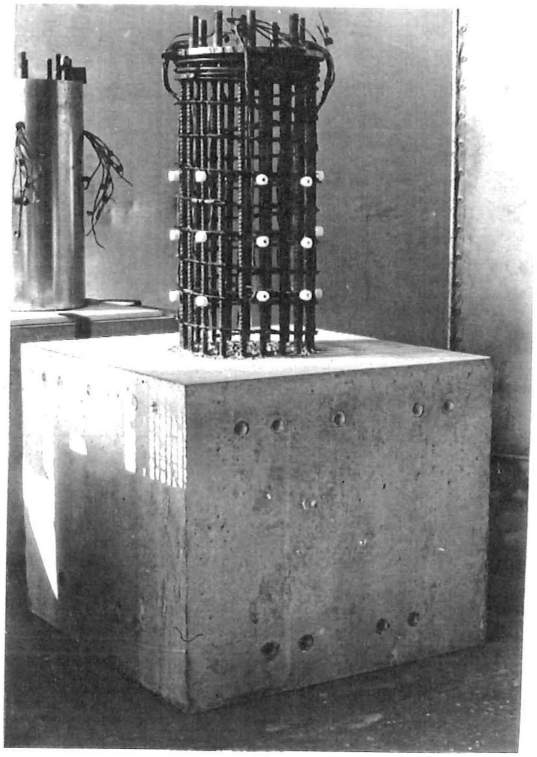

(a) Overall view

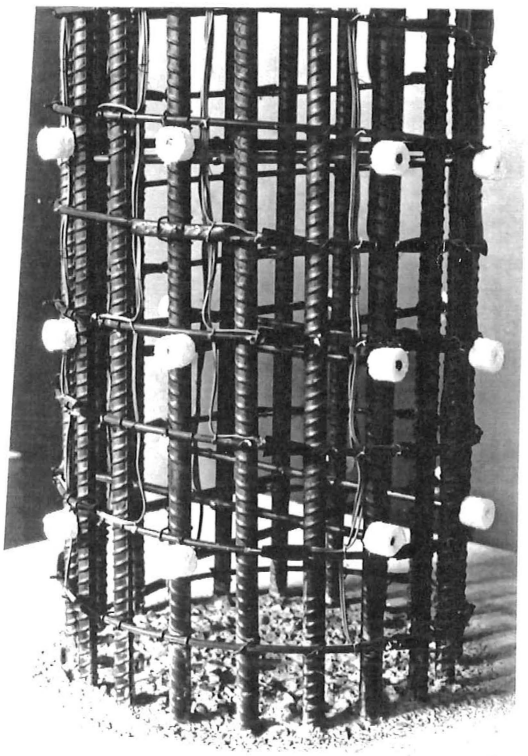

(b) Close-up showing construction joint

Fig. C.14 : Typical column reinforcement cage with instrumentation

the column head, and laterally supported. Four holes were pre-drilled on the sheet metal mould to provide outlets for the leads from strain gauges. All joints were sealed with joint sealant to avoid leakage of mortar paste. The column units were concreted vertically in three layers. Three concrete cylinders per each unit were made for the determination of compressive and splitting tensile strengths. After the initial set, the concrete was cured as for the base block.

Before testing, the column and its base were given two thin layers of white paint to facilitate crack identification.

C.8 INSTRUMENTATION OF THE COLUMN UNITS

C.8.1 Force and Displacement Measurements

A 10 MN capacity DARTEC Universal Testing Machine was used to apply the axial compression load to the column unit, while the lateral forces were applied through 1 MN capacity hydraulic jacks. These forces were measured by load cells which were calibrated using an Avery Universal Testing Machine. Measurements to an accuracy of ± 1 kN were expected.

As the column unit was subjected to bi-directional lateral deflections and possibly also to twist, four displacement measurements (l_1 to l_4) as shown in Fig. C.15, were made to define the deflections in north - south and east - west directions, as well as the angle of twist. If the angle of twist was very small, the measurements along l_1 and l_2 only would have been sufficient to determine the displacement of the column unit. Displacements and twist at the levels of 765 mm and 300 mm above the column base were measured by four 200 mm travel and four 100 m travel Sakae linear potentiometers respectively. These eight potentiometers were mounted on an instrumentation frame, shown in Fig. C.3. Since the instrumentation frame was fixed to the top surface of the massive column base, the displacements, which were measured relative to this plane, were considered to be the absolute displacements of the column.

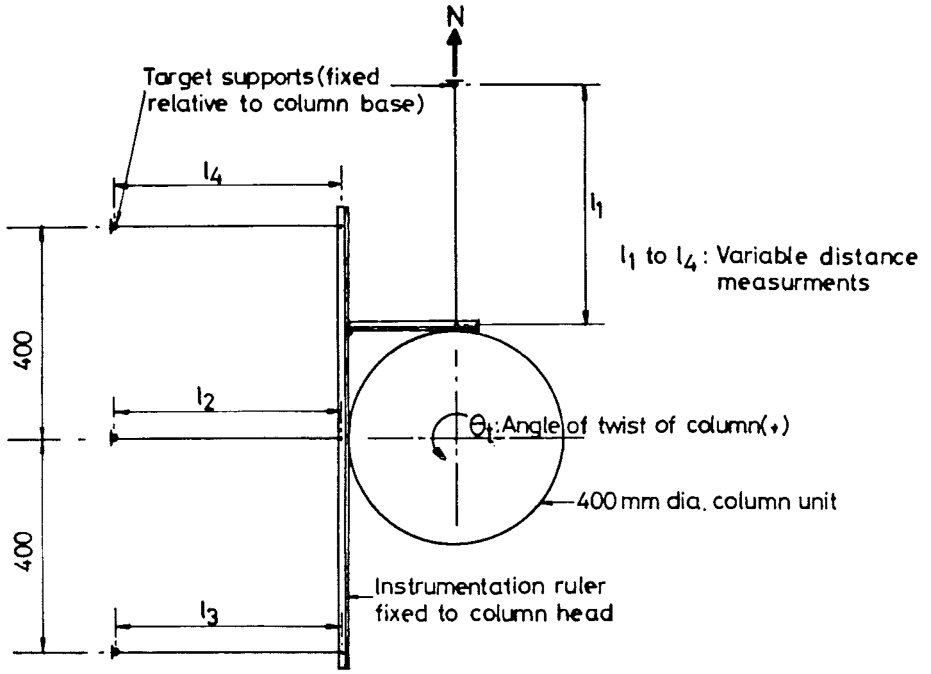

Fig. C.15 : Layout of instrumentation to measure the displacements and angle of twist of a column

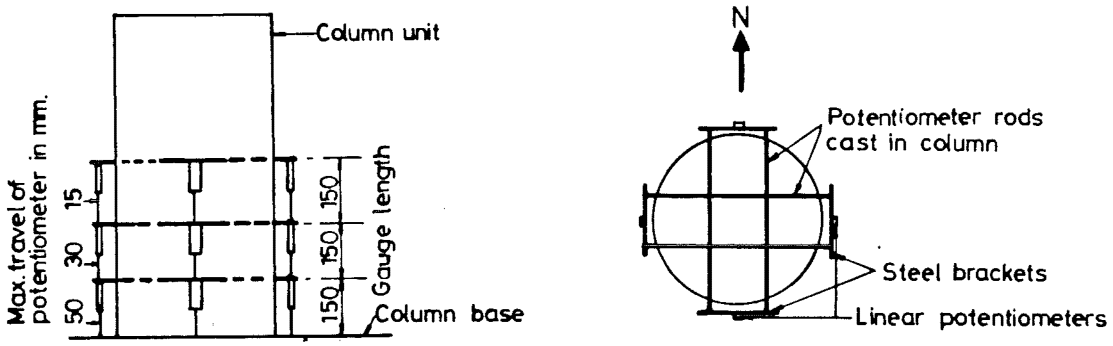

(a) Elevation (b) Plan view

Fig. C.16 : Layout of potentiometers for curvature measurements

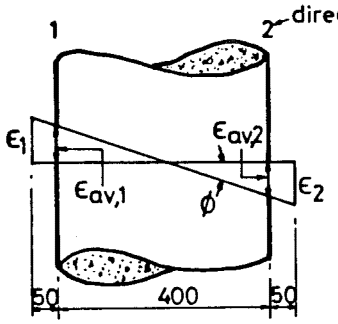

$\varepsilon_1 = \Delta_{gauge,1}$/gauge length

-ve for compression
+ve for tension

$\varepsilon_2 = \Delta_{gauge,2}$/gauge length

curvature, $\Phi = (\varepsilon_1 - \varepsilon_2)/500$ rad/mm

$\varepsilon_{av,1} = \varepsilon_1 - 50\,\Phi$

$\varepsilon_{av,2} = \varepsilon_2 + 50\,\Phi$

Fig. C.17 : Curvature and average concrete strain calculations

C.8.2 Column Curvatures

A series of Sakae linear potentiometers, with travels ranging from 15 mm to 50 mm, were aligned vertically at three levels in the four principal directions (north, south, east, and west) as shown in Fig. C.16. Each potentiometer was mounted on a steel bracket which in turn was attached to two 8 mm diameter horizontal steel rods (also referred as potentiometer rods). The rods passed through the core concrete at levels shown in Fig. C.16 with a basic gauge length of 150 mm. To avoid interference with measurements due to spalling of the cover concrete at advanced displacements, a small volume of cover concrete around the ends of the potentiometer rods was removed. This was achieved by plugging 20 mm long, 20 mm diameter polystyrene studs to the ends of the potentiometer rods before placing the column sheet metal mould.

The potentiometers measured the changes in length, Δ_{gauge}, over the gauge length concerned. With this information and the assumption of plane sections remained plane after deformation, average column curvatures, Φ, over the gauged lengths, and the average concrete strains, ε_{av}, could be calculated, as illustrated in Fig. C.17.

C.8.3 Strains Measurements along the Spiral Reinforcement

To measure strains along the spiral reinforcement, in each unit approximately a quantity of 48, 5 mm Showa N11-FA-5-120-11 electrical resistance strain gauges were attached along the top centre line of the column spirals in eight selected directions with respect to the centre of the circular section (Fig. C.18). Most of the gauges were located along potential shear cracks to provide information on the shear transfer mechanisms and the spiral confining effects on the core concrete. The preparation for affixing, waterproofing and protection of electrical resistance strain gauges and the corresponding leads, was carried out in accordance with the established practice adopted in the structural testing laboratory of the University of Canterbury.

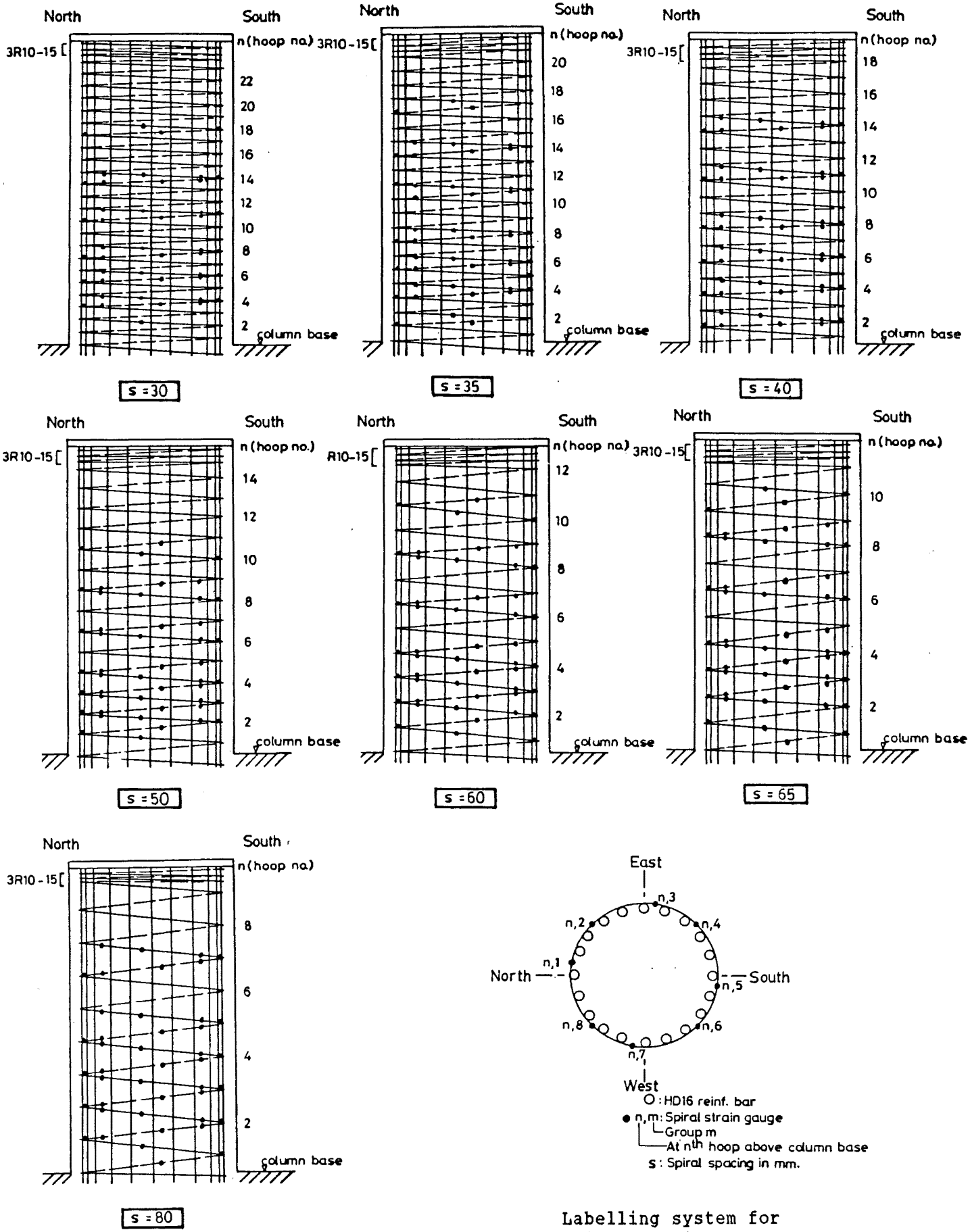

Labelling system for spiral strain gauges

Fig. C.18 : Distribution of spiral strain gauges

C.8.4 Data Acquisition System

The data acquisition system, which consisted mainly of a Cedacs II Digital Data Logger with 64 channels and an IBM Personal Computer, was used to record readings from load cells, potentiometers, and strain gauges for each scan. Electrical signals from the instrumentation, representing raw data, were transformed by the logger into ditigal numbers ranging from +2047 to -2047, and stored in the mini-floppy disk in the computer at the selected scans as determined during the progression of the test. Before testing, each channel of the logger was calibrated against its connected instrument. The readability of each type of instrument by the logger is listed in Table C.III. During testing, a complete set of updated raw data from the 64 channels and the displacements of the column head were displayed on the screen at each scan. This provided immediate information on the current status of the column unit.

In addition, three X-Y plotters were used to give a continuous record of (i) force - displacement hysteretic curves resolved in north-south principal axis, (ii) force - displacement hysteretic curves resolved in east-west principal axis, and (iii) the displacement orbit. Both (i) and (ii) were recorded by Watanabe WX 4421 X-Y plotters, whereas (iii) was recorded by Hewlett-Packard X-Y plotter. All displacements were measured at 765 mm above the column base.

During the test trial run, it was found that when the readings from the load cell were simultaneously recorded by both the X-Y plotter and logger, electric noises generated from the plotter affected the stability of the raw data for the load cell readings. To solve this problem, a Budd Strain Indicator was connected to each load cell to enable data to be read manually. Two digital volt meters were also hooked to the potentiometers which measured variations in the distances l_1 and l_3 (Fig. C.15). These meters provided continuous readings for the displacements at the column head.

When the maximum number of instrumentation readings exceeded 64, extra readings, usually from less critical strain gauges, were recorded manually by a Showa Strain Indicator.

Table C.III : Readability of different measuring instruments

Instrument		linear potentiometers					spiral strain gauge
		max. travel in mm					
		200	100	50	30	15	
Readability	value	0.1	0.05	0.025	0.015	0.0075	1.465×10^{-6}
	unit	mm/integer					/integer
Max. measured value	value	200	100	50	30	15	0.03
	unit	mm					-

C.8.5 Testing Procedures

Just prior to testing the column unit, compressive and tensile splitting tests of the concrete cylinders were carried out to determine the concrete compression and tension strengths. These were used to compute the ideal strength of the column in terms of the applied horizontal force. Complete sets of readings were taken before the application of the lateral force and after the introduction of axial compression load, if any, in order to establish the initial zero readings for later data reduction.

In general, the column was tested according to the predetermined loading pattern shown in Figs. C.4 to C.7. However, when the column indicated a significant reduction of resistance during the repeated load cycle, a few additional load cycles at the same displacement ductility level were applied till the resistance of the column became relatively stable. Then, the column was loaded again to the next higher ductility level. The unit was considered to have failed if the residual strength of the column in all loading directions became less than 60% of its ideal flexural strength, V_{if}. The test was then terminated.

In order to minimize the development of undesirable torsion in the column unit when subjected to bi-directional 'b' type displacement pattern, the lateral force perpendicular to the displacement path was always maintained at zero. This could be achieved by releasing pressure built in the horizontal hydraulic jack perpendicular to the displacement path. During an inelastic load cycle, there would be a certain amount of lateral force acting on the column at the zero displacement position (denoted as 'x' in Fig. C.19) after the completion of a displacement path (either first or second displacement path as shown in Fig. C.5a). In order to remove this force before the commencement of the following displacement path in the perpendicular direction, the column was further moved by an offset displacement, Δ_2, as shown in Fig. C.19, and then unloaded. In general, the column would return back to the zero displacement position with zero lateral load condition if the magnitude of Δ_2 was made equal to that of Δ_1 as illustrated in Fig. C.19. However, under 's' or 'r' type displacement path, no such effect would be made to achieve zero lateral force at the zero displacement position after the completion of a predetermined displacement path.

For each displacement path, a complete set of readings would be recorded at the control points along the force - displacement hysteresis curves as shown by solid dots in Fig. C.19. Crack marking was done at the onset of flexural cracks, diagonal cracks, and at each displacement peak. Photographs of cracks were made at the last displacement peak of each load cycle. They provided visual records of the progression of damage throughout the loading history.

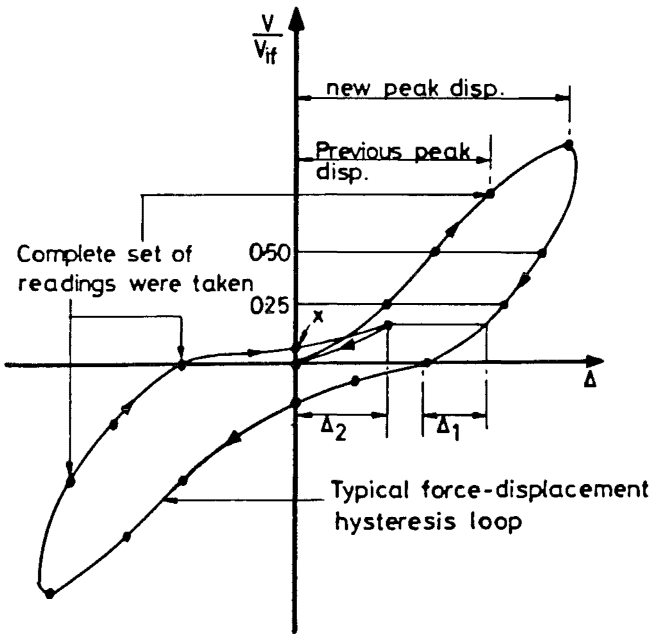

Fig. C.19 : Criteria of data recording

C.9 MATERIAL PROPERTIES OF COLUMN UNITS

C.9.1 Column Reinforcement

For each type of reinforcement bar, six monotonic tensile tests were carried out in accordance to the British Standard BS 18: Part 2: 1971 Section 5 [C.5]. The average stress - strain curves for the transverse (spirals) and longitudinal reinforcement bars are shown in Fig. C.20. All curves indicated an initial linear elastic portion, a yield plateau, and a strain-hardening range. The measured yield strengths were 11% to 25%, and 9% to 25% higher than specified yield values for the longitudinal and transverse reinforcement respectively. Table C.IV shows the measured yield strengths of steel reinforcement in each column unit.

No.	bar mark	steel grade	yield strain	yield stress (MPa)	Young's Modulus (MPa)	strain hardening	fracture strain	ultimate stress (MPa)
1	HD16	380	0.0022	423	192270	0.0175	0.28	577
2	HD16	380	0.0024	475	197920	0.0192	0.35	625
3	R6	275	0.0020	343	175000	0.0235	0.30	473
4	R10	275	0.0015	300	200000	0.0200	0.35	438

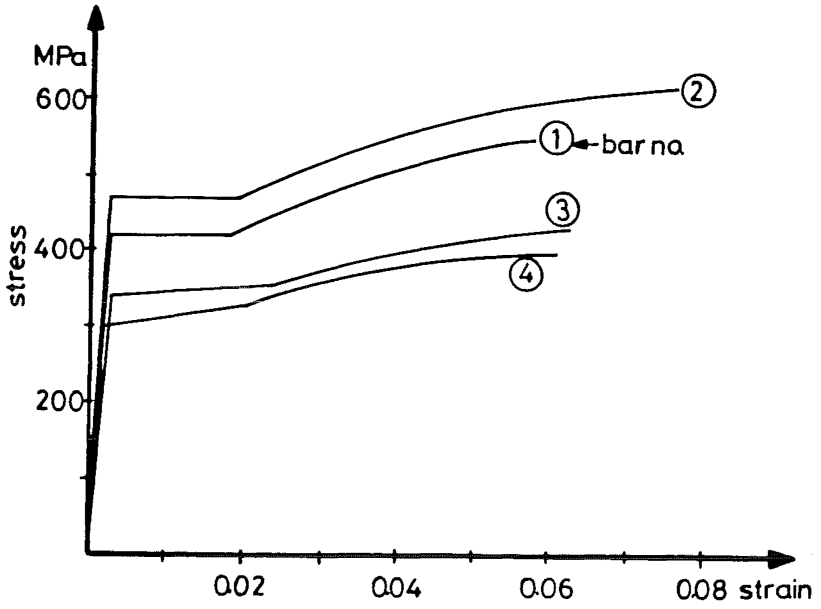

Fig. C.20 : Experimental stress - strain curves for column steel

C.9.2 Concrete Strength

The compressive strength and splitting tensile strength of the concrete were obtained from 200 x 100 mm diameter concrete cylinders, and were tested according to the procedures specified in NZS 3112: Part 2: 1986 [C.6] Sections 6 and 8 respectively. Measured concrete properties of the test units at the date of testing are listed in Table C.IV. The average measured compressive strength of column units was 7 MPa higher than the design strength.

Table C.IV : Measured material properties of test units

Unit	1	2	3	4	5
	f'c		ft	fyt	fyl
	col.	base	col.	spiral	longit.
no.	MPa	MPa	MPa	MPa	MPa
1	38	57	4.10	300	423
2	37	58	3.24	340	475
3	37	48	3.24	300	475
4	42	52	4.17	340	475
5	41	37	4.17	340	475
6	42	54	4.17	340	475
7	39	58	3.30	340	475
8	39	52	3.31	340	475
9	27	51	2.53	340	475
10	37	48	3.22	300	475
11	42	37	4.17	340	475
12	27	60	2.55	300	475
13	39	52	3.93	340	475
14	38	46	3.90	300	423
15	27	59	2.61	300	475
16	38	57	3.60	340	475

3 : splitting tensile strength, f_t
4 : yield strength of spiral, f_{yt}
5 : yield strength of longitudinal steel, f_{yl}

CHAPTER D
EXPERIMENTALLY OBSERVED BEHAVIOUR OF CIRCULAR COLUMNS SUBJECTED TO UNI- AND BI-DIRECTIONAL SHEAR FORCES

D.1 INTRODUCTION

This chapter reports the experimental results from 16 test columns. The major variables studied are :

1. Displacement pattern : a. uni-directional 'u'
   b. bi-directional 'b', 's', & 'r'
   (see Section C.3.1)

2. Axial compression load intensity : $P_l/(f'_c A_g)$ = 0, 0.19, 0.39
   (see Section C.2.3)

Fig. D.1 shows an axial load - moment interaction diagram for a test column, based on measured material properties, taking concrete compressive strength, f'_c = 39 MPa (typical value), and strength reduction factor = 1.0.

3. Volumetric spiral content : ρ_s = 0.39% to 2.46%
   (see Section C.2.3)

The spiral content of each test column is shown in Fig. D.2. Also in the same figure, the spiral content demands by NZS 3101 [D.1] and ACI 318-83 [D.2] code requirements for shear and confinement of a typical test column are represented by curves (based on f'_c = 39 MPa, yield strength of spiral, f_{yt} = 320 MPa, diameter of spiral, d_s = 364 mm, and a flexural overstrength factor = 1.22). It is noted that when $P_l/(f'_c A_g) \leq 0.1$, the spiral content demand increases with axial compression load intensity under NZS 3101 seismic shear design provisions. This is the result of greater flexural strength developed under higher axial compression load ratio. In general, the spiral contents provided in the test columns did not completely satisfy either code requirements.

In order to avoid repetitions in the presentation, general observations relevant to force - displacement relationships, relative strengths, strains, deformations, and other features of behaviour, which apply to all or to the majority of test units, are reported in Section D.2. Further details of the above-mentioned aspects and the general performance of each test column will be individually described in subsequent sections.

As a rule, the first unit in each group is presented in greater detail. Similar features of behaviour for other units will summarized only, and only unusual aspects will be described.

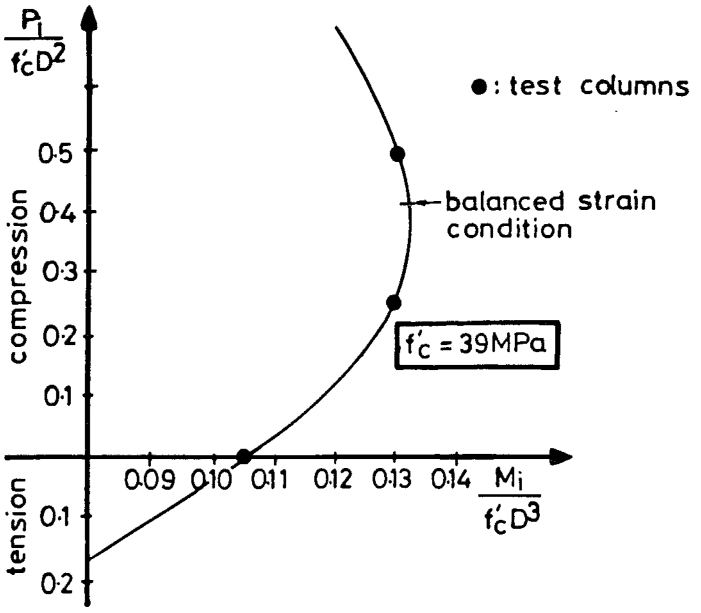

Fig. D.1 : Typical ideal moment capacity of test columns

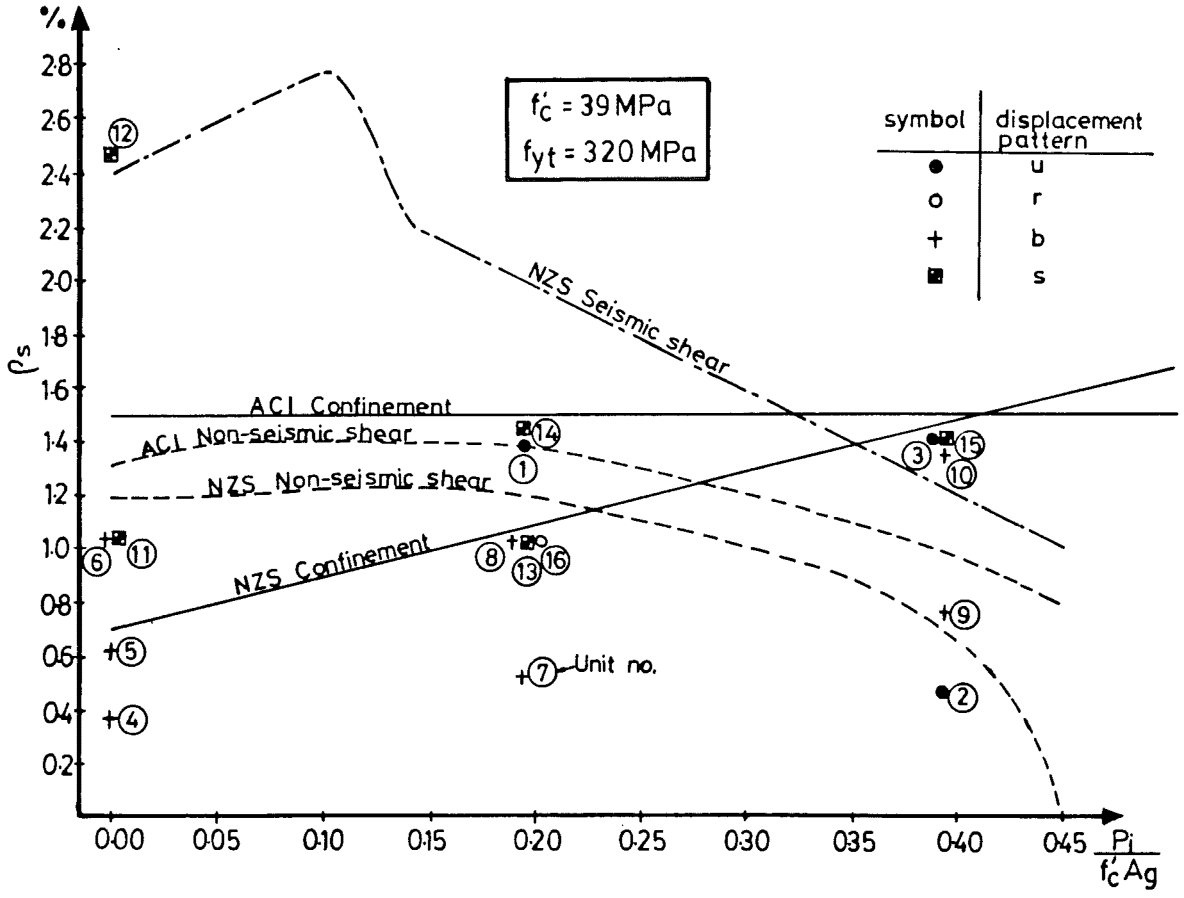

Fig. D.2 : Spiral steel contents of test columns vs code requirements

D.2 GENERAL OBSERVATIONS

D.2.1 Vectorial Representation of Forces and Displacements

When a test unit was subjected to 'u' or 'b' displacement patterns, as defined in Section C.3.1, the lateral force was applied by one hydraulic jack along the displacement direction. However, under the 's' or 'r' displacement patterns, the displacement was controlled by lateral forces being simultaneously applied by the two hydraulic jacks, acting at right angles to each other. Therefore, it is more convenient to represent the effects of applied lateral forces (or force) by an equivalent force vector, V, acting at the centre of the circular column, and an associated torque, T_t, as shown in Appendix III. Furthermore, in order to evaluate effects on the behaviour of various parameters, the V vector was normalized in terms of the column's ideal flexural strength, V_{if} (Section C.3.1).

Similarly, the distortions of the column are defined by the translational displacement vector of the column's centre, Δ, and the torsional rotation relative to the column base, θ_t, both measured at 765 mm above the column base.

D.2.2 Definitions and Determination of Forces and Displacements

With the knowledge of the measured material properties (Table C.IV) and reinforcement details (Table C.I), the ideal flexural strength, V_{if} (as defined in Section C.3.1), of each test column was calculated. The yield displacement of a column, Δ_y, was determined experimentally by the procedure described in Section C.3.2. The values of V_{if} and Δ_y of each test unit are listed in columns 3 and 6 of Table D.I.

Some control parameters and experimental findings are also included in this table. These parameters, evaluated from the measured material properties, are : the axial compression load intensity, $P_i/(f'_c A_g)$, volumetric spiral content, ρ_s, the volumetric spiral content required to resist the entire shear force, V_{if}, by spirals using the 45° truss model, ρ_{45}, the volumetric spiral content in terms of NZS 3101 code requirement for confinement, ρ_{sNZ}, and the shear strength derived from non-seismic provisions of NZS 3101, V_{iv}. Experimental findings, which are expressed in terms V_{if}, are: the strength developed at the first occurrence of horizontal flexural cracks, V_{fl}, that at the occurrence of inclined cracks, V_{cr}, and the maximum

Table D.I : Experimental findings and control parameters of test columns

Unit		1	2	3	4	5	6	7	8	9	10	11	12	13	14	15
		ρ_s	$\frac{P_1}{f'_c A_g}$	V_{1f}	$\frac{\rho_s}{\rho_{sNZ}}$	$\frac{\rho_s}{\rho_{45}}$	Δ_y	$\frac{\Delta_y}{h}$	$\frac{V_{fl}}{V_{1f}}$	$\frac{V_{cr}}{V_{1f}}$	$\frac{V_{max}}{V_{1f}}$	at μ	μ_o	$\frac{V_{1v}}{V_{1f}}$	m	μ_c
no.	notation	%	-	kN	-	-	mm	%	-	-	-	-	-	-	-	-
1	2R10-60u	1.450	0.19	373	1.29	0.60	4.80	0.627	0.27	0.59	1.30	6	6	1.12	1.24	9.3
2	4R6 -65u	0.476	0.39	393	0.37	0.22	3.15	0.412	0.56	0.87	1.31	3.6	2	0.92	1.42	2.2
3	4R10-60u	1.450	0.39	387	0.99	0.57	3.24	0.424	0.46	0.84	1.63	6	6	1.27	1.42	5.6
4	0R6 -80b	0.387	0.00	330	0.52	0.21	7.06	0.923	0.13	0.38	0.97	1.25	<1.25	0.62	1.22	≤1.0
5	0R6 -50b	0.619	0.00	330	0.84	0.33	6.77	0.885	0.15	0.36	1.06	2	2	0.74	1.22	2.0
6	0R6 -30b	1.032	0.00	330	1.40	0.56	6.32	0.826	0.17	0.37	1.09	3	4	0.97	1.22	≥8.0
*7	2R6 -60b	0.516	0.19	402	0.51	0.23	5.65	0.739	0.32	0.62	1.14	2	* 2	0.74	1.24	2.0
8	2R6 -30b	1.032	0.19	402	1.03	0.46	5.85	0.765	0.20	0.62	1.24	3	4	0.97	1.24	5.4
9	4R6 -40b	0.774	0.39	346	0.85	0.40	3.33	0.435	0.23	0.75	1.23	3	4	1.07	1.42	3.5
10	4R10-65b	1.340	0.39	387	0.92	0.53	3.40	0.444	0.31	0.91	1.41	4	5	1.22	1.42	5.1
11	0R6 -30s	1.032	0.00	330	1.40	0.56	6.32	0.826	0.18	0.38	1.03	2	3	0.97	1.22	≥8.0
12	0R10-35s	2.460	0.00	308	4.64	1.24	6.32	0.826	0.13	0.38	1.05	3	5	1.60	1.22	≥8.0
13	2R6 -30s	1.032	0.19	402	1.03	0.46	5.85	0.765	0.27	0.58	1.19	3	4	0.97	1.24	5.4
14	2R10-60s	1.450	0.19	373	1.29	0.60	4.80	0.627	0.26	0.59	1.16	3	5	1.12	1.24	9.3
15	4R10-60s	1.420	0.39	346	1.35	0.66	3.33	0.435	0.33	0.72	1.40	4	6	1.34	1.42	6.7
16	2R6 -30r	1.032	0.19	399	1.03	0.46	5.85	0.765	-	-	1.30	4	≥4	0.96	1.24	5.2

Note: All symbols are defined in the list of notation.
*: The failure of Unit 7 was caused by external electric interference at $\mu = 2$. In this case, μ_o was assumed to be 2

measured strength, V_{max}, including P-Δ effect, if applicable. The equivalent shear force due to P-Δ effect, is $(P_i \Delta)/L$, where L is the shear span of test columns (L = 800 mm). Another important quantity is the dependable displacement ductility level, μ_o, which is the largest observed displacement ductility level relevant to a specific displacement pattern, at which the resistance is not less than 80% of that corresponding with the ideal flexural strength, V_{if}.

Finally, the last two columns of Table D.I show Ang's proposal for the flexural strength enhancement factor, m, and displacement ductility capacity, μ_c, with respect to the uni-directional cyclic loading (Section B.2.4).

D.2.3 Average Concrete Strains

Table D.II shows the average concrete strains, ε_{pav} and ε_{cav}, at the first application of axial compression load and at the occurrence of local crushing of the cover concrete respectively (see Section C.8.3 for the derivation of average concrete strains). The strain ε_{cav} was not evaluated for units subjected to 's' or 'r' type displacement patterns because the position of maximum concrete strain was not in line with the orientation of curvature measurement.

As the strain given in Table D.II was the average over the nominal gauge length of 150 mm, the actual concrete strain at crushing would have been higher. Nevertheless, they can be taken as reference data for design purposes.

D.2.4 Axial Deformation

During the testing, the axial deformation of test columns was also monitored. For a unit with no axial compression load, the length of the column grew with increasing imposed displacement ductility. The net extension at the end of testing was between 4 mm to 5 mm. However, a column was shortened when it was under both shear and axial compression. Fig. D.3 shows some typical experimental results. The rate of shortening increased significantly when μ was larger than μ_o.

The growth of columns can be explained by the fact that once aggregate interlock action has been mobilized to transfer shear, the relative sliding movement between two rough surfaces of an inclined crack causes the crack to open further. Even when the shear force is removed, part of these

crack openings are retained by displaced interlocking aggregates. The growth of a column results from the accumulation of these incomplete closures of flexural and diagonal cracks along its length, and permanent elongation of vertical bars after yielding due to flexure has occurred.

However, for a unit subjected to both shear, and sufficient axial compression, the above-mentioned mechanism is overridden by the wedging mechanism. The axial compression load tends to push the upper wedge, formed by diagonal cracks, downward (Fig. D.4) so that the lateral wedges are displaced and the column becomes shorter. The rate of axial compressive deformation may be promoted by crack widening at a large ductility, and by grinding of the concrete particles along inclined cracks due to repeated load cycling.

D.2.5 Force - Displacement Hysteretic Performance

Depending on the complexity of a displacement pattern and the connection of the X-Y plotters, which measured the force - displacement relation along the principal axes (North - South and East - West), the number of force - displacement hysteretic curves created from one complete cycle of loading was different for different displacement patterns. Under regular displacement patterns, the number of these curves per each load cycle was one, two and four for 'u', 'b', and 's' type displacement histories respectively (Figs. D.25, D.37, D.64). The 's' type displacement pattern created more curves because the vector components of forces and displacements, resolved in the two principal axes, were plotted. Additional sets of curves for the resultant force - total displacement relationships were drawn for the column subjected to 's' type displacement pattern (Fig. D.65).

For all test units, the initial part of the force - displacement curves at each displacement direction was almost linear when $V < 0.5V_{if}$. The column stiffness K_1, defined as V/Δ, was measured at this load level. During the cycle to $\mu = 0.75$, stiffness K_2 was measured again at the displacement peaks. These stiffness values are listed in Table D.III. It was found that up to these force levels, stiffness was generally independent of displacement sequence. The values of K_1 could be taken as the elastic stiffness of the columns.

Table D.II : Average concrete strains of test columns

Unit	1	2
	ε_{pav}	ε_{cav}
1	-0.00041	-0.00678
2	-0.00083	-0.00837
3	-0.00063	-0.00662
4	-	-0.00671
5	-	-0.00644
6	-	-0.00500
7	-0.00052	-0.00540
8	-0.00044	-0.00370
9	-0.00077	-0.00575
10	-0.00068	-0.00885
11	-	-
12	-	-
13	-0.00044	-
14	-0.00050	-
15	-0.00083	-
16	-0.00052	-

1: ε_{pav} taken at first application of axial compression load
2: ε_{cav} taken at local crushing of cover concrete

Table D.III : Initial stiffness of test columns

Unit	1	2
	K_1	K_2
	kN/mm	kN/mm
1	116	78
2	142	124
3	131	114
4	67	47
5	62	49
6	67	52
7	130	73
8	122	70
9	135	106
10	152	114
11	80	46
12	68	50
13	148	72
14	127	71
15	160	97

1: K_1 calculated at V = 0.50 V_{1f} for 'u' type displacement pattern
= 0.37 V_{1f} for 'b' type displacement pattern
= 0.27 V_{1f} for 's' type displacement pattern
2: K_2 calculated at Δ = 0.75 Δ_y

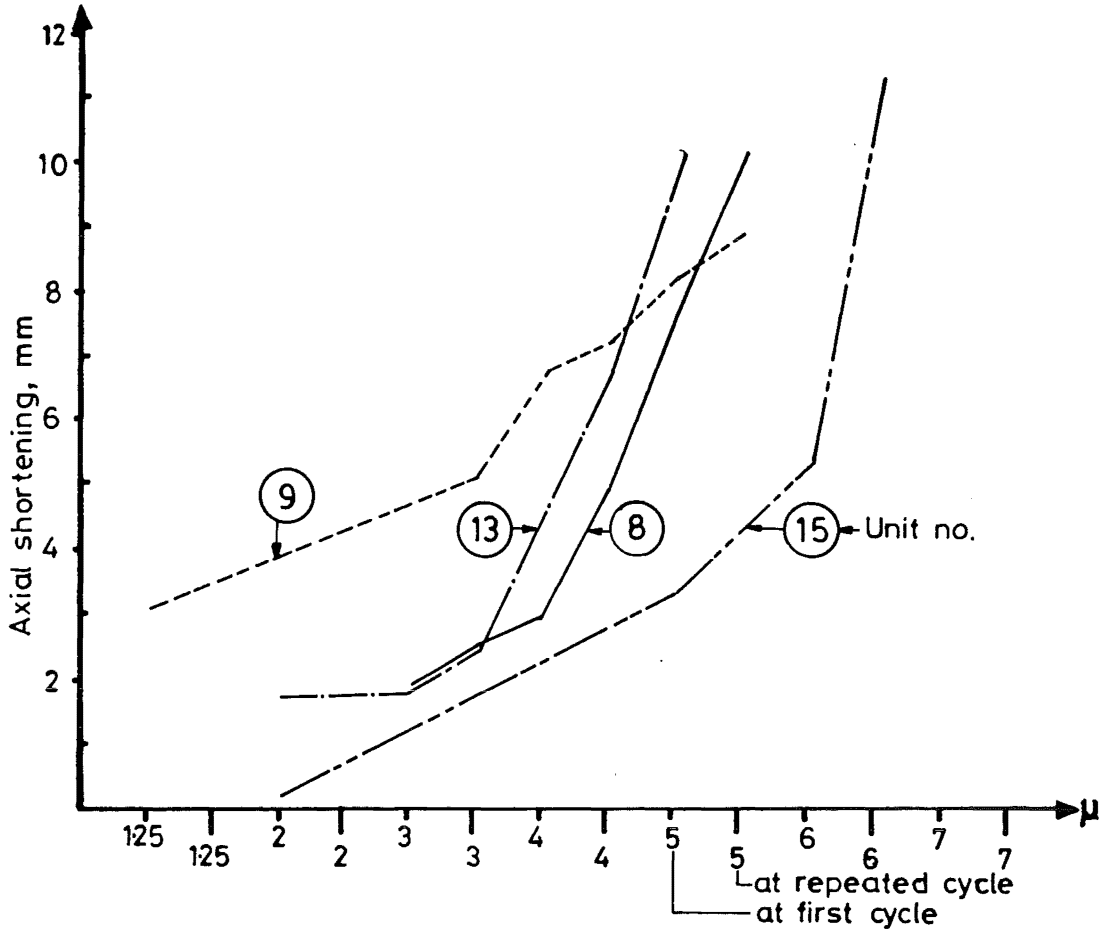

Fig. D.3 : Axial shortening vs displacement vs displacement ductility level

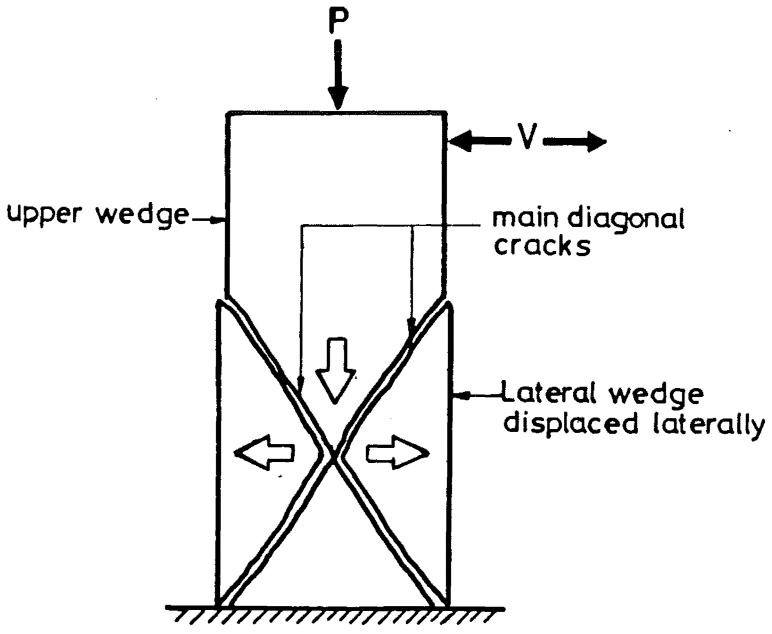

Fig. D.4 : Wedging mechanism

The reduction of stiffness at higher force levels reflected the degradation of response. This was aggravated at repeated cycles or larger displacement ductility levels.

Stiffness degradation in the form of pinching of hysteretic curves was also observed in most of the test units. This was mainly due to the closure of previously formed diagonal cracks across which diagonal concrete compression stresses had to be transferred as a result of shear reversal. Pinching was more pronounced at the second displacement path when bi-directional displacement patterns were imposed.

Strength degradation was observed at the first repeated cycle to each ductility and after V_{max} had been reached. However, the rate of strength degradation varied among test columns.

Special turning points appeared in the resultant force - total displacement hysteretic curves of a column subjected to 's' type displacement patterns (Fig. D.65). In order to have a better appreciation of such response, a three dimensional representation of force - displacement relation was constructed (Fig. D.5). These turning points occurred at Positions '3' and '5' in the first quarter of the displacement cycle. Similar features were also observed in the other quarters. Using Fig. D.3, an explanation on such phenomena is given here.

As the column was displaced from Positions '1' to '2', the lateral force increased, as expected, in a similar manner to that when using 'u' or 'b' type displacement patterns. At Position '2', the flexural compression zone of the column section, which was bounded by the neutral axis 2-2, is shown by the shaded areas 'I+II+III' (Fig. D.5c). As expected, the orientation of neutral axis depended on the direction of the total displacement vector. When the column was further displaced from Positions '2' to '3', the direction of the total displacement vector, as well as the orientation of neutral axis gradually changed. As a result, there was also a change in the vertical strain distribution. This change, which was small at the start, caused a rapid unloading in area 'I'(previously in compression) (Fig. D.5c) without any immediate build-up of compression force in area 'IV' which was previously in tension. At this stage, the compression in areas 'II+III' remained more or less the same. The result was a loss of compression in area 'I' which caused a drop in the moment of resistance or lateral force carrying capacity. At Position '3', this reduction of strength ceased. Usually, strength developed at Position '3' was very close to that

at Position '2'. The magnitudes of the displacement vectors at these two positions were almost equal. From Positions '3' to '4', the magnitude of the total displacement vector increased. The compressive forces in areas 'III+IV+V' bounded by neutral axis 4-4 in Fig. D.5c increased, and higher flexural resistance was usually achieved. During the unloading stage (i.e. from Positions '4' to '5'), the lateral force component parallel to the N-S principal axis reduced more rapidly than that parallel to the E-W principal axis. At Position '5',the N-S force component became zero. Displacement from Positions '5' to '6' caused further reduction of the E-W force component but a build-up of the N-S force component in the reverse direction occurred. This retarded the rate of releasing the total force. In some occasions, the resultant force at Position '6' was higher than that at Position '5'. As expected, during the displacement from Positions '6' to '7', both lateral force components were reduced. The E-W force component became zero at Position '7', and then increased in the reverse direction during the displacement towards Position '8', i.e. '1'.

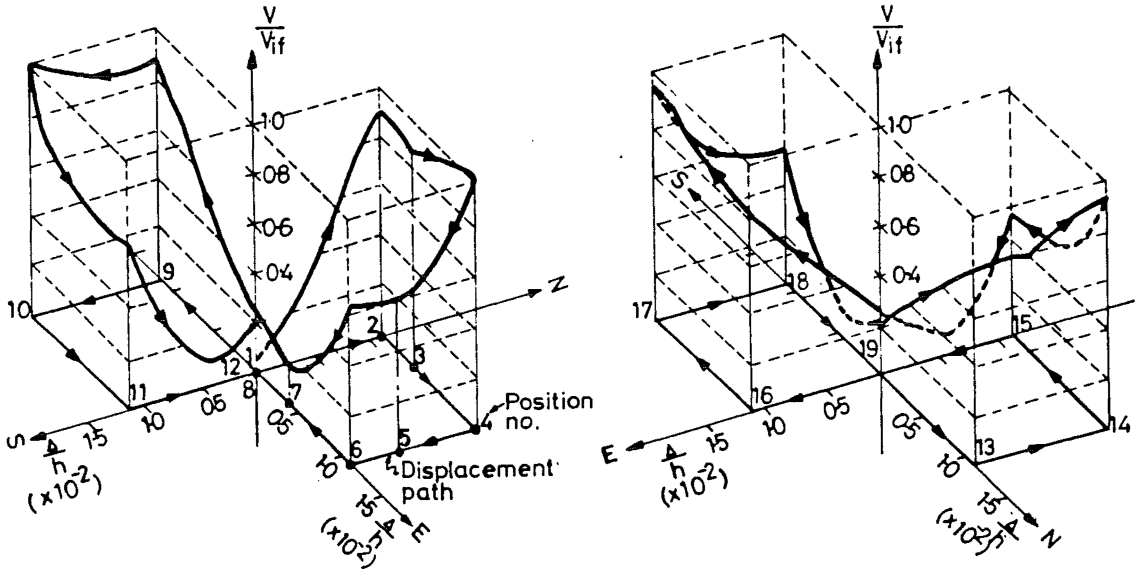

(a) First displacement path (Unit 11, μ = 2)

(b) Second displacement path (Unit 11, μ = 2)

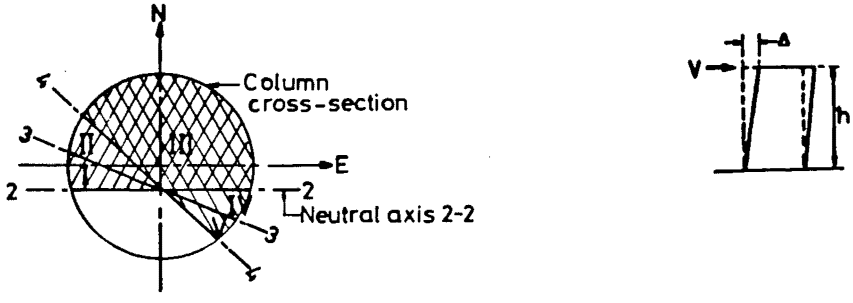

(c) Extent of concrete compression zone

Fig. D.5 : Typical force - displacement relation of unit subjected to 's' displacement patterns

The force V and displacement Δ vectors were parallel to each other under 'u' or 'b' type displacement patterns. In cases of 's' or 'r' type displacement histories, the angle Δα between these two vectors varied at different displacement positions (Fig. D.6). Δα was small during loading paths '1-2-3-4' because V and Δ were increased in similar direction. However, Δα became more significant during the unloading path '4-5-6-7-8' because the directions of the load components were reversed at Positions '5' and '7' (Fig. D.6). While approaching the zero displacement position, the direction of the imposed displacement, Δ, was very sensitive to small variations of the instrumental readings. Hence, a large value of Δα at or near the zero displacement position ('1', '8', '12') should not be considered to have any particular significance.

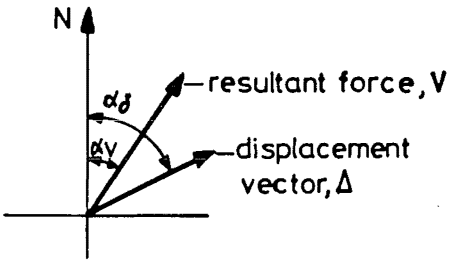

$\Delta\alpha = \alpha_\delta - \alpha_v$

Definition of angular deviation

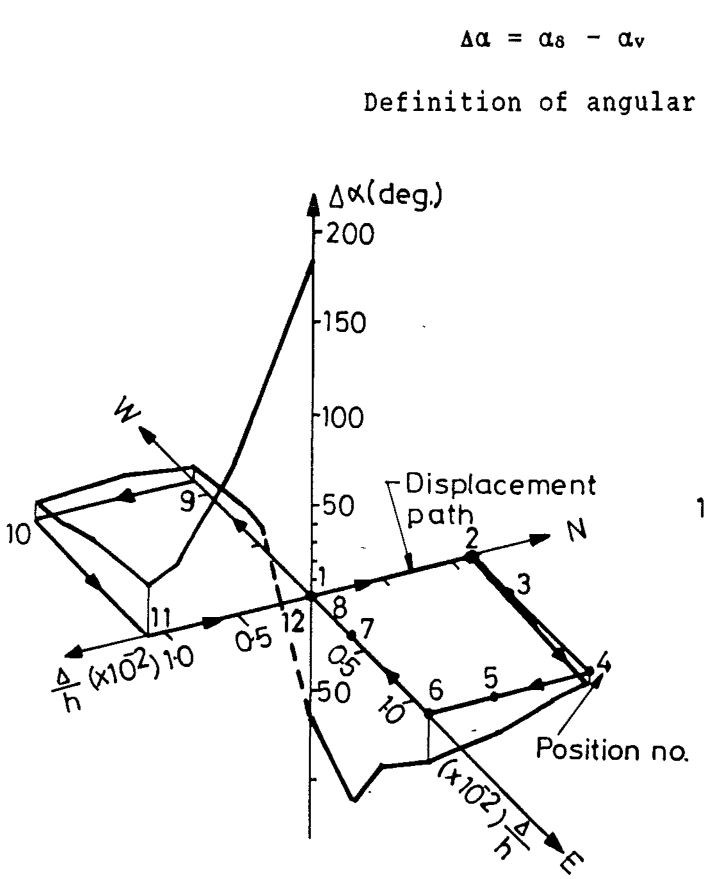

(a) First displacement path (Unit 11, μ = 2)

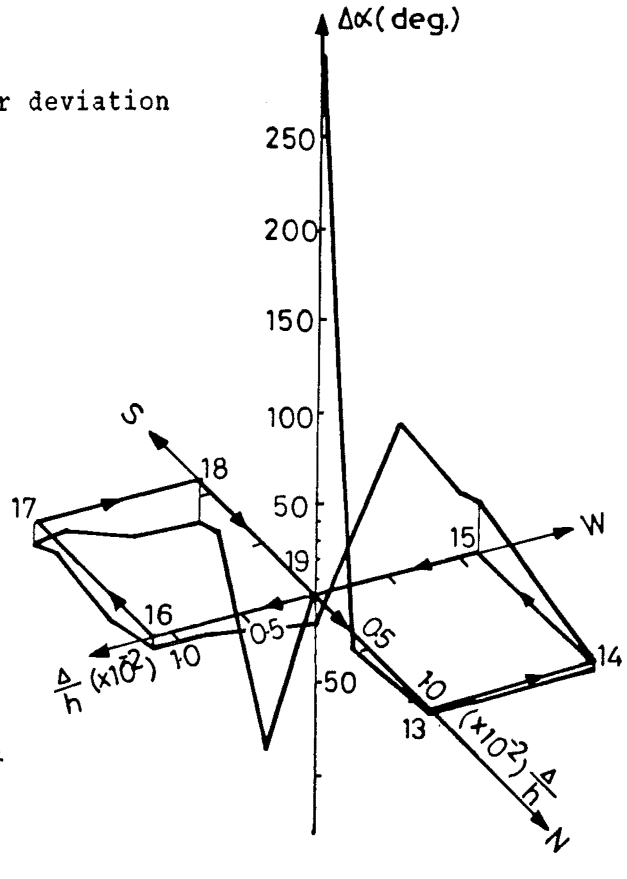

(b) Second displacement path (Unit 11, μ = 2)

Fig. D.6 : Typical force vector - displacement vector relation for a unit subjected to 's' displacement patterns

D.2.6 Curvature Profiles and Components of Deflections

Curvature profiles were formed by joining the average measured curvature values (Section C.8.1) by straight lines at the mid-points of the successive gauge lengths for each displacement peak. Any yield penetration into the base block, which may have occurred, had been included in curvature measurements over the first gauge length. As expected, under 'b' type displacement pattern, only one set of curvature profiles was significant. Readings for the orthogonal set of curvature profiles remained practically zero. Therefore, one diagram for each set of curvature profiles, corresponding to a direction of loading, was produced. Under 's' type displacement pattern, both sets of the curvature profiles were simultaneously active. Two diagrams per each set of curvatures were then drawn.

During the elastic load cycle, as expected, the curvature profile of each column unit followed the profile of linear bending moment. At the onset of plasticity, curvature profiles became non-linear. The spread of plasticity was confined to the critical region (plastic hinge) at the column base. The general trend was that curvature increased with an increase of ductility. This consistent pattern of curvature distribution indicated the dominant flexural behaviour (Fig. D.26). For some column units, this consistent pattern of curvature distribution was disturbed at large ductilities (Fig. D.42). The sense of curvature near the loading end was opposite to that near the base. This could be the result of shear deformations.

Yield curvatures and curvature ductilities of test columns are discussed in Section E.7.3. Usually, the yield curvature of a test unit is indicated in its measured curvature profiles. For columns subjected to 's' displacement histories, the directions of displacement peaks do not coincide with the orientation of curvature instrumentation, so that a proper assessment of experimental curvatures at displacement peaks becomes impossible. Therefore, for these columns, yield curvatures are not indicated in the corresponding measured curvature profiles.

In a slender member, the total deflection, Δ, is usually dominated by distortions due to flexure and yield penetration. However, for a squat member, the deflection due to shear represents a large proportion in the total deflection. Deflection due to flexure and yield penetration can be calculated by utilizing the area of either the theoretical or experimental curvature profile of the member.

For each column unit, the relation of deflections calculated from the experimentally obtained curvature profile, Δ_f, and the measured total deflections, Δ, is shown graphically in Sections D.3 to D.5. In general, the initial part of Δ_f-Δ curve was almost linear which implied the constant proportion of, Δ_f, deflection due to flexure to total deflection, Δ. At large ductilities or at the onset of irregularity of curvature profile, the gradient of Δ_f-Δ curves decreased. In other words, deformations due to shear became larger. The ratio $r_f = \Delta_f/\Delta$, was calculated at several values of μ to provide numerical comparison of the flexural component in the total deflection.

D.2.7 Spiral Strain Distribution and Spiral Forces

In general, negligible spiral strains were measured before the formation of inclined cracks. Subsequently, strain readings increased as the load continued to increase. Unloading to zero lateral force did not release all spiral strains. Instead, these residual strains accumulated at every successive zero load condition. This phenomenon was observed during both elastic and inelastic load cycles. During an elastic load cycle, this residual strain was due to incomplete closure of inclined cracks. When a spiral first entered the yield state, plastic deformation took place and the strain was increased significantly. During unloading, only a relatively small elastic recovery was necessary to bring the spiral back to the zero stress state. The magnitude of the residual strain would be similar to the previously obtained plastic tensile strain. In the subsequent load cycles, the spiral could develop the yield strength again only if its strain reached or exceeded the previous peak value. When the lateral force was released again, higher residual strains remained. This phenomenon was amplified with the presence of axial compression. Because of the concrete wedging action (Section D.2.4), spiral stress was only partly released even though the lateral load was removed.

As expected, spiral strain depended on the direction of applied shear (Fig. D.44). Higher strain would be obtained if the strain gauge was crossed by a inclined crack, or located in the flexural compression zone where spirals tended to confine the core concrete. Strain readings also increased with repeated load cycles, or with an increase of ductility.

From the experimental stress - strain curves for spirals, shown in the materials section of Chapter C.9.1, the force - strain relation of a spiral can be developed and this is shown in Fig. D.7. This simple relation

is based on the assumption that spirals would not be subjected to compression in any situation. When the column is subjected to a lateral force, irrespective of the direction of horizontal force, the spirals act as tension members in the analogous truss model to transfer shear. Also, when the column is subjected to axial compression, the spirals confine the core concrete and are always in tension. At a zero load state, tension in spirals is either totally or partially released. However, at large ductility or near the failure stage, some strain readings did indicate compression in spirals. This was probably caused by bending of the spirals due to dowel action after the widths of diagonal cracks became large.

In general, when major inclined cracks opened, as the result of applied shear, the forces in spirals crossed by these cracks did not decrease with increase of ductility, or repeated cycles to a constant ductility level.

Spiral force distribution patterns provided vital information for the assessment of spiral contribution to shear resistance and confinement. It is difficult to determine separately the proportions of spiral forces due to shear and confining effect when the column is subjected to both shear and axial compression loads. A special condition : the stress state of spirals at zero shear condition after the completion of each load cycle was studied. For this purpose, the term called average spiral stress σ_{av} is introduced. This was derived from gauges that were installed not higher than 500 mm above the column base. Values of σ_{av} after the completion of each cycle of loading will be reported in Sections D.3 to D.5. These values were further converted to equivalent confining stresses on core concrete in Section E.5, where confining stresses at zero lateral force and roles of spiral reinforcement are discussed.

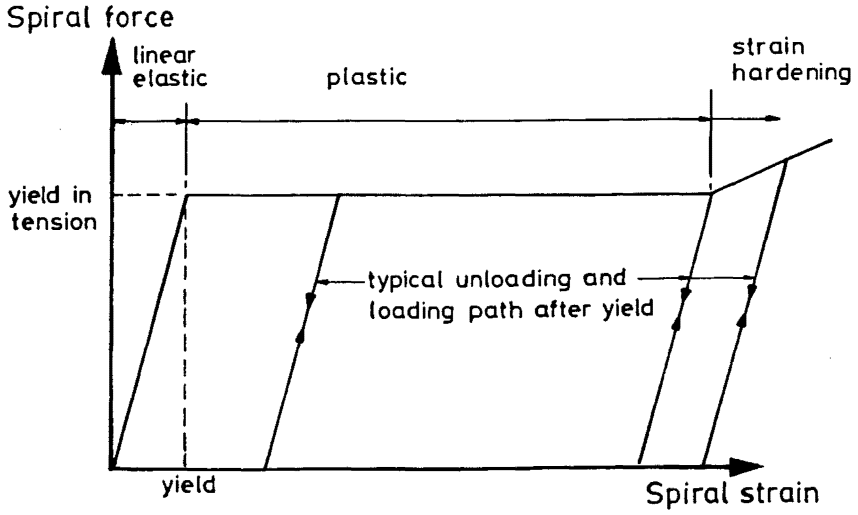

Fig. D.7 : Force - strain relation of spiral

D.2.8 Torque T_t and Twist θ_t

When a test column is displaced, the lateral force might not be acting through its centre. In such case, a torque T_t is created, inducing also twist θ_t. The latter was measured in all test columns. The torque was calculated as shown in Appendix III. It is noted that the torque is a function of displacement vector Δ and twist θ_t. A larger torque was always induced at the third displacement peak (NW direction) of 's' type displacement pattern. This is the result of the way the lateral force is applied rather than the weakness of a test column in a particular direction.

Fig. D.8 shows the observed magnitudes of twist, θ_t, and torque, T_t, in relation to displacement ductility, μ, for some typical test units. Tests revealed that θ_t and T_t were not significant for units subjected to 'u' or 'b' type displacement patterns. When units were subjected to 's' type displacement pattern, θ_t and T_t became large but only at large ductilities.

The torsion resisting mechanism of a circular reinforced concrete column is best illustrated using the well-known Rausch's Space Truss Analogy [D.3]. As the inner part of concrete core does not contribute much to the ultimate torsional resistance, the space truss is essentially a reinforced concrete tube. After the formation of helical diagonal cracks (torsional cracks), the diagonal concrete members interact with longitudinal steel bars and spirals (or hoops) to form a space truss. Torsional shear stress is then resisted by developing compressive stress in the diagonal concrete struts, and tensile stress in both longitudinal steel and spirals (or hoops). At large imposed ductilities, axial load, bending, shear, and torsion co-exist in a column, the interaction becomes complex and relevant predictions are out of the scope of this research.

It is certain that additional torque, induced in the test columns, has had adverse effects on shear capacity. Estimation of stress induced in reinforcement by this torque is shown in Appendix IV. Results indicated that the effect of torque on test columns subjected to 's' type displacement patterns (the worst case) could be neglected during the major part of their displacement history. However, when the strengths of these columns were less than $0.8V_{if}$ at high ductility levels, torque suddenly increased at the third (NW) displacement peak. In most of cases, tests had to be terminated because of large twist.

During the testing, torsional rotations relative to column base were also measured at 300 mm above column base. At the occurrence of large torque, the magnitudes of these rotations at this level were 70% to 80% of the corresponding rotations measured at the top of column. This confirmed that the major part of the total twist occurred in the column plastic hinge region.

D.2.9 Performance Of Column Base Blocks

When a column unit was subjected to lateral force, a few hair cracks were formed on the top surface of the column base block. For the purposes of this study, this base block behaved as a rigid foundation.

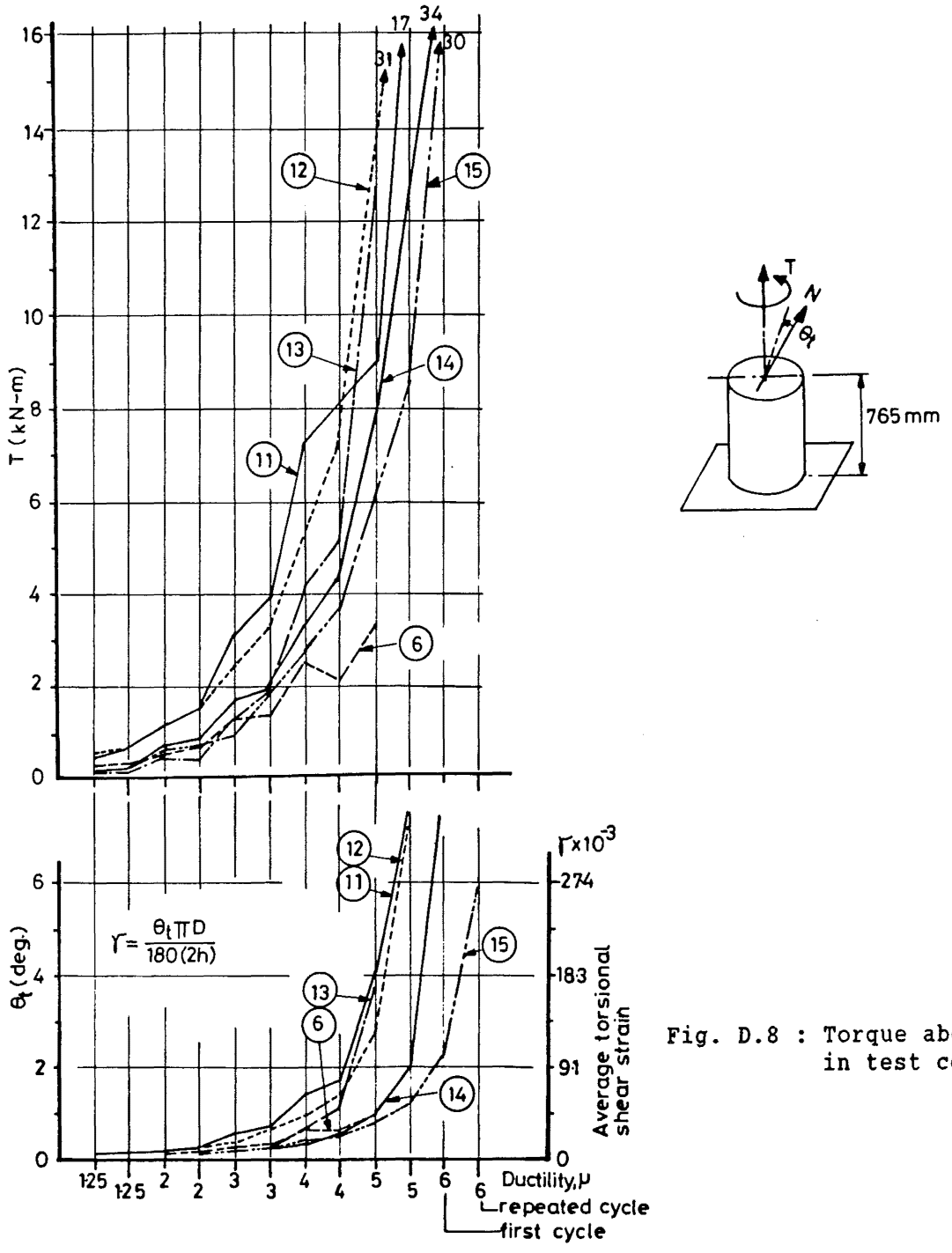

Fig. D.8 : Torque abd twist in test columns

D.3 COLUMNS SUBJECTED TO UNIDIRECTIONAL 'u' DISPLACEMENT PATTERN

In the following sections (D.3 to D.6), reference should be made to Tables C.I, C.IV, and D.I, and Fig. C.19 which summarise the properties and significant strength parameters of each test unit. When the planned displacement patterns are concerned, Figs. C.4 to C.7 are to be referred to.

For reference purposes, the pictures of all column units taken at various stages of loading are shown in Figs. D.9 to D.24. The notation used with the pictures is expressed as follows:

i/j[North]

- Loading stage: j^{th} cycle to displacement ductility level of i
- Photograph taken at north of test unit

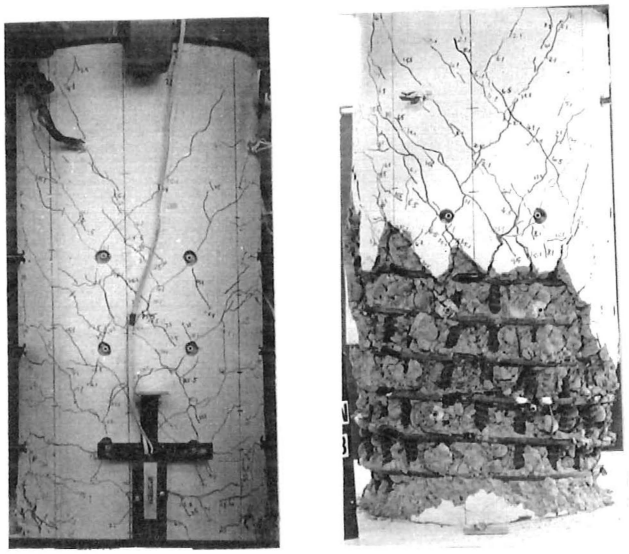

(a) 4/1[South] (b) END[North]

Fig. D.9 : Unit 1 at different stages of loading

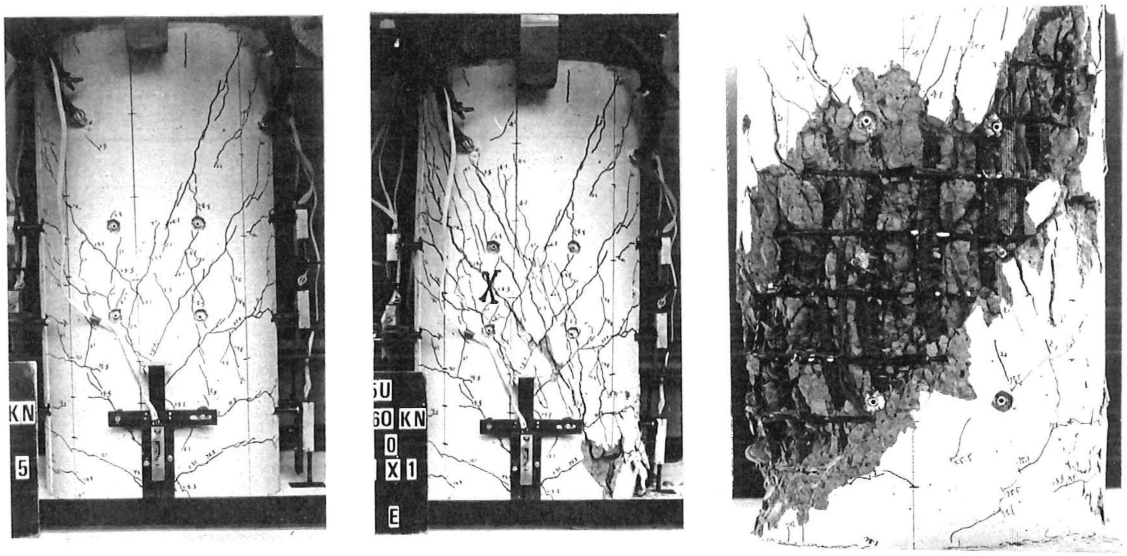

(a) 2/5[South] (b) 4/1[South] (c) END[North]

Fig. D.10 : Unit 2 at different stages of loading

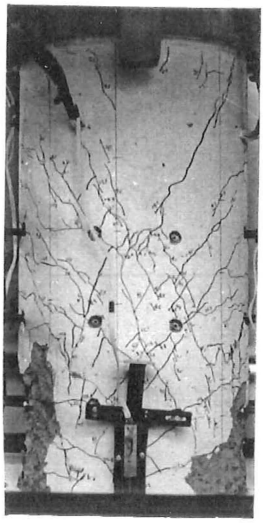

(a) 4/5[South]

(b) END[South]

Fig. D.11 : Unit 3 at different stages of loading

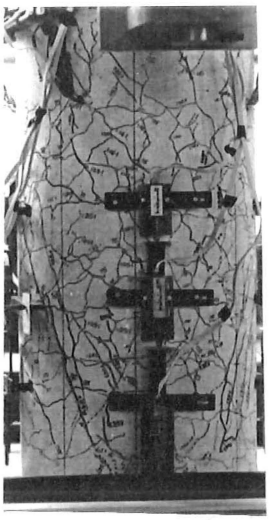

(a) 1.25/1[South]

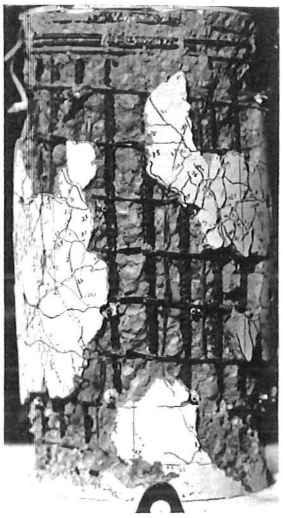

(b) END[West]

Fig. D.12 : Unit 4 at different stages of loading

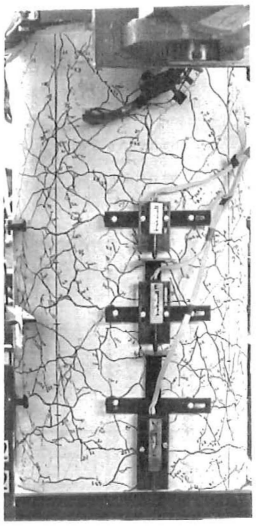

(a) 2/2[South]

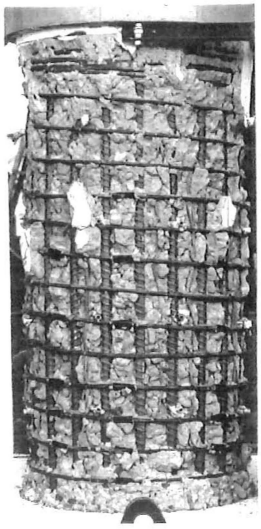

(b) END[North]

Fig. D.13 : Unit 5 at different stages of loading

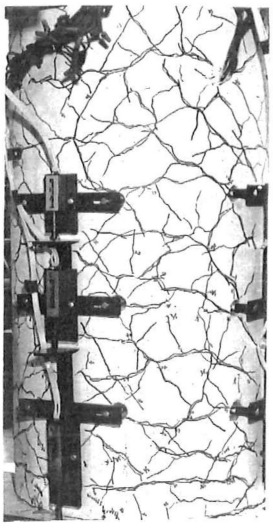

(a) 2/2[SE]

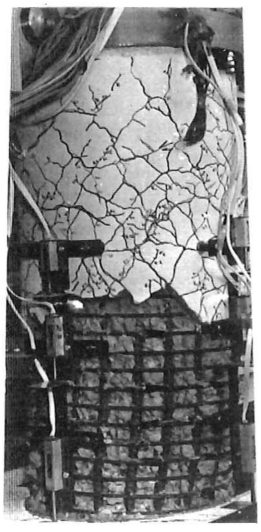

(b) END[NE]

Fig. D.14 : Unit 6 at different stages of loading

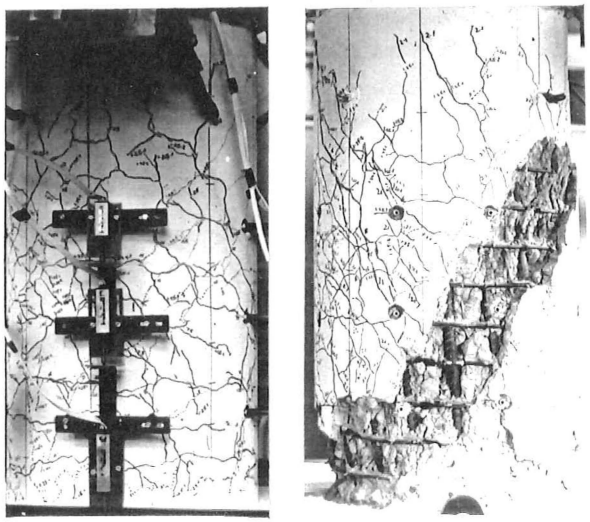

(a) 1.25/2[South] (b) END[West]

Fig. D.15 : Unit 7 at different stages of loading

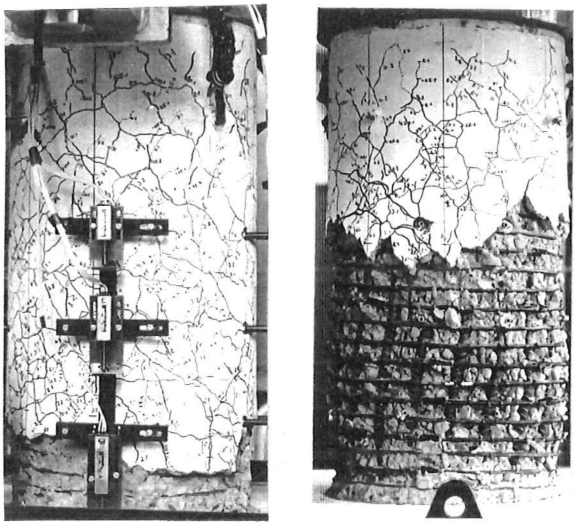

(a) 4/1[South] (b) END[West]

Fig. D.16 : Unit 8 at different stages of loading

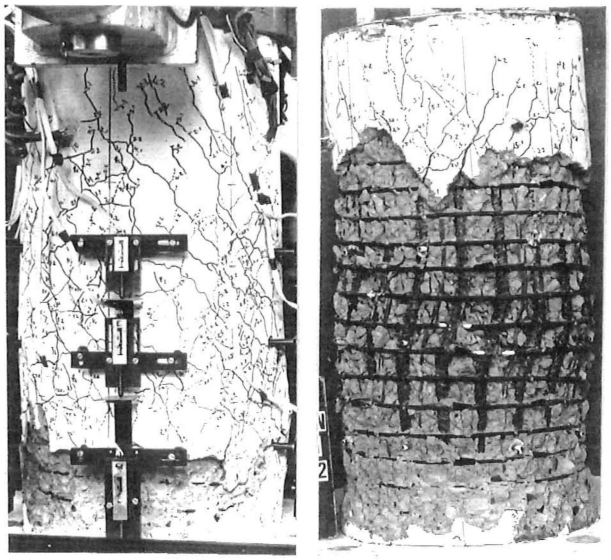

(a) 4/2[South] (b) END[NE]

Fig. D.17 : Unit 9 at different stages of loading

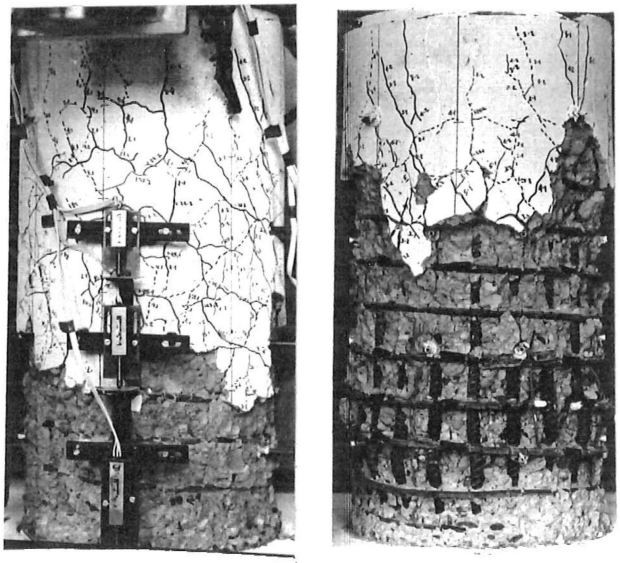

(a) 4/2[South] (b) END[East]

Fig. D.18 : Unit 10 at different stages of loading

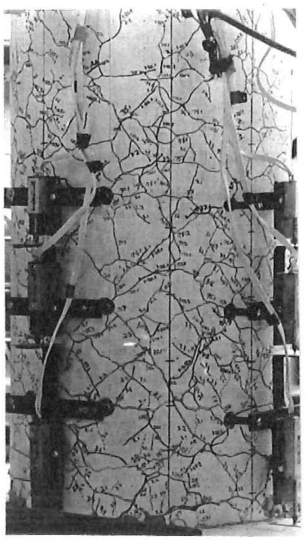

(a) 3/2[SE]

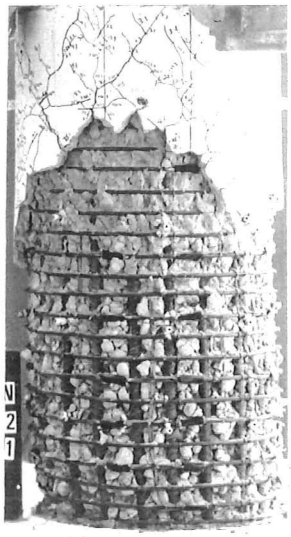

(b) END[SE]

Fig. D.19 : Unit 11 at different stages of loading

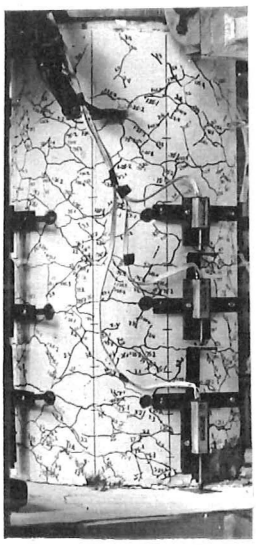

(a) 3/2[SE]

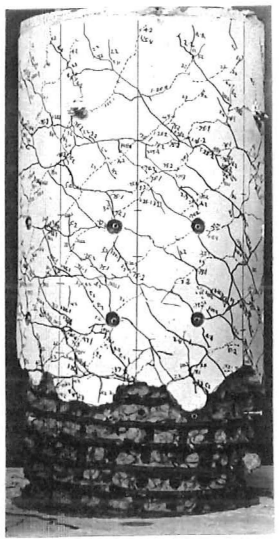

(b) END[North]

Fig. D.20 : Unit 12 at different stages of loading

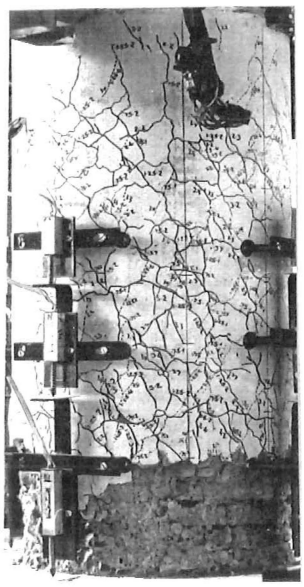

(a) 4/2[NE]

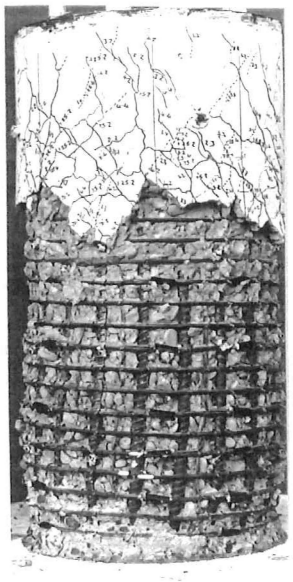

(b) END[NE]

Fig. D.21 : Unit 13 at different stages of loading

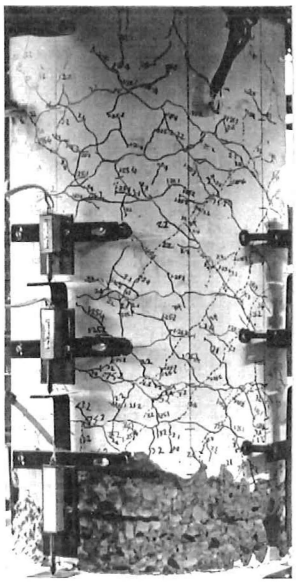

(a) 3/2[NE]

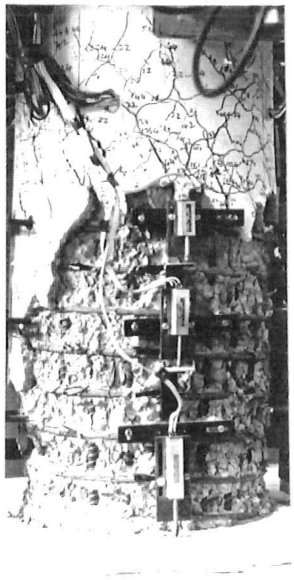

(b) END[East]

Fig. D.22 : Unit 14 at different stages of loading

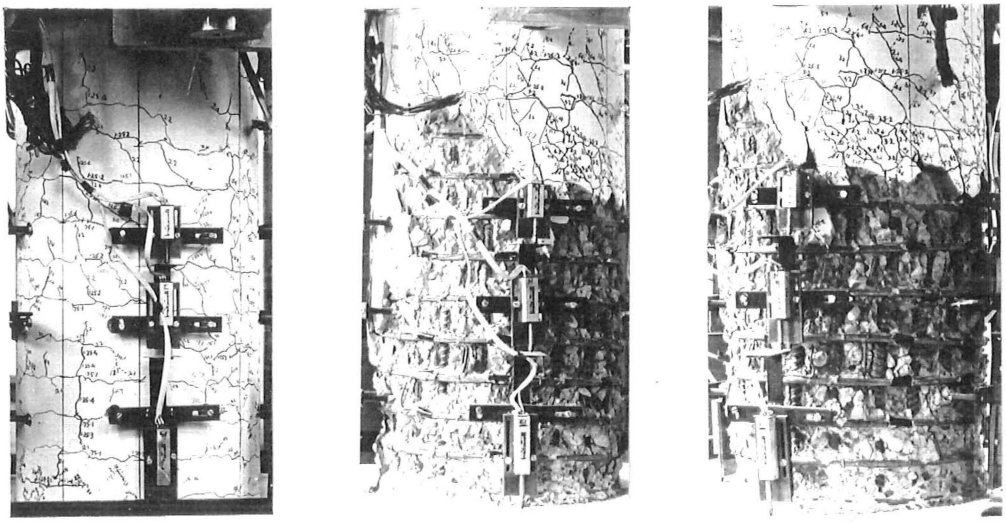

(a) 2/2[South] (b) 6/2[East] (C) END[NE]

Fig. D.23 : Unit 15 at different stages of loading

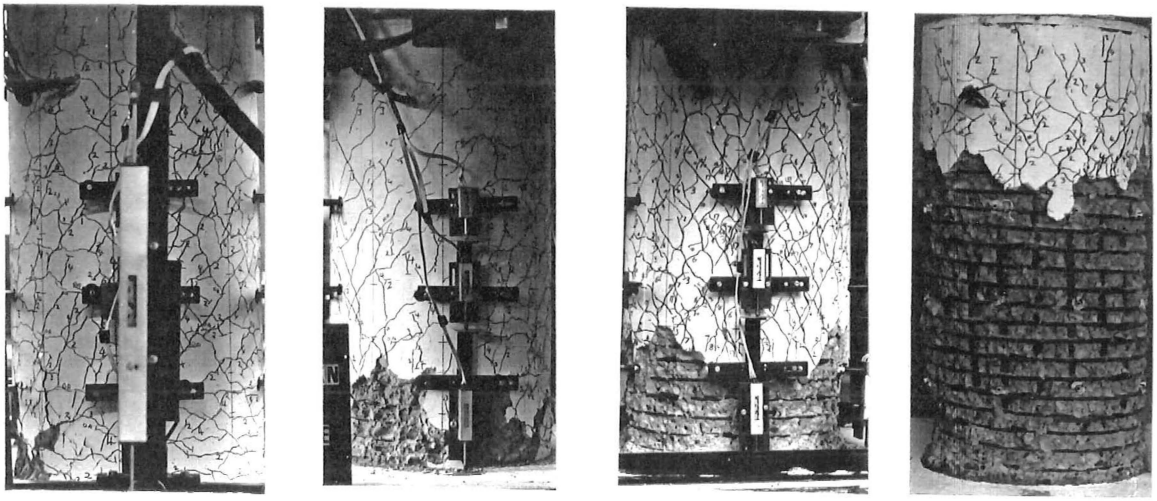

(a) 5/pt.4[North]* (b) 5/pt.4[East] (c) 4/pt.17[South] (d) END[North]

* 5/pt.4 denotes control point 4, at $\mu = 5$

Fig. D.24 : Unit 16 at different stages of loading

D.3.1 Unit 1 [2R10-60u]

D.3.1.1 Force - displacement hysteretic performance

During the initial cycle with displacement ductility, μ, equal to 0.75, the force - displacement relation was not linear (Fig. D.25). The lateral resistance reached the ideal flexural strength, V_{if}, at the displacement $\Delta = 1.3\Delta_y$, whereas the maximum measured resistance, $V_{max} = 1.30V_{if}$ occurred at the first displacement peak in the first cycle to $\mu = 6$.

At $\mu \leq 6$, the variation of strengths at displacement peaks within the same cycle was small with a maximum difference of 3%. There were some reductions in both strength (6% maximum) and stiffness in each first repeated cycle. However, hysteretic response became remarkably stable in subsequent repeated cycles.

At $\mu = 8$, the rates of strength and stiffness degradation increased in repeated cycles. Some pinching of hysteretic loops was also noted. During the second repeated cycle, the resistance reached $0.92V_{if}$ at the first displacement peak. While approaching the second displacement peak with $\Delta = 7.3\delta_y$, the resistance was temporarily held at $0.5V_{if}$ a spiral fracture took place. The axial shortening of the column instantaneously exceeded the pre-set limit of 20 mm. In order to protect the instrumentation from damage, the applied axial load P was reduced to $0.015f'_cA_g$. The residual strength then became $0.33V_{if}$.

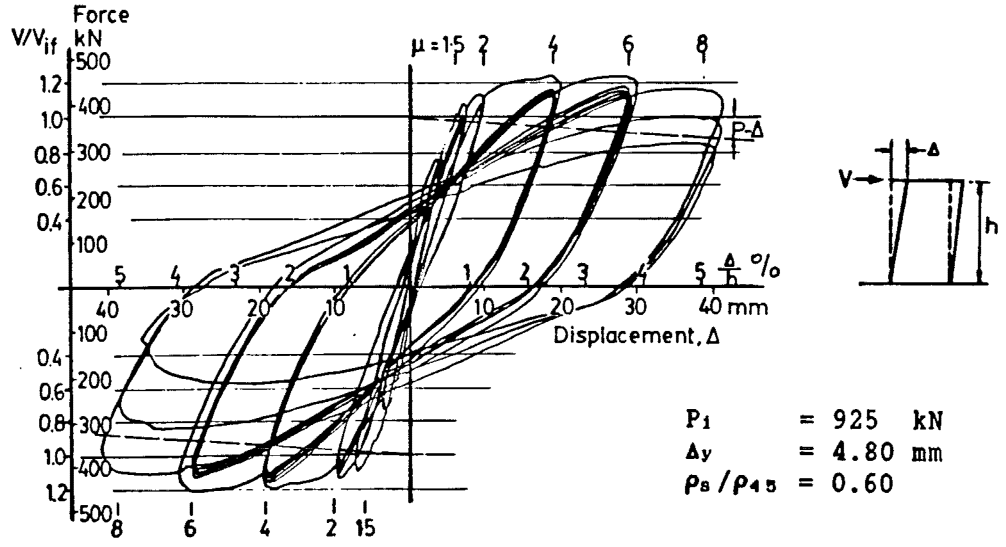

Fig. D.25 : Force - displacement hysteretic curves - Unit 1

D.3.1.2 General performance

Horizontal flexural and inclined cracks were observed at $0.27V_{if}$ and $0.59V_{if}$ respectively. At $\mu = 0.75$, cracks extended over the full height of the column. Most of the new inclined cracks developed as extensions of existing horizontal cracks. Some vertical cracks also formed at the corresponding tension side of the column in the region between 400 mm to 600 mm above the column base.

At $\Delta = 1.22\Delta_y$, local crushing of cover concrete was noted at the flexural compression zone at the bottom of the column. More new cracks developed during the first cycle to $\mu = 1.5$.

At $\mu = 2$, few new inclined cracks appeared. The inclinations of major cracks were about 45° to the vertical. Large flexural cracks were concentrated at the levels of 0 mm, 100 mm, and 200 mm above the column base.

At $\mu = 4$, the existing cracks extended further, and new cracks, at about 30° to the vertical, formed (Fig. D.9a).

At $\mu = 6$, the crack pattern fully developed. Cover concrete spalling extended to 50 mm and 200 mm above the column base at $\mu = 2$ and 6 respectively. No apparent axial shortening was recorded.

At $\mu = 8$, opening of cracks concentrated at the major diagonal cracks. Buckling of some longitudinal bars in the flexural compression zone was also seen in the first repeated cycle. At the first displacement peak of the second repeated cycle, core concrete around the buckled longitudinal steel bars became loose. Axial shortening was 3.85 mm. When the column was displaced to $7.3\Delta_y$ in the reversed direction, fracture of spiral took place (Fig. D.9b). The test was terminated.

D.3.1.3 Curvature profiles and components of deflections

At $\mu \leq 6$, the curvature profiles were consistent with typical flexure performance (Fig. D.26). For a given μ, the profiles were similar in both loading directions, and remained stable at repeated cycles. The length of the plastic hinge was about 250 mm. Fig. D.26 also shows the yield curvature of this unit. For the calculation of yield curvature, and curvature ductility of test columns, Section E.7.3 is to be referred to.

Fig. D.27 shows the components of deflections. The values of r_f, which is defined as the ratio of deflection calculated from the experimentally obtained curvature profile, Δ_f, to measured total deflection, Δ, at displacement peaks were about 0.78 at $\mu \leq 6$. This confirmed the flexure dominant behaviour of the column up to this stage.

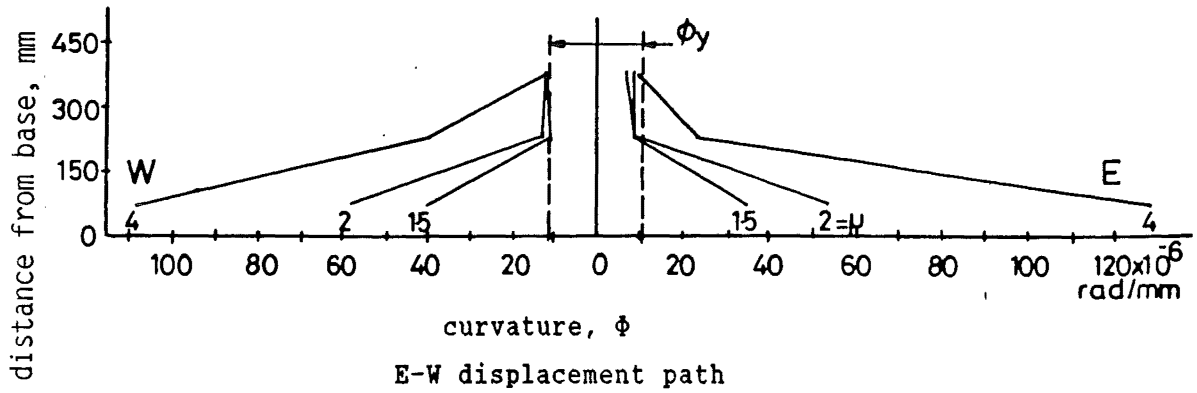

Fig. D.26 : Measured curvature profiles - Unit 1

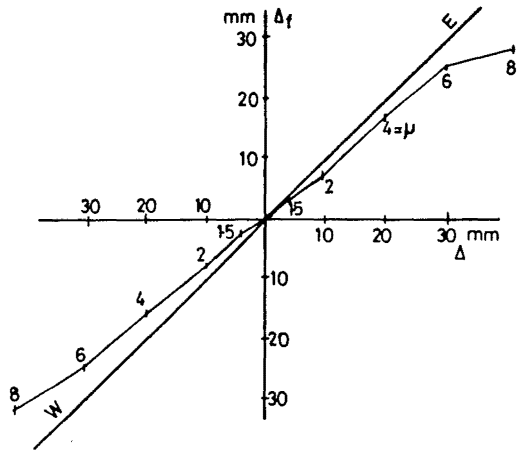

Fig. D.27 : Components of deflections - Unit 1

D.3.1.4 Spiral strain distributions and spiral forces

Fig. D.28 shows the spiral strain distribution. At the peak displacement in the first repeated cycle to $\mu = 1.5$, some spirals in the region of inclined cracks showed yield.

At each displacement peak in cycles to $\mu \geq 2$, spirals crossed either by an inclined crack, consistent with shear, or located in the flexural compression zone at the lower part of the column, reached yield stress.

At zero lateral force, the values of average spiral stresses, normalized by the corresponding spiral yield strength σ_{av}/f_{yt} (Section D.2.7), were approximately 0.18 , 0.36, 0.42, 0.29, 0.20, and 0.90 after the completion of load cycles to μ = 0.75, 1.5, 2, 4, 6, and 8 respectively.

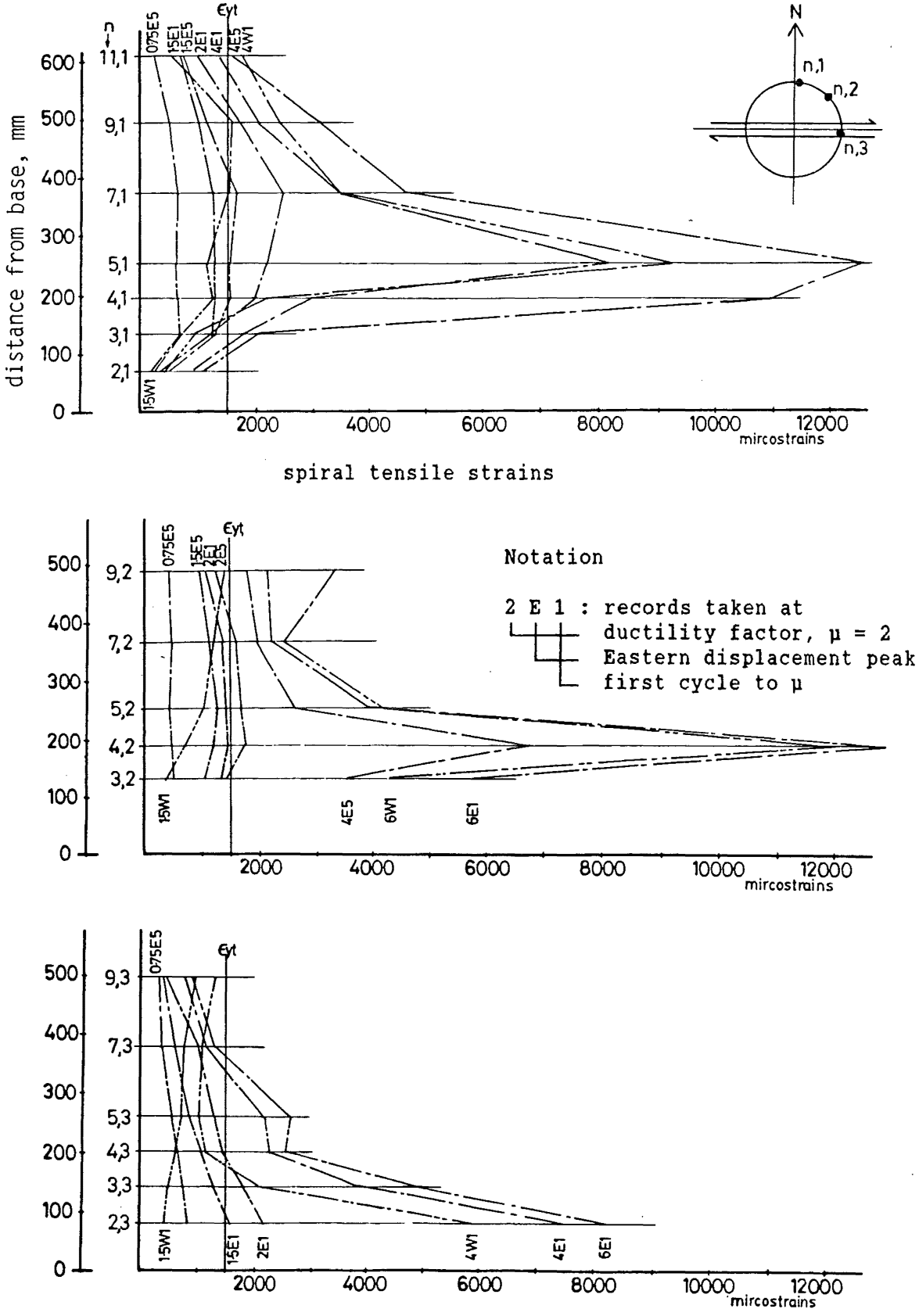

Fig. D.28 : Spiral strain distributions - Unit 1

D.3.2 Unit 2 [4R6-65u]

D.3.2.1 Force - displacement hysteretic performance

During the initial cycle to μ = 0.75, the force - displacement relation was almost linear (Fig. D.29). However, in subsequent load cycles, the force - displacement relation became slightly nonlinear. The lateral resistance reached the ideal flexural strength, V_{if}, in the first cycle to μ = 1.5. However, it was reduced to $0.95V_{if}$ in the repeated load cycles with the same ductility.

The maximum measured resistance, $V_{max} = 1.31V_{if}$ occurred at the displacement $\Delta = 3.6\Delta_y$. At $\Delta = 3.8\Delta_y$ (Point 'a' of Fig. D.29), the axial deformation suddenly increased beyond the pre-set limit of 20 mm. The axial compression load was automatically reduced to 70 kN ($P_i/(f'_cA_g) = 0.015$) for safety purposes. At the same time, the valve of the pump driving the horizontal load jack was closed. The top of column drifted eastward and finally became stable at $7\Delta_y$ with the residual resistance of $0.6V_{if}$ (Point 'b'). In order to complete this load cycle, the residual resistance was released. The design axial load ($P_i/(f'_cA_g) = 0.39$) was re-applied to the column at Point 'c'. At $\Delta = 3.5\Delta_y$ and $4\Delta_y$ westward, V reached $0.85V_{if}$ and $0.7V_{if}$ respectively. The direction of the load was then reversed. At $\Delta = 3.6\Delta_y$ eastward (Point 'd'), a resistance was temporarily maintained at $0.25V_{if}$. The axial deformation again reached the limit of 20 mm. The axial load was then cut off. The final drift of the column was $4.4\Delta_y$ and the residual resistance reduced to $0.05V_{if}$.

The force - displacement curves did not show pinching or energy dissipation of any significance. At $\mu \leq 2$, the response was very stable also during the repeated cycles.

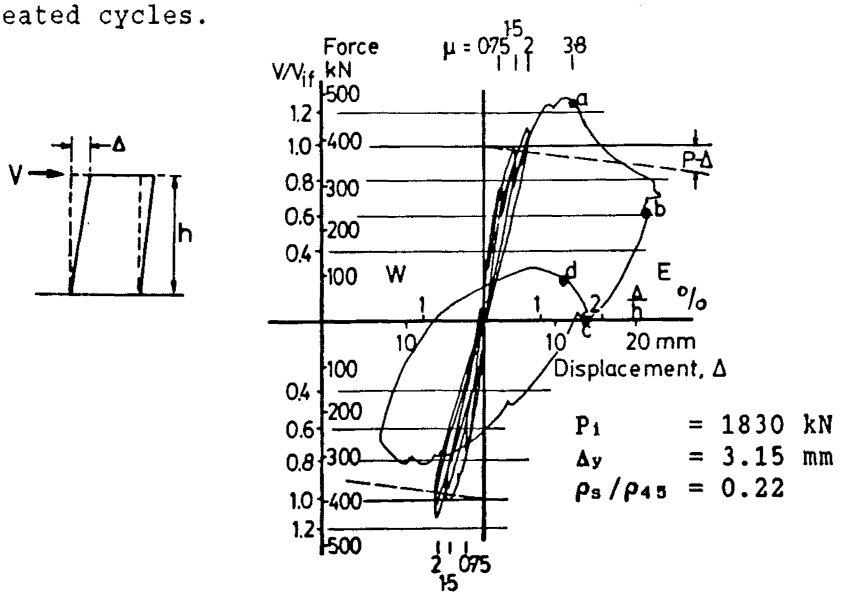

Fig. D.29 : Force - displacement hysteretic curves - Unit 2

D.3.2.2 General performance

Horizontal flexural and inclined cracks were formed at $V = 0.56V_{if}$ and $0.87V_{if}$ respectively. After the cycle to $\mu = 1.5$, inclined cracks at 40° to the vertical developed over the full height of the column.

At $\mu = 2$, existing cracks became extended. Some short inclined cracks at 20° to 30° to the vertical became visible (Fig. D.10a). These grew in numbers to form a band of major diagonal cracks at $\Delta = 3.6\Delta_y$. Large cracks were concentrated at these areas. When the column lost its axial load carrying capacity at the first time, the cover concrete at the eastern side near the column base spalled. Buckled longitudinal bars became visible. No fracture of spiral was noted. The failure was associated with sliding down on a steep diagonal plane shown 'x' in Fig. D.10b.

Before the second reduction of axial load carrying capacity had taken place, all the inclined cracks, formed by the previous loading eastward, were open in a more or less uniform way, that is, no excessive opening at any particular cracks was seen. The column visibly dilated laterally. The lateral resistance at this stage was very low. When the column failed, the cover concrete along the previous diagonal failure plane spalled. All the exposed longitudinal steel bars were buckled. Fracture of spiral was found at four locations. The core concrete was loose. This failure was likely the result of crushing of core concrete together with the sliding down at the previous diagonal failure plane (Fig. D.10c).

D.3.2.3 Curvature profiles and components of deflections

At $\mu \leq 3$, the curvature profiles maintained the shape typical of the flexural performance (Fig. D.30). For a given μ, the profiles were similar in both loading directions and remained stable at repeated cycles. The length of the plastic hinge was about 250 mm. Curvatures were rather small throughout the test.

Fig. D.31 shows the components of deflections. The ratio r_f at each displacement direction was about 0.73 at $\mu \leq 3$. This further confirmed the flexure dominant behaviour of the column up to this stage.

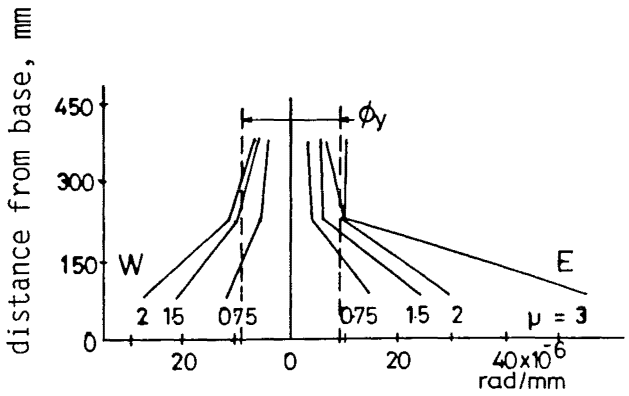

Fig. D.30 : Measured curvature profiles - Unit 2

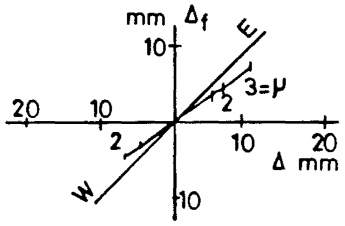

Fig. D.31 : Components of deflections - Unit 2

D.3.2.4 Spiral strain distributions and spiral forces

Fig. D.32 shows spiral strain distributions. During the cycle at $\mu = 0.75$, negligible spiral strains were recorded. Spirals started to yield at $\mu = 2$. At $\mu = 3$, the strains noticeably increased in the region of inclined cracks. Strain exceeding 3% was found in some locations at $\Delta = 3.6\Delta_y$.

At each displacement peak in cycles to $\mu \geq 2$, spirals crossed by inclined cracks, consistent with shear, reached yield stress.

At the zero lateral force, the values of σ_{av}/f_{yt} were 0.06, 0.33, and 0.47 after the completion of cycles to $\mu = 0.75$, 1.5, and 2 respectively.

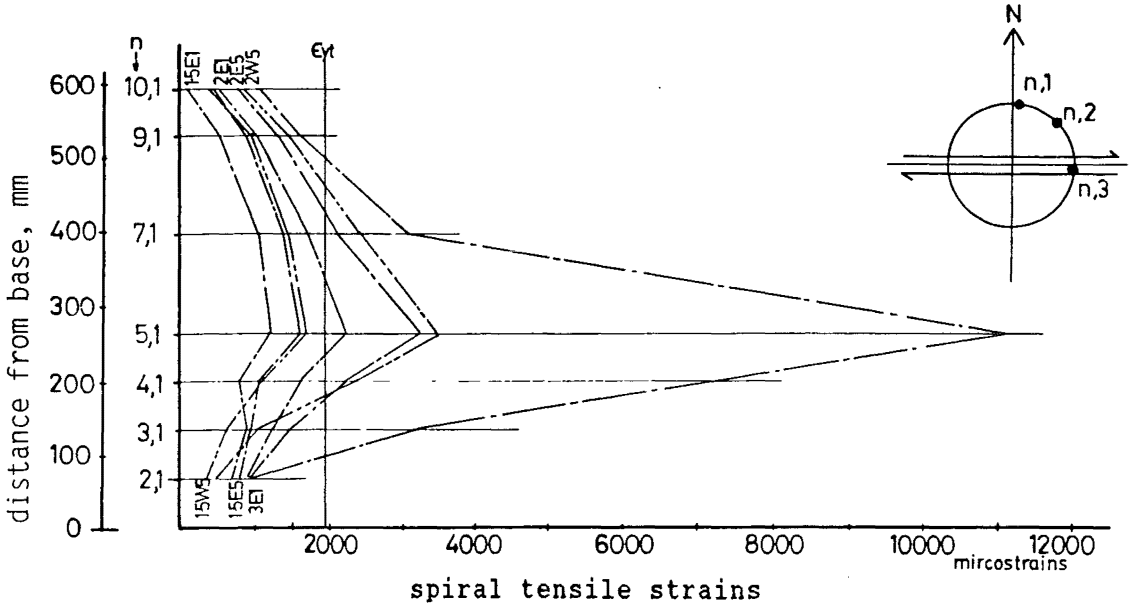

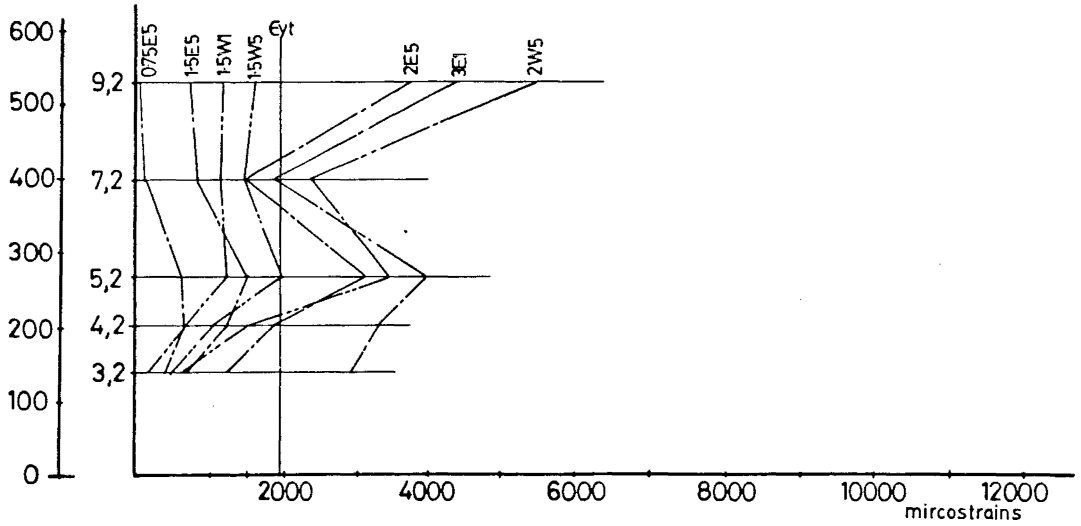

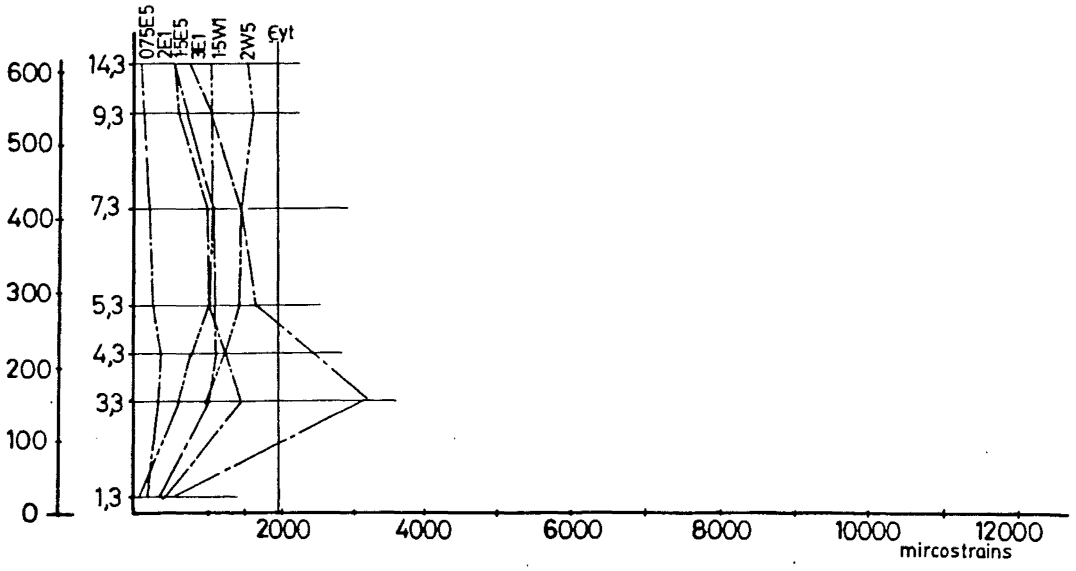

Fig. D.32 : Spiral strain distributions - Unit 2

D.3.3 Unit 3 [4R10-60u]

D.3.3.1 Force - displacement hysteretic performance

The force - displacement relation during the initial elastic cycle was very similar to that of Unit 2. At μ = 1.5, the lateral resistance reached $1.06V_{if}$ (Fig. D.33). The maximum measured strength, V_{max}, equal to $1.63V_{if}$ was recorded during the first cycle at μ = 6.

At $\mu \leq 6$, there was some reduction in both strength and stiffness in the first repeated cycle. However, hysteretic response became very stable in subsequent repeated cycles. During loading eastward of the third cycle with μ = 8, the rates of strength and stiffness degradation increased. At $\Delta = 7\Delta_y$, buckling of the longitudinal bars in the flexural compression zone caused a sudden drift to the final displacement of $10\Delta_y$. At this stage, the column still carried the applied axial compression with a lateral force resistance of $0.89V_{if}$.

No pinching was observed in the hysteretic response. The overall performance, also showing significant strength enhancement due to the increased compression strength of the confined concrete, may be considered to be excellent.

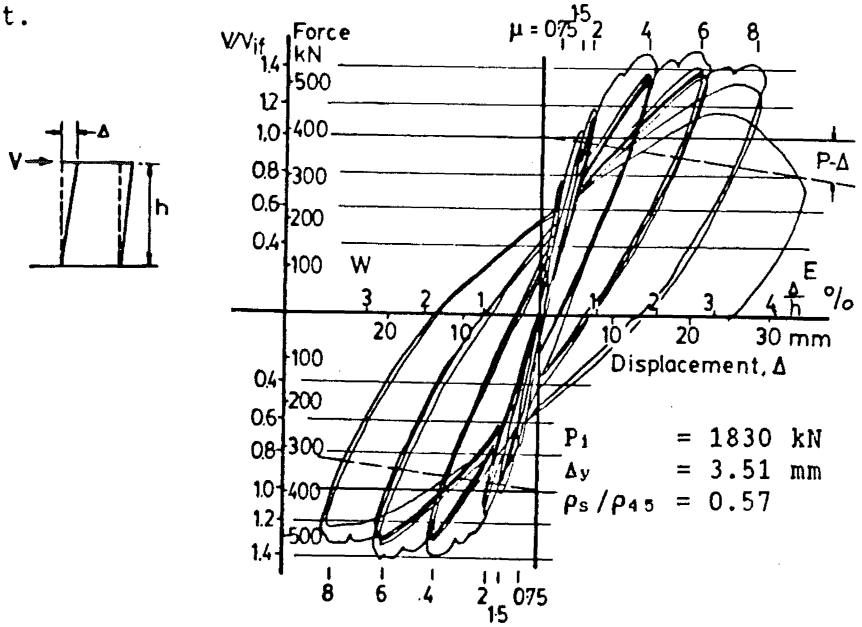

Fig. D.33 : Force - displacement hysteretic curves - Unit 3

D.3.3.2 General performance

Horizontal flexural and inclined cracks were noted at $V = 0.46V_{if}$ and $0.84V_{if}$ respectively. At μ =1.5, the inclined cracks at 40° to the vertical extended over the full height of the column. As ductility increased, the existing cracks extended further, and new cracks at about 35° to the vertical formed.

Spalling of cover concrete first appeared at μ=3. At μ = 4, the crack pattern fully developed as seen in Fig. D.11a.

The column failed due to buckling of some longitudinal bars during the third cycle to μ = 8 (Fig. D.11b). Cover concrete spalling extended to 450 mm above the column base. The core concrete remained relatively intact. No fracture of spiral was found. Throughout the loading history, the opening of inclined cracks was more or less uniform.

D.3.3.3 Curvature profiles and components of deflections

The curvature profiles of this unit were very regular at all displacement levels (Fig. D.34). At μ ≥ 6, the length of plastic hinge increased to about 250 mm. The large curvature ductility developed is indicative of predominant flexural response, consistent with the hysteretic loops in Fig. D.33.

Fig. D.35 shows the components of deflections. The value of r_f at each displacement direction was approximately 0.75 throughout the loading history.

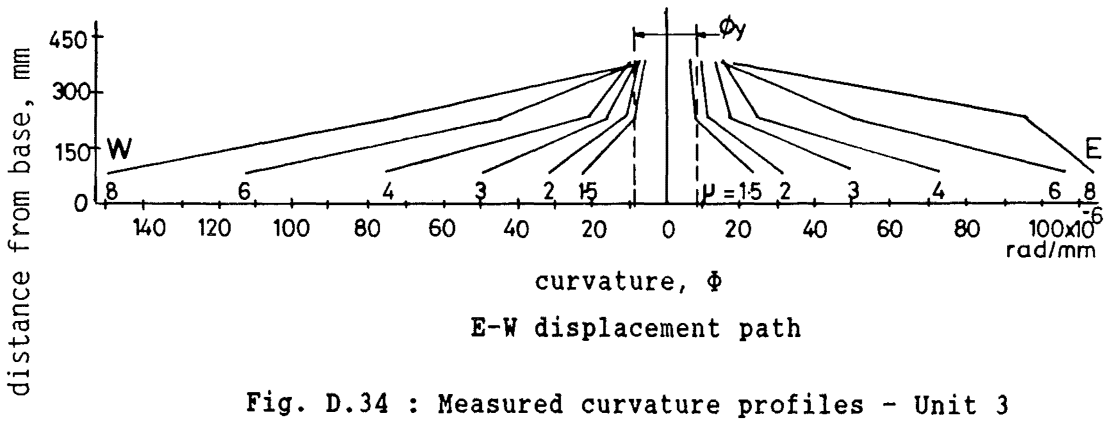

Fig. D.34 : Measured curvature profiles - Unit 3

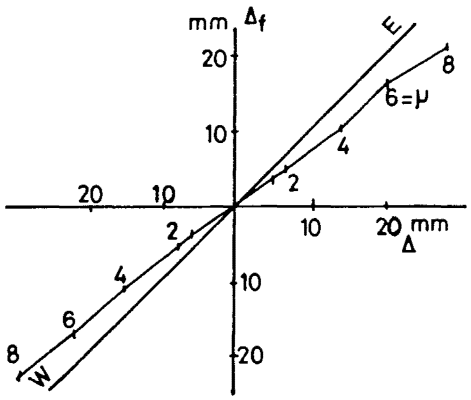

E-W displacement path

Fig. D.35 : Components of deflections - Unit 3

D.3.3.4 Spiral strain distributions and spiral forces

During the cycle to V = $0.75V_{if}$, negligible spiral strain readings were recorded. Some spirals started to yield at μ = 4 (Fig. D.36). At μ = 8, spiral strains significantly increased. Throughout the loading history, only two strain readings exceeded 3%. At each displacement peak in cycles to μ ≥ 4, spirals crossed either by an inclined crack, consistent with shear, or located in the flexural compression region reached yield stress.

The values of σ_{av}/f_{yt} at zero lateral force were 0.10, 0.32, 0.40, 0.44, 0.42, and 0.46 after the completion of cycles to μ = 0.75, 1.5, 2, 4, 6, and 8 respectively.

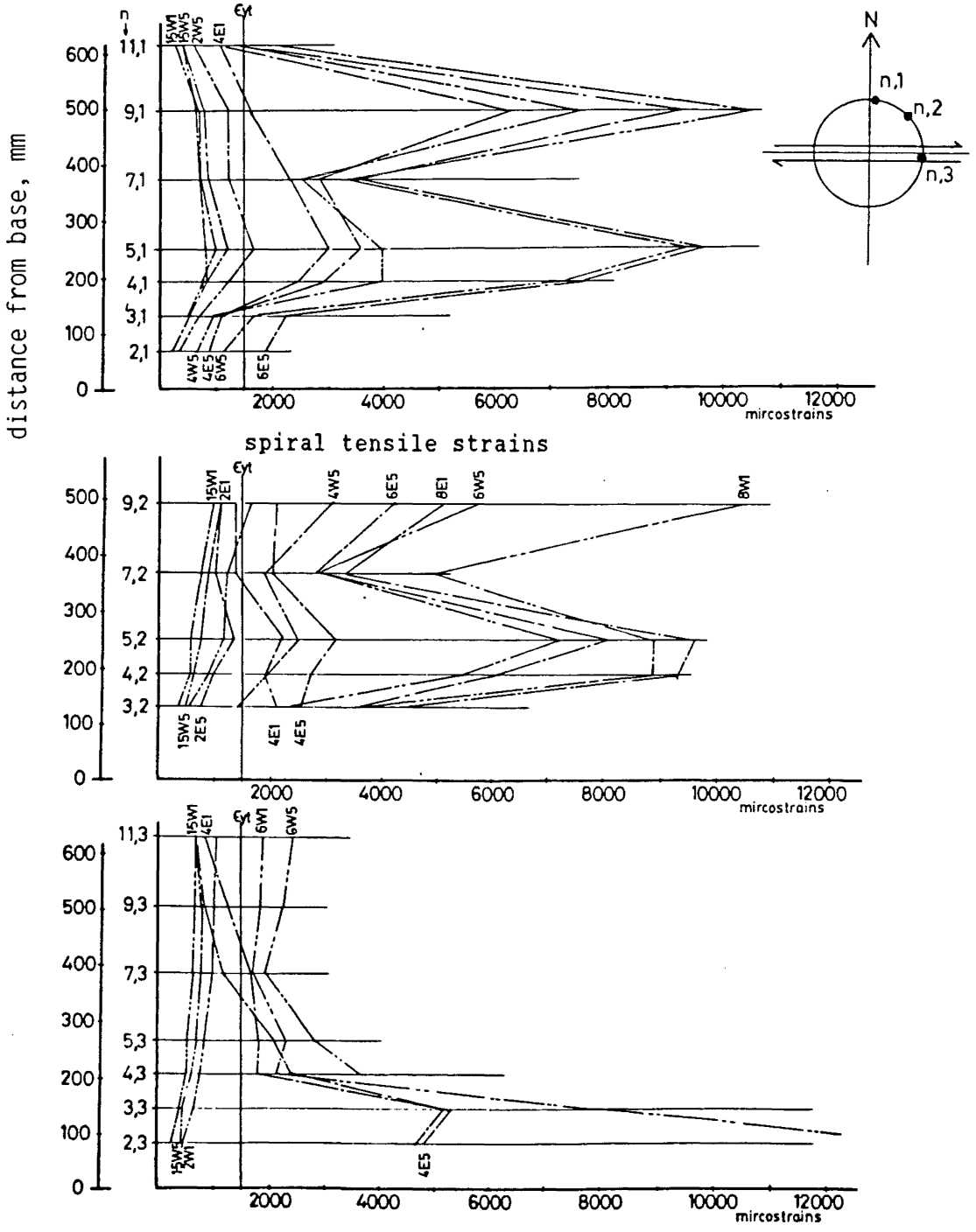

Fig. D.36 : Spiral strain distributions - Unit 3

D.4 COLUMNS SUBJECTED TO BI-DIRECTIONAL 'b' DISPLACEMENT PATTERN

D.4.1 Unit 4 [OR6-80b]

D.4.1.1 Force - displacement hysteretic performance

During the cycle to $\mu = 0.75$, the force - displacement relation was not linear. The maximum measured strength, $V_{max} = 0.97V_{if}$ occurred during the first displacement path (North-South, see Fig. C.5) in the first cycle to $\mu = 1.25$. However, the resistance was less than 80% of V_{if} in the repeated cycle to the same ductility.

Within a cycle, the resistance varied with different displacement peaks (Fig. D.37). The ratios of strengths, listed in the sequence of displacement peaks were about 1.00 : 0.90 : 0.80 : 0.88, and 1.00 : 0.86 : 0.66 : 0.70 at $\mu = 1.25$, and 3 respectively.

At $\mu \leq 2$, loss in strength during the repeated cycle was 16% to 30% of that developed first in the first displacement path, and 14% to 20% of that developed first in the second displacement path (East-West). During the first repeated cycle to $\mu = 2$, the degradation of strength became pronounced. An additional repeated cycle was applied. The strength was then relatively stable at $0.56V_{if}$ in the first displacement path, and $0.46V_{if}$ in the second displacement path.

In the first cycle to $\mu = 3$, the strengths developed were $0.75V_{if}$ and $0.65V_{if}$ in the first displacement path, and $0.5V_{if}$ and $0.53V_{if}$ in the second displacement path. The column was finally deflected northward to $5\Delta_y$ with a residual strength of $0.67V_{if}$.

Pinching of the hysteretic curves was noted already at $\mu = 1.25$ and became very pronounced with increased ductility.

D.4.1.2 General performance

Horizontal flexural cracks firstly appeared at $V = 0.13V_{if}$. Spiral strain gauge readings indicated that inclined cracks occurred at $V = 0.38V_{if}$. However, they became visible only at $V = 0.62V_{if}$. After the cycle to $V = 0.75V_{if}$, the inclined cracks extended over the full height of the column.

At μ = 1.25, four sets of major corner to corner cracks, at 20° to 30° to the vertical, developed at four displacement peaks respectively (Fig. D.12a). Local crushing of cover concrete near the column base was also observed.

At μ = 2, few new cracks formed. Spalling of cover concrete also occurred. During the second repeated cycle, more extensive spalling of cover concrete was observed.

No sign of fracture or buckling of spirals and longitudinal bars was found at the end of the test (Fig. D.12b). The core concrete remained well confined. Cracks within the confined core were also identified. Some of them cut across coarse aggregate particles. As expected, they was continuation of the surface cracks.

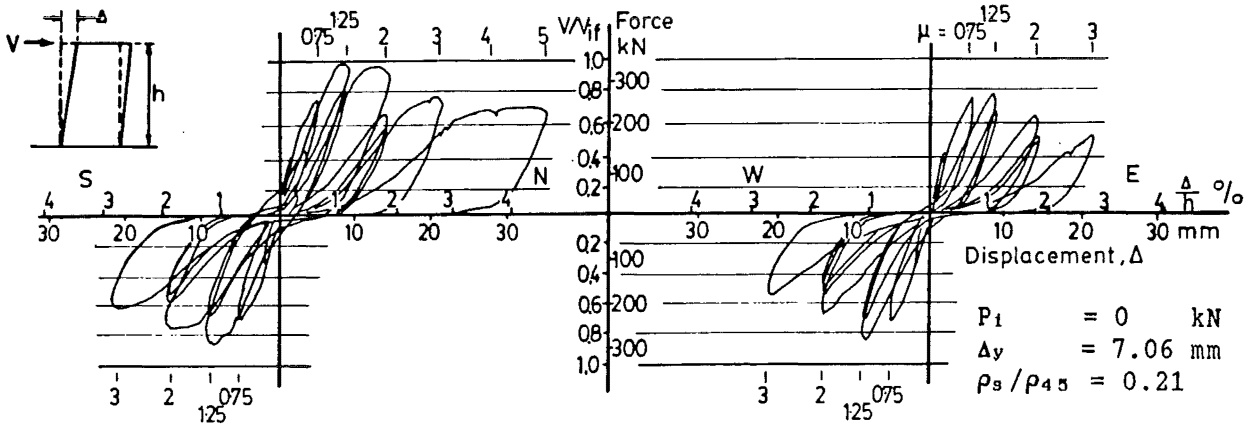

(a) First displacement path (b) Second displacement path

Fig. D.37 : Force - displacement hysteretic curves - Unit 4

D.4.1.3 Curvature profiles and components of deflections

At μ = 1.25, curvature profiles of both displacement paths were regular and similar (Fig. D.38). At μ = 2, the curvature profiles of the second displacement path became irregular. The sign of curvature near the loaded end was reversed. The length of plastic hinge was estimated to be 200 mm. It is seen in Fig. D.38 that curvature ductility developed was rather small.

The components of deflections are shown in Fig. D.39. At μ = 1.25, the values of r_f were 0.6 in the first displacement path, and 0.5 in the second displacement path. At μ = 2, the corresponding r_f values became 0.4 and 0.3 respectively indicating the preponderance of shear deformations.

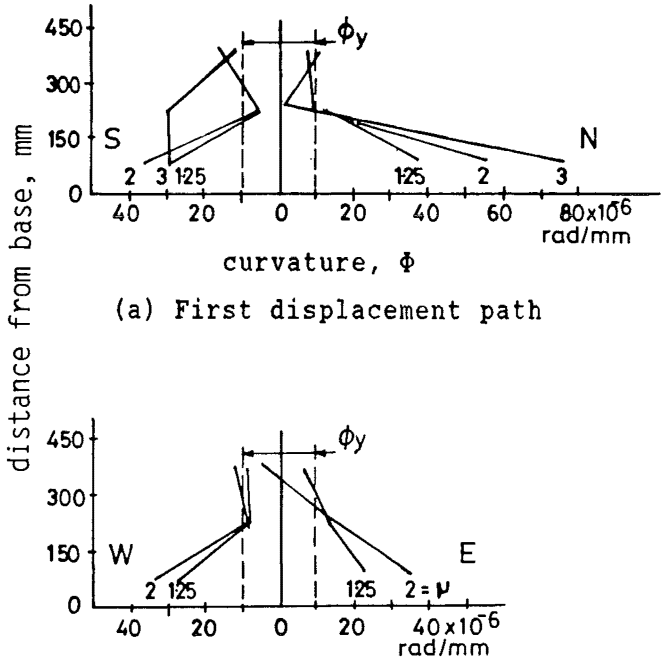

(a) First displacement path

(b) Second displacement path

Fig. D.38 : Measured curvature profiles - Unit 4

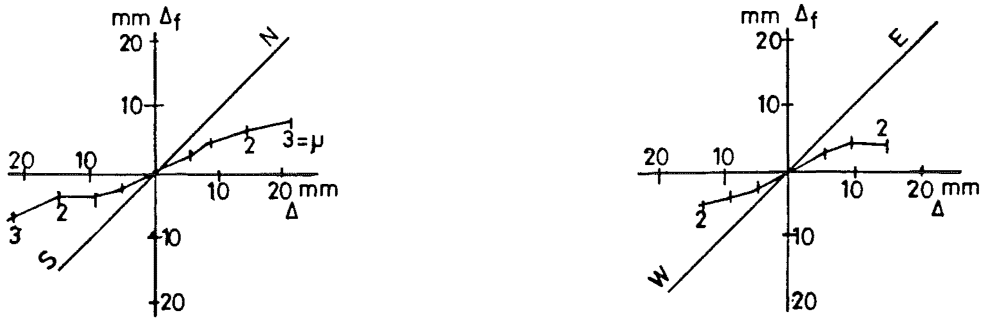

(a) First displacement path

(b) Second displacement path

Fig. D.39 : Components of deflections - Unit 4

D.4.1.4 Spiral strain distributions and spiral forces

During the initial cycle to V = 0.37 V_{if}, no spiral strains were recorded. Some spirals started to yield at the cycle with V = 0.75V_{if} (Fig. D.40). At $\mu \geq 1.25$, the strains increased well beyond yield. At $\mu = 2$, some strains exceeded 3%, a clear evidence of diagonal tension failure due to shear.

At each displacement peak of cycles to $\mu \geq 0.75$, spirals crossed by the inclined cracks, consistent with shear, reached yield stress.

At zero lateral force, the values of σ_{av}/f_{yt} were about 0.37 and 0.13 after the completion of cycles to μ = 0.75 and 1.25 respectively.

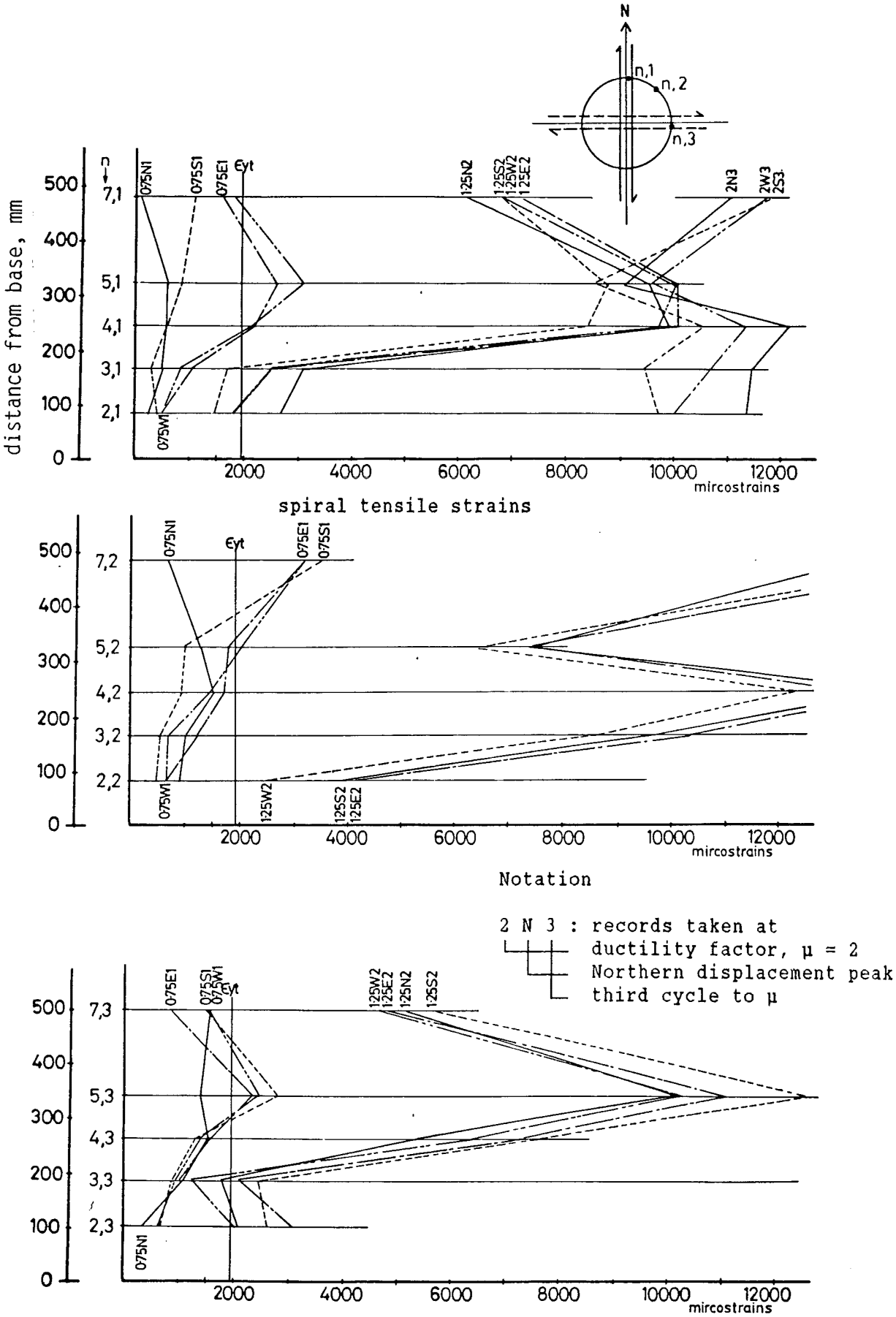

Fig. D.41 : Spiral strain distributions - Unit 4

D.4.2 Unit 5 [0R6-50b]

D.4.2.1 Force - displacement hysteretic performance

In the first cycle to μ =1.25, the resistance reached V_{if}. The maximum measured strength, V_{max} = 1.06V_{if} was recorded in the first displacement path (N-S) of the first cycle to μ =2 (Fig. D.41).

For 4 ≥ μ ≥ 1.25, the ratios of strengths, listed in the sequence of displacement peaks, were about 0.98 : 1.00 : 0.88 :0.87 in the first cycles, and 1.00 : 0.99 : 0.97 : :0.96 in the repeated cycles. Loss of strength during a repeated cycle was 13% to 24% of that developed first in the first displacement path, and 5% to 18% of that developed first in the second displacement path (E-W).

Remarkable strength degradation took place in the repeated cycle to μ =3. However, the strength was stable at 0.62V_{if} in the third and fourth cycles. The column was displaced further to μ = 4. During the first cycle, the strength was 0.79V_{if} in the first displacement path, and 0.67V_{if} in the second displacement path. These resistances rapidly reduced to 0.61V_{if} and 0.58V_{if} in the first repeated cycles. Two more cycles were applied before the end of the test. The residual strengths reduced to 0.5V_{if} in all four peak displacements.

The pattern of stiffness degradation and pinching of hysteretic curves were similar to those of Unit 4, although strengths developed throughout the test were larger.

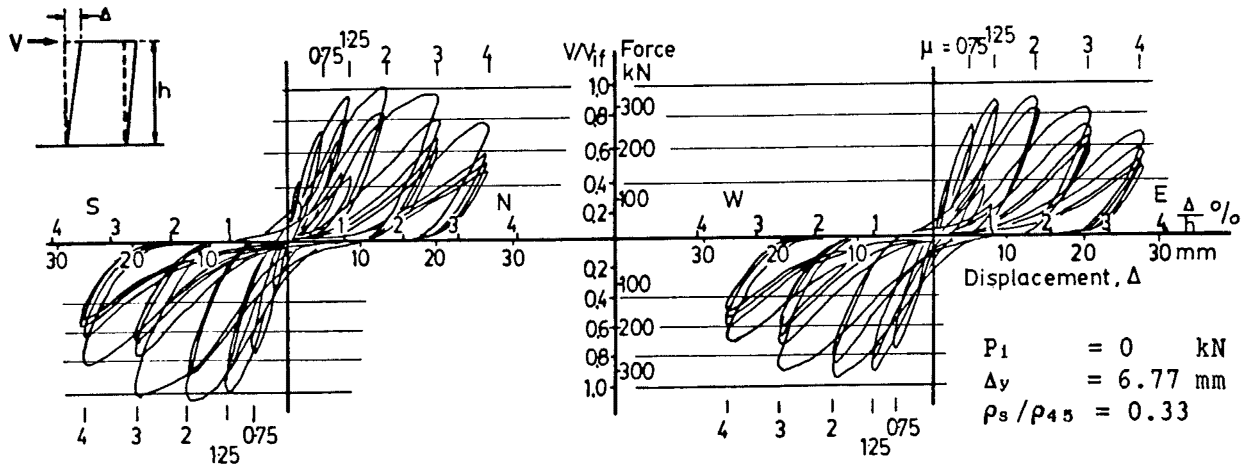

(a) First displacement path (b) Second displacement path

Fig. D.41 : Force - displacement hysteretic curves - Unit 5

D.4.2.2 General performance

Horizontal flexural cracks appeared at $V = 0.15V_{if}$. The onset of inclined cracks was observed at $V = 0.36V_{if}$ as indicated by spiral strain readings. They became visible only at $0.56V_{if}$. After the cycle to $\mu = 0.75$, the inclined cracks at 35° to the vertical extended to 600 mm above the column base.

At $\mu = 1.25$, inclined cracks developed over the full height of the column. Local crushing of cover concrete occurred at the repeated cycle.

At $\mu = 2$, inclined corner to corner cracks at 20° to 25° to the vertical formed. They became the major cracks where most of crack widening took place. Crack patterns formed during loading to each displacement peak were similar.

Spalling of cover concrete started at the repeated cycle to $\mu = 2$ (Fig. D.13a). During the third repeated cycle to $\mu = 3$, all the cover concrete of the column spalled. After the test, the core concrete was still well confined (Fig. D.13b). No fracture of spirals or buckling of longitudinal bars was found.

D.4.2.3 Curvature profiles and components of deflections

At $\mu \leq 3$, the curvature profiles were of regular flexural type (Fig. D.42). At $\mu = 4$, the sign of curvature near the loaded end was reversed. Plastic hinge rotation concentrated at the lower 200 mm region of the column.

Fig. D.43 shows the components of deflections. At $\mu = 2$, the value of r_f was about 0.62 in both displacement paths. At $\mu = 4$, these values reduced to 0.54 in the first displacement path, and 0.42 in the second displacement path.

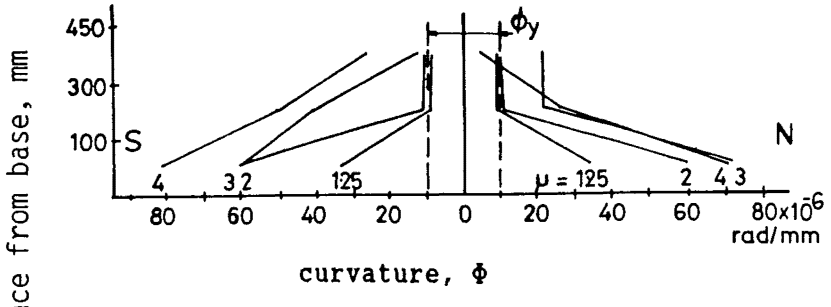

(a) First displacement path

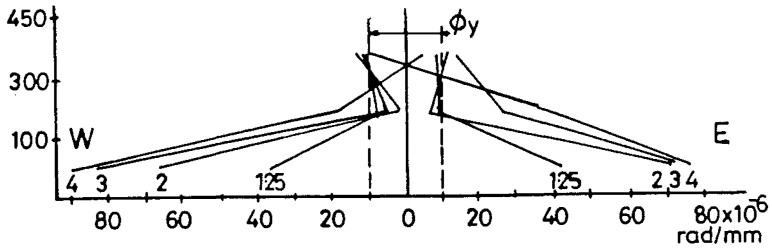

(b) Second displacement path

Fig. D.42 : Measured curvature profiles - Unit 5

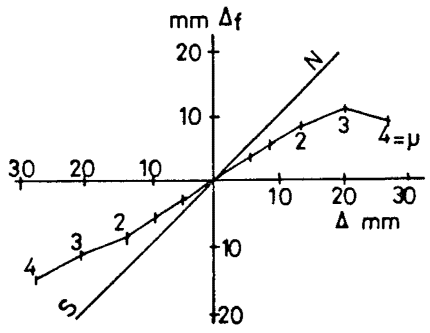

(a) First displacement path

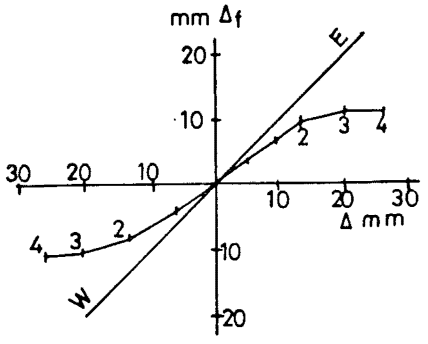

(b) Second displacement path

Fig. D.43 : Components of deflections - Unit 5

D.4.2.4 Spiral strain distributions and spiral forces

Spiral strain profiles (Fig. D.44) indicated that most spirals yielded at μ = 1.25. At $\mu \geq 3$, some spiral strains exceeded 3%.

In a cycle to $\mu \geq 1.25$, spirals crossed by inclined cracks, consistent with shear, reached yield stress at each displacement peak.

At zero lateral force, the values of σ_{av}/f_{yt} were about 0.29 and 0.10 after the completion of cycles to μ = 1.25 and 2 respectively.

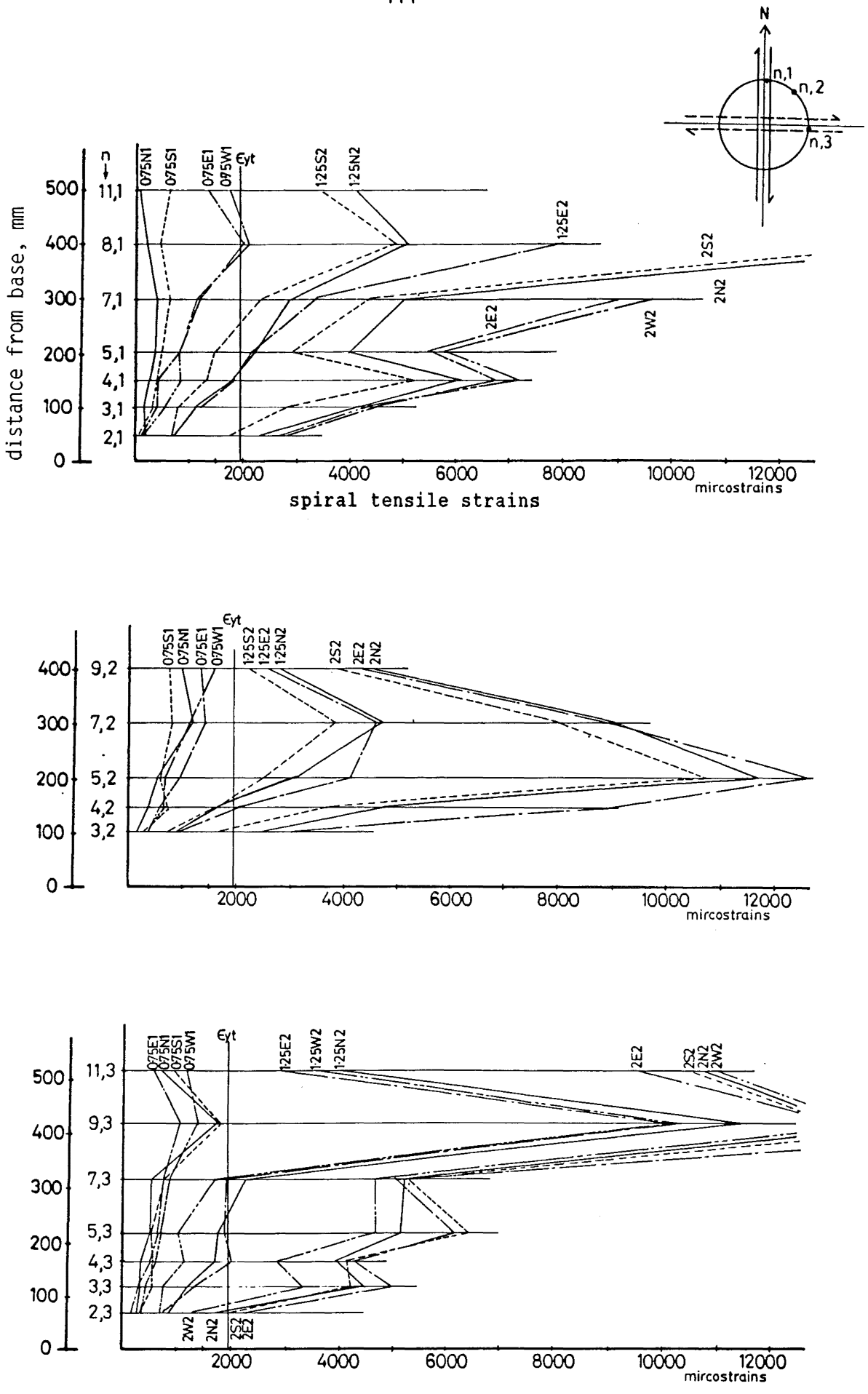

Fig. D.44 : Spiral strain distributions - Unit 5

D.4.3 Unit 6 [OR6-30b]

D.4.3.1 Force - displacement hysteretic performance

The strength reached $1.03V_{if}$ in the first cycle to $\mu = 1.25$ (Fig. D.45). The maximum measured strength $V_{max} = 1.09V_{if}$ was attained in the first cycle to $\mu = 3$.

At $1.25 \leq \mu \leq 4$, the ratios of strengths, listed in the sequence of the displacement peaks, were about 0.96 : 1.00 : 0.92 : 0.89 in the first cycles and 0.98 : 1.00 : 1.00 :0.95 in the repeated cycles. Loss in strength during a repeated cycle was 9% to 17% of that developed first in the first displacement path, and 4% to 12% of that developed first in the second displacement path.

Only at $\mu = 5$, did the degradation of strength become pronounced. In the repeated cycle, the resistance was below 80% of V_{if}. At the last cycle to $\mu = 6$, one spiral fractured. Strengths developed immediately before and after the spiral fracture were $0.65V_{if}$ and $0.53V_{if}$ respectively.

Pinching of hysteretic curves was visible at and beyond $\mu \geq 2$.

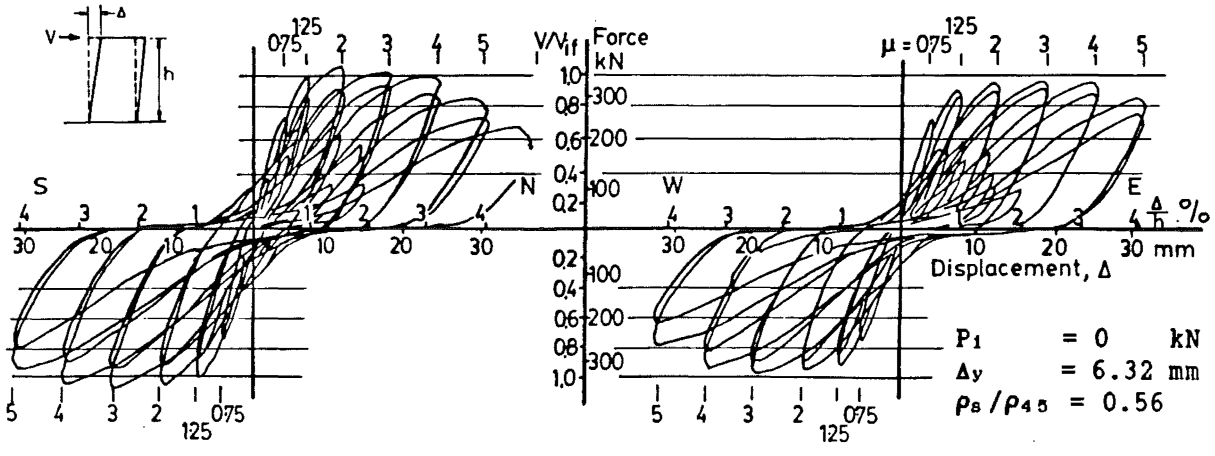

(a) First displacement path (b) Second displacement path

Fig. D.45 : Force - displacement hysteretic curves - Unit 6

D.4.3.2 General performance

Horizontal flexural and inclined cracks were observed at $0.17V_{if}$ and $0.37V_{if}$ respectively. After the cycle to $\mu = 0.75$, inclined cracks at 42° to 45° to the vertical extended to 700 mm above the column base.

Local crushing of cover concrete occurred near the column base in the repeated cycle to $\mu = 1.25$.

At $\mu = 2$, the inclination of main inclined cracks became 30° to 33° to the vertical (Fig. D.14a). Crack patterns were similar for all four displacement peaks. Some spalling of cover concrete was noted in the repeated cycle.

At $\mu = 5$, the cover concrete within 300 mm above the column base completely spalled. Finally, the column failed due to fracture of the spiral adjacent to a welded splice at $\Delta = 6\Delta_y$. The core concrete remained well confined by the spirals (Fig. D.14b).

D.4.3.3 Curvature profiles and components of deflections

At $\mu < 5$, curvature profiles at each displacement peak were regular and similar (Fig. D.46). The estimated length of plastic hinge was 200 mm. At $\mu = 5$, irregularity of curvature distribution was noted. Significant curvature ductility did develop.

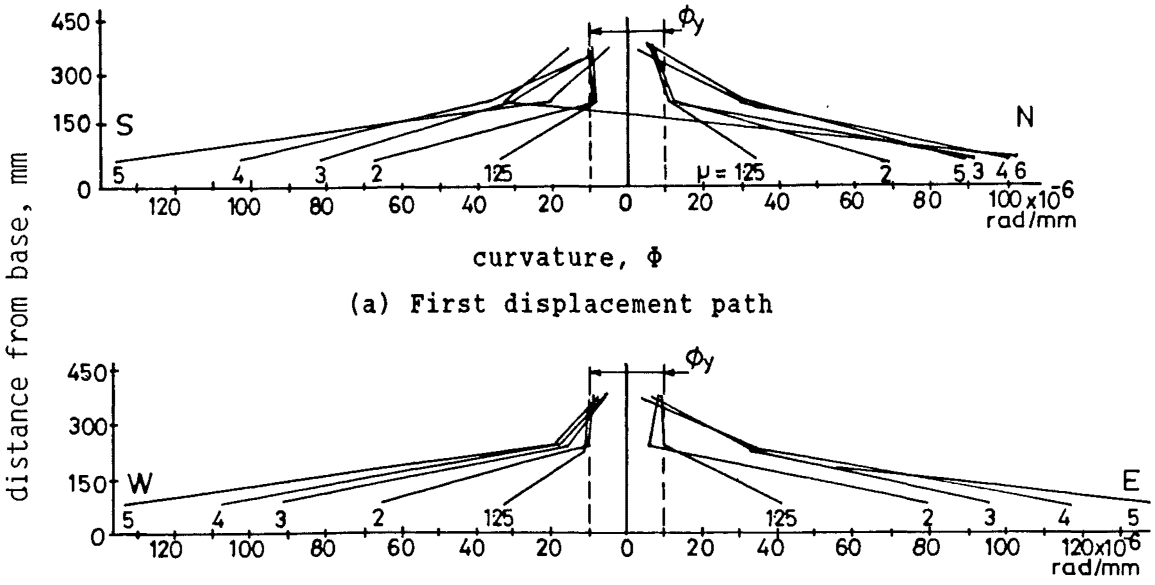

(a) First displacement path

(b) Second displacement path

Fig. D.46 : Measured curvature profiles - Unit 6

Fig. D.47 shows the components of deflections. The values of r_f at each displacement peak were about 0.73 at $\mu = 3$, and 0.48 at $\mu = 5$.

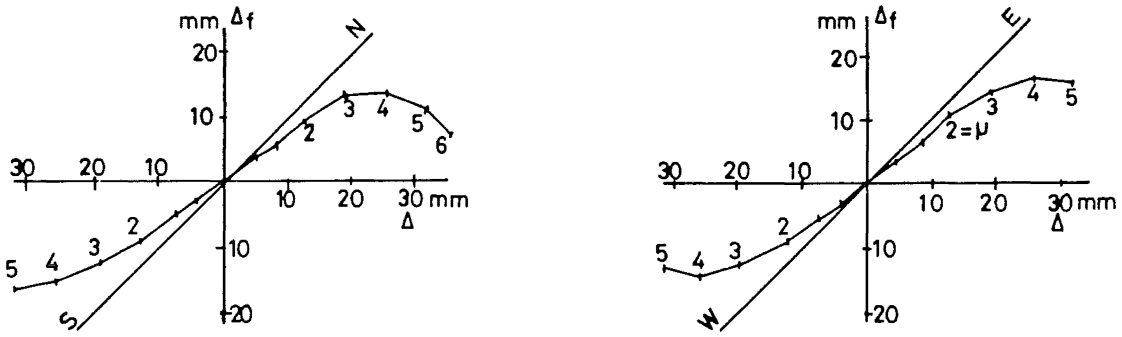

(a) First displacement path (b) Second displacement path

Fig. D.47 : Components of deflections - Unit 6

D.4.3.4 Spiral strain distributions and spiral forces

At $V = 0.37V_{if}$, only some strains were measured. Some spirals started to yield at $\mu = 2$ (Fig. D.48) . During the repeated cycle to $\mu = 4$, strain at several locations exceeded 3%.

At each displacement peak in cycles to $\mu \geq 2$, spirals intercepted by inclined cracks, consistent with shear, reached yield stress.

At zero lateral force, the values of σ_{av}/f_{yt} were about 0.24 and 0.10 after the completion of cycles to $\mu = 1.25$ and 3 respectively.

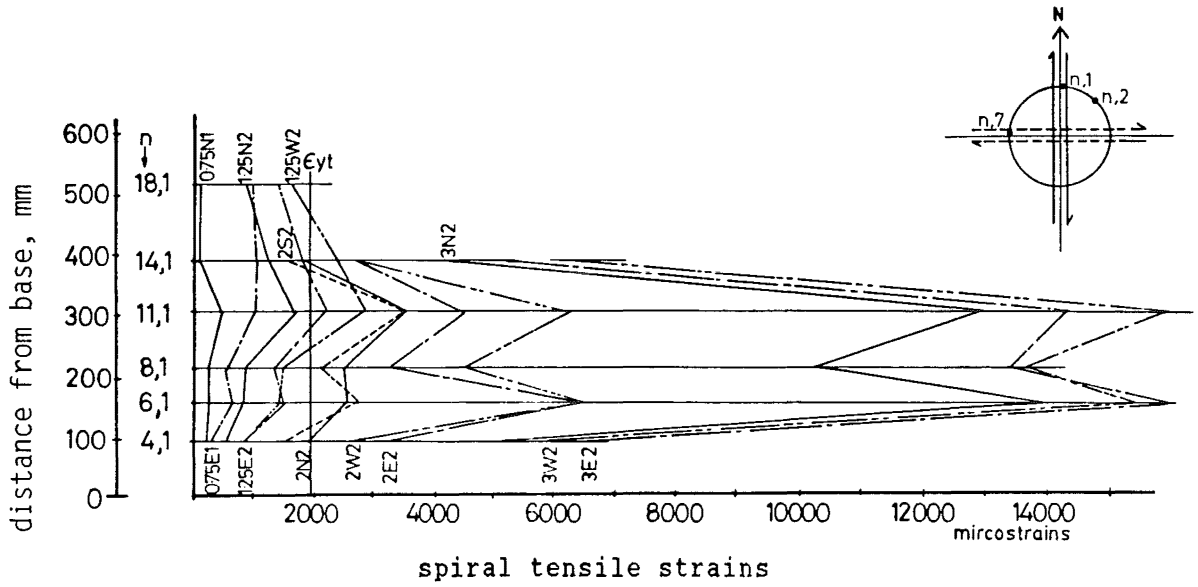

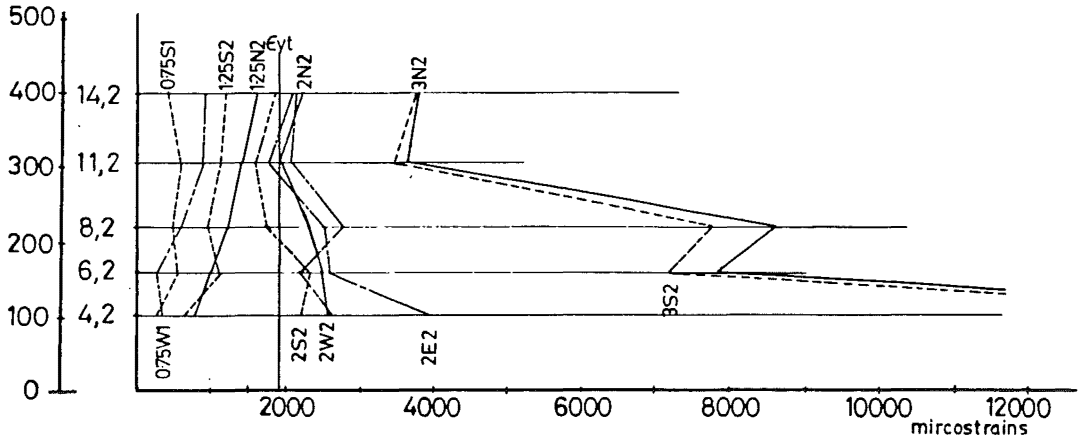

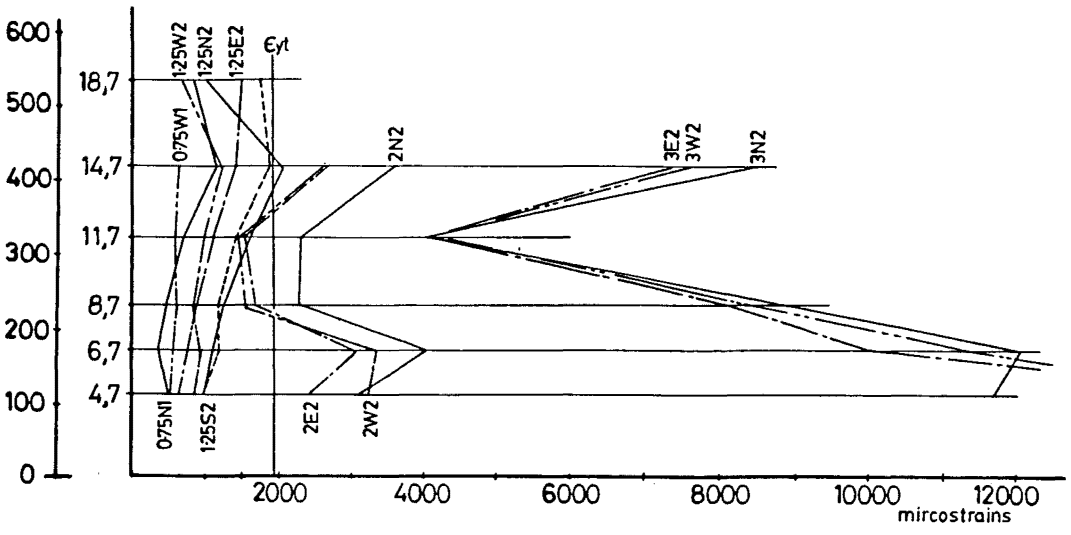

Fig. D.48 : Spiral strain distributions - Unit 6

D.4.4 Unit 7 [2R6-60b]

D.4.4.1 Force - displacement hysteretic performance

During the cycle to $\mu = 0.75$, the force - displacement relationship was no longer linear. In the first cycle to $\mu = 1.25$, the strength reached was V_{if} in the first displacement path, and it reduced to $0.92V_{if}$ in the second displacement path (Fig. D.49). In the repeated cycle, the strength was about $0.92V_{if}$ in all four displacement peaks.

In the first cycle to $\mu = 2$, the maximum measured strength $V_{max} = 1.14V_{if}$ developed at the first displacement peak. While maintaining this displaced position, an external electric interference caused the applied axial load of $0.19f'_cA_g$ to reduce suddenly by 92%. The column was instantaneously displaced northward to $9.5\Delta_y$. The residual strength was $0.65V_{if}$. When the lateral load was released, the permanent displacement was $2\Delta_y$. The initial axial compression was re-applied and this cycle was completed with the strengths $0.81V_{if}$, $0.55V_{if}$, and $0.45V_{if}$ at the subsequent displacement peaks.

The column was subjected to a final displacement in the north direction. At $\Delta = 4\Delta_y$, the strength developed was $0.51V_{if}$. Spiral fracture took place at $5\Delta_y$, and the strength reduced to $0.4V_{if}$. The column sustained the design axial compression load.

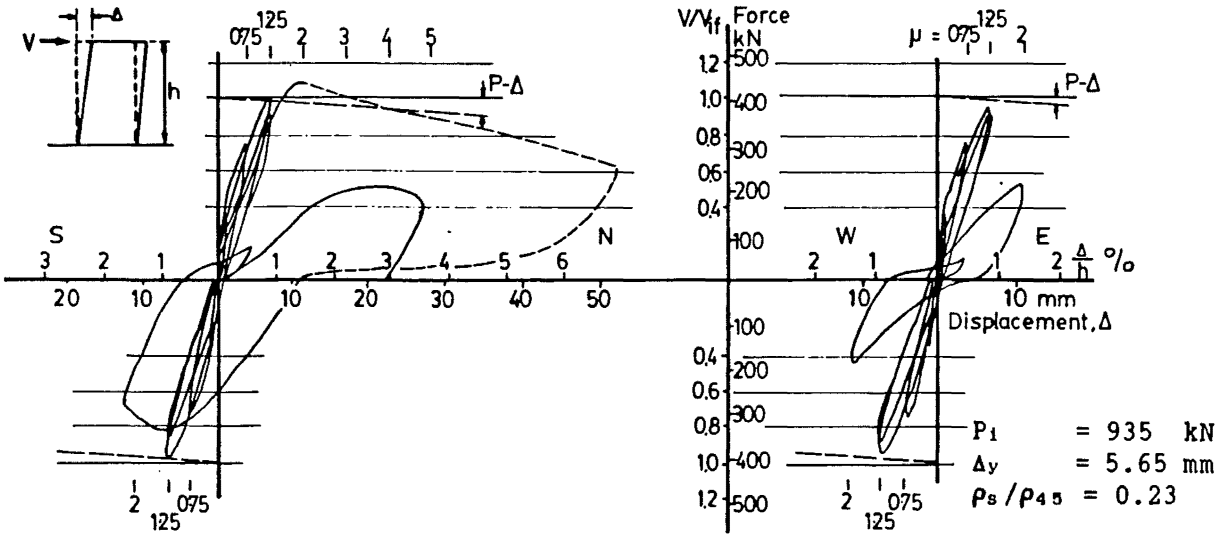

(a) First displacement path (b) Second displacement path

Fig. D.49 : Force - displacement hysteretic curves - Unit 7

D.4.4.2 General performance

Horizontal flexural and inclined cracks were observed at $0.32V_{if}$ and $0.62V_{if}$ respectively. At $\mu = 0.75$, diagonal cracks extended to 500 mm above the column base.

At $\mu = 1.25$, new and steeper cracks developed (Fig. D.15a). Crack angles were 30° to 35° to the vertical in the first displacement path, and 35° to the vertical in the second displacement path. Local crushing of cover concrete occurred before $\Delta = 1.25\Delta_y$.

After the test, a band of dislocated cover concrete along the diagonal failure plane was removed (Fig. D.15b). This revealed that one spiral was fractured.

D.4.4.3. Curvature profiles and components of deflections

At $\mu = 1.25$, curvature distribution was almost linear (Fig. D.50). After the sudden drift northward to $9.5\Delta_y$, the regular distribution of curvature was disturbed.

The value of r_f at each displacement peak was about 0.6 at $\mu = 1.25$.

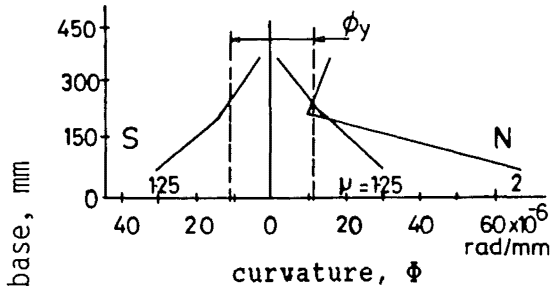

(a) First displacement path

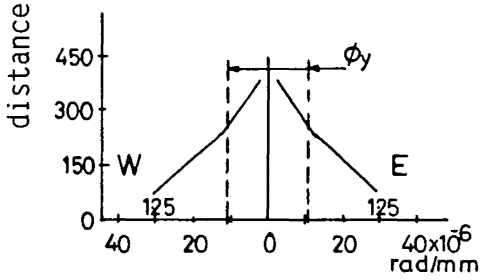

(b) Second displacement path

Fig. D.51 : Measured curvature profiles - Unit 7

D.4.4.4 Spiral strain distributions and spiral forces

Fig. D.51 shows typical spiral strain profiles for this column. Noticeable strains were recorded at μ =0.75. Some spirals started to yield in the first cycle to μ = 1.25. At the displacement to 9.5Δ_y, some strains exceeded 3%. In the repeated cycle to μ = 1.25, spirals crossed by the inclined cracks, consistent with shear, reached yield stress at each displacement peak.

At zero lateral force, the values of σ_{av}/f_{yt} were about 0.33 and 0.5 after the completion of cycles to μ = 0.75 and 1.25 respectively.

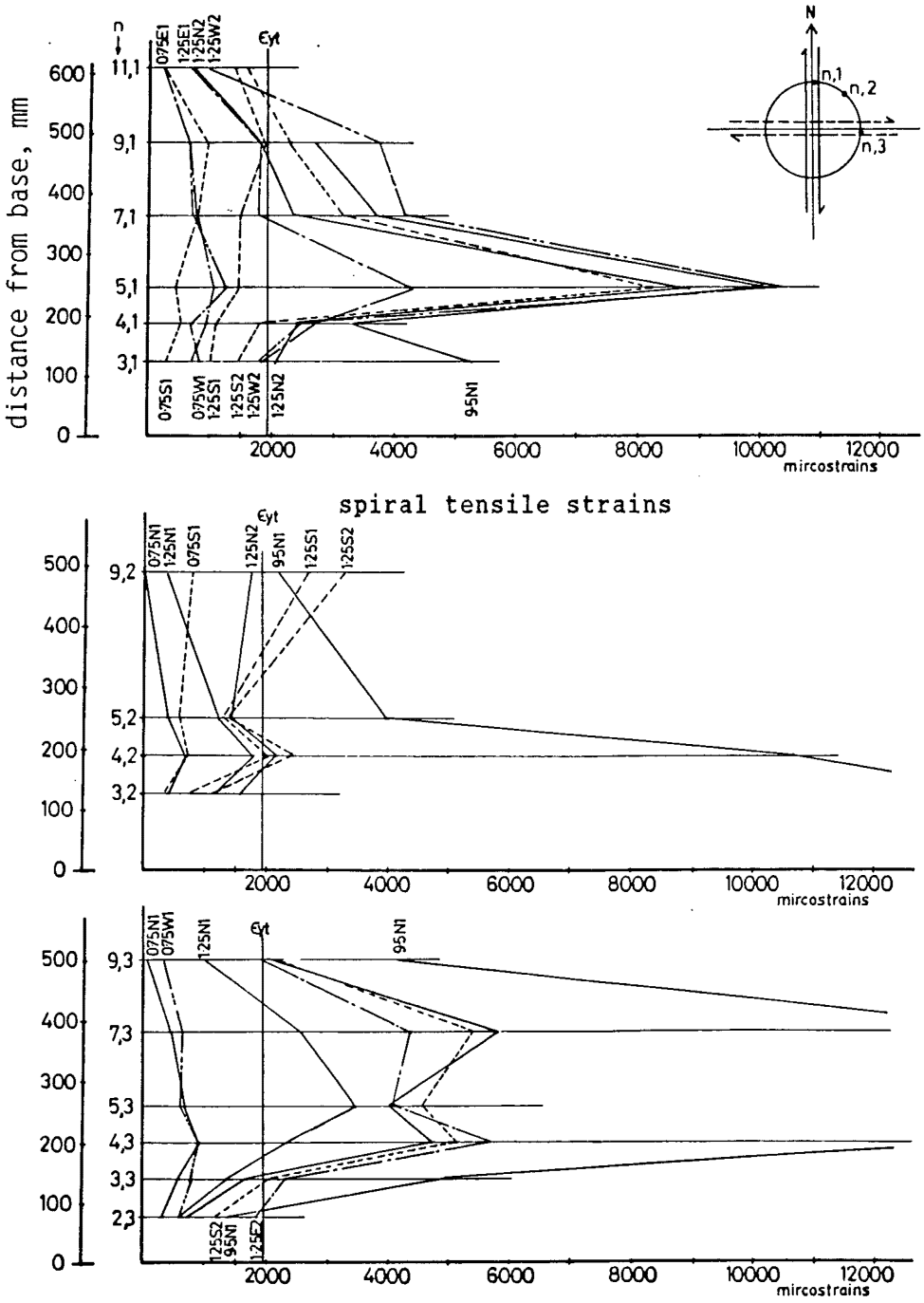

Fig. D.51 : Spiral strain distributions - Unit 7

D.4.5 Unit 8 [2R6-30b]

D.4.5.1 Force - displacement hysteretic performance

At μ = 1.25, the resistance reached V_{if}. The maximum measured resistance was $1.24V_{if}$ in the first cycle to μ = 3 (Fig. D.52).

At $\mu \leq 4$, the variation of strengths at displacement peaks was small within the same cycle with a maximum difference of 5%. At $\mu \leq 3$, loss in strength during a repeated cycle was only 3% to 7% of that developed in the first cycle. However, in the repeated cycle to μ = 4, the degradation of strength and stiffness became significant.

At μ = 5, pinching of the hysteretic curves was noted. In the repeated cycle, the strength developed was below 60% of V_{if}.

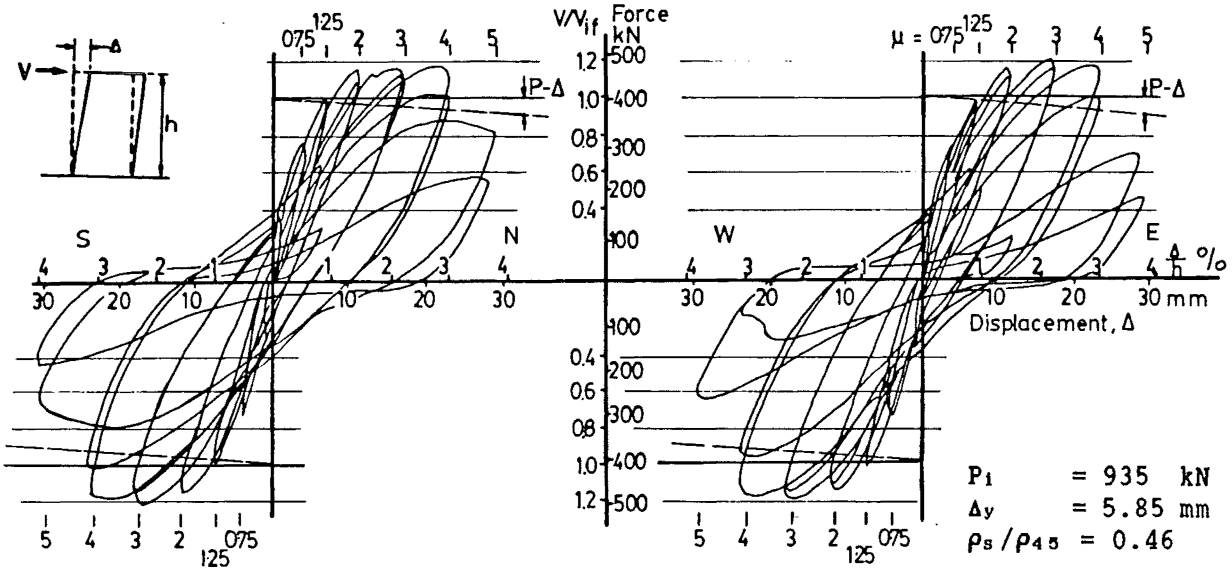

(a) First displacement path (b) Second displacement path

Fig. D.52 : Force - displacement hysteretic curves - Unit 8

D.4.5.2 General performance

Horizontal flexural and inclined cracks were observed at $0.2V_{if}$ and $0.62V_{if}$ respectively. At μ = 0.75, the cracks extended to 450 mm above the column base. Most of the new inclined cracks developed as extensions of existing horizontal flexural cracks. Some vertical cracks also formed at the corresponding tension side of the column in the region between 300 mm and 450 mm above the column base.

At μ =1.25, local crushing of some cover concrete was noted. Cracks extended to 720 mm above the column base. The inclinations of major inclined cracks were about 48° to the vertical in the first displacement path, and 40° in the second displacement path.

At larger ductilities, new inclined cracks were formed in the first cycles but not in the repeated cycles. The opening of cracks was more or less uniform. The inclinations of major inclined cracks became about 32° to the vertical (Fig. D.16a).

Before reaching the last displacement peak of the repeated cycle to μ = 5, the column lost both its axial and lateral load resistance at the occurrence of spiral fracture and the consequent buckling of longitudinal bars.

At the end of the test, the cover concrete within 500 mm above the column base spalled completely (Fig. D.16b).

D.4.5.3 Curvature profiles and components of deflections

Fig. D.53 shows curvature profiles for this column. Irregular distribution of curvatures appeared only at the last displacement peak in the repeated cycle to μ = 4. Significant curvature ductility is evident.

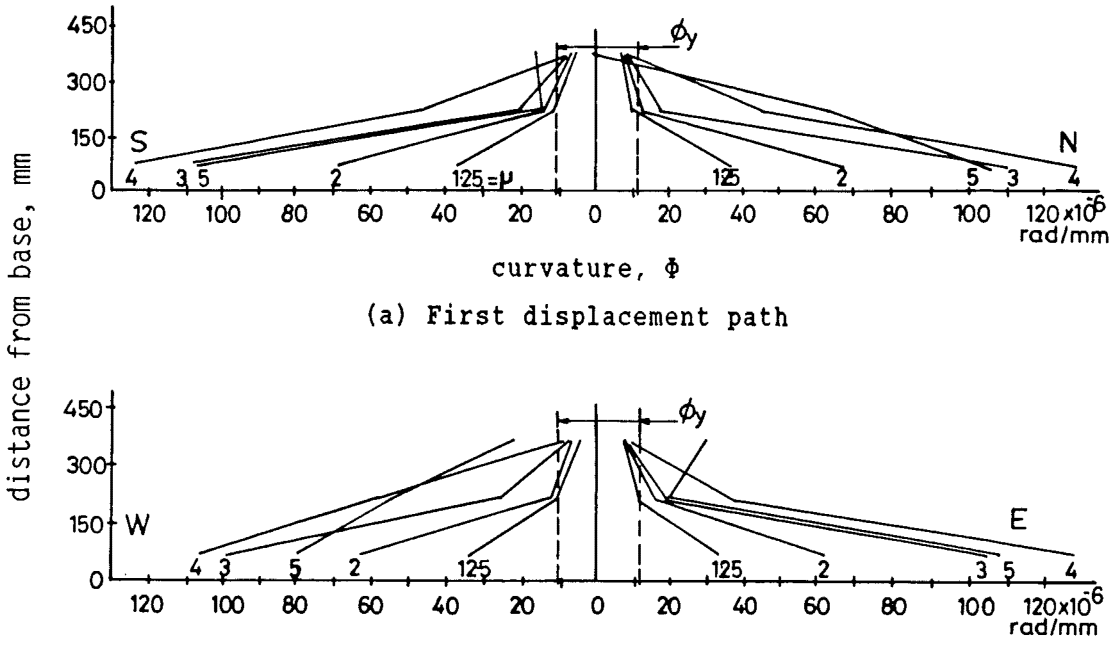

(a) First displacement path

(b) Second displacement path

Fig. D.53 : Measured curvature profiles - Unit 8

Fig. D.54 shows the components of deflections. Before the occurrence of irregular distribution of curvatures, the value of r_f at each displacement direction remained stable at 0.8 indicating dominating flexural response. At $\mu = 5$, these values were less than 0.58 and 0.44 in the first and repeated cycles respectively.

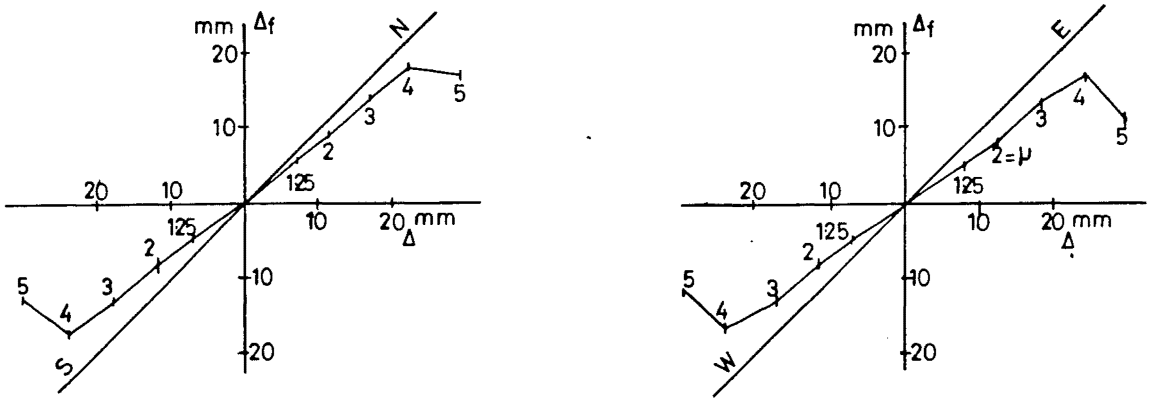

(a) First displacement path

(b) Second displacement path

Fig. D.54 : Components of deflections - Unit 8

D.4.5.4 Spiral strain distributions and spiral forces

Significant spiral strains were recorded at μ =0.75. At μ = 1.25, a few spirals started to yield (Fig. D.55). In the first cycle to μ = 5, some strains exceeded 3%.

In cycles to $\mu \geq 2$, spirals crossed by the inclined cracks, consistent with shear, reached yield stress at each displacement peak. At the same time, spirals located in the flexural compression zone near the column base were also strained to and beyond yield.

At zero lateral force, the values of σ_{sv}/f_{yt} were about 0.37, 0.42, 0.40, 0.34, and 1.0 after the completion of cycles to μ = 1.25, 2, 3, 4, and 5 respectively.

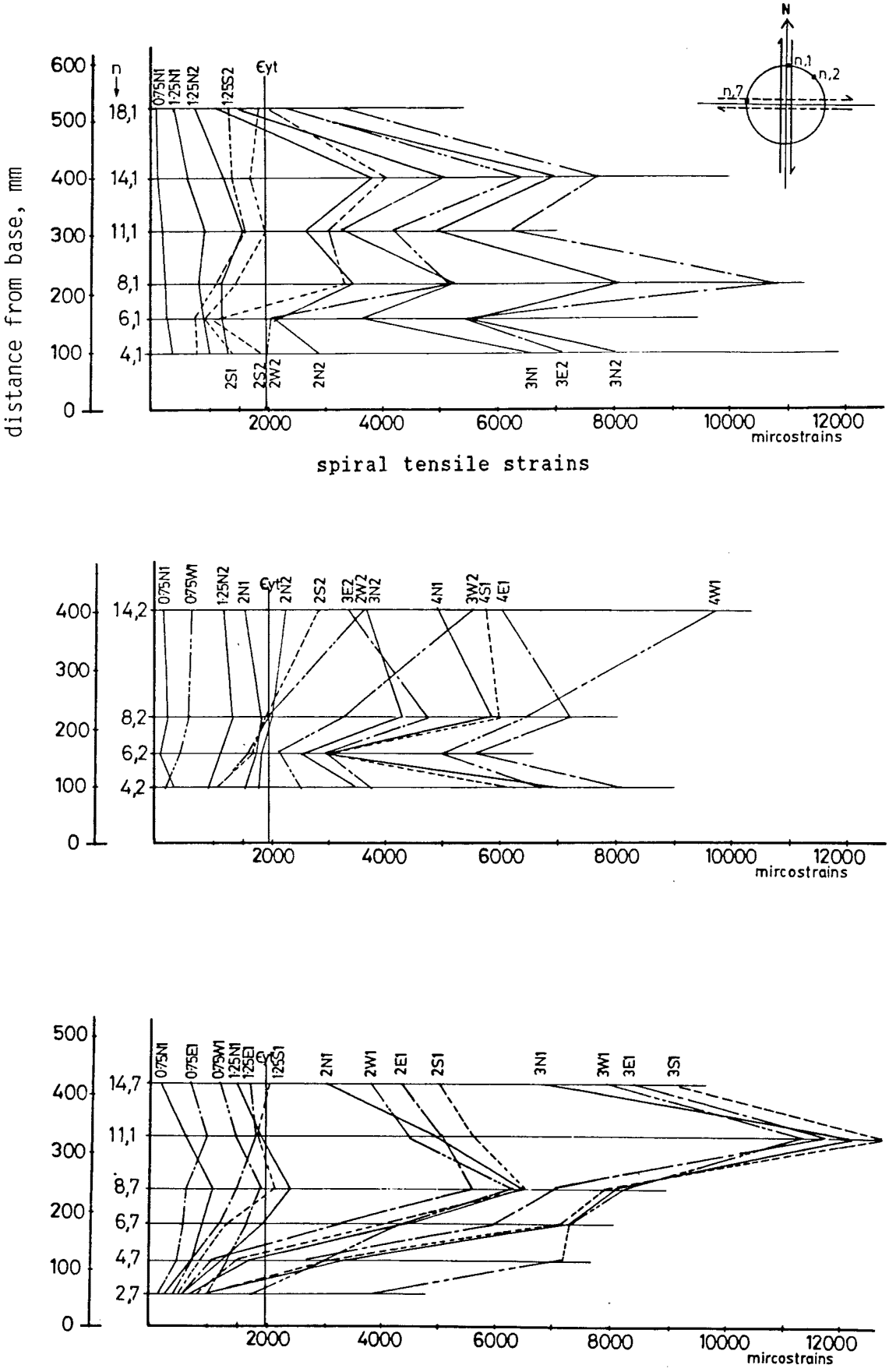

Fig. D.55 : Spiral strain distributions - Unit 8

D.4.6 Unit 9 [4R6-40b]

D.4.6.1 Force - displacement hysteretic performance

In the first cycle to $\mu = 2$, the resistance developed was $1.11V_{if}$ (Fig. D.56). The maximum measured resistance increased to $1.23V_{if}$ at the first cycle to $\mu = 3$. At $\mu \leq 3$, the variation of strength within a cycle was small with a maximum difference of only 7%.

At $1.25 \leq \mu \leq 2$, loss in strength during repeated cycles was 6% to 9% of that developed first in the first displacement path, and 2% to 7% of that developed first in the second displacement path.

Starting from the repeated cycle to $\mu = 3$, the degradation of strength and stiffness became significant. In the first cycle to $\mu = 5$, the strengths listed in the order of displacement peaks were $0.96V_{if}$, $0.82V_{if}$, $0.80V_{if}$ and $0.79V_{if}$. However, the corresponding strengths reduced to $0.77V_{if}$, $0.60V_{if}$, $0.65V_{if}$ and $0.62V_{if}$ during the repeated cycles.

The column was subjected to a final displacement northward. At $\Delta = 8\Delta_y$, the strength developed was $0.66V_{if}$. At $\Delta = 9\Delta_y$, the column failed.

Noticeable pinching of hysteretic curves was visible in the repeated cycle to $\mu = 4$ and in subsequent cycles.

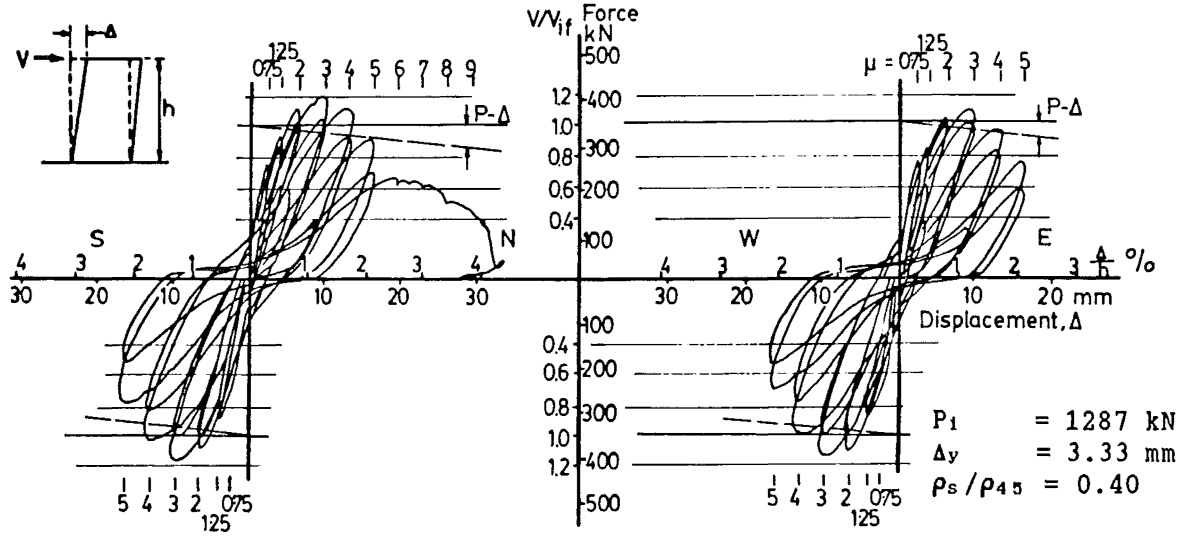

(a) First displacement path (b) Second displacement path

Fig. D.56 : Force - displacement hysteretic curves - Unit 9

D.4.6.2 General performance

Horizontal flexural and inclined cracks were observed at $0.23V_{if}$ and $0.75V_{if}$ respectively. At V = 0.75 V_{if}, flexural cracks extended to 300 mm above the column base.

At μ = 1.25, local crushing of cover concrete was noted in the repeated cycle. Cracks extended to 500 mm above the column base. At μ = 2, cracks occurred over the full height of the column. The inclinations of major inclined cracks were 30° to the vertical in the first displacement path, and 35° to the vertical in the second displacement path.

At μ = 4, new cracks developed at the upper part of the column. Crack opening concentrated at a few major diagonal cracks. Spalling of cover concrete occurred at the lower 200 mm region of the column (Fig. D.17a).

At μ = 5, spalling extended to 550 mm above the column base. At $\Delta = 9\Delta_y$, the column lost its axial and lateral load resistance at the occurrence of spiral fracture and consequent buckling of longitudinal bars (Fig. D.17b).

D.4.6.3 Curvature Profiles And Components Of Deflections

Up till μ = 4, curvature profiles maintained a flexure dominant shape (Fig. D.57). The length of the plastic hinge was about 250 mm. During the second displacement path in the repeated cycle to μ = 4, curvature distribution became irregular. Curvature ductility developed was moderate.

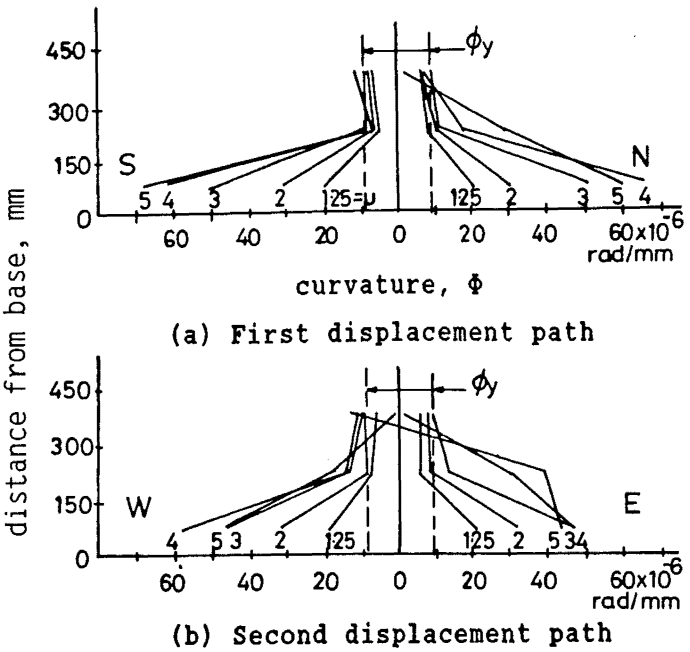

(a) First displacement path

(b) Second displacement path

Fig. D.57 : Measured curvature profiles - Unit 9

Fig. D.58 shows the components of deflections. The values of r_f at each peak displacement were about 0.65 at $\mu = 3$, and 0.49 at $\mu = 5$.

(a) First displacement path (b) Second displacement path

Fig. D.58 : Components of deflections - Unit 9

D.4.6.4 Spiral strain distributions and spiral forces

Significant spiral strains were recorded at $V = 0.75V_{if}$. In the first cycle to $\mu = 2$, a few spirals started to yield (Fig. D.59). In the subsequent cycles, spirals intercepted by the major diagonal cracks, consistent with shear, reached yield stress at each displacement peak. Some strains exceeded 3% in the first cycle to $\mu = 5$.

At zero lateral force, the values of σ_{av}/f_{yt} were about 0.28, 0.56, 0.46 after the completion of cycles to $\mu = 1.25$, 2, and 3 respectively.

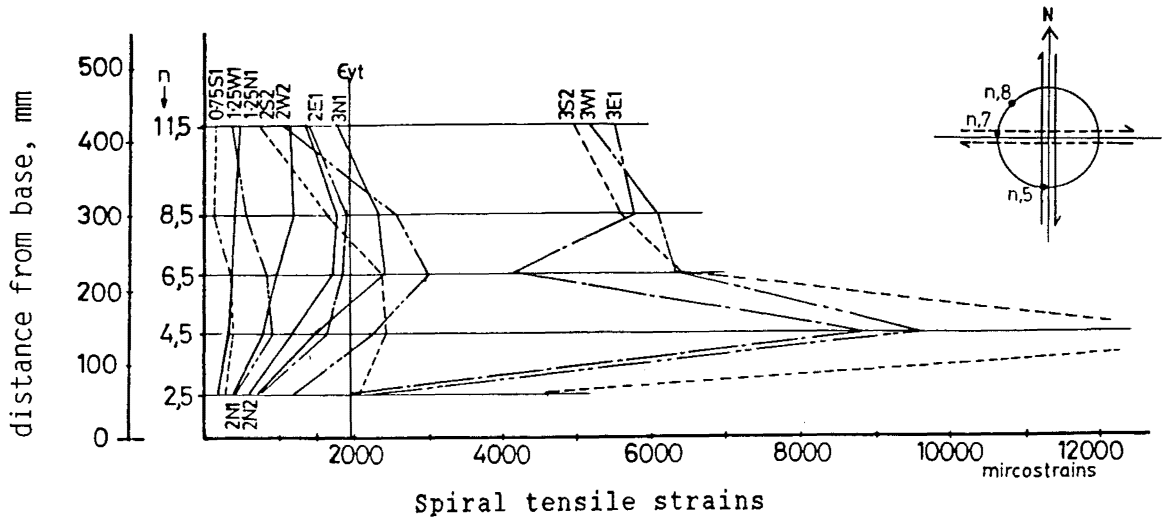

Spiral tensile strains

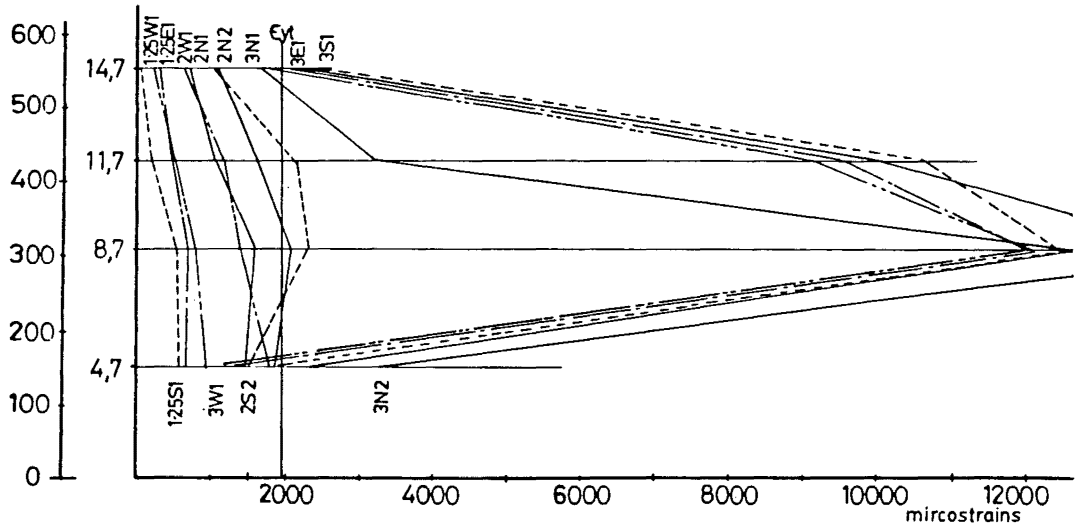

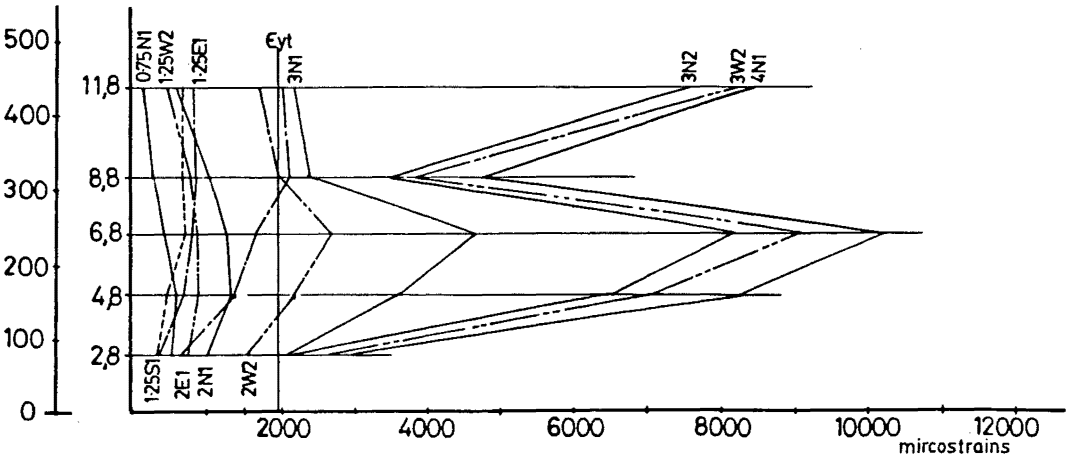

Fig. D.59 : Spiral strain distributions - Unit 9

D.4.7 Unit 10 [4R10-65b]

D.4.7.1 Force - displacement hysteretic performance

In the first cycle to $\mu = 2$, the lateral load resistance reached $1.17V_{if}$ (Fig. D.60).

During the first cycle to $\mu = 3$, maximum resistance of $1.41V_{if}$ was recorded in the first displacement path. While approaching the last displacement peak in the same cycle, the column was accidentally displaced to $4\Delta_y$ with the resistance of $1.33V_{if}$. Therefore, in the first cycle of $\mu = 4$, the last peak displacement was intentionally kept to $3\Delta_y$, and resistance of $1.14V_{if}$ was obtained.

Apart from the above-mentioned change in the displacement pattern, the variation of resistance was small with a maximum difference of only 5% within cycles to $\mu \leq 4$. Loss in strength during repeated cycles was 6% to 8% of those developed in the first cycles.

The degradation of strength and stiffness became significant at $\mu = 5$. In the repeated cycles, the strengths listed in the order of displacement peaks were $1.07V_{if}$, $1.04V_{if}$, $1.03V_{if}$, and $0.72V_{if}$.

Throughout the test, there was no sign of pinching of the hysteretic curves. Strength enhancement due to confinement was evident.

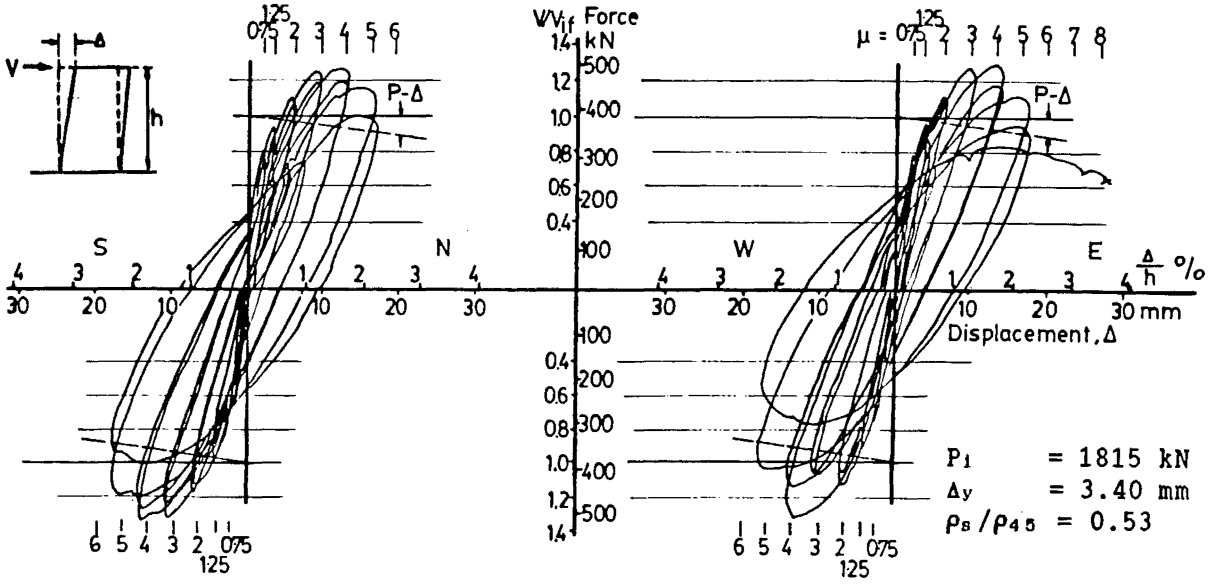

(a) First displacement path (b) Second displacement path

Fig. D.60 : Force - displacement hysteretic curves - Unit 10

D.4.7.2 General performance

Horizontal flexural and inclined cracks were observed at $0.31V_{if}$ and $0.91V_{if}$ respectively. At $\mu = 1.25$, inclined cracks extended to 450 mm above the column base. The inclinations of major inclined cracks were about 45° to the vertical in the first displacement path, and 30° to the vertical in the second displacement path.

Local crushing of cover concrete occurred before reaching displacement of $2\Delta_y$. At $\mu = 2$, the crack pattern fully developed over the entire column. Spalling of cover concrete was noted at the lower 150 mm region of the column.

During displacements at larger ductilities, few new inclined cracks formed. The opening of cracks was more or less uniform. At $\mu = 4$, spalling of cover concrete extended to 450 mm above the column base (see Fig. D.18a).

In the repeated cycle to $\mu = 5$, buckling of longitudinal bars in the flexural compression zone was observed in each displacement peak. Spalling of cover concrete extended to 600 mm above the column base. Axial shortening was 11 mm.

The column was then displaced eastward as far as possible. At the displacement of $8\Delta_y$, the column lost its axial load resistance when fracture of the spiral took place. A slight loss of core concrete around the buckled longitudinal bars was noted (Fig. D.18b).

D.4.7.3 Curvature profiles and components of deflections

Curvature profiles (Fig. D.61) and components of deflections (Fig. D.62) indicated the flexure dominant behaviour of the column at $\mu \leq 4$ with corresponding limited curvature ductility. The value of r_f at each displacement peak was around 0.75. The length of plastic hinge was about 250 mm.

At $\mu = 5$, curvature profiles did not conform with the previous pattern.

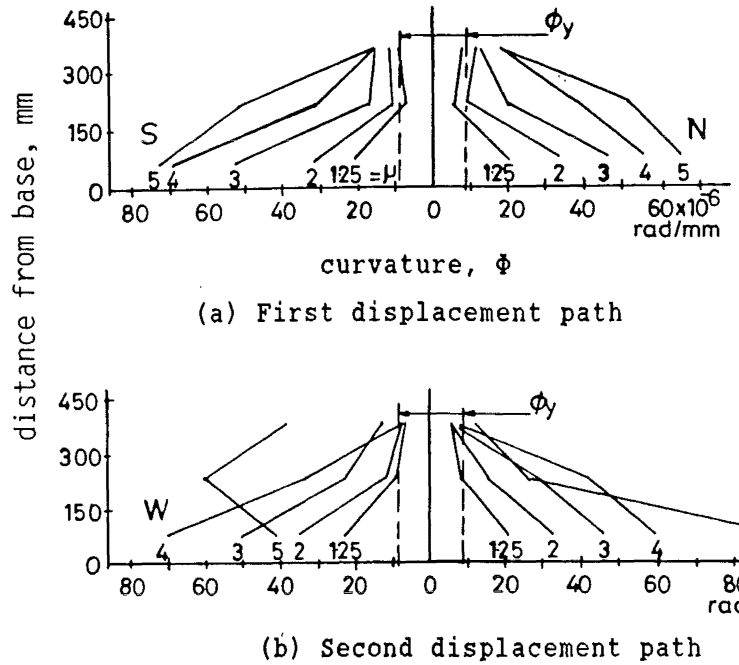

(a) First displacement path

(b) Second displacement path

Fig. D.61 : Measured curvature profiles - Unit 10

(a) First displacement path

(b) Second displacement path

Fig. D.62 : Components of deflection - Unit 10

D.4.7.4 Spiral strain distributions and spiral forces

Some spirals started to yield in the first cycle to μ = 2 (Fig. D.63). In subsequent cycles, spirals crossed either by the inclined cracks, consistent with shear, or located in the flexural compression zone near the column base reached yield stress at each displacement peak. In the repeated cycle to μ = 5, spiral strain exceeded 3% only at one location.

At zero lateral force, the values of σ_{sv}/f_{yt} varied between 0.40 and 0.60 after the completion of cycles to $\mu \geq 2$.

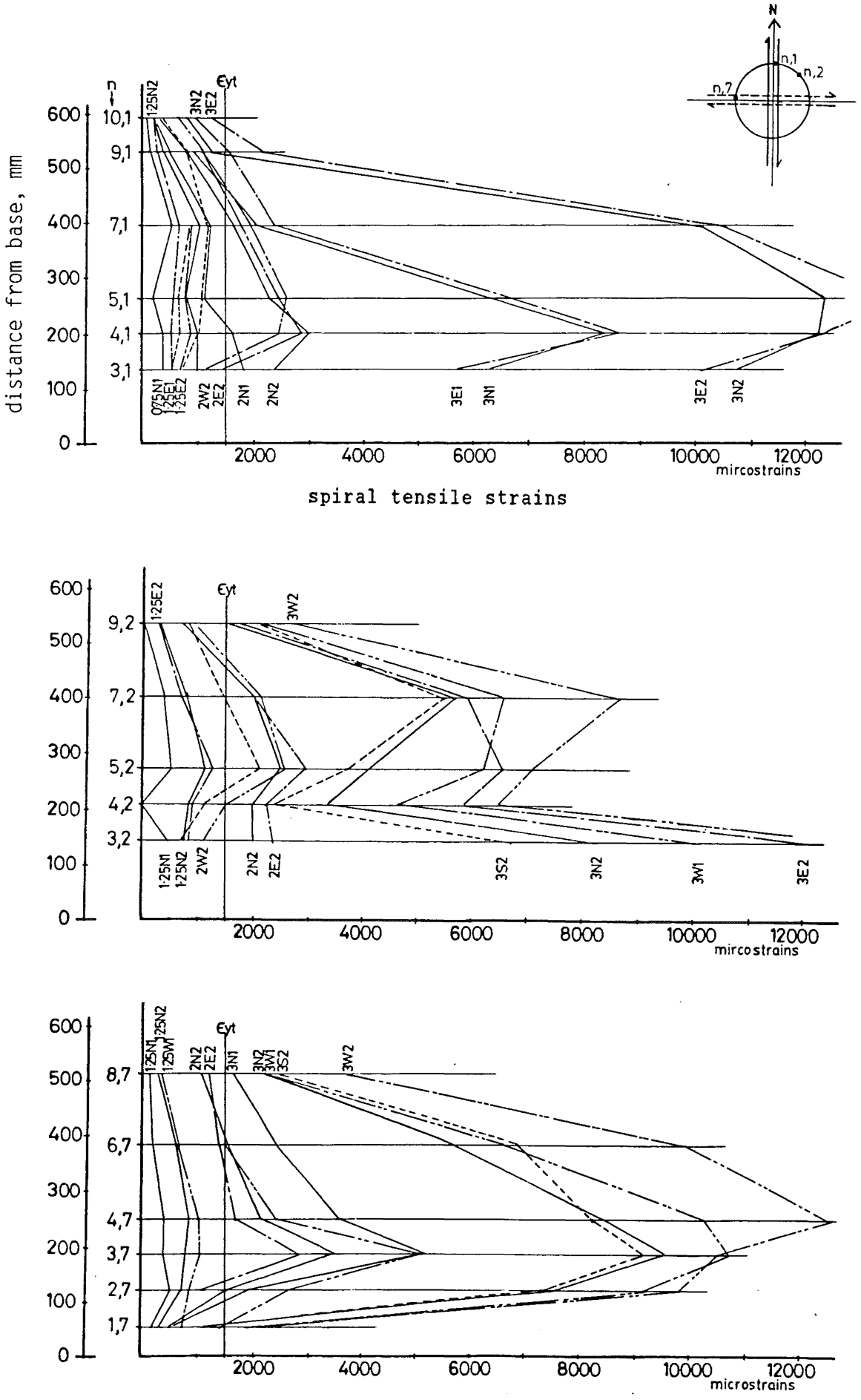

Fig. D.63 : Spiral strain distributions - Unit 10

D.5 COLUMNS SUBJECTED TO BI-DIRECTIONAL 's' DISPLACEMENT PATTERN

D.5.1 Unit 11 [OR6-30s]

D.5.1.1 Force - displacement hysteretic performance

Fig. D.64 shows the force - displacement hysteretic curves of the column for (a) the component of the lateral force in North-South directions, V_y, vs the component of the displacement measured along North-South directions, $\Delta y'$, and (b) the component of the lateral force in East-West directions, V_x, vs the component of the displacement measured along East-West directions, $\Delta x'$.

The resultant lateral force, V, against the total displacement, Δ, is shown in Fig. D.66. As defined in Section C.3.1, the displacement ductility factor, μ, is the ratio of the displacement, Δ, measured between a displacement peak and the zero displacement position, to the corresponding experimentally established yield displacement, Δ_y. For this unit, the maximum measured resistance of $1.03V_{if}$ was developed in the first displacement path (NE-SW, see Fig. C.6) in the first cycle to $\mu = 2$.

At $\mu \leq 4$, the strengths attained in the second displacement path (NW-SE) were about 90% of those attained in the first displacement path to the same cycle. Loss in strength during a repeated cycle was 9% to 14% of that developed first in the first displacement path, and 2% to 13% of that developed first in the second displacement path. During the repeated cycle to $\mu = 4$, the strength attained in the second displacement path was 75% of V_{if}.

At $\mu = 5$, the rate of strength degradation increased. In the first cycle, the strengths developed were $0.77V_{if}$, $0.80V_{if}$, $0.68V_{if}$, and $0.65V_{if}$ (listed in the order of displacement peaks). In the repeated cycle, the corresponding strengths became $0.62V_{if}$, $0.65V_{if}$, $0.59V_{if}$, and $0.56V_{if}$.

The column was finally subjected to one cycle to $\mu = 8$ along the North-South direction. Strengths developed were $0.67V_{if}$ and $0.78V_{if}$ respectively.

Significant pinching of the hysteretic loops was observed at $\mu \geq 4$.

The characteristics of turning points found in the resultant force - total displacement hysteretic curves (Fig. D.65) have been discussed in Section D.2.5. In here, quantitative assessments of variations of strength at these points are reported. At $\mu \geq 1.25$, the loss in strength at the turning point at a loading stage, identified as Position '3' in Fig. D.5, varied between 5% and 15% of that attained just before the change of displacement direction, identified as Position '2'. On the other hand, gain in strength at the turning point at an unloading stage, identified as Position '6', varied between 0% and 17% of that just previously developed at zero lateral force in one of the hydraulic jacks, identified as Position '5'. However, this gain did not take place when the pinching of the corresponding hysteretic loop became significant. The relative values of such strength loss or gain were similar in all other units subjected to 's' displacement pattern. Therefore, this phenomenon is not described again in the reports for Units 12 to 15.

D.5.1.2 General performance

Horizontal flexural and inclined cracks were observed at $0.18V_{if}$ and $0.38V_{if}$ respectively. In the cycle to $\mu = 0.75$, inclined cracks developed over the full height of the column. The inclinations of major inclined cracks were 35° to 40° to the vertical in the first displacement path, and 40° to 45° to the vertical in the second displacement path.

At $\mu = 3$, crack patterns fully developed (see Fig.D.19a). The inclinations of cracks were about 30° to 35° to the vertical.

New cracks formed in the second displacement path were relatively short. As they met existing cracks which had been developed in the first displacement path, they ceased to propagate across these existing cracks. Instead, they tended to follow existing crack paths at least for a short distance, until a path of least cracking resistance was found within a previously uncracked region. Then, new cracks branched out. This phenomenon was also identified in other units subjected to this 's' displacement pattern.

At the end of the test, cover concrete in the lower 550 mm region of the column spalled completely (Fig. D.19b). No fracture of spiral or buckling of longitudinal bars was detected. The core concrete remained well confined.

D.5.1.3 Curvature profiles and components of deflections

At $\mu \leq 3$, curvature profiles recorded for each displacement peak were regular and similar (Fig. D.66). The length of plastic hinge was about 200 mm. At $\mu = 5$, curvature distribution became irregular.

Fig. D.67 shows the components of deflections. The values of r_f at each displacement peak were about 0.75 at $\mu \leq 3$, and 0.42 at $\mu = 5$.

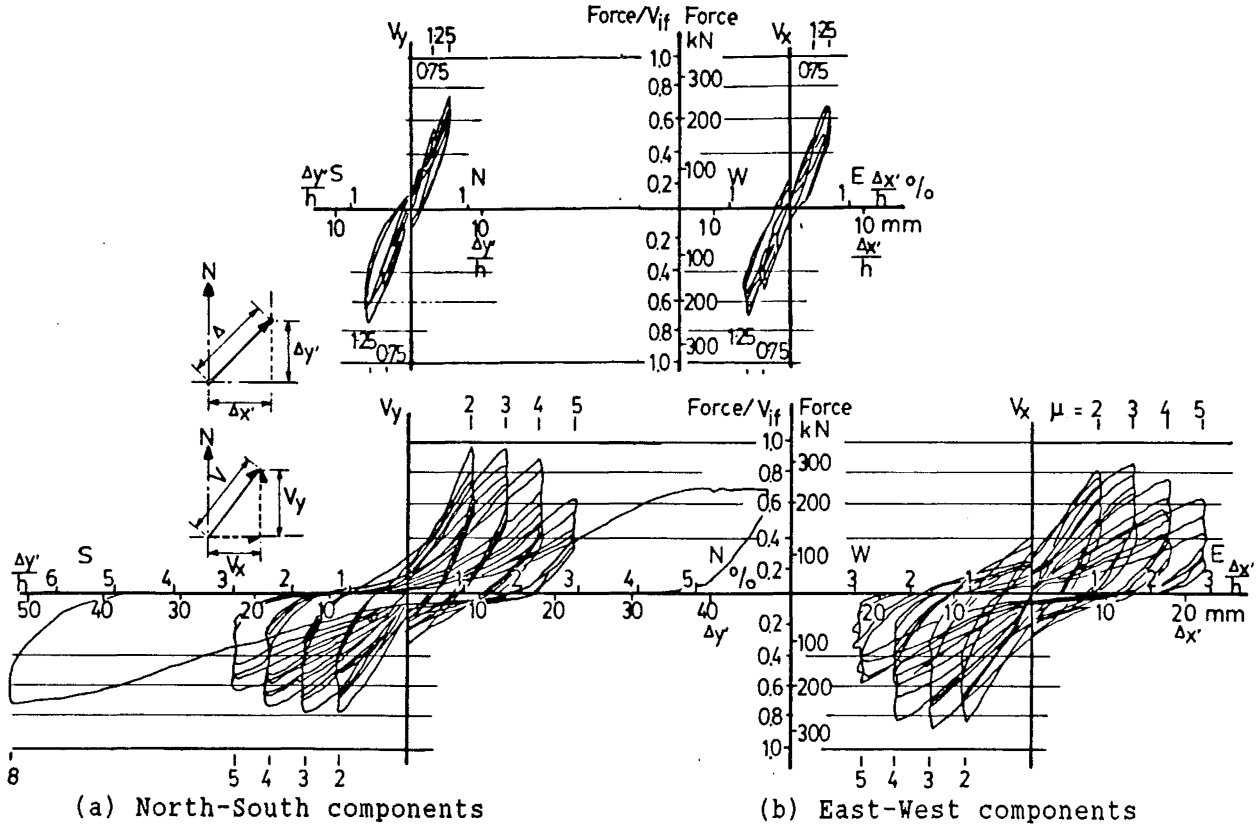

Fig. D.64 : Force - displacement hysteretic curves for displacement components - Unit 11

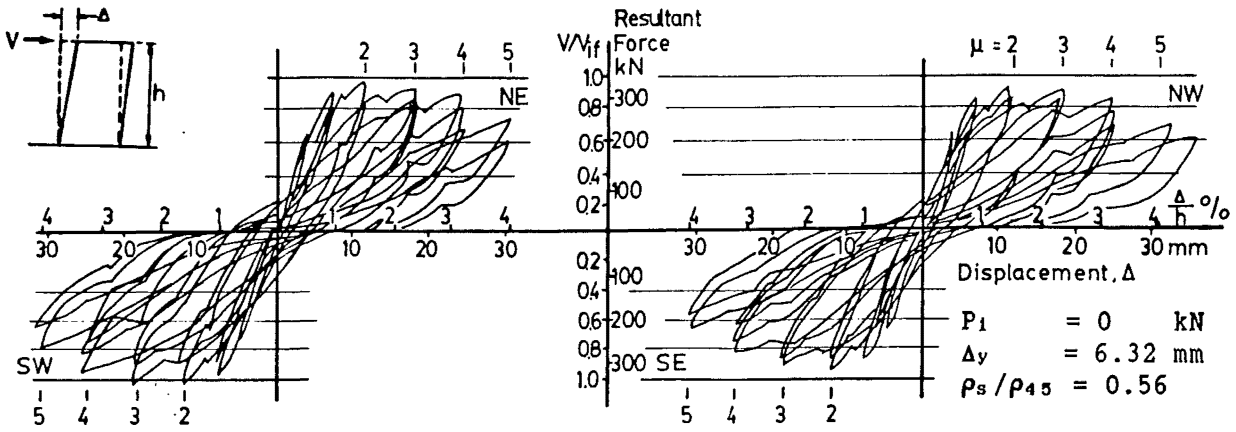

(a) First displacement path (b) Second displacement path

Fig. D.65 : Resultant force - total displacement hysteretic curves - Unit 11

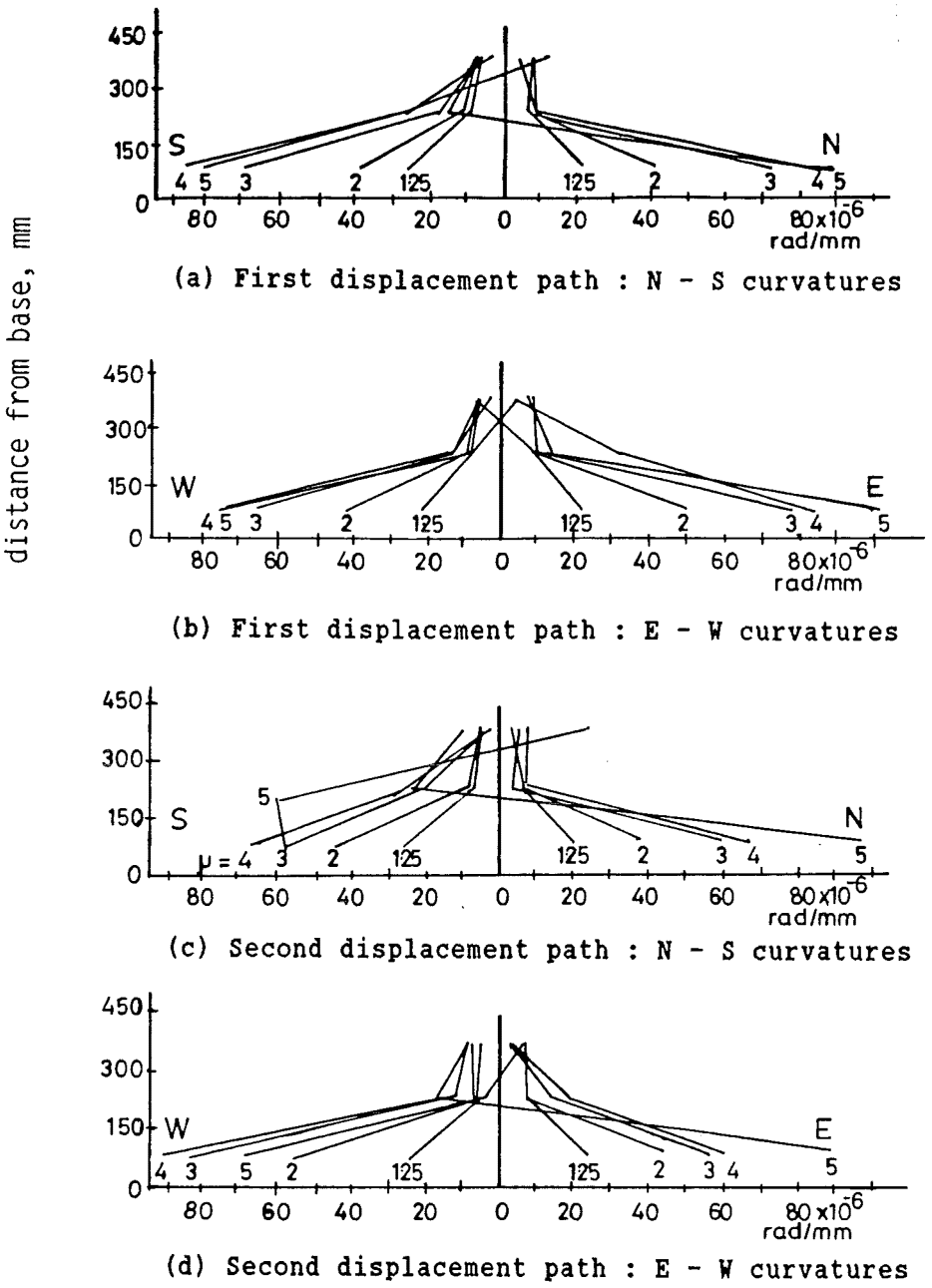

(a) First displacement path : N - S curvatures

(b) First displacement path : E - W curvatures

(c) Second displacement path : N - S curvatures

(d) Second displacement path : E - W curvatures

Fig. D.66 : Measured curvature profiles - Unit 11

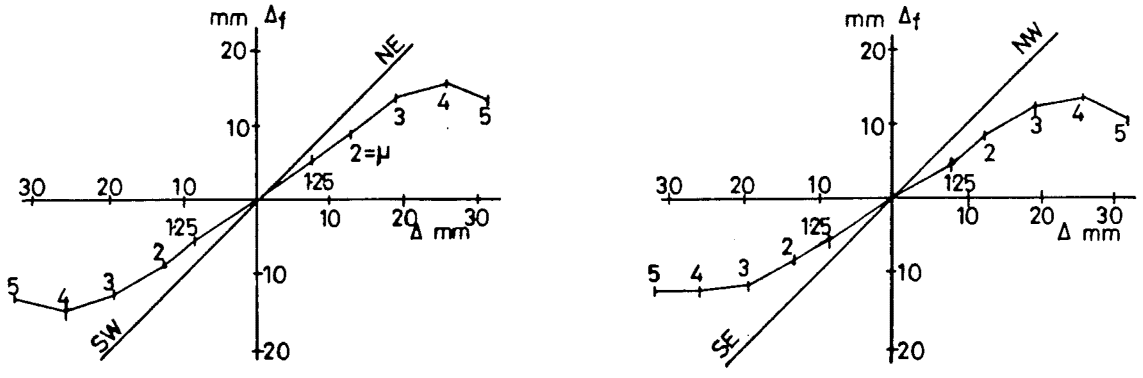

(a) First displacement path

(b) Second displacement path

Fig. D.67 : Components of deflections - Unit 11

D.5.1.4 Spiral strain distributions and spiral forces

Significant spiral strains were recorded at $V = 0.37V_{if}$. During the repeated cycle to $\mu = 1.25$, some spirals started to yield (Fig. D.68). In the first cycle to $\mu = 4$, strain exceeded 3% at some locations.

At each displacement peak in cycles to $\mu \geq 2$, spirals intercepted by the inclined cracks, consistent with shear, attained yield stress.

At zero lateral force, the values of σ_{av}/f_{yt} were about 0.20, 0.30, 0.35, and 0.20 after the completion of cycles to $\mu = 0.75$, 1.25, 2, and 3 respectively.

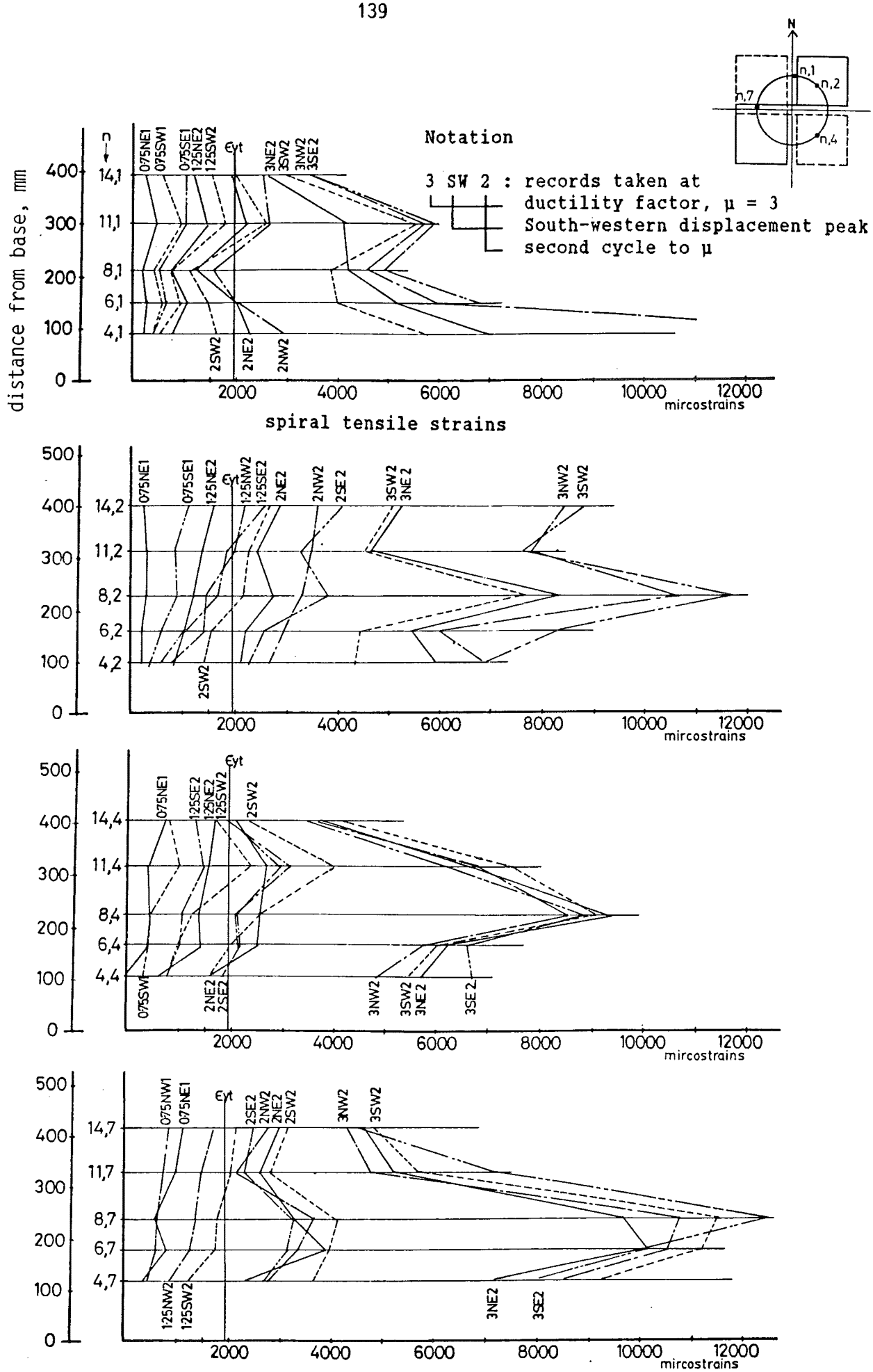

Fig. D.68 : Spiral strain distributions - Unit 11

D.5.2 Unit 12 [0R10-35s]

D.5.2.1 Force - displacement hysteretic performance

The force - displacement hysteretic curves are shown in Figs. D.69 and D.70. In the first cycle to $\mu = 2$, a resistance of $1.04V_{if}$ was recorded. The maximum measured resistance of $1.05V_{if}$ occurred at the first displacement path in the first cycle to $\mu = 3$.

At $1.25 \leq \mu \leq 4$, the ratios of strengths listed in the order of displacement peaks were about 1.00 : 0.98 : 0.93 : 0.90 in the first cycles, and 0.95 : 1.00 : 0.99 : 0.96 in the repeated cycles. Loss in strength during a repeated cycle was 8% to 17% of that developed first in the first displacement path, and 2% to 7% of that developed first in the second displacement path.

At the third displacement peak of the repeated cycle to $\mu = 5$, the resistance reduced to $0.8V_{if}$. The test was terminated because of significant twisting of the column.

No significant pinching of the hysteretic curves was observed throughout the loading history.

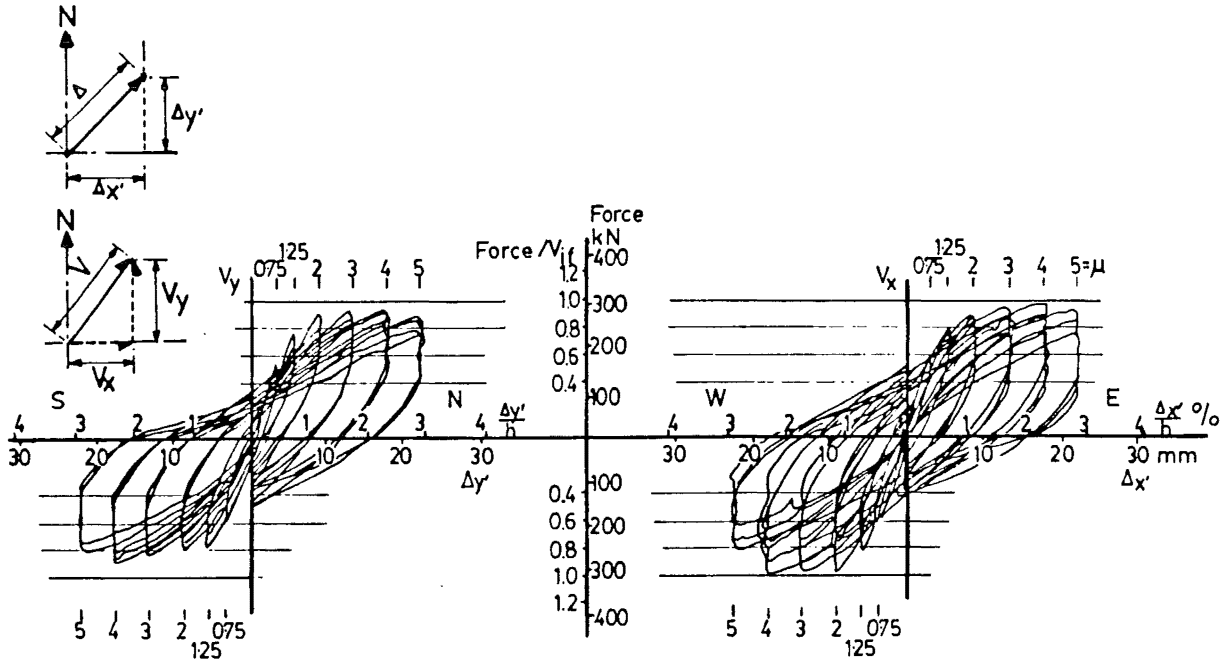

(a) North-South components (b) East-West components

Fig. D.69 : Force - displacement hysteretic curves for displacement components - Unit 12

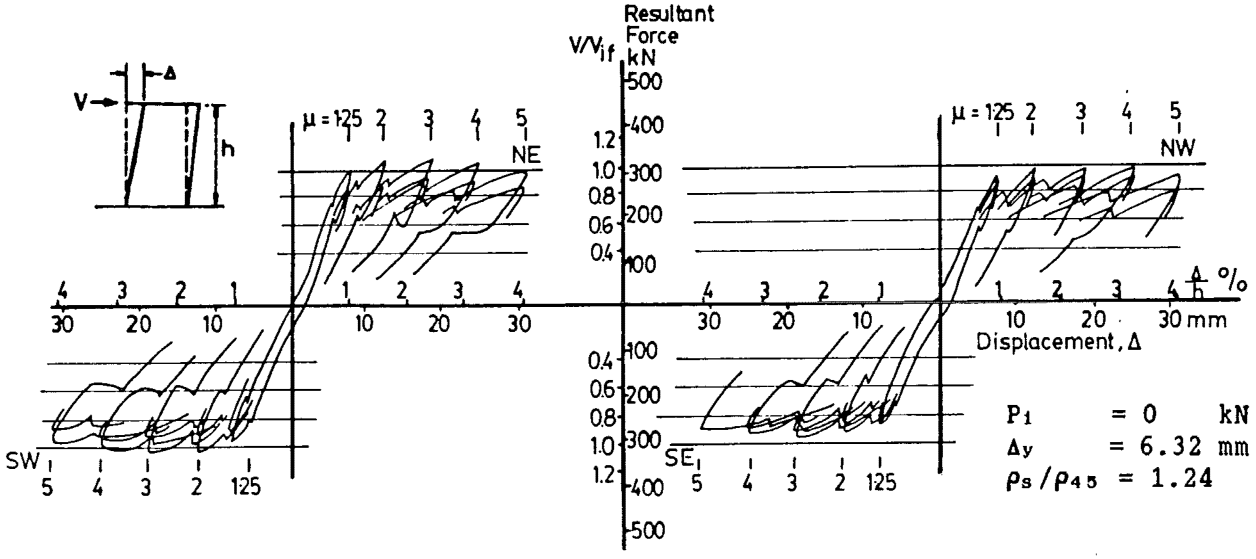

(a) First displacement path (b) Second displacement path

Fig. D.70 : Resultant force - total displacement hysteretic curves - Unit 12

D.5.2.2 General performance

Horizontal flexural and inclined cracks appeared at loads of $0.13V_{if}$ and $0.38V_{if}$ respectively. At $\mu = 0.75$, cracks extended to 600 mm above the column base.

At $\mu = 1.25$, local crushing of cover concrete took place near the column base.

At $\mu = 3$, crack patterns fully developed over the entire column. The inclinations of main diagonal cracks were about 45° to the vertical in the first displacement path, and 40° to the vertical in the second displacement path. Spalling of cover concrete extended to 90 mm above the column base (Fig. D.20a).

At the end of the test, the cover concrete in the lower 250 mm region of the column spalled completely. No fracture of spiral or loss of core concrete was found (Fig. D.20b).

During the testing, the opening of inclined cracks was more or less uniform. The widths of the flexural crack at base of column were 1 mm, 2 mm, 3 mm, and 4.5 mm at the displacement peaks to μ =1.25, 2, 3, and 4 respectively.

D.5.2.3 Curvature profiles and components of deflections

At $\mu \leq 3$, regular distribution of curvature was observed in all four displacement peaks (Fig. D.71). At $\mu \geq 4$, reliable readings for curvature calculation could not be obtained due to twisting of the column. The length of plastic hinge was about 200 mm. The development of significant curvature ductility is evident.

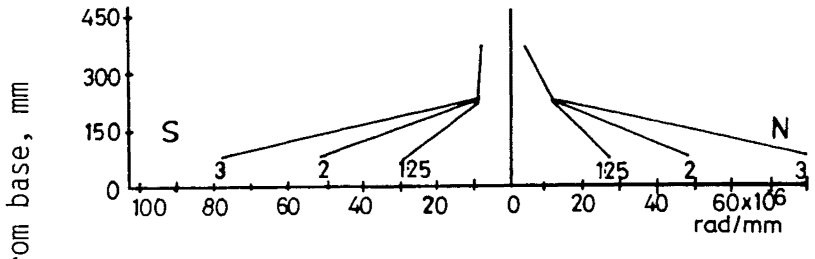

(a) First displacement path : N - S curvatures

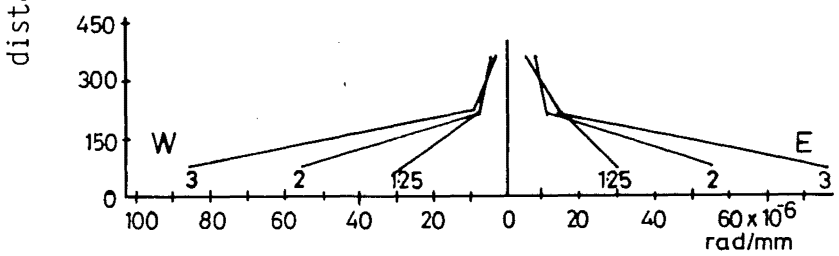

(b) First displacement path : E - W curvatures

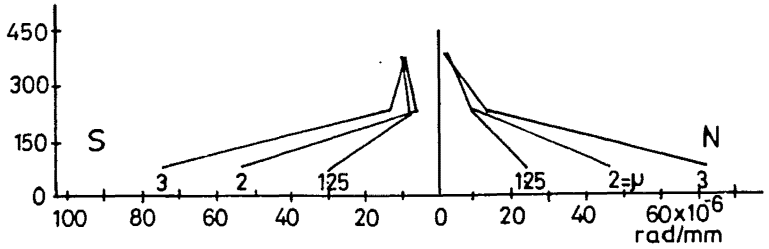

(c) Second displacement path : N - S curvatures

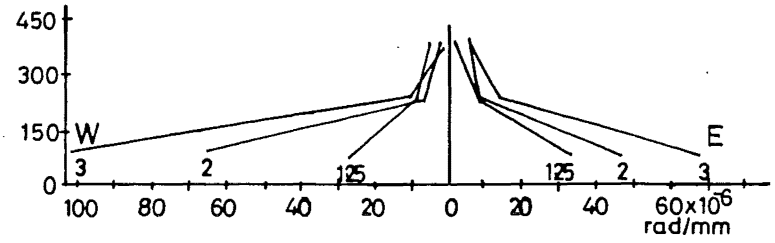

(d) Second displacement path : E - W curvatures

Fig. D.72 : Measured curvature profiles - Unit 12

Fig. D.72 shows the components of deflections. The value of r_f at each displacement peak was about 0.73 at $\mu \leq 3$.

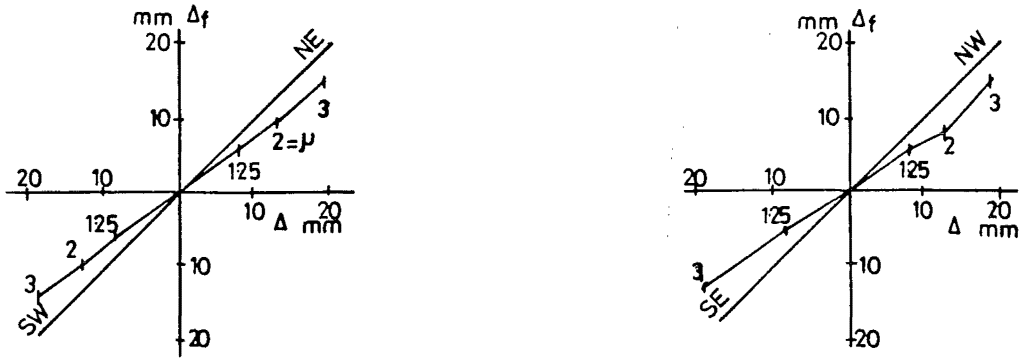

(a) First displacement path (b) Second displacement path

Fig. D.72 : Components of deflections - Unit 12

D.5.2.4 Spiral strain distributions and spiral forces

At $\mu = 2$, only two spiral strain readings indicated yielding (Fig. D.73). At $\mu = 4$, a few gauge locations near the column base gave strain values in excess of 3%.

At displacement peaks in cycles to $\mu \geq 3$, spirals crossed by the inclined cracks, consistent with shear, developed yield stress.

At zero lateral force, the values of σ_{av}/f_{yt} were about 0.22 and 0.24 after the completion of cycles to $\mu = 1.25$ and 4 respectively.

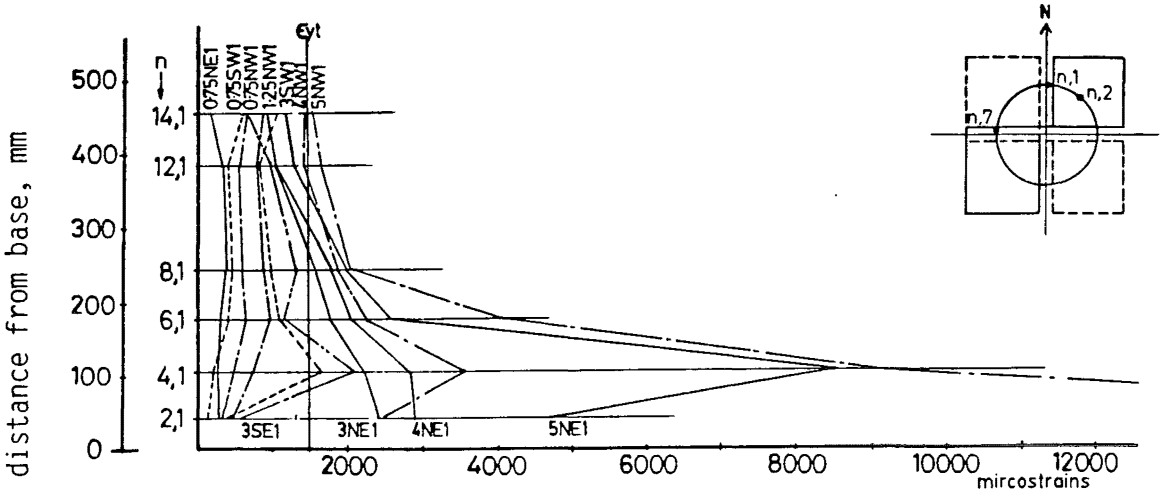

spiral tensile strains

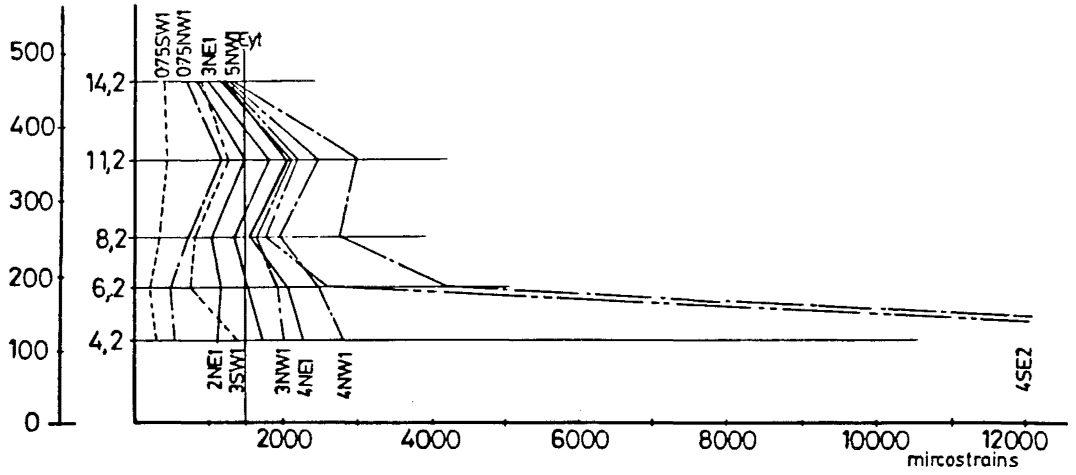

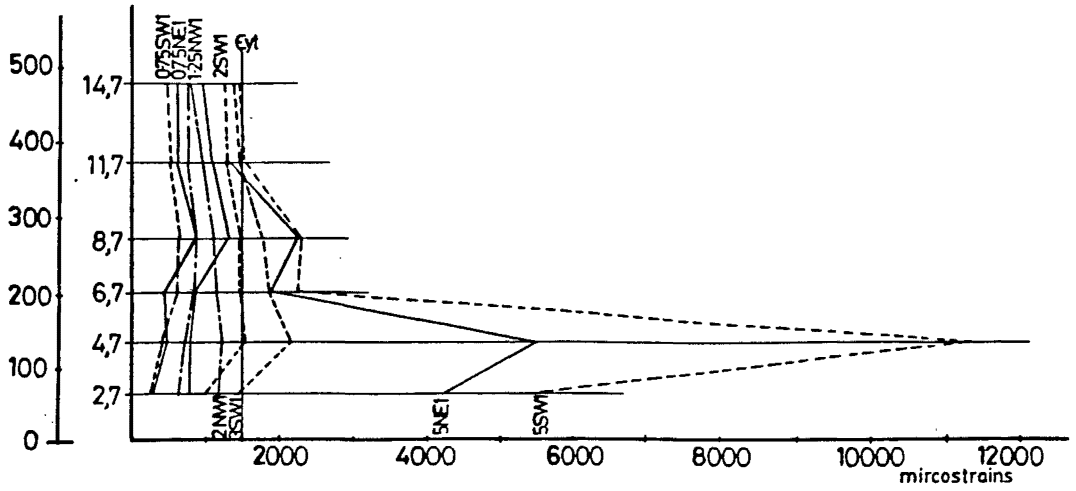

Fig. D.73 : Spiral strain distributions - Unit 12

D.5.3 Unit 13 [2R6-30s]

D.5.3.1 Force - displacement hysteretic performance

During loading towards the first displacement peak (NE) with an intensity of V = $0.37V_{if}$, the lateral force in the E-W direction was accidentally increased to $0.52V_{if}$ instead of $0.27V_{if}$. The resultant resistance of the column at this stage became $0.58V_{if}$, with a total displacement $0.68\Delta_y$.

In the first cycle to $\mu = 2$, the resistance reached $1.13V_{if}$ (Figs. D.74 and D.75). The maximum measured resistance of $1.19V_{if}$ occurred at the first displacement path of the first cycle to $\mu = 3$.

At $1.25 \leq \mu \leq 3$, the ratios of strengths listed in the order of displacement peaks were approximately 1.00 : 1.00 : 0.96 : 0.97 in the first cycles, and 0.94 : 1.00 : 0.96 : 0.95 in the repeated cycles. Loss in strength during a repeated cycle was 4% to 10% of that developed first in the first displacement path, and 4% to 7% of that developed first in the second displacement path.

The rates of degradation of strength and stiffness started to increase during the second displacement path of the first cycle to $\mu = 4$. In the repeated cycle, the observed strengths, listed in the order of displacement peaks, were $0.87V_{if}$, $0.92V_{if}$, $0.82V_{if}$, and $0.84V_{if}$.

In the first cycle to $\mu = 5$, the corresponding resistances became $0.76V_{if}$, $0.76V_{if}$, $0.54V_{if}$, and $0.64V_{if}$ respectively.

Significant pinching of hysteretic loops appeared at the repeated cycle to $\mu = 4$ and during subsequent cycles.

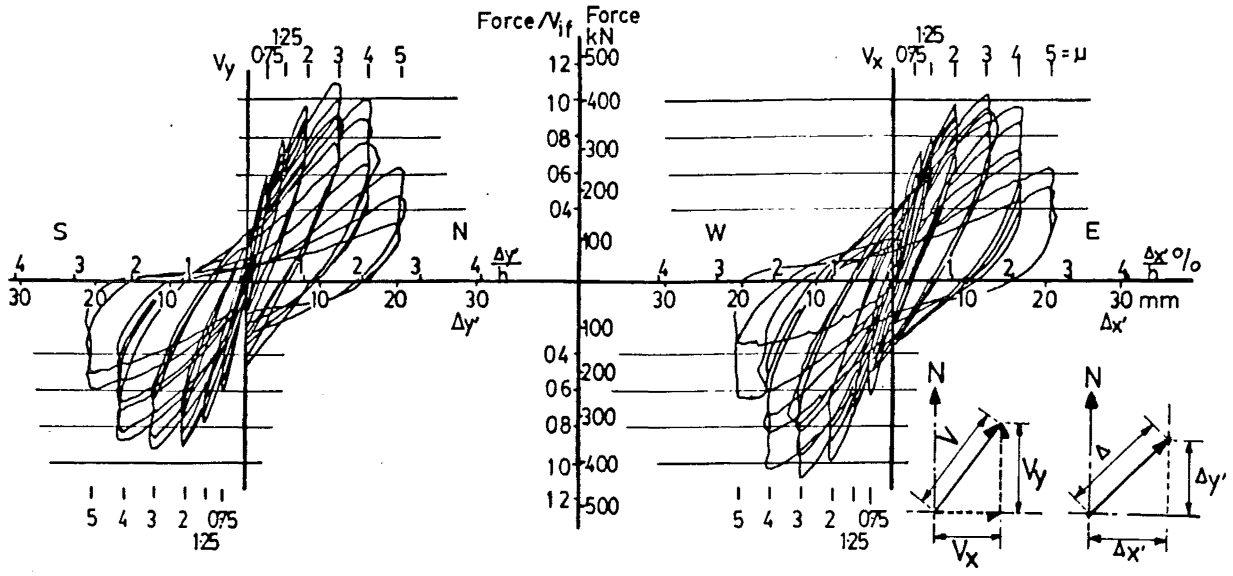

(a) North-South components (b) East-West components

Fig. D.74 : Force - displacement hysteretic curves for displacement components - Unit 13

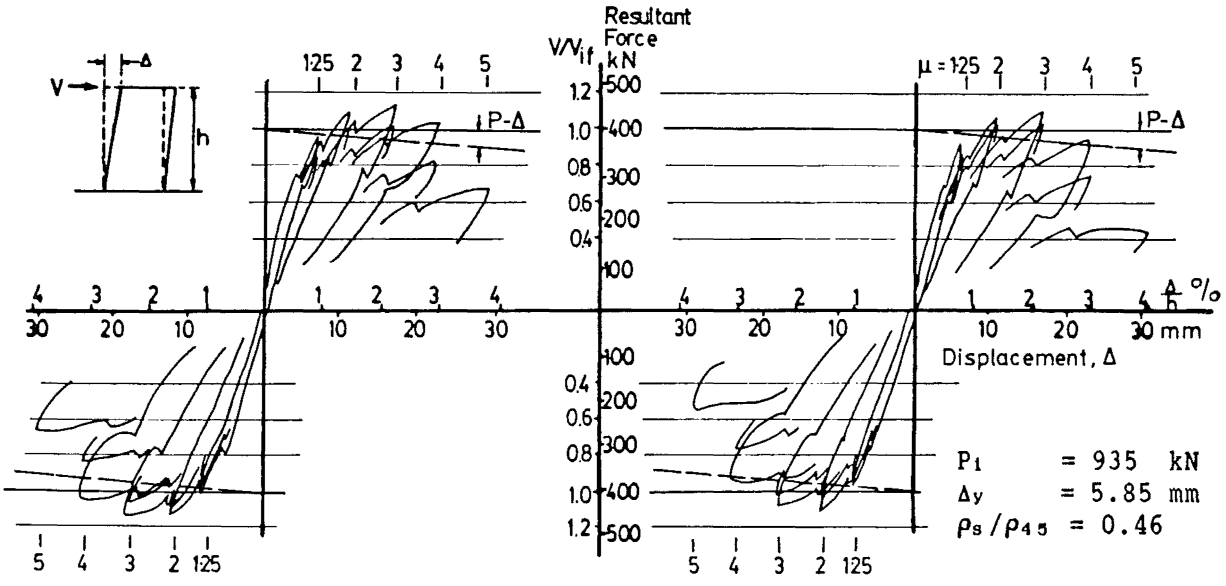

(a) First displacement path (b) Second displacement path

Fig. D.75 : Resultant force - total displacement hysteretic curves - Unit 13

D.5.3.2 General performance

Horizontal flexural and inclined cracks appeared at $0.17V_{if}$ and $0.58V_{if}$ respectively. At $\mu = 0.75$, cracks extended to 500 mm above the column base.

At $\mu = 1.25$, local crushing of cover concrete took place. Cracks developed over the full height of the column.

At $\mu = 3$, crack patterns fully developed. Inclinations of main diagonal cracks were about 35° to the vertical in the first displacement path, and 30° in the second displacement path (Fig. D.21a). Spalling of cover concrete extended to 200 mm above the column base.

In the first cycle to $\mu = 5$, some longitudinal bars buckled. Spiral fracture occurred at the first loading north during the subsequent repeated cycle. Resistance dropped instantaneously. However, the column held the required axial load of $P_i = 0.19f'_cA_g$. The cover concrete completely spalled in the lower 500 mm region of the column. There was no loss of core concrete (Fig. D.21b).

D.5.3.3 Curvature profiles and components of deflections

Regular distribution of curvatures was maintained before the repeated cycle to $\mu = 4$ (Fig. D.76). The length of plastic hinge was about 250 mm.

Fig. D.77 shows the components of deflections. The value of r_f at each peak displacement was about 0.67 at $\mu \leq 3$.

D.5.3.4 Spiral strain distributions and spiral forces

During the first cycle to $\mu = 1.25$, some spirals started to yield. At $\mu = 5$, some strains exceeded 3%.

At $\mu \geq 2$, spirals intercepted by the major diagonal cracks, consistent with shear, reached yield stress at each displacement peak (Fig. D.78).

At zero lateral force, The values of σ_{av}/f_{yt} were approximately 0.25, 0.47, 0.48, and 0.26 after the completion of cycles to $\mu = 0.75$, 1.25, 2, and 3 respectively.

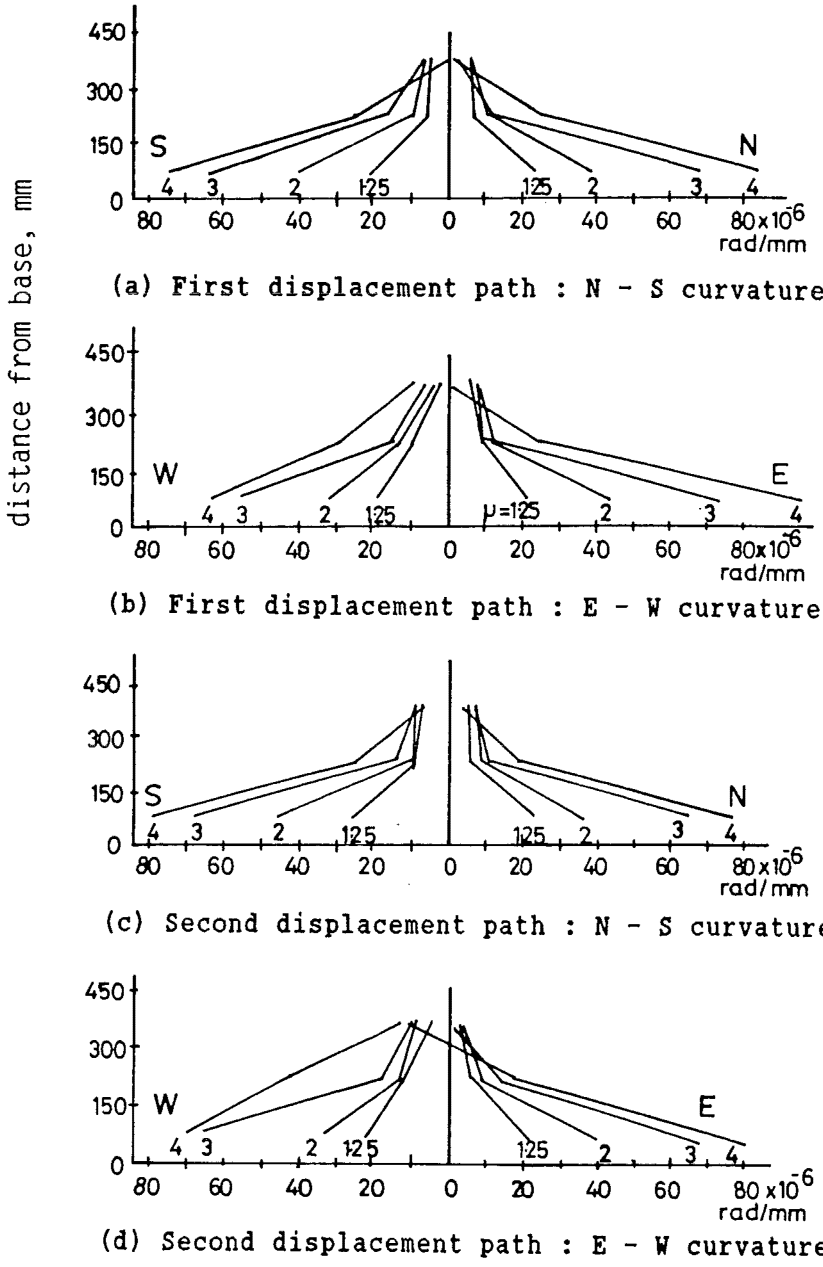

(a) First displacement path : N - S curvatures

(b) First displacement path : E - W curvatures

(c) Second displacement path : N - S curvatures

(d) Second displacement path : E - W curvatures

Fig. D.76 : Measured curvature profiles - Unit 13

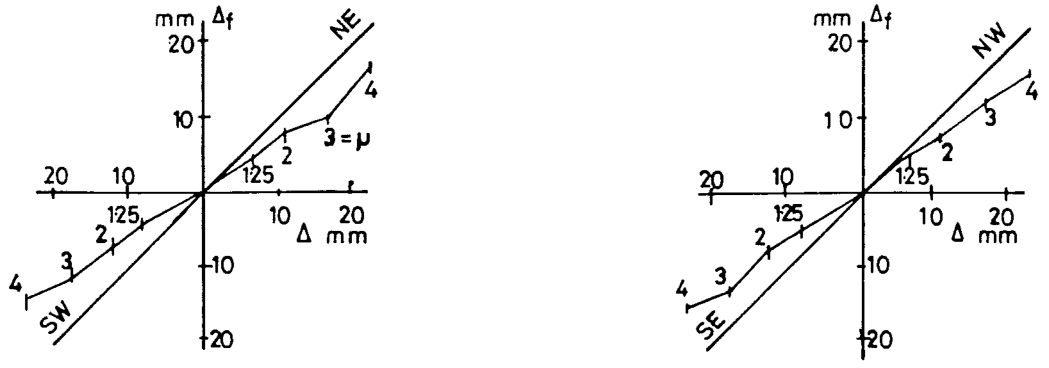

(a) First displacement path

(b) Second displacement path

Fig. D.77 : Components of deflections - Unit 13

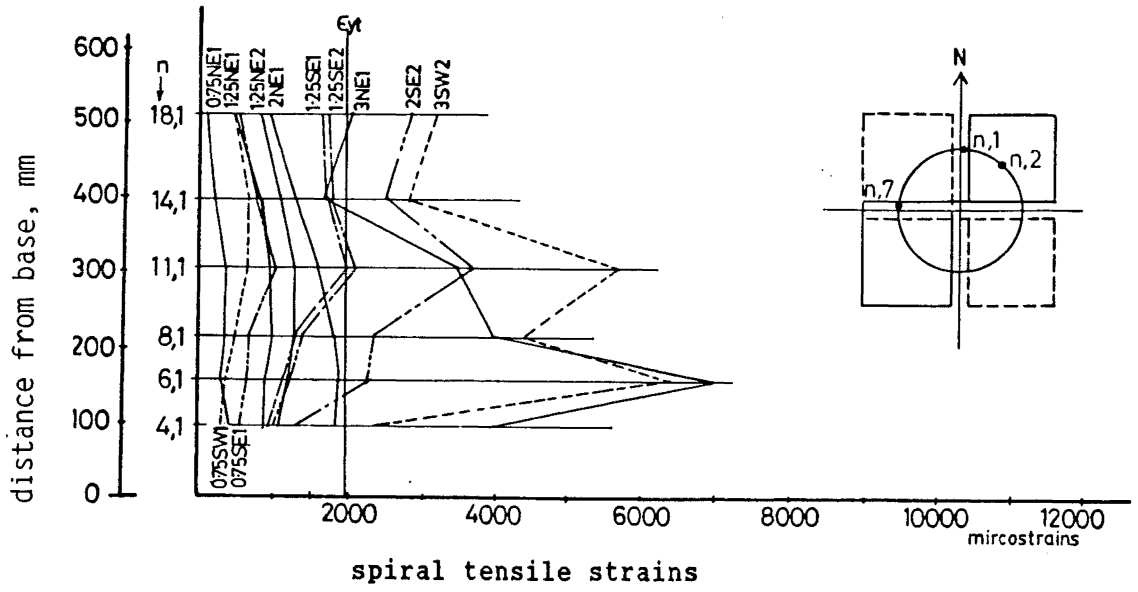

spiral tensile strains

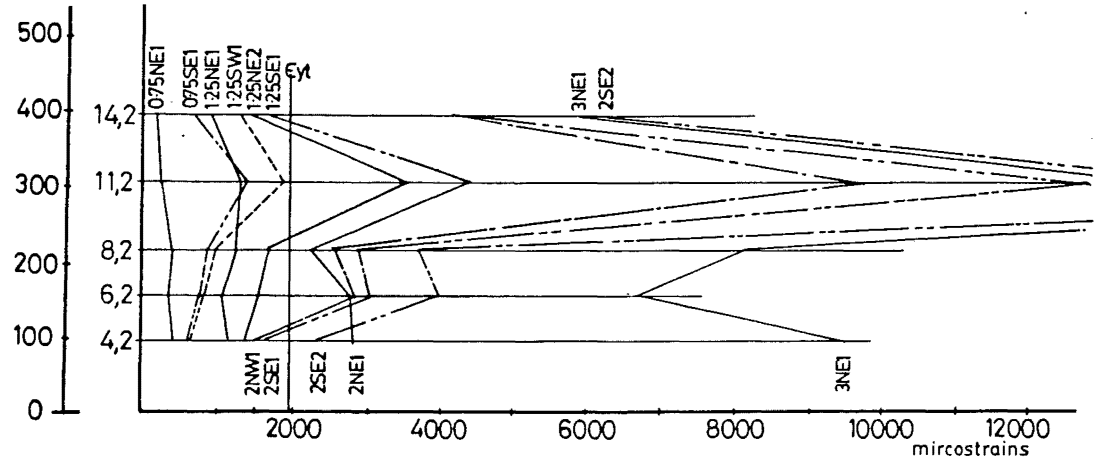

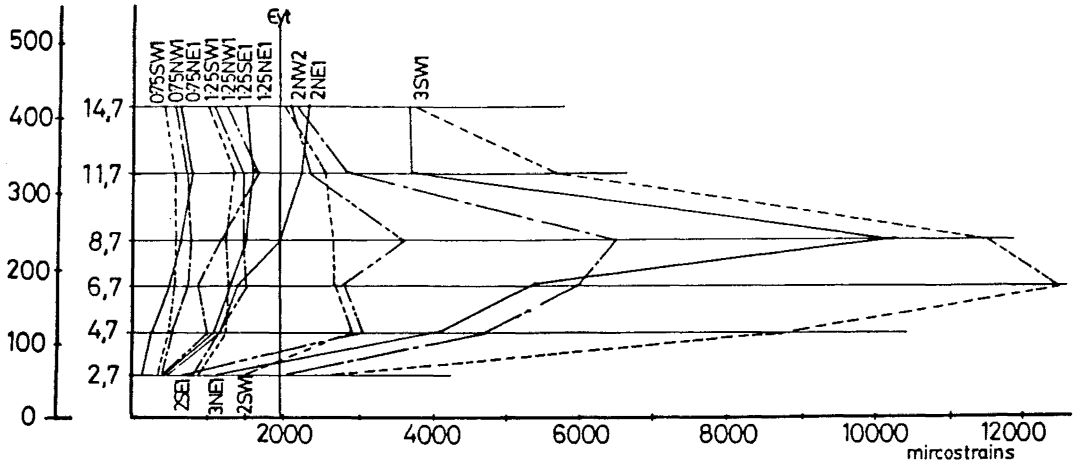

Fig. D.78 : Spiral strain distributions - Unit 13

D.5.4 Unit 14 [2R10-60s]

D.5.4.1 Force - displacement hysteretic performance

The force - displacement hysteretic curves are shown in Figs. D.79 and D.80. In the first cycle to $\mu = 2$, a resistance of $1.10V_{if}$ was recorded. The maximum measured resistance of $1.30V_{if}$ was observed at the first displacement peak in the first cycle to $\mu = 3$, whereas the resistances at the other displacement peaks in the same cycle were $1.16V_{if}$, $1.13V_{if}$, and $1.09V_{if}$. For the other cycles to $\mu \leq 5$, the variation of strengths at displacement peaks in the same cycle was small with a maximum difference of 3%. Loss in strength during repeated cycles was 3% to 20% of that developed first in the first displacement path, and 1% to 8% of that developed first in the second displacement path.

During the first cycle to $\mu = 6$, the strengths attained at the first two displacement peaks were $0.99V_{if}$. However, the test was terminated because of significant twisting of the column at the third displacement peak. The residual strength reduced to $0.75V_{if}$.

D.5.4.2 General performance

Horizontal flexural and inclined cracks appeared at $0.26V_{if}$ and $0.59V_{if}$ respectively. At $\mu = 0.75$, cracks extended to 600 mm above the column base.

At $\mu = 1.25$, local crushing of cover concrete took place at the bottom of the column. The inclination of major cracks was about 44° to the vertical.

At $\mu = 3$, the crack pattern fully developed. The inclination of major cracks became about 35° to 40° to the vertical (Fig. D.22a).

During the repeated cycle to $\mu = 5$, buckling of longitudinal bars in the flexural compression zone was noted. Spalling of cover concrete extended to 100 mm and 500 mm above the column base at $\mu = 2$ and 5 respectively.

At the end of the test, the cover concrete in the lower 700 mm region spalled completely. No fracture of spiral or loss of core concrete was detected (Fig. D.22b).

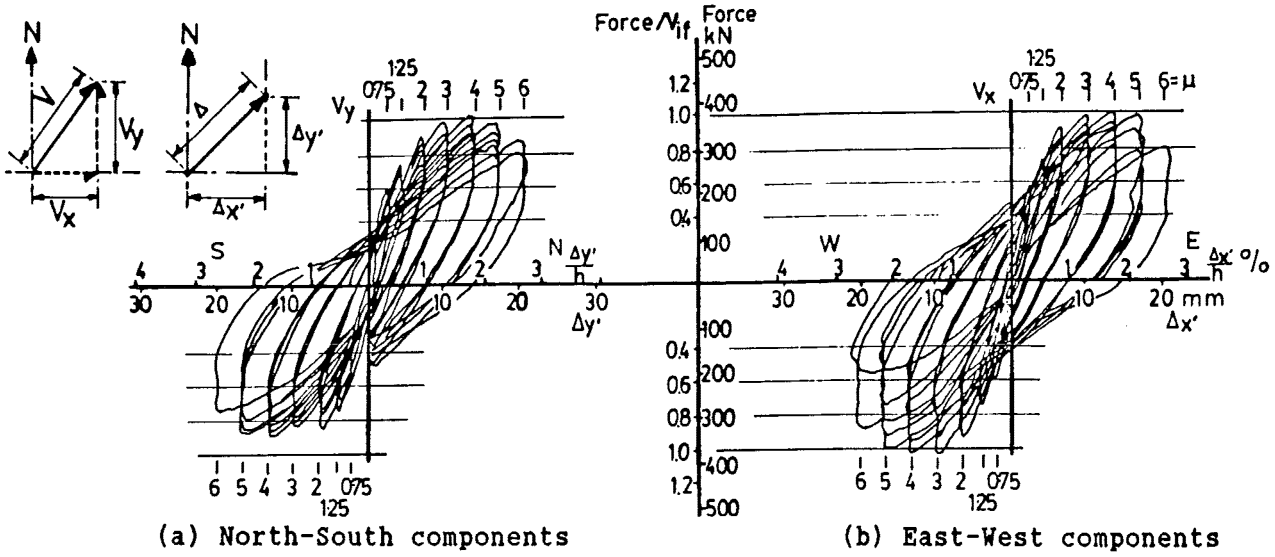

Fig. D.79 : Force - displacement hysteretic curves for displacement components - Unit 14

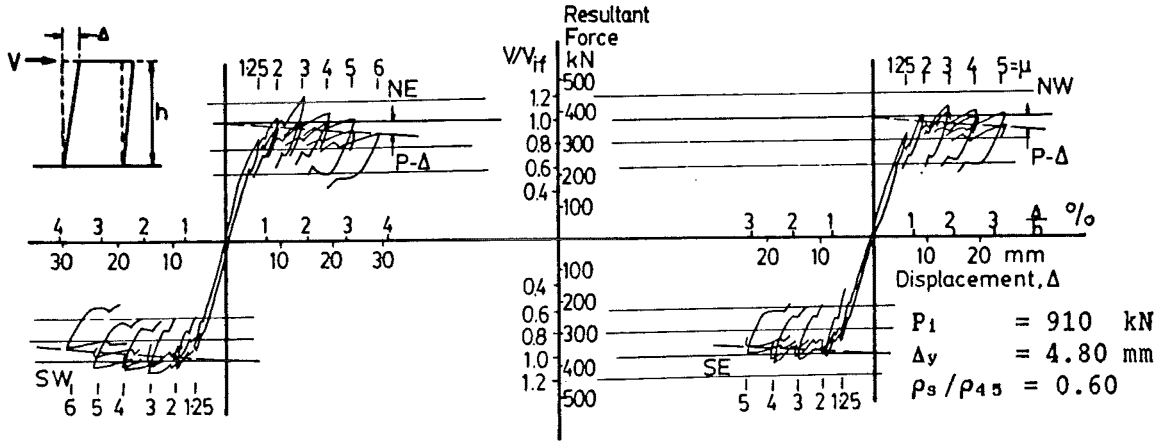

Fig. D.80 : Resultant force - total displacement hysteretic curves - Unit 14

D.5.4.3 Curvature profiles and components of deflections

At $\mu \leq 5$, regular distribution of curvature was recorded in all displacement peaks (Fig. D.81). The length of plastic hinge was about 250 mm. The development of significant curvature ductility was evident.

Fig. D.82 shows the components of deflections. At $\mu \leq 5$, the value of r_f at each displacement direction was about 0.76, which confirmed the flexure dominant behaviour of the column up to this stage.

D.5.4.4 Spiral strain distributions and spiral forces

During the repeated cycle to $\mu = 1.25$, only a few spiral strain readings indicated yielding (Fig. D.83). At $\mu = 5$, a few gauge locations near the column base gave strain values in excess of 3%.

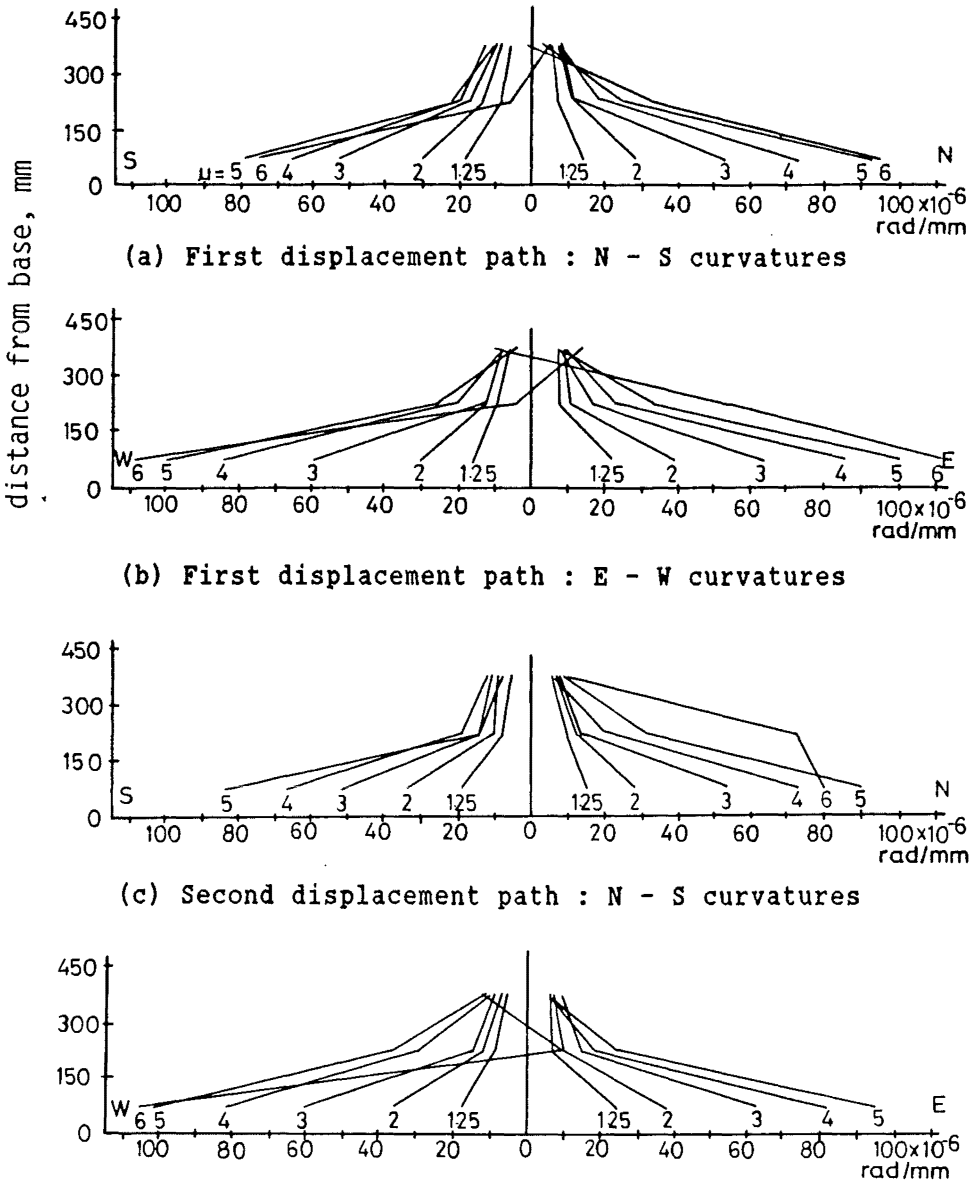

(a) First displacement path : N - S curvatures

(b) First displacement path : E - W curvatures

(c) Second displacement path : N - S curvatures

(d) Second displacement path : E - W curvatures

Fig. D.81 : Measured curvature profiles - Unit 14

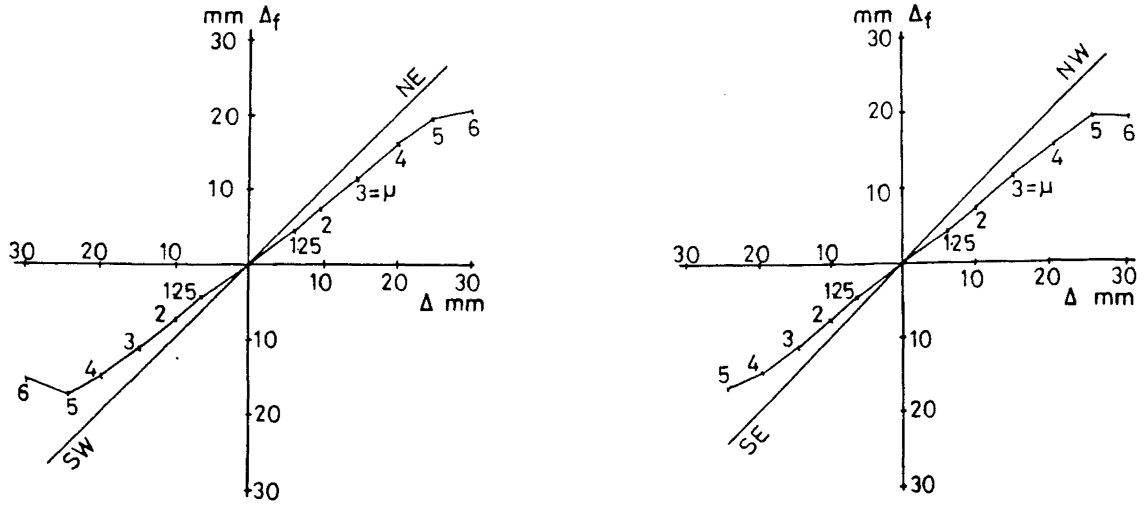

(a) First displacement path

(b) Second displacement path

Fig. D.82 : Components of deflections - Unit 14

At the displacement peaks in cycles to $\mu \geq 2$, spirals crossed by inclined cracks, consistent with shear, reached yield stress.

At zero lateral force, values of σ_{av}/f_{yt} were about 0.48, 0.38, 0.32, and 0.27 after the completion of load cycles to μ = 1.25, 2, 3 and 4 respectively.

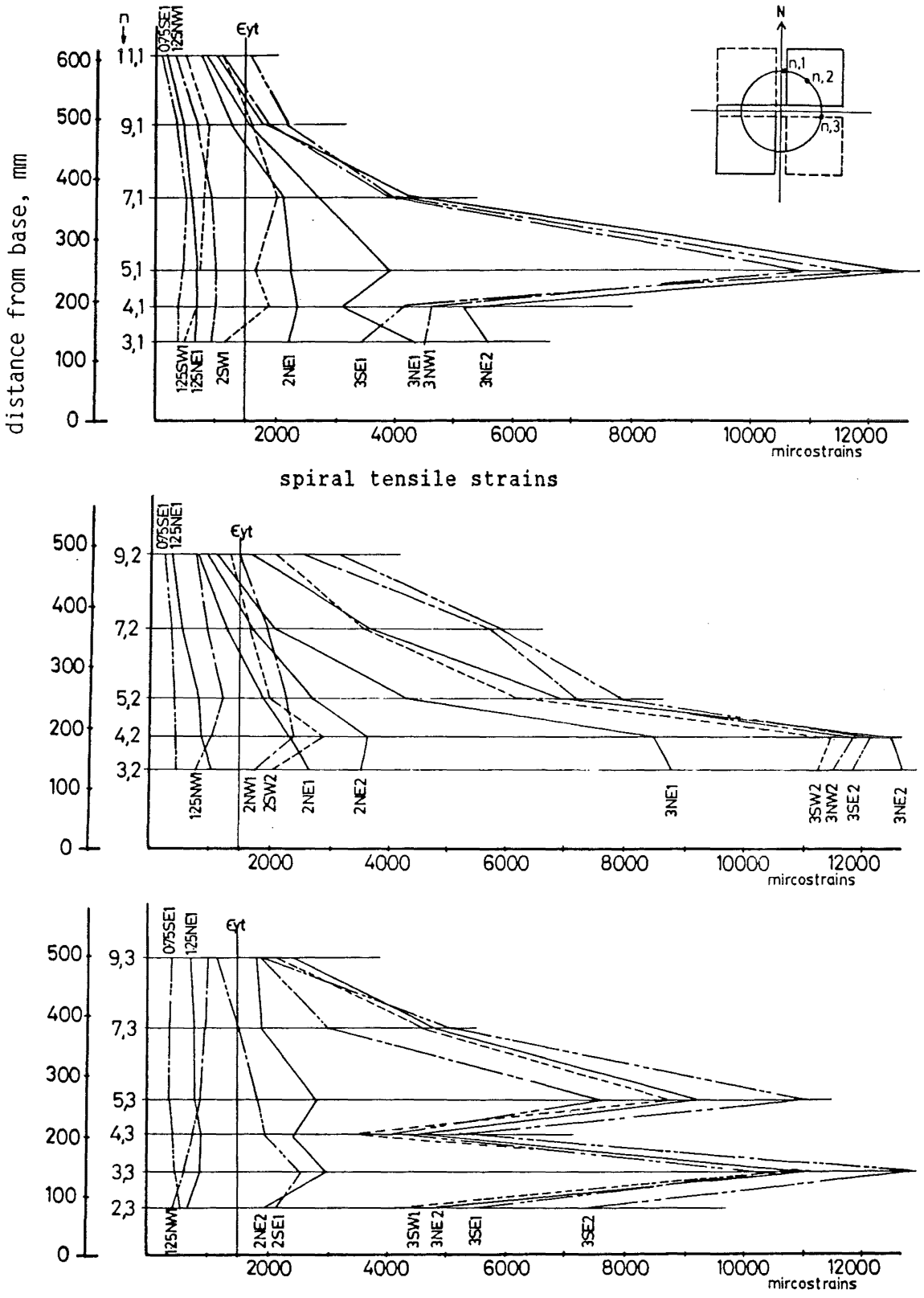

Fig. D.83 : Spiral strain distributions - Unit 14

D.5.5 Unit 15 [4R10-60s]

D.5.5.1 Force - displacement hysteretic performance

A resistance of $1.12V_{if}$ was recorded in the first cycle to $\mu = 2$, whereas the maximum resistance of $1.40V_{if}$ was observed at the first displacement path in the first cycle to $\mu = 4$ (Figs. D.84 and D.85).

At $1.25 \leq \mu \leq 5$, the ratios of strengths listed in the order of displacement peaks were approximately 0.94 : 1.00 : 0.93 : 0.95 in the first cycles, and 0.94 : 1.00 : 0.97 : 0.96 in the repeated cycles. Loss in strength during a repeated cycle was only 2% to 8% of that developed in the first cycle.

Rates of degradation of strength and stiffness became significant only in the second displacement path in the first cycle to $\mu = 6$. During the repeated cycle, the developed strengths varied between $0.87V_{if}$ and $1.05V_{if}$.

At the first displacement peak to $\mu = 7$, the resistance was $0.84V_{if}$.

No pinching of hysteretic curves was observed throughout the loading history. The large applied axial compression load resulted in a very significant increase of stiffness and corresponding decrease in yield displacement. As a consequence, $\mu = 6$ could be attained at a top deflection of less than 2% of the column height.

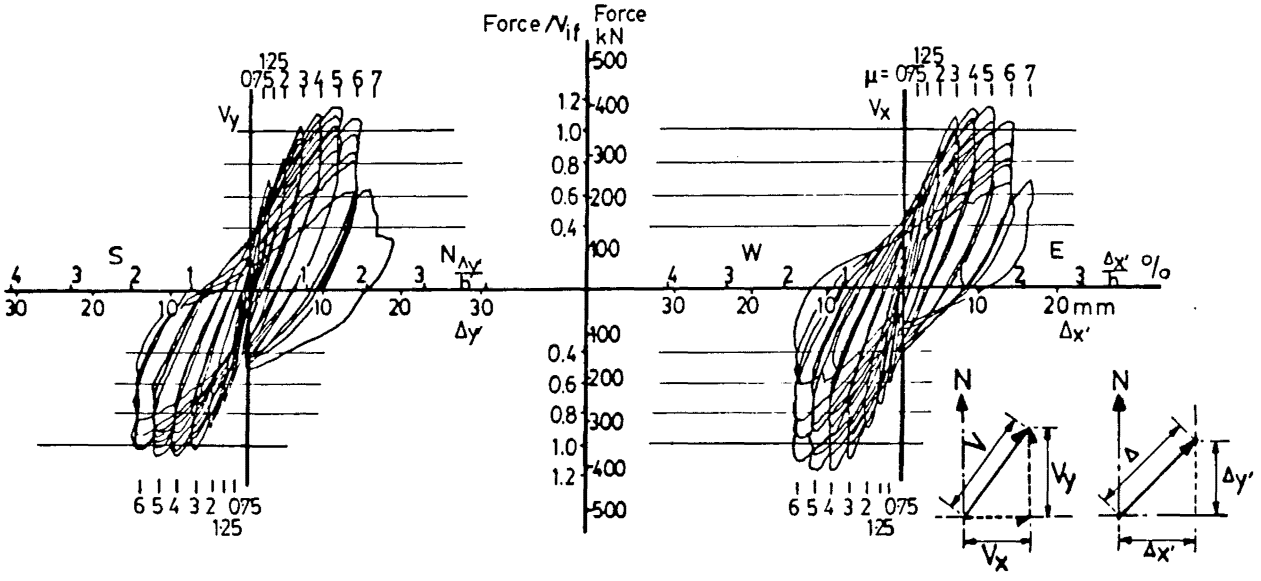

(a) North-South components (b) East-West components

Fig. D.84 : Force - displacement hysteretic curves for displacement components - Unit 15

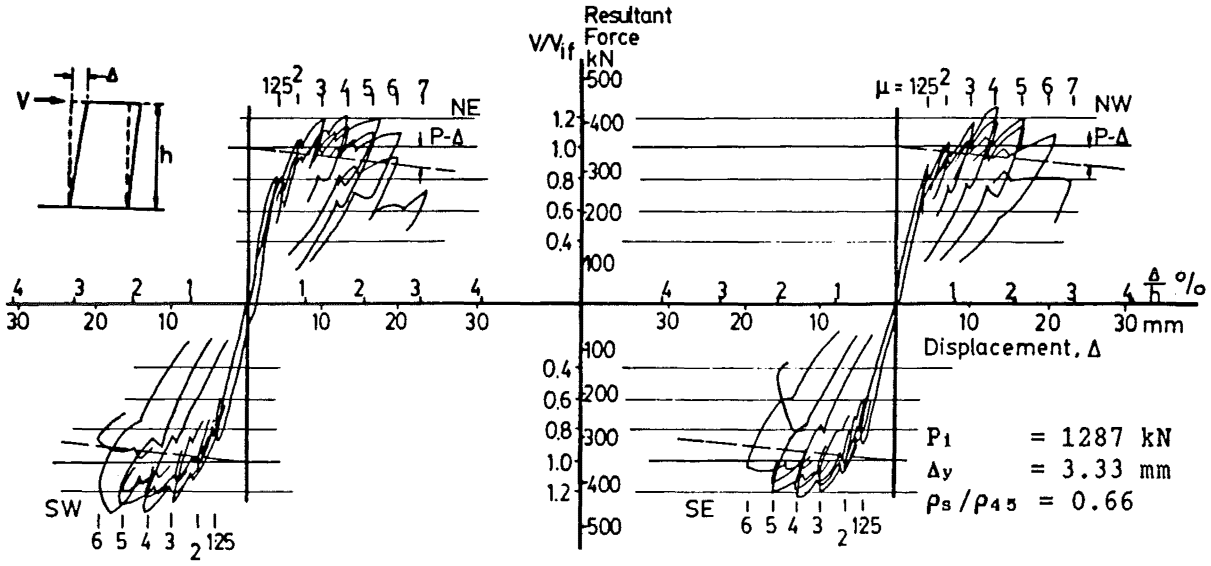

(a) First displacement path (b) Second displacement path

Fig. D.85 : Resultant force - total displacement hysteretic curves - Unit 15

D.5.5.2 General performance

Horizontal flexural and inclined cracks occurred at loads of $0.33V_{if}$ and $0.72V_{if}$ respectively. At $\mu = 0.75$, the flexural cracks extended to 500 mm above the column base. They lined up with spiral locations.

Cracks progressively developed over the full height of the column at $\mu = 1.25$ and 2 (Fig. D.23a).

At $\mu = 3$, crack patterns fully developed. The inclinations of major inclined cracks were 35° to 40° to the vertical.

Spalling of cover concrete took place at the lower 100 mm region of the column at $\mu = 3$, and this extended to 300 mm at $\mu = 5$.

The test was terminated with the SW displacement peak in the first cycle to $\mu = 7$. This became necessary because at this stage the whole system (test unit and the reaction frames) rotated more than 8° about the vertical axis of the column. The reaction frame in the south direction was about to touch one of the piers of Dartec Testing Machine.

At the end of the test, no spiral fracture or loss of core concrete was detected (Fig. D.23b).

D.5.5.3 Curvature profiles and components of deflections

At $\mu \leq 3$, curvature profiles at the displacement peaks were regular and similar (Fig. D.86). The length of plastic hinge was about 250 mm. Afterwards, shapes of curvature distribution profiles were different at different directions of displacements. However, the components of deflections at each displacement peak were similar (Fig. D.87). At $\mu \leq 6$, the value of r_f at each displacement peak was about 0.7. In spite of the moderate inelastic curvatures shown here, significant curvature ductility was developed, indicating the dominance of flexural response.

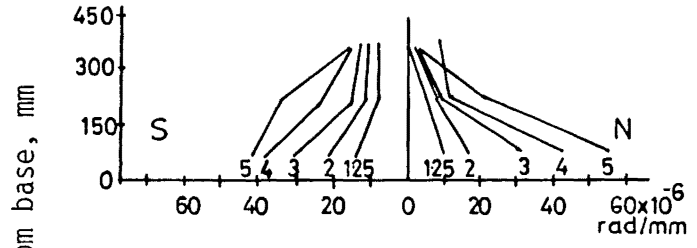

(a) First displacement path : N - S curvatures

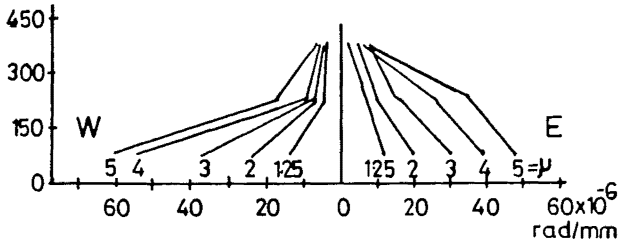

(b) First displacement path : E - W curvatures

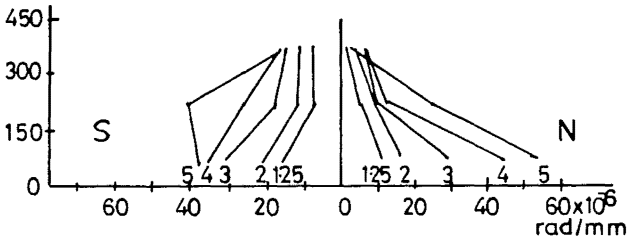

(c) Second displacement path : N - S curvatures

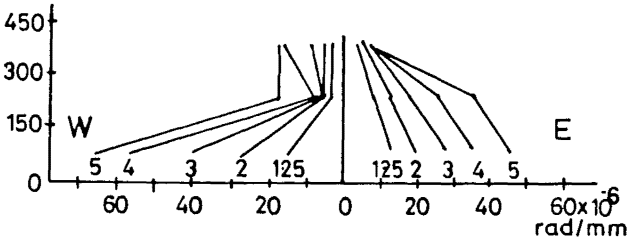

(d) Second displacement path : E - W curvatures

Fig. D.86 : Measured curvature profiles - Unit 15

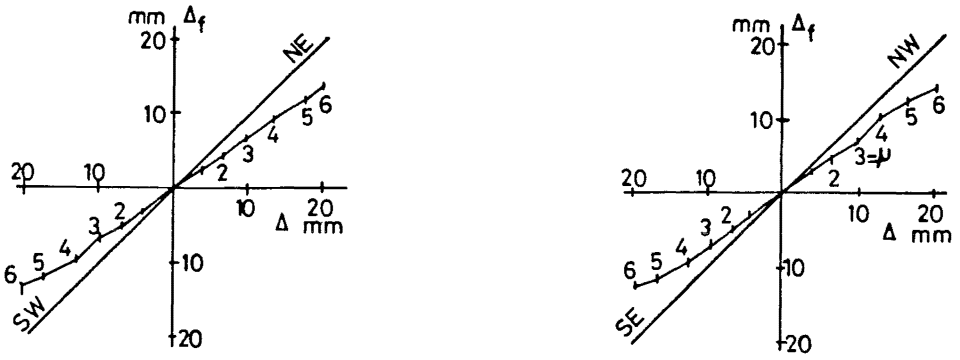

(a) First displacement path (b) Second displacement path

Fig. D.87 : Components of deflections - Unit 15

D.5.5.4 Spiral strain distributions and spiral forces

Some spirals started to yield in the first cycle to $\mu = 2$. During the repeated cycle to $\mu = 5$, some strains exceeded 3%

At displacement peaks in cycles to $\mu \geq 2$, spirals crossed by inclined cracks, consistent with shear, reached yield stress (Fig. D.88).

At zero lateral force, the values of σ_{av}/f_{yt} were 0.32, 0.52, 0,47, and 0.33 after the completion of cycles to $\mu = 1.25$, 2, 3, and 4 respectively.

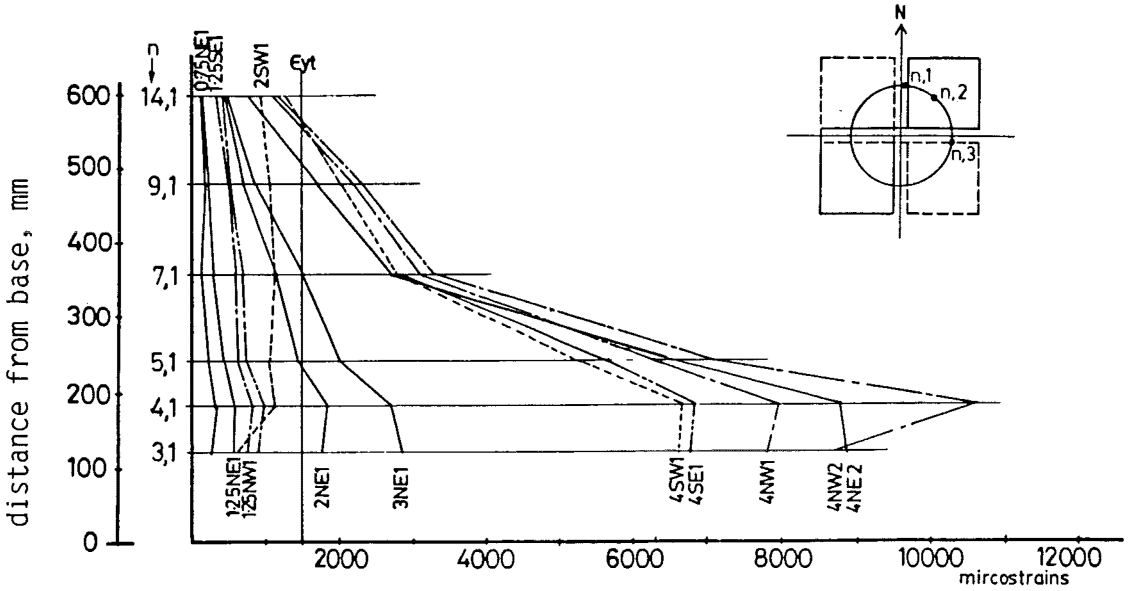

spiral tensile strains

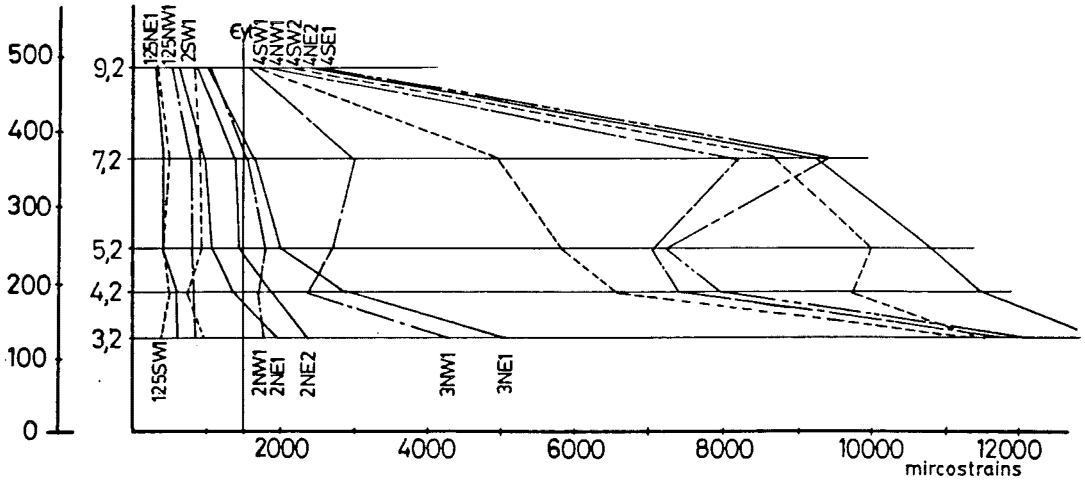

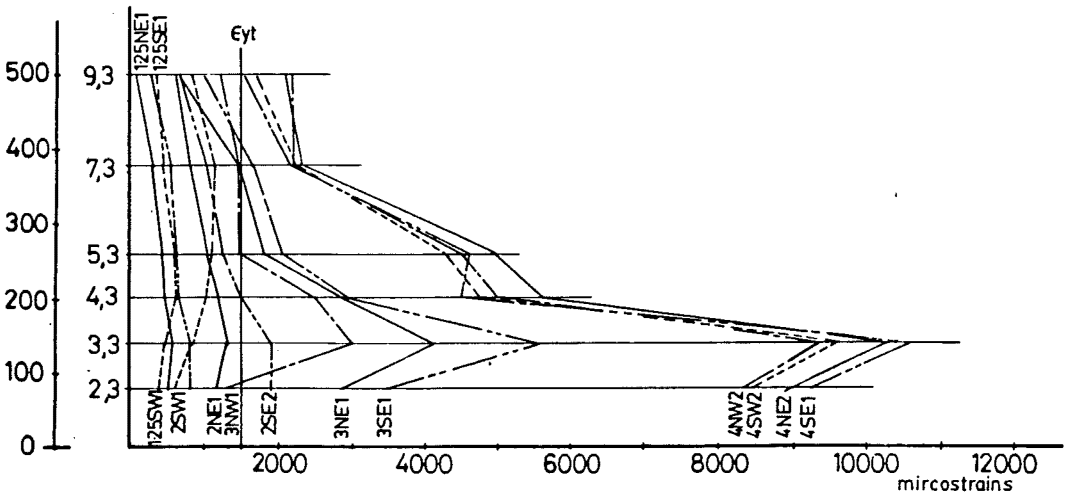

Fig. D.88 : Spiral strain distributions - Unit 15

D.6 COLUMN SUBJECTED TO BI-DIRECTIONAL 'r' DISPLACEMENT PATTERN
Unit 16 [2R6-30r]

D.6.1 Force - Displacement Hysteretic Performance

Figs. D.89 to D.91 show the force - displacement hysteresis curves of the column for components of displacement, measured separately along North-South and East-West directions respectively. The strengths, developed at various control points as identified in the special displacement pattern (Fig. C.7), are listed in Table D.IV.

During the first displacement path, the maximum measured resistance of $1.30V_{if}$ was recorded at control point 2 ($\mu = 4$) . At control point 4 ($\mu = 5$), the resistance became $1.28V_{if}$. the observed strength was only reduced to $1.16V_{if}$ at control point 7 ($\mu = 4$).

As there were no signs of distress after completing the first load path, the column was then subjected to the second displacement path. Variation of strengths at displacement peaks within the same cycle was small with a maximum difference of only 7%. At the displacement peaks in the third repeated cycle, the column still resisted $0.89V_{if}$. At this stage, some pinching of the hysteretic loops was detected.

The column was further subjected to the third displacement path, which was circular with $\mu = 4$. Strength gradually degraded from $0.94V_{if}$ to $0.75V_{if}$. Finally, the column was displaced eastward to $8\Delta_y$ while sustaining $0.95V_{if}$.

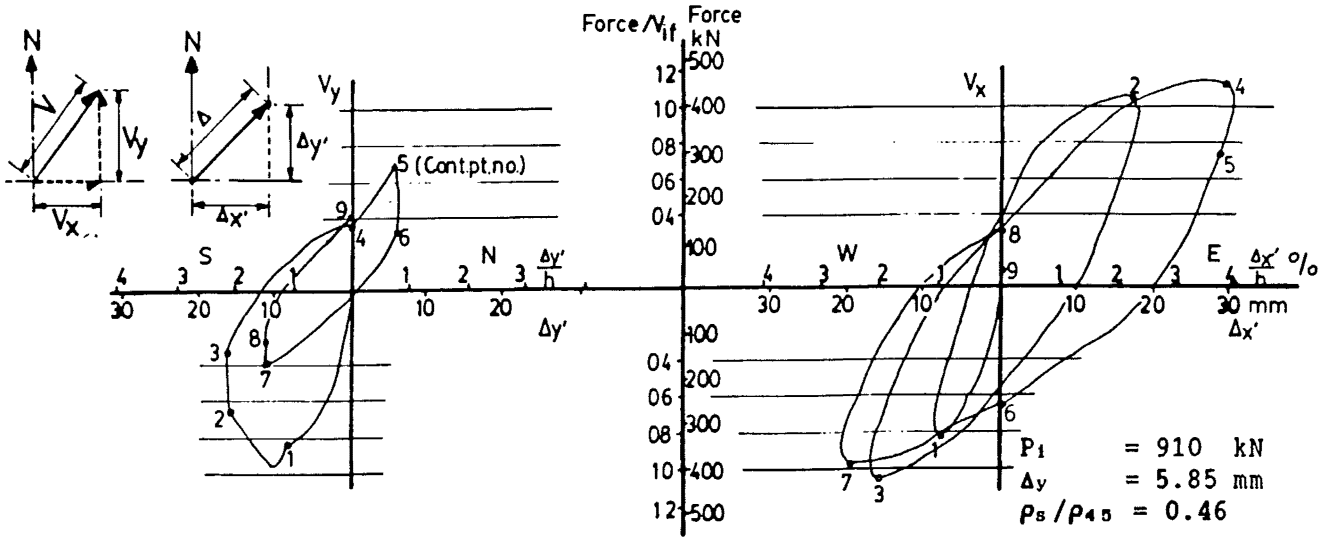

(a) North-South components (b) East-West components

Fig. D.89 : Force - displacement hysteretic curves for displacement path 1 - Unit 16

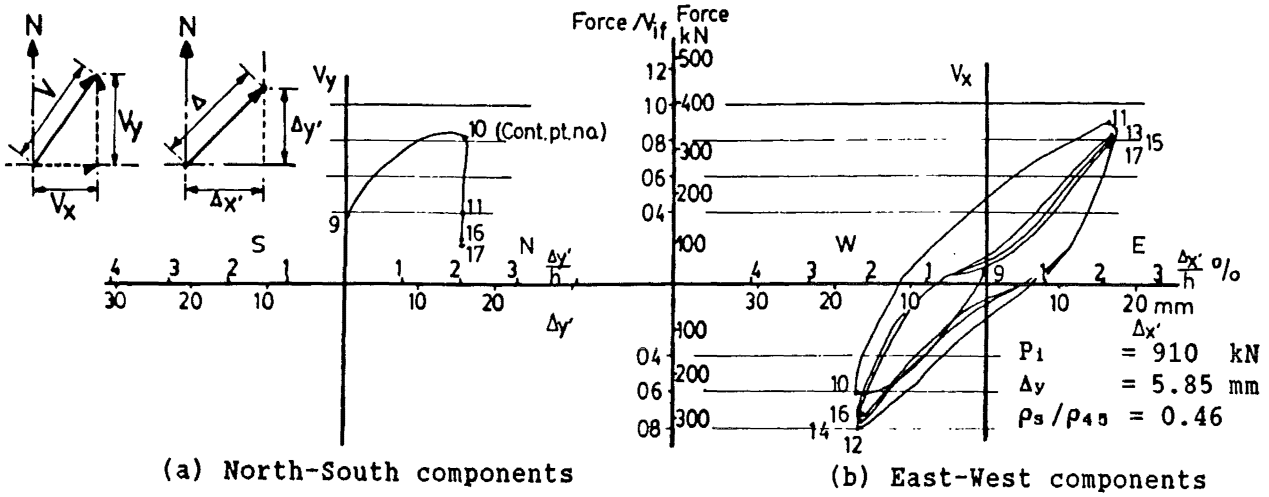

(a) North-South components (b) East-West components

Fig. D.90 : Force - displacement hysteretic curves for displacement path 2 - Unit 16

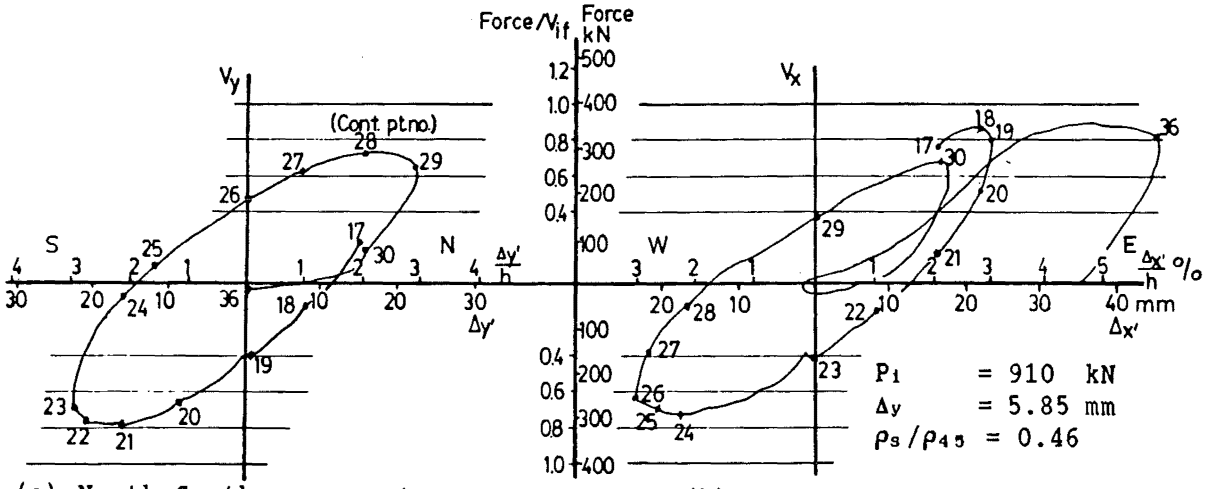

(a) North-South components (b) East-West components

Fig. D.91 : Force - displacement hysteretic curves for displacement path 3 - Unit 16

Table D.IV : Strengths developed at various control points for Unit 16

Displacement paths								
1			2			3		
control pt.	μ	V/Vif	control pt.	μ	V/Vif	control pt.	μ	V/Vif
1	2	1.22	10	4	1.12	18	4	0.94
2	4	1.30	11	4	1.04	19	4	0.90
3	4	1.08	12	4	0.94	20	4	0.95
4	5	1.28	13	4	0.96	21	4	0.94
5	5	1.08	14	4	0.92	22	4	0.91
6	1	0.77	15	4	0.92	23	4	0.87
7	4	1.16	16	4	0.89	24	4	0.83
8	2	0.45	17	4	0.89	25	4	0.79
9	0	0.36				26	4	0.79
						27	4	0.78
						28	4	0.77
						29	4	0.75
						30	4	0.75
						31	3	0.13
						32	0	0.10
						33	3	0.54
						34	5	0.93
						35	6.3	0.94
						36	8	0.95

Note : Values included P - Δ effect (see Section D.2.2)

D.6.2 General Performance

During the first displacement path, flexural and inclined cracks extended to 700 mm above the column base at control point 1 (μ = 2). The inclination of major cracks was 45° to the vertical. Local crushing of cover concrete extended to 100 mm above the column base. At higher ductilities, more new inclined cracks, consistent with shear, formed. At control point 4 (μ =5), the inclination of new cracks was approximately 35° to the vertical (Fig. D.24a). Spalling of cover concrete extended to 160 mm above the column base. At the end of this first displacement path, the axial shortening of the column was 0.28 mm.

During the second displacement path, more new inclined cracks appeared during the first cycle (control points 10 and 11). After the completion of this displacement path, spalling of cover concrete extended to 350 mm above the column base (Fig. D.24b).

As the column was displaced according to the third, i.e. circular path, spalling of cover concrete progressively extended to higher levels above the column base. At the end of the test, the cover concrete at the lower 600 mm region of the column spalled completely (Fig. D.24c). There was no sign of spiral fracture or buckling of longitudinal bars. The core concrete appeared to be in good condition. The column was still able to carry the applied axial and substantial lateral loads. The axial shortening at the end of the test was 3.54 mm.

When taking into account the simulated and rather severe displacement paths used in this test, the performance of the column (Table D.IV) was considered to be very satisfactory.

D.6.3 Curvature Profiles and Components of Deflections

The curvature profiles maintained the shape typical of flexural performance (Fig. D.92). The estimated length of plastic hinge was 250 mm. Significant curvature ductility was developed.

Fig. D.93 shows the components of deflections. The values of r_f were 0.74 and 0.62 in the first and second displacement paths respectively.

D.6.4 Spiral Strain Distributions and Spiral Forces

Except for control points 6, 8, 9, 31, 32, and 33, which are located on the unloading paths, spirals crossed by inclined cracks, consistent with shear, reached yield stress at $\mu \geq 2$ (Fig. D.94).

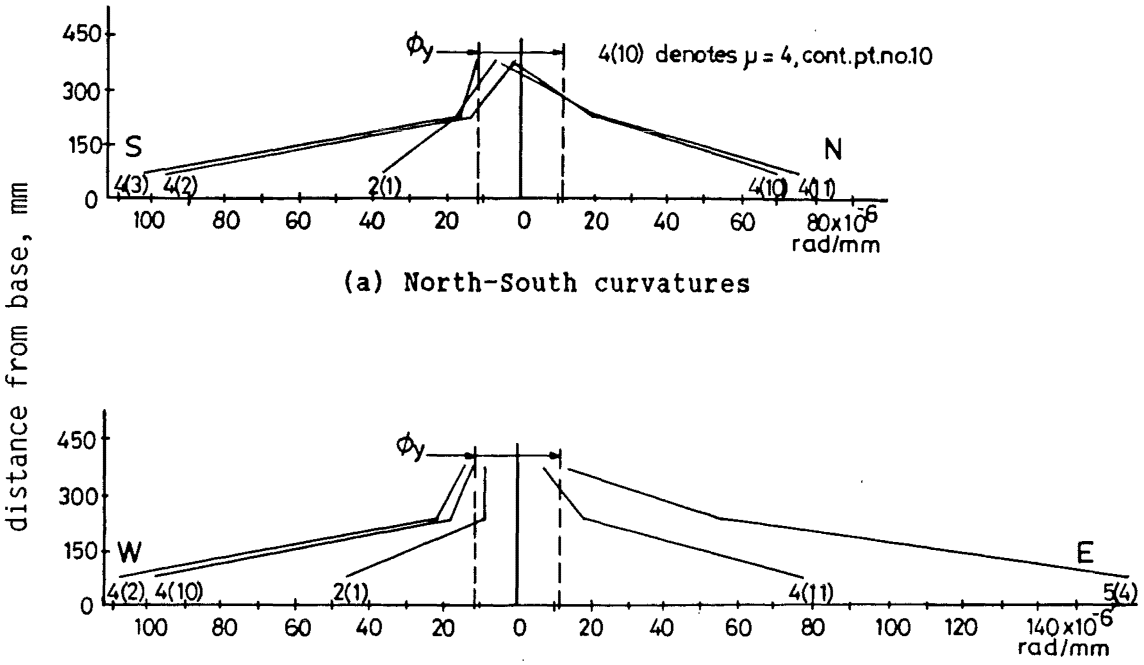

(a) North-South curvatures

(b) East-West curvatures

Fig. D.92 : Measured curvature profiles - Unit 16
(at control points 10 and 11)

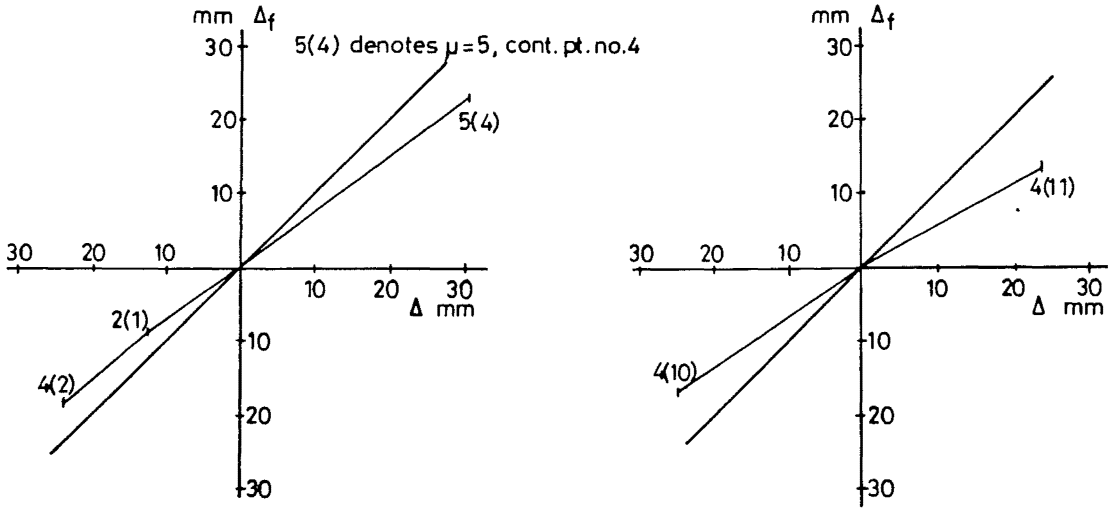

(a) Control points 1, 2, and 4 (b) Control points 10 and 11

Fig. D.93 : Components of deflections - Unit 16

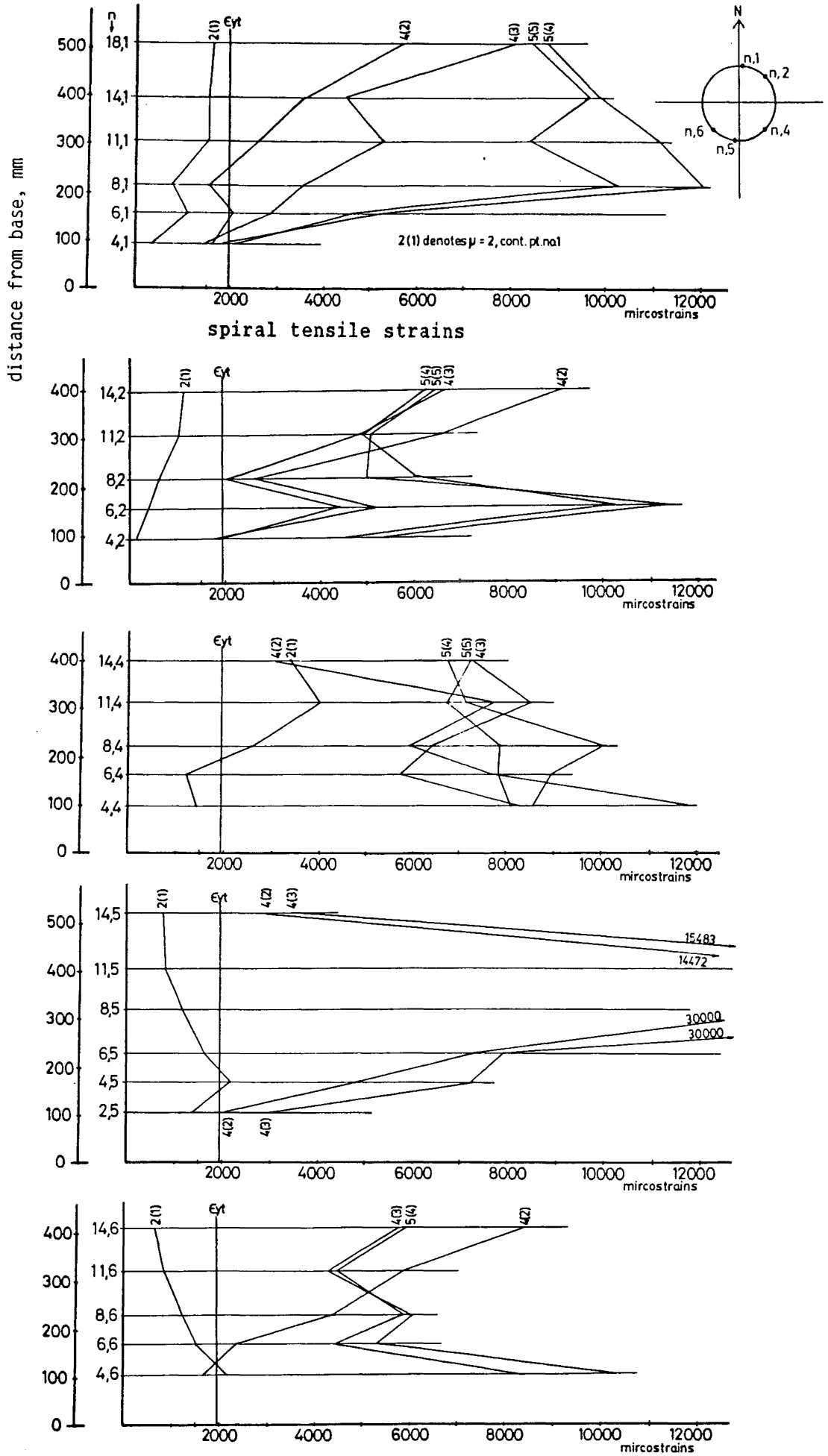

Fig. D.94 : Spiral strain distributions - Unit 16

CHAPTER E
COMPARISONS OF PERFORMANCE OF TEST COLUMNS

E.1 INTRODUCTION

In this chapter, the influence of the main parameters, namely displacement pattern, spiral steel content and axial compression load intensity, on various features of the performance of test columns are discussed, and compared.

E.2 FAILURE MODES AND FEATURES OF FAILURE

With reference to Ang's [E.1] classification of failure modes of columns, a similar strategy is used to classify the failure modes of sixteen columns in this test series. They are :

Ductile flexural failure (D-F) : $\mu_o \geq 6$,

Failure with moderate ductility (MD-S) : $4 \leq \mu_o < 6$,

Shear failure with limited ductility (LD-S) : $2 \leq \mu_o < 4$,

and Brittle shear failure (B-S) : $\mu_o < 2$,

where μ_o is the observed dependable displacement ductility capacity as defined in Section D.2.2.

Table E.I lists the failure modes of the test columns and observed features of failure. The test results cover the full range of failure modes, and provide useful data for design recommendations to be given in Chapter F.

As far as features of failure are concerned, it is noted that sudden collapse did not occur for columns with no axial compression load. For example, Unit 4 failed in brittle shear mode. However, it still sustained 66% of its ideal flexural strength, V_{if}, at the displacement of $5\Delta_y$ or drift (ratio of the tip deflection of a column to the distance from the column base to the level where dip deflection is measured, Δ/h) of 4.6% without showing any sign of instability. Similarly, Unit 11 was displaced to $8\Delta_y$ (drift of 6.6%) with residual strength of $0.66V_{if}$. Unit 6 is the only one in this group ($P_l/(f'_c A_g) = 0$) which failed with spiral fracture at the displacement of $6\Delta_y$ or drift of 5%. Since the fracture took place adjacent to a welded joint, this part of spiral was likely to be affected during the welding process.

Table E.I : Failure modes and features of failure of test columns

failure mode	Unit		ρ_s	Δ/h at μ_o		features of failure			
	no.	notation	%	%	-	longit. bars buckled	spiral fracture	sudden compress. failure	large twist
D-F	1	2R10-60u	1.450	3.76	6	yes	yes	yes	-
	3	4R10-60u	1.450	2.54	6	yes	-	-	-
	15	4R10-60s	1.420	2.61	6	-	-	-	yes
MD-S	6	0R6 -30b	1.032	3.33	4	-	yes	-	-
	8	2R6 -30b	1.032	3.06	4	yes	yes	yes	-
	9	4R6 -40b	0.774	1.74	4	yes	yes	yes	-
	10	4R10-65b	1.340	2.22	5	yes	yes	yes	-
	12	0R10-35s	2.460	4.13	5	-	-	-	yes
	13	2R6 -30s	1.032	3.06	4	-	yes	-	yes
	14	2R10-60s	1.450	3.14	5	yes	-	-	yes
	16	2R6 -30r	1.032	$\geq$3.06	$\geq$4	-	-	-	-
LD-S	2	4R6 -65u	0.476	0.82	2	yes	-	yes	-
	5	0R6 -50b	0.619	1.77	2	-	-	-	-
	7	2R6 -60b	0.516	1.48	2	-	yes	-	-
	11	0R6 -30s	1.032	2.48	3	-	-	-	yes
B-S	4	0R6 -80b	0.387	$<$1.15	$<$1.25	-	-	-	-

Notes:

D-F : Ductile flexural failure
MD-S : Failure with moderate ductility
LD-S : Shear failure with limited ductility
B-S : Brittle shear failure

It appears that the dependable ductility capacity, μ_o, decreases with increase of the severity of displacement history. The observed μ_o of a test unit subjected to uni-directional loading history was greater than that of its companion unit subjected to bi-directional loading history. However, for test units with applied axial compression, the observed μ_o of a test column subjected to bi-directional 'b' type displacement pattern was similar to that of its companion column subjected to bi-directional 's' type displacement pattern. An increase of spiral reinforcement content distinctly improved the ductility of test columns. In one case, there was evidence that axial compression load increased the μ_o. However, it will be shown in Section E.3.1 that axial compression load has significant influence on the strength envelope curves of test columns.

Although the dependable ductility, μ_o, has been used in Table E.1 as a benchmark to assist in classification, it should be noted that absolute displacements must also be considered. Irrespective of the ductility, μ, developed, it may be considered that total deflections in excess of 3% of the column height are beyond design limits. While it might be encouraging to know that deformations beyond 3% could be sustained, it is questionable whether this ability could be utilized in design. Inelastic excursions beyond the 3% drift limit are likely to result in excessive permanent deformations which would negate any attempt of repair or to strengthen bridge piers so damaged.

Because yield displacements are affected by the applied axial compression, different drifts may be associated with the same displacement ductility factor. For this reason, the observed drift at the dependable ductility, μ_o, are also listed in Table E.I. This will assist in identifying units for which drift rather than ductility should be considered as the limiting criterion for inelastic performance.

Although columns with moderate or high axial compression load can achieve moderate or ductile failure modes, these are often accompanied by buckling of longitudinal steel bars, spiral fracture, and sudden compression failure i.e. a sudden softening in the axial and lateral resistance capacity. This is evident from the test results of Units 1, 2, 8, 9, and 10. The corresponding drift at failure varied from 1.6% (Unit 2) to 5% (Unit 1).

E.3 STRENGTH ENVELOPE CURVES AND MAXIMUM MEASURED STRENGTH

E.3.1 Strength Envelope Curves

In the previous chapter, the force - displacement hysteretic performance of each test column has been individually reported. In order to further investigate influences of the main parameters (spiral reinforcement content, axial compression load intensity, and displacement pattern) on the development of strength at each ductility level, strength envelope curves are constructed as shown in Figs. E.1 to E.4. They are envelopes of the corresponding force - displacement hysteretic loops with strength and displacement normalized by the related ideal flexural strength, V_{if}, and yield displacement, Δ_y, respectively. These curves are then grouped according to the parameters which might be relevant. Furthermore, as supplementary information to Figs. E.1 to E.4, the measured initial stiffness of test columns, and drifts at various loading stages are listed in Table E.II. Their characteristics are discussed as below:

I) Ascending portions of the envelope curves

The secant stiffness of a test column, K_2, measured at $\Delta = 0.75\ \Delta_y$, depended mainly on the applied axial compression load intensity (Table E.II). The mean values of K_2 were 48 kN/mm, 73 kN/mm, and 111 kN/mm for units with $P_i/(f'_c A_g)$ equal to 0, 0.19, and 0.39 respectively. Axial compression increases stiffness and reduces curvature by increasing the depth of flexural compression zone of a section. Furthermore, it also reduces shear deformation during the elastic stage of loading by delaying the formation of inclined cracks. On the other hand, spiral steel content and displacement patterns had insignificant effect on K_2.

Another measure of stiffness at the early stage of loading is the drift at the first occurrence of $V/V_{if} = 1$. At this load level, the drifts were found to be about 1% for units with $P_i/(f'_c A_g) \leq 0.19$, and 0.6% for units with $P_i/(f'_c A_g) = 0.39$ (Table E.II). As the yield displacement is established from the stiffness at $V/V_{if} = 0.75$, the ratios of drift listed in column 6 of Table E.II are close to the ratios of stiffness at $V/V_{if} = 1$ to those at $V/V_{if} = 0.75$. The average of these ratios was 0.75. These ratios tended to increase with an increase of spiral reinforcement content which has the effect of reducing shear deformations after the formation of diagonal cracks. On the other hand, an increase of severity of loading history enhanced the loss of stiffness.

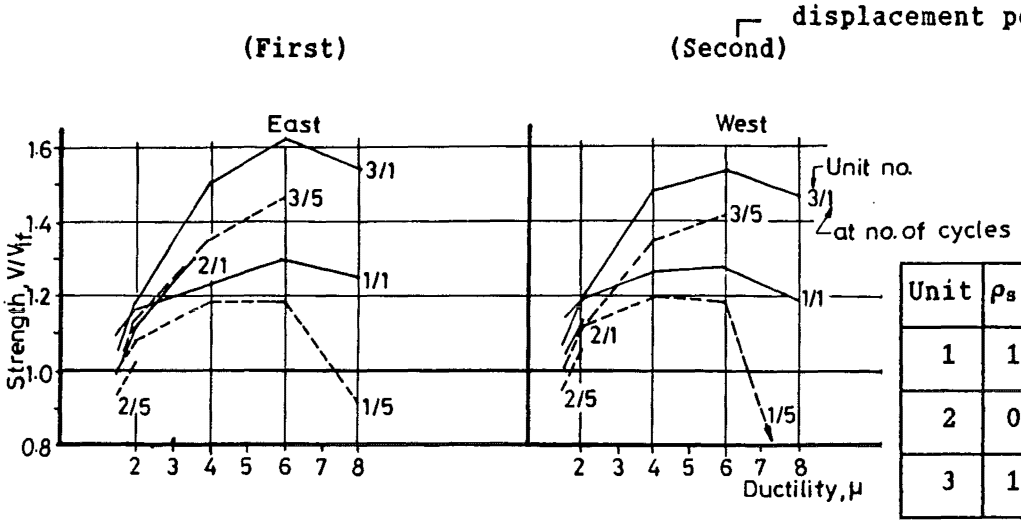

Unit	ρ_s (%)	$P_t/(f'_c A_g)$
1	1.45	0.19
2	0.48	0.39
3	1.45	0.39

Fig. E.1 : Influence of axial load and spiral content on strength envelope curves ('u' type displacement pattern)

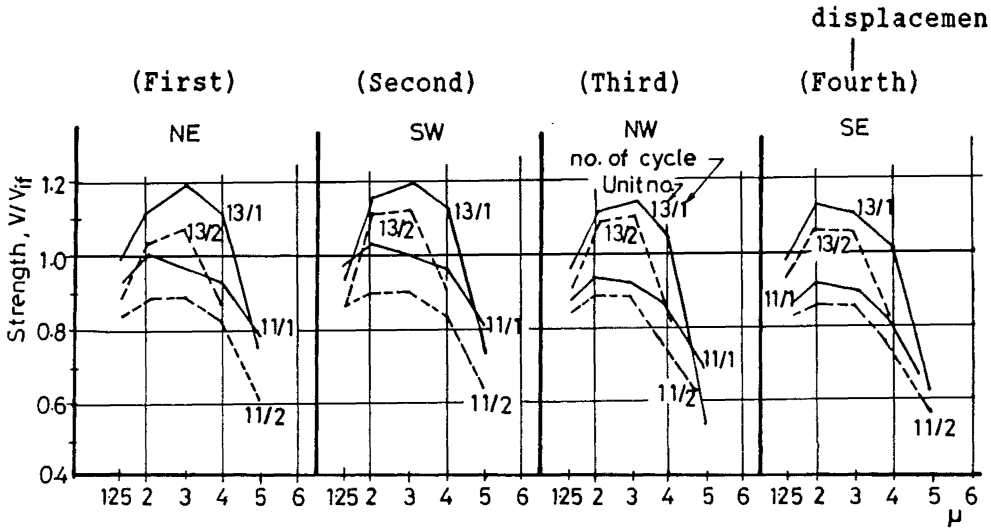

Unit	$P_t/(f'_c A_g)$
11	0
13	0.19

(a) 's' type displacement pattern, ρ_s = 1.03%

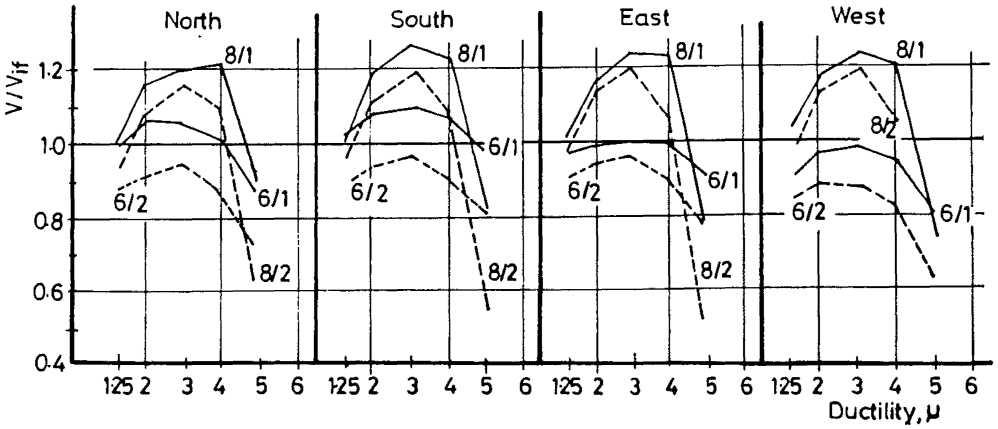

Unit	$P_t/(f'_c A_g)$
6	0
8	0.19

(b) 'b' type displacement pattern, ρs = 1.03%

Fig. E.2 : Influence of axial load on strength envelope curves

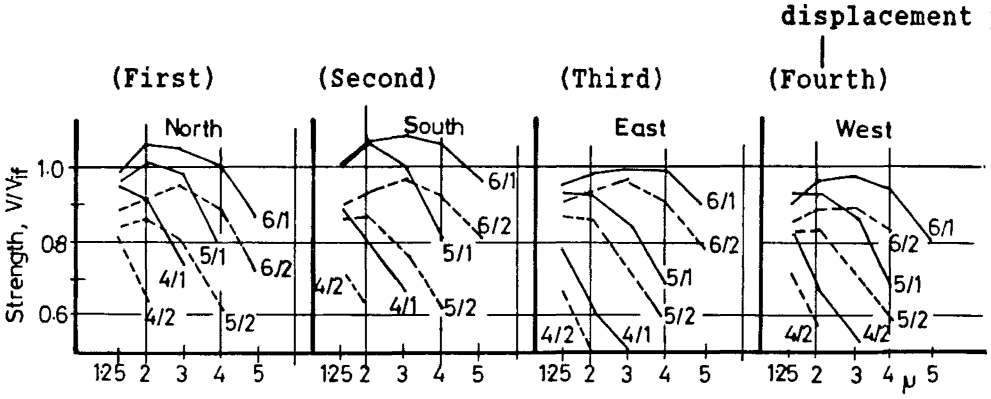

Unit	ρ_s (%)
4	0.39
5	0.62
6	1.03

(a) $P_i/(f'_c A_g) = 0$, 'b' type displacement pattern

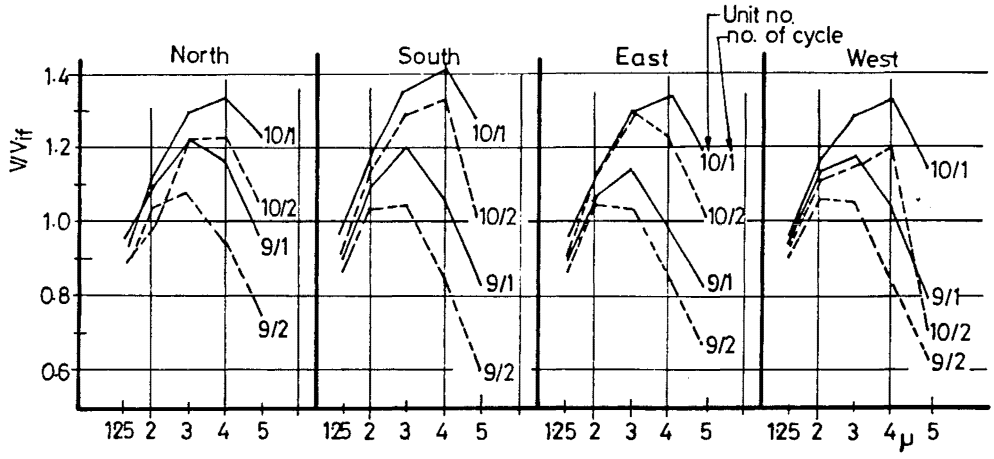

Unit	ρ_s (%)
9	0.77
10	1.34

(b) $P_i/(f'_c A_g) = 0.39$, 'b' type displacement pattern

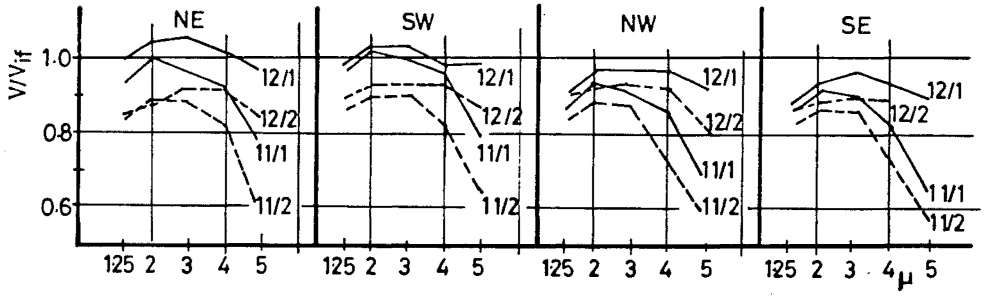

Unit	ρ_s (%)
11	1.03
12	2.46

(c) $P_i/(f'_c A_g) = 0$, 's' type displacement pattern

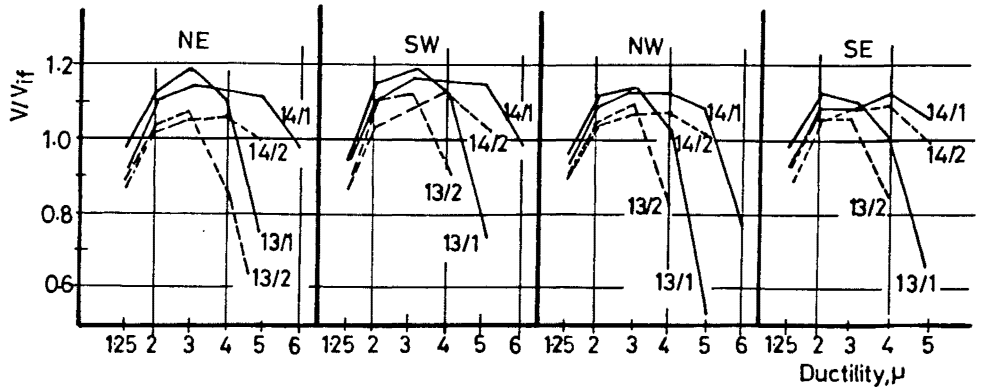

Unit	ρ_s (%)
13	1.03
14	1.45

(d) $P_i/(f'_c A_g) = 0.19$, 's' type displacement pattern

Fig. E.3 : Influence of spiral content on strength envelope curves

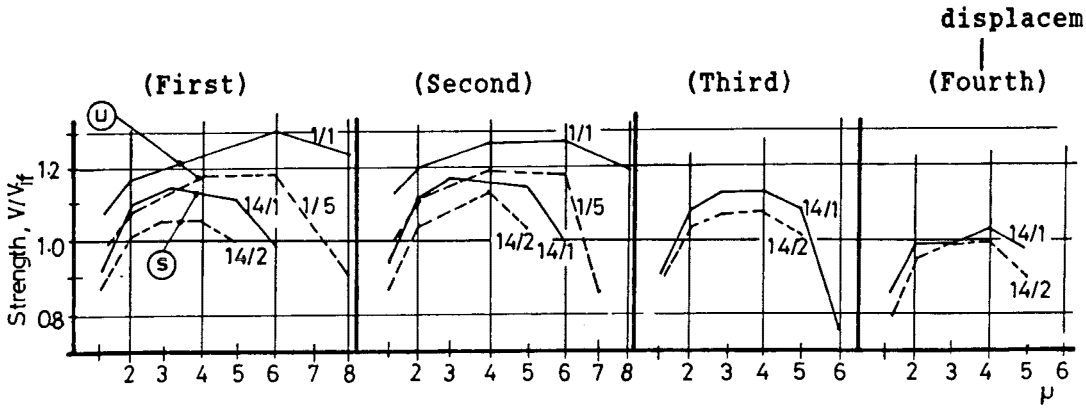

(a) $P_1/(f'_cA_g)$ = 0.19, ρ_s = 1.45%, Displacement patterns 'u' & 's'

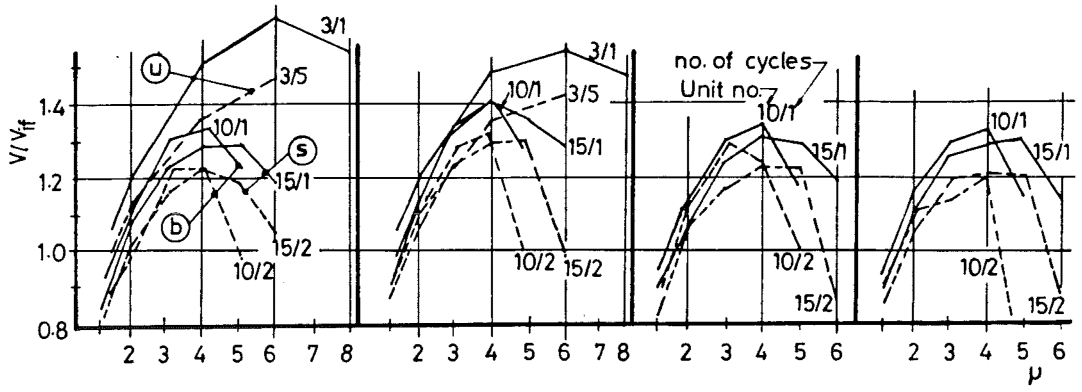

(b) $P_1/(f'_cA_g)$ = 0.39, ρ_s = 1.45% (1.34% for Unit 10), Displacement patterns 'u', 'b', & 's'

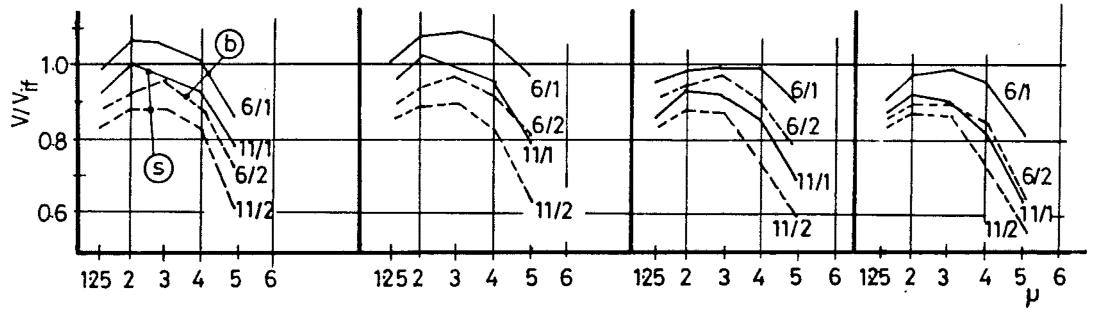

(c) $P_1/(f'_cA_g)$ = 0, ρ_s = 1.03%, Displacement patterns 'b' & 's'

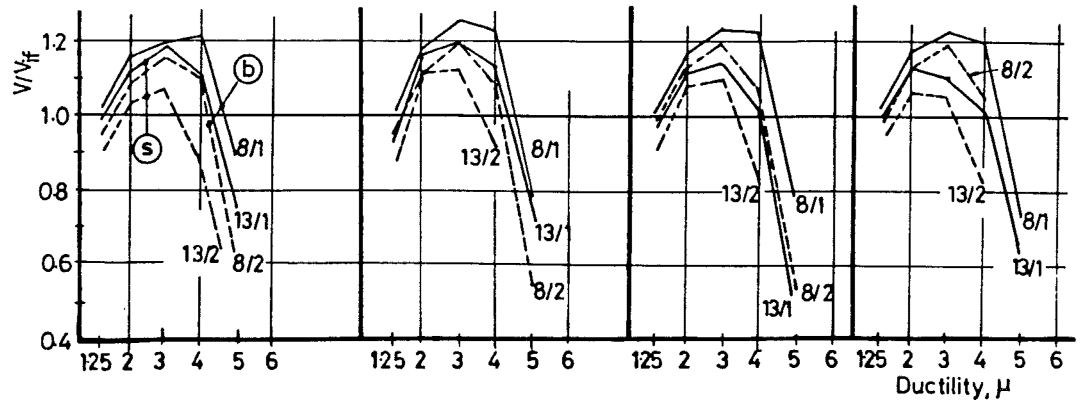

(d) $P_1/(f'_cA_g)$ = 0.19, ρ_s = 1.03%, Displacement patterns 'b' & 's'

Fig. E.4 : Influence of displacement patterns on strength envelope curves

Table E.II : Drifts of test columns at various loading stages

Unit		1	2	3	4	5	6
		K_2	Δ_y/h	Δ/h at V_{if}	Δ/h at V_{max}	μ at V_{max}	2/3
no.	notation	kN/mm	%	%	%	-	-
4	0R6 -80b	47	0.92	-	1.15	1.25	-
5	0R6 -50b	49	0.88	1.14	1.77	2	0.77
6	0R6 -30b	52	0.83	1.03	2.48	3	0.81
11	0R6 -30s	46	0.83	1.16	1.65	2	0.72
12	0R10-35s	50	0.83	1.04	2.48	3	0.80
1	2R10-60u	78	0.63	0.89	3.76	6	0.71
7	2R6 -60b	73	0.74	0.97	1.48	2	0.76
8	2R6 -30b	70	0.77	0.93	2.30	3	0.83
13	2R6 -30s	72	0.77	0.97	2.30	3	0.79
14	2R10-60s	71	0.63	0.94	1.88	3	0.67
16	2R6 -30r	-	0.77	0.92	3.06	4	0.84
2	4R6 -65u	124	0.41	0.60	1.48	3.6	0.67
3	4R10-60u	114	0.42	0.58	2.54	6	0.72
9	4R6 -40b	106	0.44	0.59	1.31	3	0.75
10	4R10-65b	114	0.44	0.56	1.78	4	0.79
15	4R10-60s	97	0.44	0.78	1.74	4	0.56

1. Secant stiffness K_2 calculated at $\Delta = 0.75\ \Delta_y$.
3. Δ/h when strength V_{if} was firstly reached.

For $\mu \geq 1.25$, the values of V/V_{if} increased with higher axial compression (Figs. E.1 and E.2) or spiral steel content (Figs. E.1 and E.3). The performance of a test column also depended on the imposed displacement pattern (Fig. E.4). As expected, the displacement pattern 's' resulted in most severe damaging effects on test columns, whereas displacement pattern 'u' was the least damaging. A more severe displacement pattern resulted in lower resistance. Nevertheless, except for Unit 4, which suffered a premature shear failure, the maximum measured strength, V_{max}, always exceeded the corresponding ideal flexural strength, V_{if}, at a displacement ductility not less than 2. There seems to be a trend whereby V_{max} developed at larger ductilities as $P_i/(f'_c A_g)$ increased (Table E.II). This is probably due to the fact that large curvatures involved large concrete strains. Thereby concrete strength and hence V_{if} were enhanced to a greater extent due to confinement. Further discussions on maximum measured strength in relation to flexural strength enhancement factor are reported in Section E.3.2.

The drift at V_{max} generally varied from 1.5% to 2.5% (Table E.II). However, for columns subjected to low axial compression and moderately severe displacement patterns, such as Units 1 and 16, the drift attained exceeded 3% if columns were designed to perform in a ductile flexural or moderate ductile manner.

Strengths at displacement peaks did not vary much within a displacement path. However, under bi-directional displacement patterns 's' and 'b', strengths attained in the first displacement path were always higher than those in the second displacement path of the same cycle. These strength variations were reduced with an increase of axial compression (Figs. E.1 and E.2). There was strength loss during repeated cycles to the same ductility level. The percentage of this strength loss in the first displacement path load cycling was higher than that in the second displacement path load cycling. Again, an increase of axial compression resulted in reduction of such strength loss.

II) Descending portions of the envelope curves

The onset of the descending portions of the envelope curves was delayed as the spiral steel content increased (Figs. E.1 and E.3) or the severity of displacement pattern was reduced (Figs. E.4). Axial compression increased the rate of strength decay (Figs. E.1 and E.2). The slopes of descending portions appeared to be insensitive to the spiral steel content.

Direct comparison between Units 13 and 15 is not possible because they are of different concrete strengths. However, the performance of Unit 15 indicates that a ductile behaviour can also be achieved with the most severe displacement pattern 's'.

Lastly, Unit 16 was subjected to random displacement pattern 'r' which consists of two simulated severe earthquake displacement paths and one circular displacement path with $\mu = 4$. Although the corresponding strength envelope curves are difficult to construct, it is easy to see that the performance of Unit 16 is better than that of the companion Unit 8 which was subjected to 'b' type displacement history. Thus, it is likely that the performance of a column subjected to displacement pattern 'b' adequately represents the performance of the same under realistic severe earthquake excitations.

E.3.2 Maximum Measured Strength

As described in Section B.2.4, the flexural strength, computed by the ACI method, is too conservative for reinforced concrete columns designed for ductile flexural response. Based on Ang's equations, Eqs. (B.38a to B.38d), the flexural strength enhancement factors, m, for columns, using Grade 380 steel are 1.22, 1.24, and 1.42 for $P_i/(f'_c A_g)$ equal to 0, 0.19, and 0.39 respectively. If Grade 275 steel are used, the corresponding m values are 1.13, 1.15, and 1.33 (Fig. B.9). Ang also suggested that the m values, derived from Eqs. (B.38a to B.38d), should be further multiplied by a factor of 1.15 in order to obtain their upper bound values, which is relevant to the capacity design.

In Section E.3.1, the influence of various parameters on V_{max}/V_{if} is evaluated with reference to the present 16 test columns. The maximum V_{max}/V_{if} values obtained were 1.09, 1.30, and 1.63 for columns with $P_i/(f'_c A_g)$ equal to 0, 0,19, and 0.39 respectively.

From Ang's test results [E.1] on circular reinforced concrete columns with aspect ratio of 2 and no axial compression load, the maximum V_{max}/V_{if} values were 1.04 and 1.15 for columns reinforced with Grades 275 and 380 steel respectively.

Thus, it is evident that the m values for circular reinforced concrete columns with low aspect ratio and negligible axial compression load are over-estimated by Ang's suggestions. Since his equations, Eqs. (B.38a to B.38d), were derived from relatively slender reinforced concrete cantilever columns with an aspect ratio of 4, significant difference in shear induced in columns due to different aspect ratios is likely to be a factor affecting the overall strength enhancement.

The performance of Unit 12 (with no axial load) of the present test series is of particular interest. This column was provided with extensive spiral content (ρ_s = 2.46%). The measured m value was found to be 1.05 which is well below the expected value of 1.22. The possibility of inadequate shear reinforcement as a main cause for reduction of the m factor may be eliminated. Another possible source of the reduction in strength enhancement is the mechanism of shear - moment transfer at the column - foundation interface. This will be shown to be an important factor to control the strength enhancement in units with low aspect ratio and negligible axial compression load.

A typical crack pattern observed in the present test columns is shown in Fig. E.5. For simplicity, only one set of cracks is drawn. Above the potential diagonal failure plane, inclined shear cracks are more or less parallel to each other. Diagonal compressive forces develop in these concrete struts. Consequently, nearly the whole cross-sectional area of core concrete is mobilized to transfer shear forces. However, below the potential diagonal failure plane, nearly all the compressive forces in these radial struts converge on the flexural compression zone at the column - foundation interface. Opening of cracks at the flexural tension zone along the base interface is largely due to yield penetration from the foundation. This crack gradually widens at higher displacement ductility levels so that shear transfer along this crack, by means of aggregate interlock, practically vanishes. Therefore the combination of high shear stress and compressive stress in concrete of the flexural compression zone can be significant enough to prohibit development of flexural overstrength.

This phenomenon becomes significant for a reinforced concrete column with low aspect ratio and low axial compression load. A low aspect ratio implies that high shear stress is required to be transmitted. Under a low axial compression load, the depth of neutral axis would be small. Thus, a relatively smaller area of flexural compression zone at the column-foundation interface is available for the transmission of shear forces.

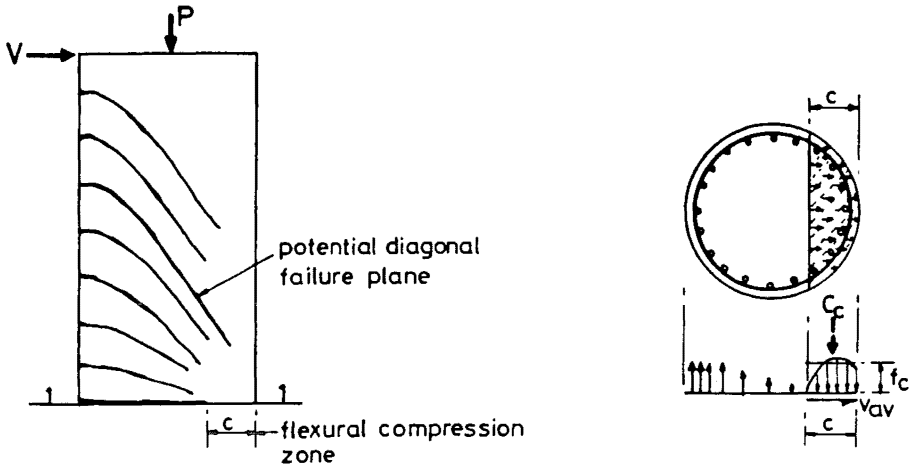

(a) Typical crack pattern (b) Stresses at Section 1 - 1

Fig. E.5 : Typical diagonal crack pattern and shear transfer at the base of a column

A brief analytic study of the columns of the present test series is used to substantiate the aforesaid statements. A typical value of the compressive strength of concrete, f'_c, is taken to be 39 MPa. When the bending moment, M, at the column base reaches the ideal flexural capacity, M_i, the ratios of the segmental area of the flexural compression zone, inclusive of the cover concrete, to the gross cross-sectional concrete area are found to be 0.28, 0.42, and 0.58 for $P_i/(f'_c A_g)$ = 0, 0.19, and 0.39 respectively. If the shear at the base, V, is assumed to be transferred within the flexural compression zone only (Fig. E.5b), the corresponding average shear stresses, v_{av}, are $0.24f'_c$, $0.20f'_c$ and $0.14f'_c$. The ratios of the vector resultant force, obtained from adding the shear, V, and the flexural concrete compression force, C_c, to only C_c, are 1.07, 1.04, and 1.02. In terms of the ratios of principal compressive stresses, f_{c2}, resulting from v_{av} and the average flexural compressive stress on concrete, f_c, to only f_c (Fig. E.5b), the corresponding ratios would become 1.14, 1.09, and 1.04. These figures imply that at the development of the ideal flexural capacity, M_i, the effect of shear transfer would increase the compressive stress at the column-foundation interface by 14% for columns with no axial compression load, and only 4% for columns with $P_i/(f'_c A_g)$ = 0.39. As an increase of the compression strength of the concrete in a column subjected to very small or no axial compression cannot be expected, it is likely that the effective flexural compression zone, i.e. c in Fig. E.5, will increase to accommodate the larger inclined compression force ($\sqrt{V^2 + C_c^2}$) without increased compression stresses. Thereby the internal lever arm will reduce, resulting in reduced strength enhancement of short columns with low axial compression. Thus, with a relatively small neutral axis depth c (Fig. E.5b), the response of the flexural compression zone will be more sensitive to the contribution of both shear and flexural compression, and to the strength of cover concrete.

E.4 SPIRAL STRAIN DISTRIBUTION

Spiral reinforcement content has insignificant effect on the onset of diagonal cracks. However, after diagonal cracking, the rate of increase of spiral strain is greater for a column with lower spiral steel content.

Other, less important factors affecting the rate of strain increase are displacement patterns and axial compression load intensity. Spirals, where crossed by diagonal cracks, were subjected to larger strains under a more severe displacement pattern. On the other hand, when the influence of axial compression load intensity was considered, it appeared that it would be more appropriate to use a drift index, Δ/h, rather than a displacement ductility level as a basis for comparison. This is because the magnitude of yield displacement is affected by the axial compression load intensity. Under a similar drift index, larger spiral strains developed in a column subjected to higher axial compression load intensity.

E.5 CONFINING STRESS AT ZERO LATERAL FORCE AND ROLES OF SPIRAL REINFORCEMENT

E.5.1 Confining Stress at Zero Lateral Force

In data presented in the previous chapter, average spiral stresses at zero lateral force, σ_{sv}, were also evaluated. From the equilibrium condition for the free body shown in Fig. E.6, the confining stress at zero lateral force, σ_{cc}, can be estimated as $\sigma_{cc} = \rho_s \sigma_{sv}/2$, where ρ_s is the volumetric spiral steel content ($\rho_s = 4 A_{sp}/(d_s s)$. This is considered to be a measure of the residual inelastic lateral deformations imposed on the diagonally cracked concrete core of the columns. It may be viewed also as a measure of damage which occurred in this core.

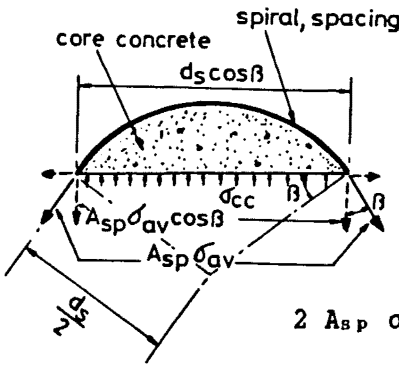

$$2 A_{sp} \sigma_{sv} \cos\beta = \sigma_{cc} d_s \cos\beta s$$

Fig. E.6 : Determination of confining stress

Fig. E.7 shows the variation of these confining stresses with loading stages. For comparison purposes, σ_{cc} is normalized in terms of the compressive strength of concrete. The loading stage i/j denotes the completion of the j^{th} cycle to displacement ductility level of i.

Values of σ_{cc} were non-zero, ranging from $0.001f'_c$ to $0.033f'_c$, after completion of cycles at low ductility levels. In general, the maximum σ_{cc} was observed immediately after the first occurrence of yield in all spirals which crossed a potential diagonal failure plane. Subsequently, σ_{cc} tended to decrease with increase of ductility levels or repeated load cycles. Some columns, such as Units 1 and 8, exhibited significant axial shortening and buckling of longitudinal bars prior to failure. Under such conditions, σ_{cc} would be suddenly increased during the last load cycle of testing.

An increase of spiral content distinctly increased σ_{cc}. A higher value of σ_{cc} resulted when axial compression was also applied. This is considered to be consistent with wedging action. However, there was no clear indication of effects of displacement patterns on σ_{cc}.

E.5.2 Roles of Spiral Reinforcement

Spiral reinforcement provides confinement to the core concrete at zero shear condition irrespective of the presence or absence of axial compression (Fig. E.8a). This is because some residual transverse deformations due to diagonal cracks and other effects remain after the removal of lateral force. The lack of fit between rugged faces of diagonal cracks, mentioned earlier, is likely to be the major source of residual spiral stresses. At this stage, spirals do not resist any external lateral load. However, when spirals have been subjected to large inelastic strain, the elastic recovery of spiral deformations may be much smaller than the width of diagonal cracks. Hence, residual stresses in spirals gradually reduce after each cyclic loading to higher ductility levels. This phenomenon, seen also in Fig. E.7, was described in Section E.5.1.

Subsequently, with gradual application of transverse force, new and wider diagonal cracks form. Shear transfer by truss mechanism then develops. Along the diagonal cracks, the compressive stresses between the concrete particles in the direction of external shear ceases as the cracks widen. On the other hand, the spiral force components in the direction of external shear and the bond forces along the longitudinal steel bars create a diagonal compression field (diagonal concrete struts) to resist shear (Fig. E.8b).

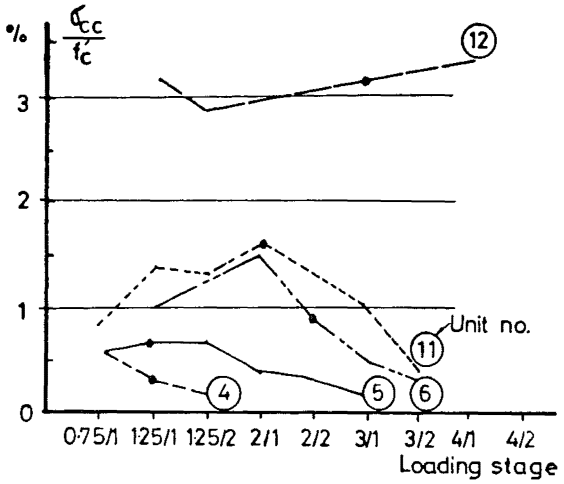

(a) Units with $P_i/(f'_c A_g) = 0$

Unit no.	σ_{cc}/f'_c (%) (all spirals yield)
1	5.7
2	2.2
3	5.9
4	1.6
5	2.6
6	4.2
7	2.3
8	4.5
9	5.0
10	5.4
11	4.2
12	13.9
13	4.5
14	5.7
15	8.0

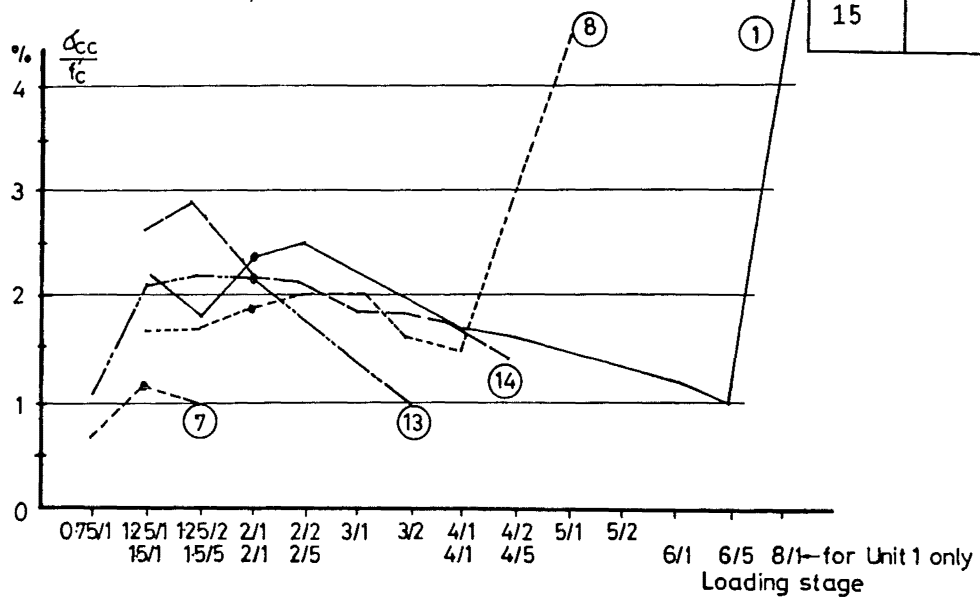

(b) Units with $P_i/(f'_c A_g) = 0.19$

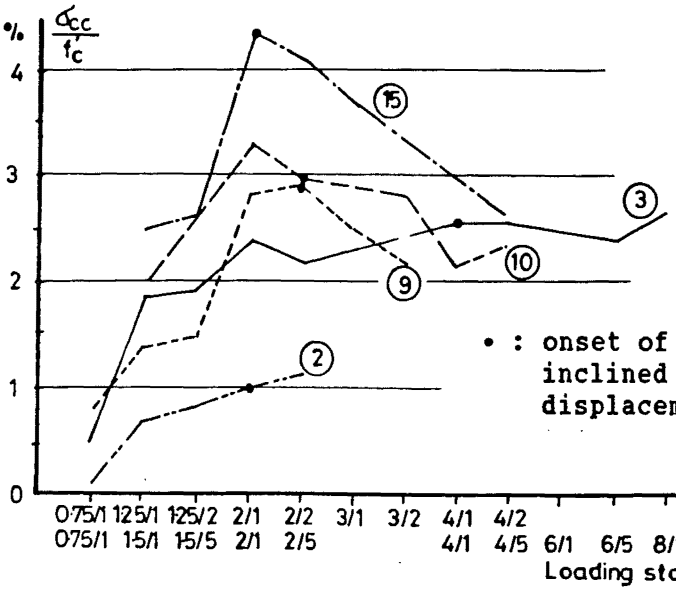

• : onset of yield in spirals, crossed by inclined cracks of that cycle at displacement peak

(c) Units with $P_i/(f'_c A_g) = 0.39$

Fig. E.7 : Observed confining stress derived from spiral strains at zero lateral force

Spiral force components perpendicular to the direction of external shear still provide some confinement to the diagonal concrete struts transverse to the direction of the applied shear. This, however, is not likely to enhance the compression strength of the concrete in the diagonal struts.

However, in the flexural compression zone, spirals are likely to act also as confining reinforcement. Referring to Fig. E.8b, the concrete element "A" in the flexural compression zone is longitudinally confined by the flexural compression, and also effectively confined by spirals and diagonal concrete struts in the transverse direction. Since the force in a diagonal concrete strut depends on the amount of the spiral content, spirals will play an important role in confinement mechanisms of the flexural compression zone, even if they perform primarily as shear reinforcement.

As shear transferred by truss mechanism requires the development of bond stress between concrete and longitudinal steel bars, deterioration of bond stress would jeopardize the effectiveness of such mechanism. Apparently, no obvious sign of any bond distress was observed from the current column tests at low ductility levels. At larger ductilities, the column core concrete around the longitudinal steel bars, particularly at the plastic hinge region, would tend to be weakened as a result of repeated "grinding". Degradation of bond stress would be expected. However, it did not appear to be the main cause of failure of test columns.

It is also realized that, at the cantilever end of test columns, the longitudinal bars were welded to the steel shear ring for anchorage purposes. Hence, even when the bond stress, along the longitudinal bars, was reduced to zero, tensile forces in these bars could still be developed. Shear force would then be transmitted by developing a concrete strut diagonally across the whole span of the column. At the loading end of the column, the compressive force in this diagonal concrete strut would be balanced by the shear force, and the tensile forces in the longitudinal bars. However, this mechanism would only take place after a severe loss of bond stress at high ductility levels. It was likely that the test columns had already failed due to significant reduction in strength or fracture of spiral steel, before this shear carrying mechanism was mobilized.

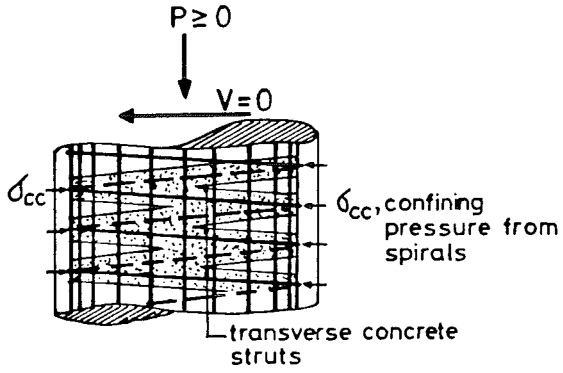

(a) At zero shear condition

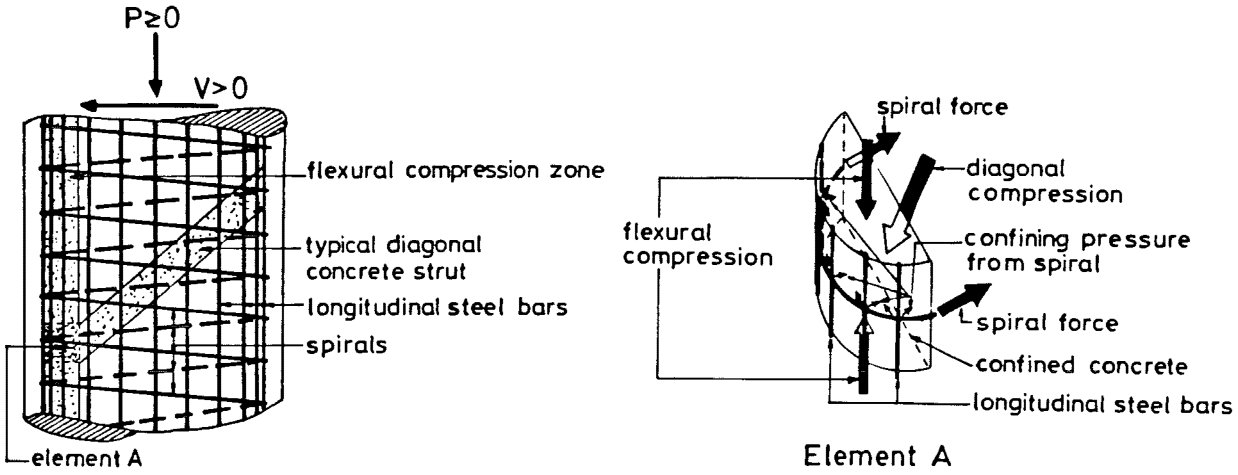

(b) At non-zero shear condition

Fig. E.8 : Roles of spiral reinforcement

E.6 SHEAR CARRIED BY CONCRETE MECHANISM

Using the truss analogy, shear carried by spirals, V_s, is evaluated by summing up across the shear failure plane the components of spiral forces in the direction of external load V. The difference between V and V_s is then assumed to be the shear carried by concrete mechanism, V_c, i.e. mechanisms other than the diagonal compression field.

However, there are difficulties in assessing the appropriate shear failure plane. Shear failure surfaces seldom form as a perfect plane, especially for a unit with large spiral content or which was subjected to displacement pattern 's'. Angles of inclination of diagonal cracks, being an indication of the inclination of diagonal compression, often varied according to different directions of loading. Moreover, at high ductility levels, excessive spalling of cover concrete made crack identification practically impossible. Therefore, the inclination of a shear failure plane θ was approximated by taking the average of the measured inclinations of potential shear failure surfaces formed during different directions of loading. Spiral forces across a shear failure plane were then estimated from the measured spiral strains in the neighbourhood.

Figs. E.9 to E.11 show estimated components of shear resistance, V_c and $V_s = V - V_c$, at different ductility levels. Two different expressions of shear are shown. The first expression is average shear stress, v, normalized by the square root of the concrete compressive strength, f'_c, where $v = 4V/(\pi d_s^2)$, and d_s is the diameter of the concrete core. The other expression is the shear force normalized by the column's ideal flexural strength V_{if}. The ductility level i/j denotes the j^{th} cycle to displacement ductility level of i. The stage at which yielding of spirals was first observed and the mean inclination of diagonal cracks, θ, are also recorded in these figures.

The index $v/\sqrt{f'_c}$ indicates the relative magnitude of shear in terms of the tensile strength of the concrete. This can be related to the magnitudes envisaged by some codes [E.2, E.3]. For example, it is recommended in NZS 3101 [E.2] that in potential plastic hinge regions, the ultimate shear stress be limited to $v_u \leq 0.9\sqrt{f'_c}$. On the other hand, because of considerations of a potential diagonal compression failure due to shear, $v_u \leq 0.2f'_c \leq 6$ MPa is specified. It is found that with the exception of Unit 3, the maximum measured shear stresses, v_{max}, in this test series did not exceed NZS 3101 requirements. The value of v_{max} of Unit 3 was 6.2 MPa

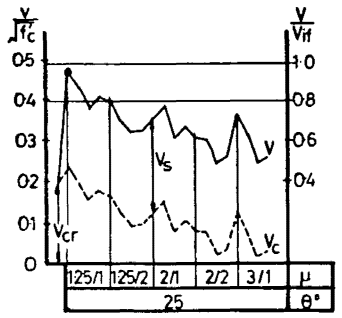

(a) Unit 4

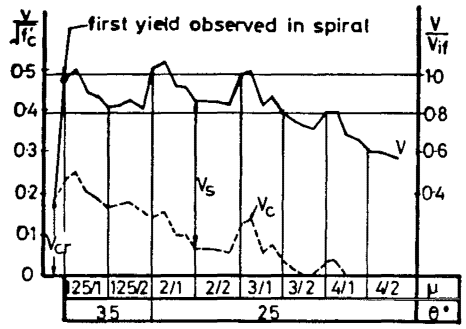

(b) Unit 5

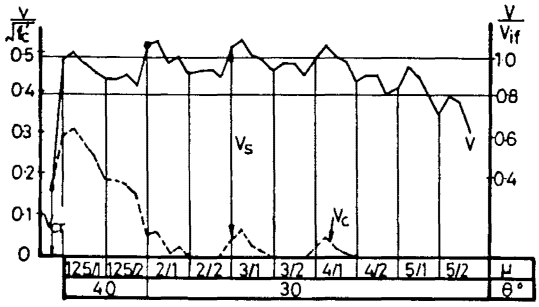

(c) Unit 6

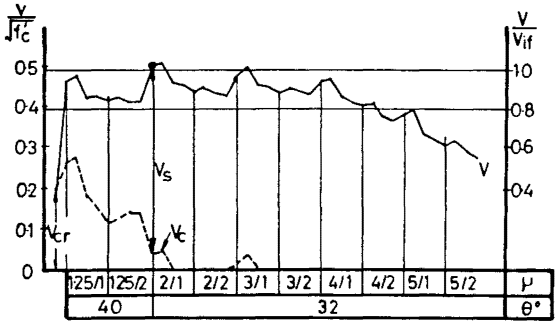

(d) Unit 11

Fig. E.9 : Components of shear resistance for units with $P_1/(f'_c A_g) = 0$

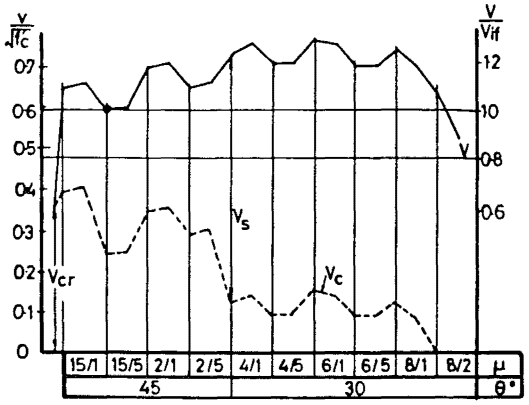

(a) Unit 1

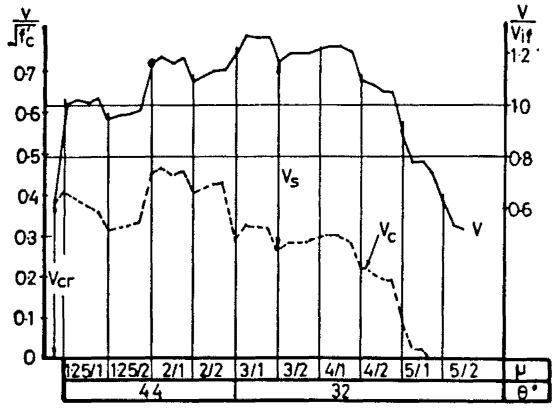

(b) Unit 8

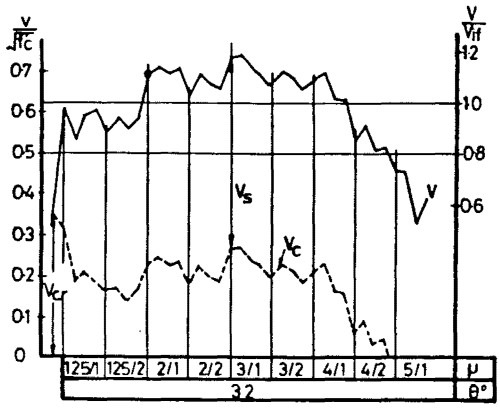

(c) Unit 13

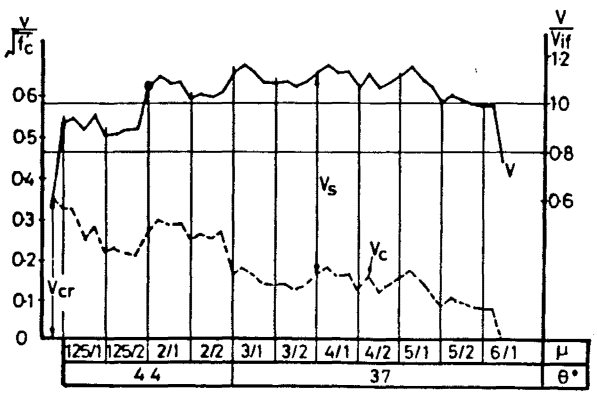

(d) Unit 14

Fig. E.10 : Components of shear resistance for units with $P_1/(f'_c A_g) = 0.19$

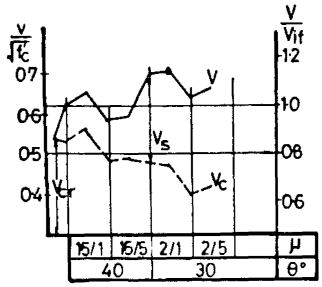

(a) Unit 2

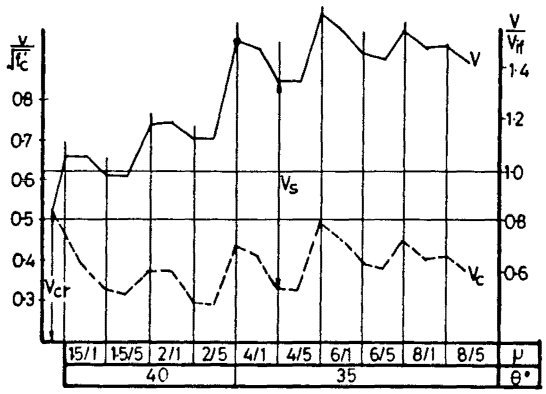

(b) Unit 3

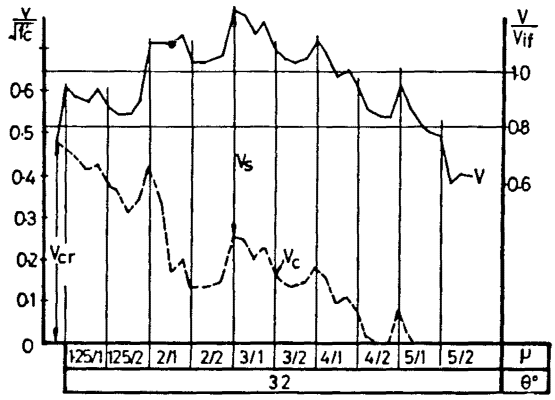

(c) Unit 9

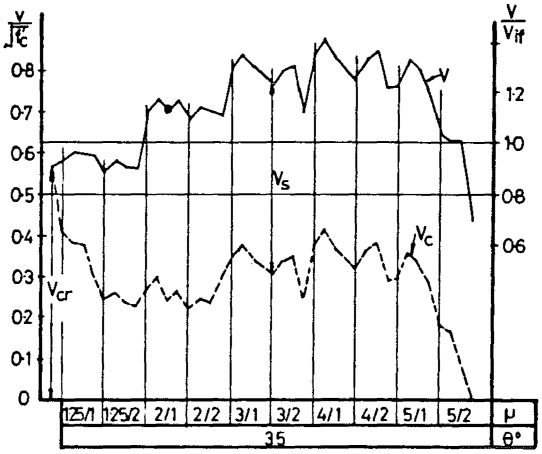

(d) Unit 10

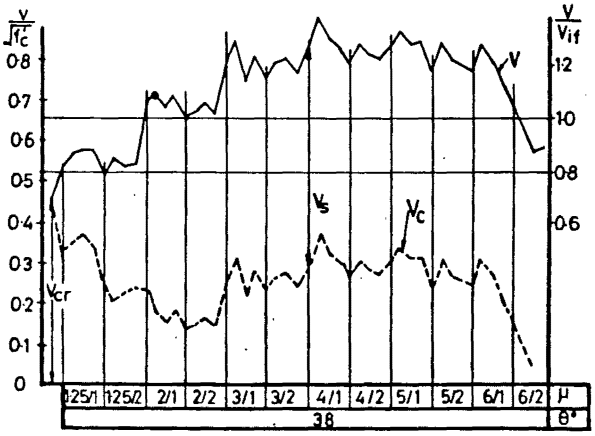

(e) Unit 15

• : Spirals, crossed by inclined cracks, reached yield stress first at this displacement peak

Fig. E.11 : Components of shear resistance for units with $P_i/(f'_c A_g) = 0.39$

which was greater than 0.9 $\sqrt{37}$ MPa. Since these code specified stress limits are based on nominal rather than on actual (measured) strength properties, it is implied that the stresses achieved in tests could well be 10 to 15% larger than specified. Nevertheless, it is considered that the shear stresses induced in these tests are likely to be larger than those that could be expected in real bridge piers when subjected to similar ductility demands. This is because of the relatively large vertical reinforcement content used, which results in large flexural strength.

As expected, shear carried by concrete mechanism at the onset of diagonal cracks, V_{cr}, increased with axial compression intensity. This is because axial compressive stress allows larger shear stresses to be applied before the principal tensile stress reaches the tensile strength of concrete. It is also evident that shear carried by concrete mechanism, V_c, at low displacement ductility levels, after the onset of diagonal cracking, increased more than V_{cr}. However, during the subsequent cycles to higher ductilities, $\mu \geq 2$, V_c decreased as the imposed ductility level was increased. In particular, under the condition of no axial compression, the rate of deterioration of V_c was so fast that V_c eventually vanished, even before significant degradation of total strength became apparent.

The rate of deterioration of V_c is also greater for more severe displacement patterns. Under bi-directional displacement patterns, V_c developed in the second displacement path was always lower than that developed in the first displacement path of the same loading cycle.

Repeated cycles at a given ductility level also reduced V_c as compared with the value achieved in the first cycle to the same ductility. Lastly, the increase in the amount of spiral reinforcement content appeared to have no significant influence on V_c.

In view of degradation of V_c, any increase in the overall shear resistance at higher ductility levels appears to be due to an increase in V_s. As observed, this has been achieved by developing higher stresses in the spirals, or because of new sets of the diagonal cracks with smaller inclinations.

E.7 PLASTIC HINGES, CURVATURE PROFILES AND CURVATURE DUCTILITY

E.7.1 Plastic Hinges

The formation of a plastic hinge was observed in all test columns. The lengths of these hinges, which were estimated from curvature profiles, shown in Chapter D, were approximately 250 mm and 200 mm for the columns with and without axial compression respectively. Spiral reinforcement content or displacement pattern had no apparent influence on the length of plastic hinge.

E.7.2 Curvature Profiles

The general trend confirmed that curvatures increased with an increase of displacement ductility level. Before significant strength degradation has taken place, the curvature profiles maintained the shape typical of flexure performance, and were similar in each displacement direction. Curvature profiles did not vary much during repeated cycles to a constant ductility level. After the occurrence of significant strength degradation, curvature profiles above the plastic hinge region became irregular.

At a given displacement ductility level, curvatures in the plastic hinge region were smaller for columns with less spiral reinforcement content. This can be explained by the fact that a column with low spiral content showed early onset of yielding of spirals. Shear deformations then became significant fractions of the total deformation. Hence, for a given ductility level, less flexural rotation was required.

Displacement patterns did not show an influence on the distribution of curvatures. However, more severe displacement patterns resulted in irregular curvature profiles already at low displacement ductility levels.

E.7.3 Curvature Ductility

Before an examination of curvature ductility of circular reinforced concrete columns can be made, it is necessary to define the yield curvature, Φ_y. If the moment - curvature relationship of a column is elasto-plastic (Fig. E.12), the yield displacement, Δ_y, can be expressed as $\Delta_y = \Phi_y L^2/3$ for a cantilever column with a triangular bending moment distribution. In this expression, effects of tension stress penetration at the foundation, and shear deformations are not considered.

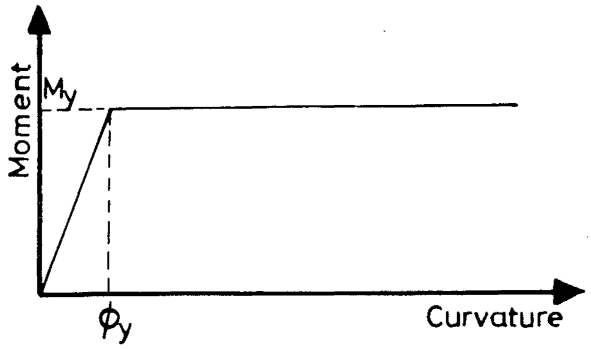

Fig. E.12 : Idealized elasto-plastic moment - curvature relationship

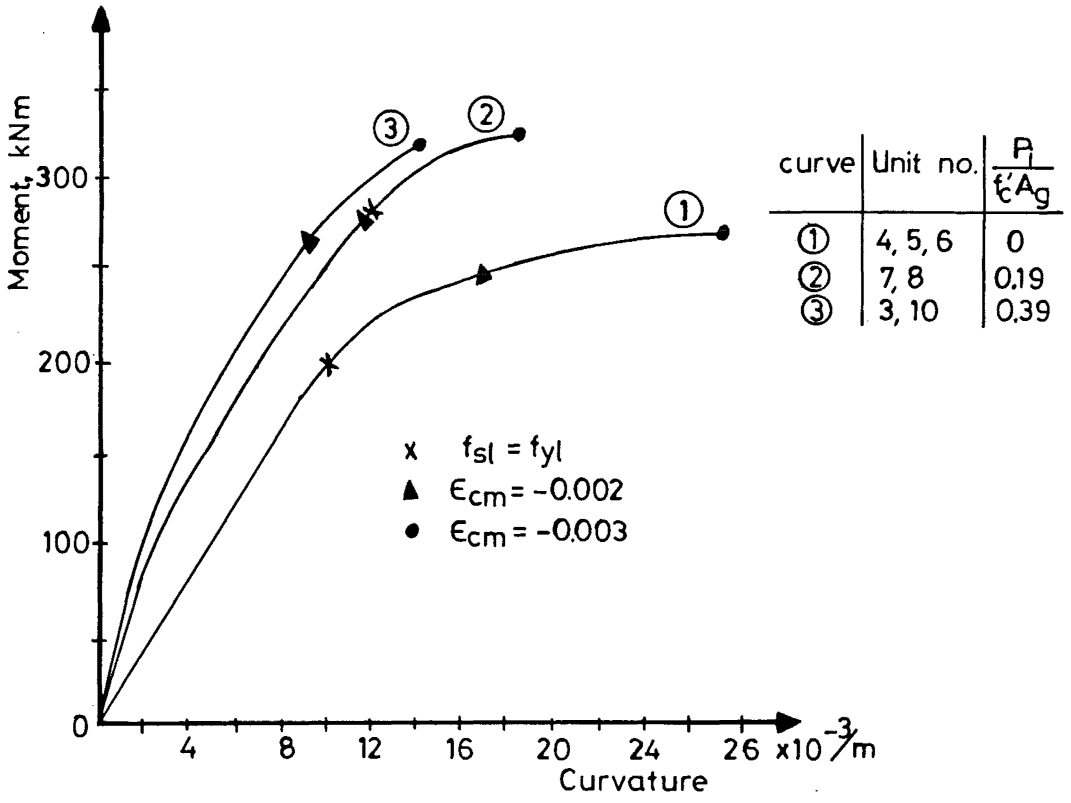

Fig. E.13 : Theoretical moment - curvature relationships

Fig. E.13 shows theoretical moment - curvature curves of some test columns. A typical calculation procedure for these curves is shown in Appendix V. The analyses were based on measured material properties (Section C.9). The stress - strain relation of concrete was determined from Eqs. (E.1a to E.1c), proposed by Kent and Park [E.4] for unconfined concrete.

$$\text{when } \varepsilon_c \geq -0.002, \quad f_c = f'_c \left[\frac{\varepsilon_c}{0.001} + \left(\frac{\varepsilon_c}{0.002}\right)^2\right] \tag{E.1a}$$

$$\varepsilon_c < -0.002, \quad f_c = -f'_c \left[1 + Z\,(\varepsilon_c + 0.002)\right] \leq -0.2\, f'_c \tag{E.1b}$$

$$\text{where} \quad Z = \frac{0.5}{\left(\frac{3 + 0.29\, f'_c}{145\, f'_c - 1000}\right) - 0.002} \tag{E.1c}$$

f_c and ε_c are negative for compression

f'_c in MPa units

As observed, the moment - curvature curves of the test columns are far from being elasto-plastic. Moreover they cannot be used as a sole source of column deformations. It is shown in Section F.3 that the components of deflections resulting from tension stress penetration along the vertical column bars in the foundation, and shear have significant contributions to the total deflections of test units. In general, flexural deformation accounts for only 47% to 65% of the total deformation at $\mu = 0.75$ (Table F.I). Therefore, it is inappropriate to relate yield curvature directly to yield displacement. In this project, yield curvature, Φ_y, is the curvature at the stage when the tension steel at the extreme tension fibre yields or when the strain in con-crete at the extreme compression fibre reaches 0.002, whichever occurs first.

The values of the theoretical yield curvatures, Φ_y, of some test units, together with the corresponding concrete strains at the extreme compression fibre, ε_{cm}, and the steel strains at the extreme tension fibre, ε_{ls}, are listed in Table E.III. In general, the steel strain criterion governs the yield curvatures of the units with no axial load. On the other hand, yield curvatures are determined by the concrete strain criterion for those units with axial compression intensity, $P_l/(f'_c A_g)$, equal to 0.19 or 0.39.

Table E.III also shows the maximum measured curvatures, Φ_{max}, at the first potentiometer level near the column base. Units subjected to 's' type displacement pattern are not listed in this table because most of them are companion units of those listed. Moreover, as the directions of displacement peaks do not coincide with the orientation of curvature instrumentation, a proper assessment of experimental curvatures at displacement peaks becomes impossible for columns subjected to 's' type displacement patterns.

Table E.III : Yield curvatures and curvature ductilities of test columns

Unit no.	1	2	3	4	5	6	7	8	9	10	11
	$\frac{P_i}{f'_c A_g}$	Φ_y	at Φ_y		Φ_{max} at μ		L_d	Φ'_{max}	μ_ϕ	μ_ϕ/μ	$\mu_{\phi I}/\mu$
	-	rad/m	ε_{cm}	ε_{ls}	rad/m	-	mm	rad/m	-	-	-
	-	$x10^{-3}$	-	-	$x10^{-3}$	-	-	$x10^{-3}$	-	-	-
1	0.19	11.67	-0.0020	0.0023	238.0	8	253	128.5	11.0	1.34	1.23
2	0.39	8.88	-0.0020	0.0013	54.8	3	251	29.6	3.3	1.10	1.18
3	0.39	8.88	-0.0020	0.0013	150.0	8	276	78.0	8.8	1.10	1.23
4	0.00	9.80	-0.0013	0.0024	29.9	1.25	265	15.8	1.6	1.28	1.10
5	0.00	9.80	-0.0013	0.0024	71.7	3	314	35.1	3.6	1.20	1.35
6	0.00	9.80	-0.0013	0.0024	141.0	5	260	76.1	7.7	1.54	1.42
7	0.19	11.66	-0.0020	0.0023	31.3	2	251	16.9	1.4	0.70	1.13
8	0.19	11.66	-0.0020	0.0023	107.0	5	265	56.7	4.9	0.98	1.21
9	0.39	9.02	-0.0020	0.0014	65.8	5	267	34.9	3.9	0.78	1.21
10	0.39	8.88	-0.0020	0.0013	72.9	5	276	37.9	4.3	0.86	1.21
16	0.19	11.64	-0.0020	0.0023	164.1	5	253	88.6	7.6	1.52	1.21

2, 3, 4 : evaluated from moment-curvature analysis
5, 6 : experimentally obtained values
7 : L_d calculated from Eq. (E.10)
8 : Φ'_{max} calculated from Eq. (E.9)
9. $\mu_\phi = \Phi'_{max}/\Phi_y$
11. $\mu_{\phi I}$ obtained from Eq. (E.11)

Considering the set-up of potentiometers for curvature measurements (Section C.8.2), the maximum measured curvature near the column base, Φ_{max}, in fact, includes the effects of tension stress penetration along column steel bars in the column base block. Since yield curvature, Φ_y, does not include any stress penetration, it would be appropriate to define the curvature ductility factor, μ_ϕ as:

$$\mu_\phi = \Phi'_{max}/\Phi_y \qquad (E.2)$$

where Φ'_{max} is the maximum curvature near the base of the column, excluding effects of tension stress penetration along column bars in the foundation (Fig. E.14b). The values of Φ'_{max} can be estimated from Φ_{max} as follows:

Since Φ_{max} is the average curvature measured over the gauge length, L_g, (Fig. E.14b), the rotation of the column, θ_g, at the first potentiometer level is:

$$\theta_g = \Phi_{max} L_g \qquad (E.3)$$

Let δ be the slip of the column steel bar at the extreme tension fibre due to tension stress penetration into the foundation (Fig. E.14a).

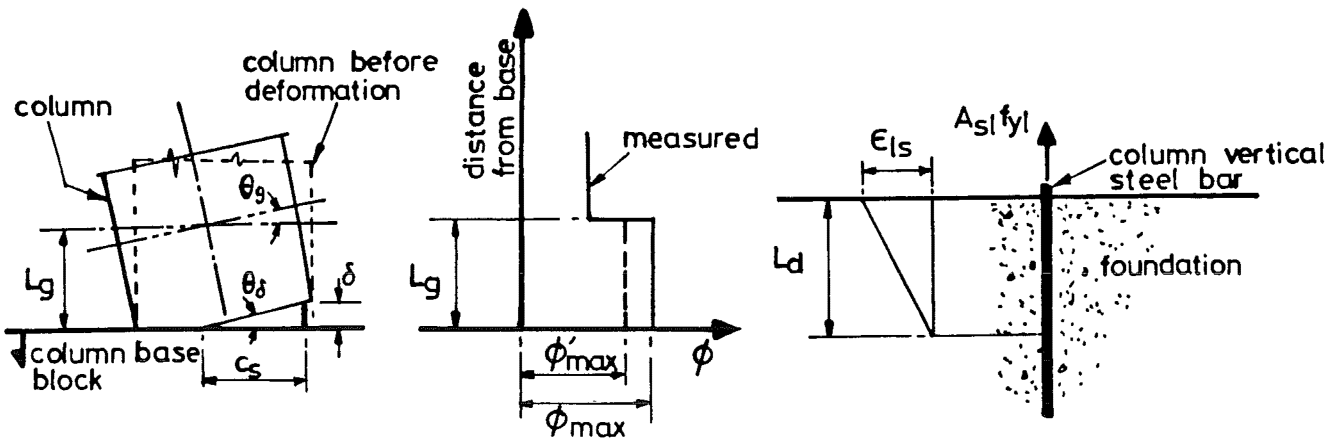

(a) deformation (b) average curvature distribution (c) strain distribution of column bar in foundation

Fig. E.14 : Effects of tension stress penetration along column bars in the foundation

The rotation of the column at the column base due to δ is:

$$\theta_\delta = \delta / c_s \qquad \text{(E.4)}$$

where c_s is the distance from the centre of the column bar at the extreme tension fibre to the neutral axis.

Thus, θ_g can also be expressed as

$$\theta_g = \Phi'_{max} L_g + \theta_\delta \qquad \text{(E.5)}$$

Combining Eqs. (E.3 to E.5), we obtain

$$\Phi'_{max} = \Phi_{max} - \delta/(c_s L_g) \qquad \text{(E.6)}$$

Since no strain gauge was installed in the test units to monitor the strain distributions of column steel bars in the column base block, it is assumed that the strain of the column bar at the extreme tension fibre is ε_{ls} at the column - foundation interface, and linearly reduces to zero over the development length, L_d, inside the foundation (Fig. E.14c). Hence, the value of δ is

$$\delta = \varepsilon_{ls} L_d / 2 \qquad \text{(E.7)}$$

On the other hand, ε_{ls} can be approximated by

$$\varepsilon_{ls} = \Phi'_{max} c_s \qquad \text{(E.8)}$$

Substituting Eqs. (E.7 and E.8) into Eq. (E.6), we obtain

$$\Phi'_{max} = \frac{\Phi_{max}}{1 + L_d/(2 L_g)} \qquad \text{(E.9)}$$

The development length, L_d, may be expressed by Eq. (E.10), which is taken from ACI 318-89 Clause 12.2 recommendation [E.3].

$$L_d = 0.02\, A_{sl}\, f_{yl} / \sqrt{f'_c} \qquad \text{(E.10)}$$

where A_{sl} = cross-sectional area of the column vertical bar

f_{yl} = yield strength of the column vertical bar

f'_c = measured concrete compressive strength of the column base block

The values of L_d, Φ'_{max}, μ_{ϕ}, and μ_{ϕ}/μ are listed in Table E.III. It is apparent that μ_{ϕ}/μ values are very low. For normal slender beams and columns, μ_{ϕ}/μ is of the order of 3. This can be partly explained by the fact that the curvature ductility depends significantly on the imposed displacement ductility, μ, the equivalent length of plastic hinge, L_p, and the distance from the section of maximum moment to the point of counterflexure, L. For example, if the behaviour of a cantilever column is assumed to be elasto-plastic, and the plastic rotation is concentrated at the centre of the plastic hinge, the curvature ductility of this idealized column, $\mu_{\phi I}$, can be expressed as:

$$\mu_{\phi I} = 1 + \frac{\mu - 1}{3\,\frac{L_p}{L}\left[1 - 0.5\,\frac{L_p}{L}\right]} \qquad \text{(E.11)}$$

The derivation of this equation can be found in references [E.1] and [E.5]. It assumes that deformations are due to flexure only, i.e. shear deformations are not included in the determination of μ. As the plastic hinge length, L_p, is normally a function of the column depth, D, Eq. (E.11) implies that $\mu_{\phi I}$ increases as the slenderness of a column or displacement ductility increases.

It is noted that the μ expressed in Eq. (E.11) is defined differently from the experimentally determined μ used in this project. The latter included deflections due to shear deformations. However, before any significant strength degradation, shear deformations account for about 29% of the measured total deflection even at small displacement levels (Section E.8). That is, the contributions of shear deformations to the total deflection, and to the experimentally established yield displacement are of similar ratio. As a result, shear deformations will not effectively affect the derivation of the experimentally determined μ, before the occurrence of significant strength degradation. Column 11 of Table E.III lists the $\mu_{\phi I}/\mu$ values for some test units, in which the observed values of L_p (Section E.7.1) were applied. Apparently, $\mu_{\phi I}/\mu$ values are consistent with the corresponding μ_{ϕ}/μ values (Column 10 of Table E.III). In other words, Eq. (E.11) can be used to estimate the curvature ductility of test columns provided that suitable expressions for the lengths of plastic hinges are used.

E.8 COMPONENTS OF DEFLECTIONS

The index r_f is defined as the ratio of deflection calculated from the experimentally obtained curvature profile, to the measured total deflection. This index has been extensively used to quantify the flexural performance of test columns. It should be aware that the experimentally obtained curvature profile includes the effects of tensile stress penetration along the column bars into the foundation block.

Before the occurrence of significant strength degradation, the average value of r_f was 71% with a standard deviation of 6%. This indicates that even at small displacement levels, shear deformations represent a considerable fraction of total deflection, irrespective of the amount of spiral reinforcement content.

In general, an increase of spiral steel content increased r_f. This was to be expected because the increased spiral steel content delayed extensive yielding due to shear and hence lead to smaller shear deformations at higher ductilities. Axial compression load intensity or displacement patterns did not appear to affect r_f.

At residual strength less than 80% of the column's ideal flexural strength, V_{if}, r_f varied between 40% and 50%, depending on the spiral steel content. No reliable information with respect to r_f could be extracted during the subsequent displacement history.

E.9 ENERGY DISSIPATION PERFORMANCE

Energy dissipation during hysteretic response is one of the important parameters used to quantify the performance of a structure under seismic attack. For a member with good inelastic properties, the major part of the input energy induced by ground motions can be dissipated during inelastic deformations. The area enclosed by a lateral force - displacement hysteretic loop $\oint V.ds$ represents the energy dissipation during inelastic deformations. For a member with a perfect bi-linear elasto-plastic response, the energy which is dissipated from one complete uni-directional load cycle to the displacement ductility level, μ, is referred as the ideal energy dissipation, E_I. The magnitude of $E_I = 4(\mu - 1) V_{if} \Delta_y$, which is the shaded area as shown in Fig. E.15.

According to the definitions adopted here, the energy dissipation E is the area enclosed by the lateral force - displacement hysteretic loop (or loops) generated from the completion of one displacement path. Hence, one hysteretic loop is formed from one complete displacement path under uni-directional 'u' type or bi-directional 'b' type displacement pattern (Figs. D.25 and D.37). In the case of bi-directional 's' type displacement pattern, completing one displacement path generates non-zero components of displacement and force in both N-S and E-W directions. As a result, two hysteretic loops are created (Fig. D.74). In this circumstance, the energy dissipation $E = \oint V.ds = \oint V_x dx + \oint V_y dy$, where V_x and V_y are components of the shear vector, V, perpendicular to each other. Similarly, dx and dy are components of the displacement vector, ds.

In this section, the energy dissipation E for each displacement path, normalized in terms of the corresponding ideal energy dissipation E_I is compared and studied. The term E/E_I is called the relative energy dissipation index.

For a bi-directional displacement pattern, each load cycle consists of two displacement paths. Accordingly, two values of E/E_I per each cycle are obtained, one for the first and one for the second displacement path. Unless otherwise stated, the average of these two E/E_I values, calculated from one complete displacement cycle, is used to represent the relative energy dissipation index of that cycle.

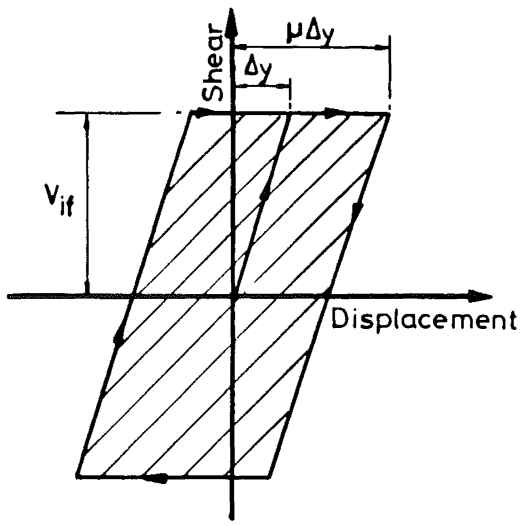

Fig. E.15 : Ideal energy dissipation, E_i

E.9.1 Influence of Spiral Reinforcement Content

An increase in spiral reinforcement content distinctly improved the energy dissipation performance of columns at all stages of the loading (Figs. E.16). When the E/E_i values of the first cycle to each displacement ductility level, μ, were compared, the spiral steel content did not appear to have any significant effect on E/E_i at $\mu \leq 2$ for columns with axial compression load. However, at high ductility levels, E/E_i values were noticeably smaller for columns with lower spiral reinforcement content. This reduction is a result of degradation of strength and pinching of hysteretic loops due to shear effects.

As expected, E/E_i decreased at repeated cycles to the same ductility level. The loss in E/E_i at repeated cycles could have been reduced by increasing the spiral reinforcement content. In all test units, the loss of energy dissipation during the first repeated cycle was not less than 12% of that developed in the first cycle to a given ductility level. When the number of repeated cycles to the same ductility level exceeded two, energy dissipation remained relatively constant. This is also evident from the loops shown in Figs. D.25 and D.42. More stable hysteretic performance was exhibited during the second and subsequent repeated cycles to a given ductility level.

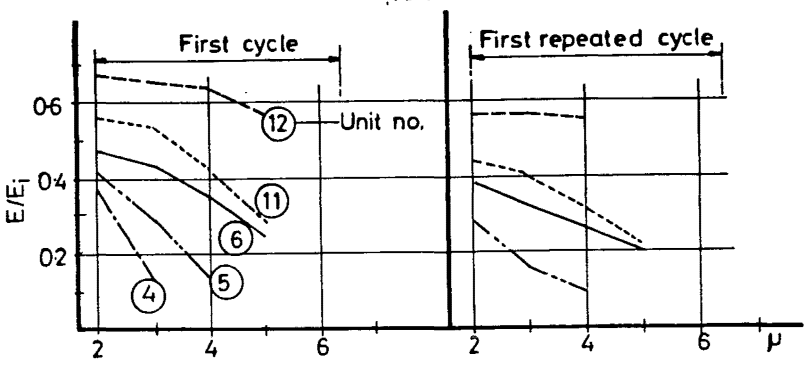

(a) Units with $P_i/(f'_cA_g) = 0.00$

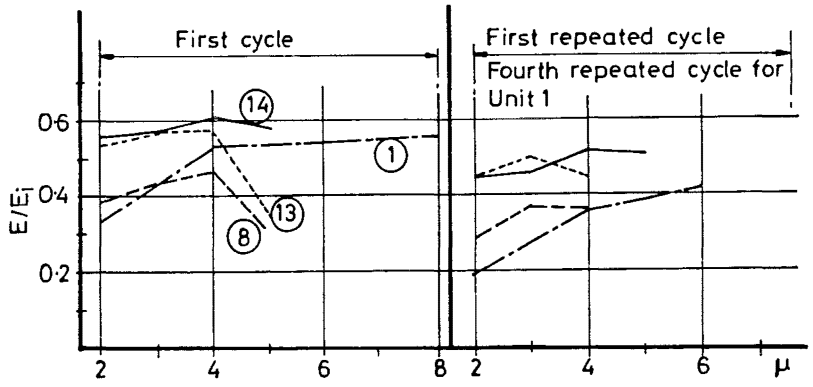

(b) Units with $P_i/(f'_cA_g) = 0.19$

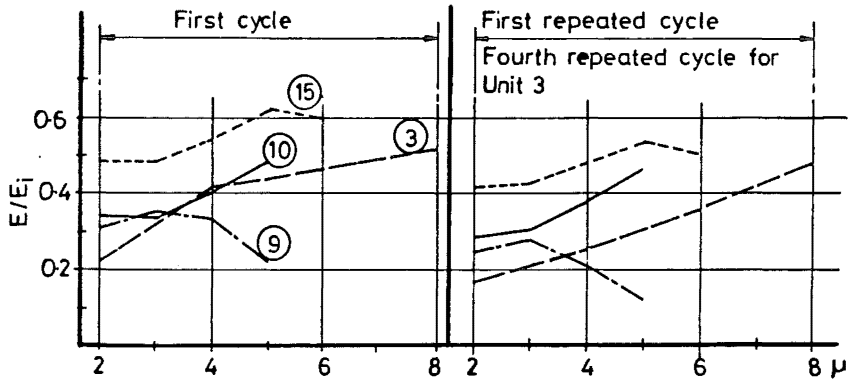

(c) Units with $P_i/(f'_cA_g) = 0.39$

Fig. E.16 : Relative energy dissipation indices at different imposed ductility levels for different axial compression intensities

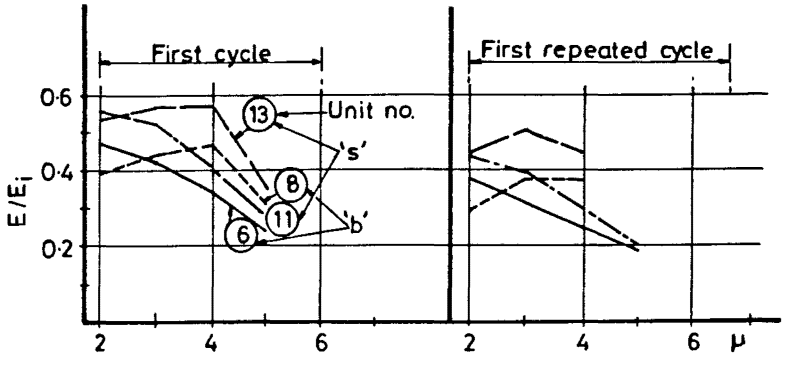

Fig. E.17 : Comparison of relative energy dissipation indices at different imposed ductility levels for different displacement patterns

E.9.2 Influence of Axial Compression Load

The presence of axial compression load on test columns did not appear to have any significant effect on increasing the maximum value of E/E_i when compared with that of the companion units with no axial load. However, larger energy dissipation i.e. the maximum value of E/E_i, occurred at the imposition of larger ductilities. In general, energy dissipation for column with axial compression load was found to increase slightly with progressively increasing ductility (Fig. E.17). This is because for a column with axial compression load, the adverse effect of a reduction of stiffness on energy dissipation is usually compensated by the beneficial effect on the same due to a gain in strength. This strength gain is mainly due to the increase of the compressive strength of confined concrete developed at higher ductility levels (Table D.I).

It was also found that using a bi-directional displacement pattern, the relation between energy dissipation performance during the second displacement path and that during the first displacement path of the same cycle depended mainly on the axial compression load intensity. The ratios of relative energy dissipation index of the second displacement path to that of the first displacement path of the same cycle are approximately 88%, 93%, and 96% for columns with $P_i/(f'_c/A_g)$ equal to 0, 0.19, and 0.39 respectively. Thus, the larger the axial compression load, the smaller the difference in the energy dissipation performances during the two displacement paths of the same cycle.

E.9.3 Influence of Displacement Pattern

It was observed that a column subjected to the least destructive uni-directional 'u' type displacement pattern maintained good energy dissipation at higher ductility levels. Companion units subjected to other displacement patterns have often failed at the same ductility. However, before significant degradation of strength has taken place, a column subjected to 's' type displacement pattern exhibited better energy dissipation performance. This is in comparison to that of its companion units subjected to 'u' type or 'b' type displacement patterns (Figs. E.16c and E.17). The longer path involved in doing work under 's' type displacement pattern, to achieve the same magnitude of peak displacement as that in the other displacement patterns, has the beneficial effect of developing larger E/E_i values.

E.10 INFLUENCE OF RELATIVE STRENGTH INDEX V_{iv}/V_{if} ON DUCTILITY

Previous research [E.1] found that there was an approximate linear relation between the displacement ductility, μ, and the design shear strength, V_{iv}, recommended by the current New Zealand non-seismic code provision [E.2]. In order to investigate whether such a relation also exists in the present test series, plots of μ at maximum observed strength, V_{max}, and dependable displacement ductility, μ_o, versus V_{iv}/V_{if} were prepared. They are shown in Figs. E.18 and E.19 respectively.

In general, both μ at V_{max} and μ_o tended to increase as the relative strength index increased. It was then attempted to use best-fit straight lines based on regression analysis to represent such relations. In each cases, an individual best-fit straight line was derived for each type of displacement patterns. The equations of these lines are:

$$\mu \text{ at } V_{max} = 6.58\,(V_{iv}/V_{if}) - 2.26 \geq 1 \qquad \text{(E.12a)}$$
for uni-directional 'u' type displacement pattern

$$= 4.13\,(V_{iv}/V_{if}) - 1.11 \geq 1 \qquad \text{(E.12b)}$$
for bi-directional 'b' type displacement pattern

$$= 1.28\,(V_{iv}/V_{if}) + 1.47 \geq 1 \qquad \text{(E.12c)}$$
for bi-directional 's' type displacement pattern

$$\mu_o = 6.58\,(V_{iv}/V_{if}) - 2.26 > 0 \qquad \text{(E.13a)}$$
for uni-directional 'u' type displacement pattern

$$= 6.94\,(V_{iv}/V_{if}) - 3.18 > 0 \qquad \text{(E.13b)}$$
for bi-directional 'b' type displacement pattern

$$= 2.86\,(V_{iv}/V_{if}) + 1.17 > 0 \qquad \text{(E.13c)}$$
for bi-directional 's' type displacement pattern

Reasonable linear correlation between μ at V_{max} and relative strength index was found only for uni-directional 'u' type or bi-directional 'b' type displacement patterns. Correlation between μ_o and relative strength index was found to be weak in all test units. Relative strength index alone is considered to be insufficient to predict reliable ductility potential.

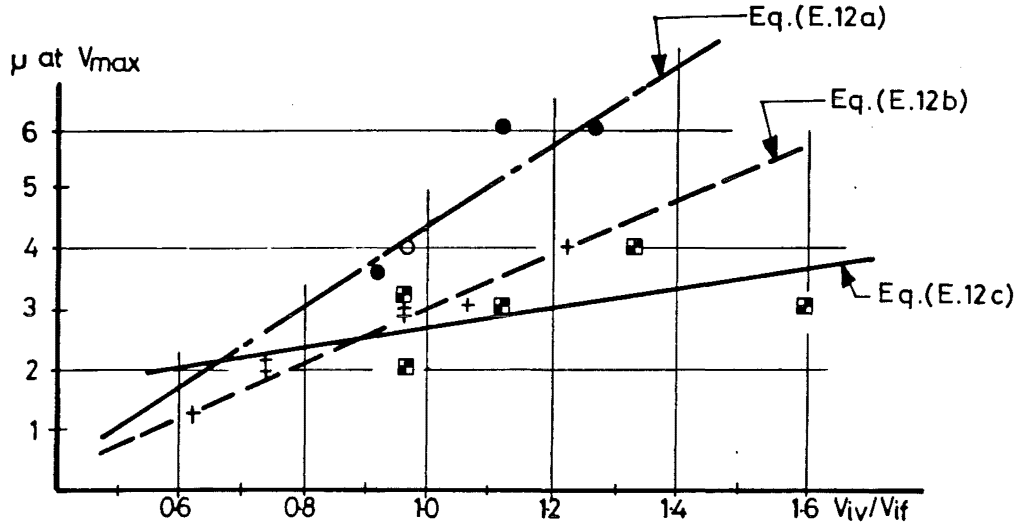

Fig. E.18 : Displacement ductility level, μ, at V_{max} as a function of strength ratio V_{iv}/V_{if}

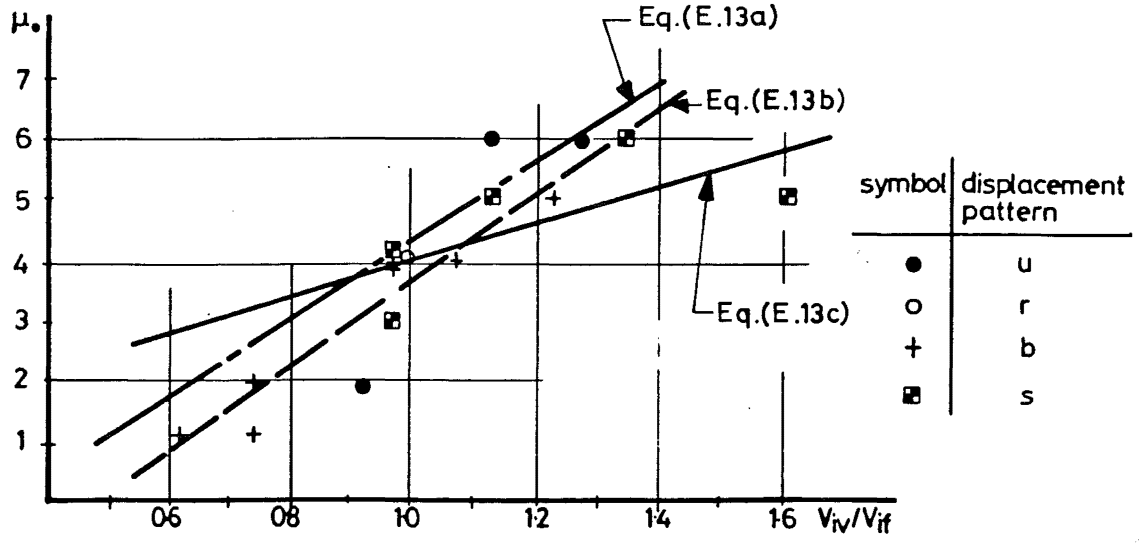

Fig. E.19 : Dependable displacement ductility level, μ_o, as a function of strength ratio V_{iv}/V_{if}

CHAPTER F
DESIGN RECOMMENDATIONS

F.1 INTRODUCTION

This chapter presents design recommendations on two topics:

1) An approach to evaluate elastic deformations in reinforced concrete circular cantilever columns (Section F.2),

2) A proposal of seismic shear design for reinforced concrete circular columns (Section F.3).

F.2 AN APPROACH TO EVALUATE ELASTIC DEFORMATIONS IN REINFORCED CONCRETE CIRCULAR CANTILEVER COLUMNS

An approach to evaluate the elastic deformations in reinforced concrete circular cantilever columns, particularly with low aspect ratios, when subjected to lateral and axial loads, is presented in this section. This approach is simple and it leads to a reasonable agreement with the present test results at the lateral force, V, equal to $0.75V_{if}$.

An improved prediction of column deflection due to lateral forces may assist in a more realistic assessment of "service" performance. Also it enables a more accurate estimate of the dynamic properties of bridge structures to be made. An important relationship, used in the design of bridge columns, is that between absolute lateral displacements and the displacement ductility factor. A more realistic evaluation of column stiffness enables a corresponding estimate of the reference yield displacement, Δ_y, to be made. This in turn, leads to an improved estimate of the total displacement associated with a displacement ductility ratio on which the design of the structure may have been based.

The top end deflection of a reinforced concrete cantilever column, Δ, can be expressed as:

$$\Delta = \Delta_{fl} + \Delta_{ts} + \Delta_b + \Delta_s \qquad (F.1)$$

where Δ_{fl} = deflection due to flexure

Δ_{ts} = deflection due to the effects of diagonal tension cracks

Δ_b = deflection due to bar elongation within the foundations

Δ_s = deflection due to core distortions caused by shear

These deflection components are derived subsequently.

F.2.1 Deflection Due to Flexure

With the knowledge of the distribution of bending moments along a reinforced concrete column, the corresponding theoretical curvature profile can be determined from the theoretical moment-curvature relationships (Appendix V). Integration of the curvature gives the deflection at the top of the column due to flexure, Δ_{fl}, as

$$\Delta_{fl} = \int_0^L \Phi_x (L - x) dx \qquad (F.2)$$

where x = distance measured from the column support (Fig. F.1b)

L = height of the column

Φ_x = curvature corresponding to bending moment, M_x, at section x due to lateral force V (Fig. F.1c)

F.2.2 Deflection Due to the Effects of Diagonal Tension Cracks

When the lateral force V on a column is larger than that causing diagonal cracks, V_{cr}, diagonal tension cracks are formed. Diagonal tension cracks lead to larger tension forces T_x or strains in the flexural reinforcement than is implied by the bending moment diagram at sections away from the section of maximum bending moment. These additional strains in the flexural reinforcement will increase deformations. A diagonal crack leads to discontinuity within a transverse section of the member. Consequently the plane section hypothesis used for the definition of curvature is violated. However, for design purposes, deflections due to flexure and diagonal tension cracks may be estimated by integration of the curvature corresponding to the internal moment $T_x(jd)$ distribution (Fig. F.1) [F.1]; that is

$$\text{when } V \geq V_{cr}, \quad \Delta_{fl} + \Delta_{ts} = \int_0^L \Phi_x' (L - x) dx \qquad (F.3)$$

where Φ_x' = curvature corresponding to the internal moment $T_x(jd)$ at section x. It is approximately equal to the curvature at bending moment $M = T_x(jd)$ from moment - curvature analysis [F.1].

$T_x(jd)$ is calculated from Eqs. (F.5 and F.7)

From the test results of this project, it is proposed V_{cr} be expressed by Eq. (F.4). It based on best-fit straight line technique for observed values.

$$v_{cr}/\sqrt{f'_c} = 0.19(1 + 4.7\, P_i/(f'_c\, A_g))\alpha_1 \qquad (f'_c \text{ in MPa}) \qquad (F.4)$$

where $v_{cr} = V_{cr}/A_e$

$\alpha_1 = 2.0\, D/L \geq 1.0$

As shown in Table F.I, the average ratio of the values given by Eq. (F.4) to those of the test results is 1.02, with coefficient of variation 7%.

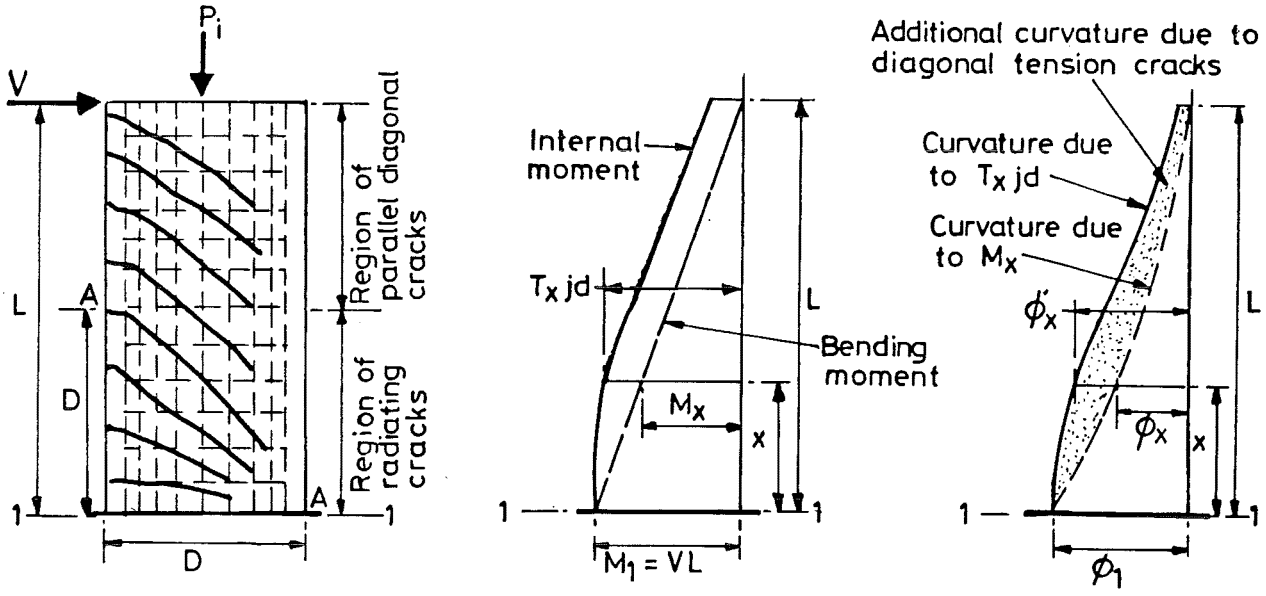

(a) Typical crack pattern

(b) Bending and internal moment diagrams

(c) curvature diagrams

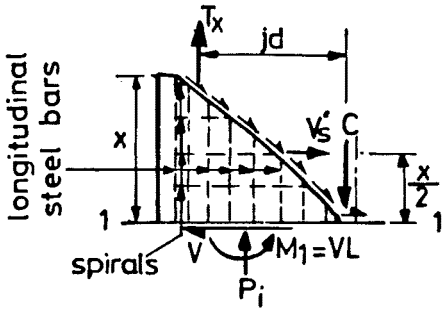

(d) Forces acting on a free body bound by a radiating crack

Fig. F.1 : Internal moment and curvature diagrams as affected by shear

Table F.I : Column shear strength at onset of diagonal cracks

Unit no.	1	2	3
	$v_{cr}/\sqrt{f'_c}$		
	predicted	measured	(1)/(2)
1	0.36	0.35	1.03
2	0.54	0.54	1.00
3	0.54	0.53	1.02
4	0.19	0.19	1.00
5	0.19	0.18	1.06
6	0.19	0.18	1.06
7	0.36	0.38	0.95
8	0.36	0.38	0.95
9	0.54	0.47	1.15
10	0.54	0.57	0.95
11	0.19	0.19	1.00
12	0.19	0.22	0.86
13	0.36	0.36	1.00
14	0.36	0.35	1.03
15	0.54	0.45	1.20

mean: 1.02
standard deviation: 0.07

The internal moment $T_x(jd)$ diagram can be evaluated from the equilibrium of a free body bound by inclined sections, such as Fig. F.1d. It is clear that $T_x(jd)$ depends on the shear carried by spirals crossing the section concerned. In Section E.6, estimated components of shear resistance , V_c and $V_s = V - V_c$, at different ductility levels have been discussed. At a low ductility level ($\mu < 1$), the shear carried by spirals, V_s, crossing a 45° diagonal, section A - A, may be approximated by Eq. (F.5)

$$V_s = V - V_{cr} \qquad \text{(F.5)}$$

where V_{cr} is obtained from Eq. (F.4)

It is also assumed that spirals contribute at a uniform rate (force per unit length) to shear resistance over the entire height of the column. Then, in the region of a radiating diagonal crack ($x \leq D$), the shear carried by spirals crossing the diagonal crack originating at a distance x from the support, is V_s' (Fig. F.1d).

where $V_s' = V_s\ x/D$ (F.6)

From the equilibrium condition of a free body shown in Fig. F.1d,

$$T_x(jd) = V\ L - (V_s'\ x)/2$$

$$= V\ L - (V_s\ x^2)/(2\ D) \qquad \text{when } x \leq D \qquad \text{(F.7a)}$$

At a 45° crack, when $x \approx D$,

$$T_x(jd) = V\,L - (V_s\,D)/2 \qquad \text{(F.7b)}$$

Similarly, in the region outside the potential plastic hinge ($D \le x \le L$),

$$T_x(jd) = V(L - x + D) - (V_s\,D)/2 \quad \text{when } x \ge D \qquad \text{(F.7c)}$$

The increase of internal tension force above values implied by conventional flexural analysis is generally referred to as the phenomenon of tension shift.

When the lateral force, V, is smaller than that at the onset of diagonal cracks, V_{cr}, only flexural cracks are formed. The internal moment $T_x(jd)$ diagram is then identical to the bending moment diagram, and the deflection due to the effects of diagonal tension cracks, Δ_{ts}, is zero; i.e.

$$\text{when} \quad V < V_{cr}, \quad \Delta_{ts} = 0 \qquad \text{(F.8)}$$
$$\text{and} \quad \Delta_{fl} \text{ is obtained from Eq. (F.2).}$$

F.2.3 Deflection Due to Bar Elongation Within the Foundations

The rotation of a column at the column - foundation interface, θ_δ, due to the tension stress penetration along column steel bars inside the foundation has been derived in Section E.7.3. From Eqs. (E.4 and E.7), θ_δ is expressed as

$$\theta_\delta = \varepsilon_{ls}\,L_d/(2\,c_s) = \Phi_l\,L_d/2 \qquad \text{(F.9)}$$

where ε_{ls} = strain of the column bar at the extreme tension fibre at the column - foundation interface

L_d = development length required to develop tensile stress, f_{sl}, of the column bar at the extreme tension fibre at the column - foundation interface

Φ_l = theoretical curvature of the column at the column - foundation interface

The values of ε_{ls}, f_{sl}, and Φ_l are calculated from the moment - curvature analysis with the moment $M = V\,L$. The development length, L_d, may be determined from Eq. (F.10). This equation is modified from ACI 318-89 Clause 12.2 recommendation [F.2]. A discussion on Eq. (F.10) is presented in Section F.2.5.

$$L_d = 0.02\, A_{sl}\, f_{sl}/\sqrt{f'_c} \qquad \text{(F.10)}$$

where A_{sl} = cross-sectional area of the column vertical bar

f'_c = measured concrete compressive strength of the column support (in MPa)

The top deflection of the column due to bar elongation within the foundations, Δ_b, is given by

$$\Delta_b = \theta_b\, L = (\Phi_1\, L\, L_d)/2 \qquad \text{(F.11)}$$

Applying Eq. (F.11), the values of Δ_b for some test columns at the displacement ductility factor, $\mu = 0.75$ (lateral force $V = 0.75\, V_{if}$), were calculated and these listed in Table F.II.

It is seen that anchorage deformations at this stage of lateral force applications account for column deflection of only 0.04 to 0.16% of the column height.

Table F.II : Deflection due to bar elongation within the foundations for some test columns, calculated at 756 mm above column base

1	2	3	4	5	6	7	8
Unit	V	f'_c	Φ_1	f_{sl}	ε_{ls}	L_d	Δ_b
-	kN	MPa	x10-6/mm	MPa	-	mm	mm
1	280	57	9.0	329	0.00171	175	0.60
2	295	58	7.4	198	0.00100	105	0.30
3	290	48	7.4	198	0.00100	115	0.33
4	248	52	9.9	475	0.00240	265	1.00
5	248	37	9.9	475	0.00240	314	1.19
6	248	54	9.9	475	0.00240	260	0.98
7	302	58	9.3	376	0.00190	199	0.70
8	302	52	9.3	376	0.00190	210	0.75
9	260	51	8.4	243	0.00123	137	0.44
10	290	48	7.4	198	0.00100	115	0.33

2: $V = 0.75\, V_{if}$
3: f'_c = measured concrete compressive strength of column base block
7: L_d obtained from Eq. (F.10)
8: Δ_b obtained from Eq. (F.11)

F.2.4 Deflection Due to Core Distortion Caused by Shear

For columns with low aspect ratios, the core distortion caused by shear may be significant. Therefore, for such members, it is necessary to be able to assess the magnitude of deflection due to core distortion.

The shear stiffness K_v is defined as the magnitude of shear force that when applied to a column of unit length, will cause a unit shear displacement of one end relative to the other. In the uncracked portion of a column, shear deformation can be satisfactorily predicted using the principles of elasticity. As suggested by Park and Paulay [F.1], the shear stiffness of an uncracked elastic column of unit length is

$$K_v = 0.4\, E_c\, A_q / f \qquad \text{(F.12)}$$

where E_c = modulus of elasticity of concrete
A_q = area contributed to the shear stiffness
f = form factor to allow for the nonuniform distribution of shear stress

The modulus of elasticity of normal weight concrete, E_c, may be considered to be $4730\sqrt{f'_c}$ MPa [F.1].

Analytical and experimental studies [F.1] have shown that the shear stiffness of a diagonally cracked member was approximately 10 to 30% of the shear stiffness of the uncracked member, depending on the amount of shear reinforcement provided [F.1]. For this reason, the deflection due to core distortion caused by shear was derived under two conditions: (a) before the formation of diagonal cracks, and (b) after the formation of diagonal cracks.

a) Before the formation of diagonal cracks

It was evident that before the lateral force V exceeded that causing diagonal cracks, V_{cr}, some flexural cracks had been formed on the test columns (Chapter D). At this stage of loading, the shear stiffness of test columns can be expected to be a little less than that at the uncracked state as expressed by Eq. (F.12). It is suggested that K_v of circular columns with minor flexural cracks might be approximated by $K_v = 0.25\, E_c\, A_g$. This assumption is further discussed in Section F.2.5.

Hence, when $V \le V_{cr}$, the deflection due to core distortion caused by shear, Δ_s is given by

$$\Delta_s = V L/(0.25\, E_c\, A_g)$$
$$\approx V L/(1200\, \sqrt{f'_c}\, A_g) \qquad (f'_c \text{ in MPa}) \qquad \text{(F.13)}$$

b) After the formation of diagonal cracks

When the lateral force V is larger than V_{cr}, diagonal cracks will be formed. The estimation of deflection due to core distortion after the formation of diagonal cracks, Δ_s, is based on the following assumptions:

1. The total core distortion caused by shear is considered as the sum of core distortions due to shear resisted by "concrete mechanism", V_c (Section E.6), and that by spirals, V_s. Although the one contributed by "concrete mechanism" is difficult to determine, its magnitude can be conservatively assessed by Eq. (F.13).

At a low ductility level ($\mu < 1$), V_s may be approximated by Eq. (F.5), i.e. V_c is assumed to be V_{cr}.

2. For the purpose of simplicity, shear carried by spirals, V_s, is approximated by using the model of the analogous truss, as shown in Fig. F.2. It comprises spirals and 45° diagonal concrete struts as web members. For the purpose of determining the web distortion only, the axial stiffness of the vertical chord members is assumed to be infinitely large.

3. Across a diagonal crack, the spirals are equally stressed to the same level below yield strength.

Applying the Williot's principles to the analogous truss, the web distortion per length d_s, Δ_4, can be found from Figs. F.2b and F.2c [F.1] as follows:

$$\Delta_4 = \Delta_3 + \sqrt{2}\,\Delta_1 \qquad \text{(F.14)}$$

where Δ_3 = elongation of spirals

Δ_1 = shortening of the diagonal concrete strut

Based on Eq. (I.6) in Appendix I, the strain of spiral, ε_s, is

$$\varepsilon_s = 2\,V_s\,s/(\pi\,A_{sp}\,d_s\,E_{st}) \qquad \text{(F.15)}$$

where E_{st} = modulus of elasticity of spiral steel

The diameter of strained spiral is $(1 + \varepsilon_s)d_s$, so that

$$\begin{aligned}\Delta_3 &= (1 + \varepsilon_s)d_s - d_s \\ &= \varepsilon_s\,d_s \\ &= 2\,V_s\,s/(\pi\,A_{sp}\,E_{st}) \qquad \text{(F.16)}\end{aligned}$$

The calculation of the stress of the elliptical diagonal concrete strut of circular members is complicated. Fortunately, in the truss model, the axial stiffness of the diagonal concrete strut is generally much greater than that of transverse reinforcement. Therefore, the contribution of shortening of the diagonal concrete strut, Δ_1, to Δ_4 can be neglected without incurring a significant error in the estimation. Therefore

$$\Delta_4 \approx 2\, V_s\, s/(\pi\, A_{sp}\, E_{st}) \qquad (F.17)$$

Hence, when $V \geq V_{cr}$, the end deflection due to shear distortion can be approximated by

$$\Delta_s \approx V_{cr}\, L/(1200\, \sqrt{f'_c}\, A_g) + \Delta_4\, L/d_s$$

$$\approx \frac{V_{cr}\, L}{1200\, \sqrt{f'_c}\, A_g} + \frac{2(V - V_{cr})\, s\, L}{\pi\, d_s\, A_{sp}\, E_{st}} \qquad (F.18)$$

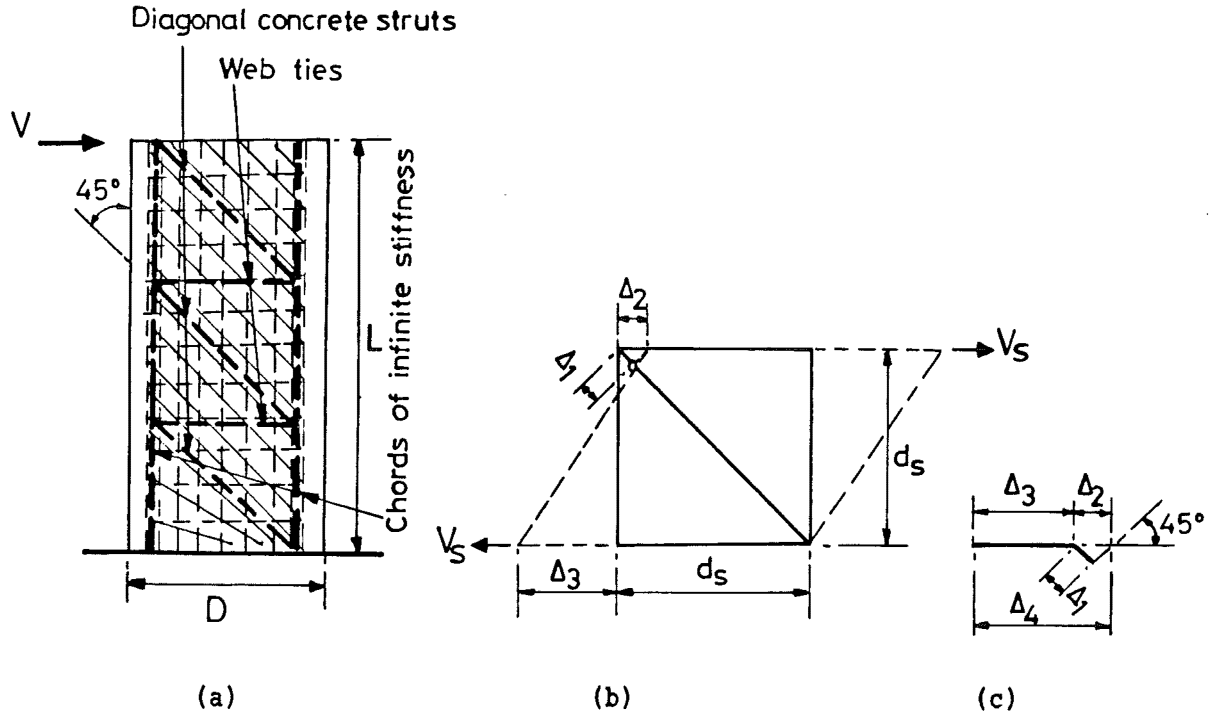

Fig. F.2 : Core distortions of a reinforced concrete member caused by shear

F.2.5 A Comparison of Predicted Deflections of Test Columns with Corresponding experimentally Observed Values At $\mu = 0.75$

During the testing of the column specimens, the end deflections of the columns were measured at 765 mm above the column base. These experimentally observed end deflections at the displacement ductility factor, $\mu = 0.75$, i.e. at $V = 0.75\ V_{if}$, were then compared with the corresponding predicted values evaluated by the approach outlined in Sections F.2 to F.2.4. The results are shown in Table F.III.

It is seen that column top deflections at this level of applied lateral force are of the order of 0.26 to 0.82% of the column height.

Table F.III : Deflections of test columns at 765 mm above column base at $\mu = 0.75$

Unit no.	1	predicted					expt.	
	1	2	3	4	5	6	7	8
	V	V_{cr}	$\Delta_{fl} + \Delta_{ts}$	Δ_b	Δ_s	Δ	Δ	(6)/(7)
	kN	kN	mm	mm	mm	mm	mm	-
1	280	226	2.40	0.60	0.47	3.47	3.60	0.96
2	295	342	1.46	0.30	0.25	2.01	2.36	0.85
3	290	334	1.45	0.33	0.25	2.03	2.43	0.84
4	248	128	2.60	1.00	2.70	6.30	5.30	1.19
5	248	127	2.60	1.19	1.72	5.51	5.08	1.08
6	248	128	2.60	0.98	1.08	4.66	4.74	0.98
7	302	234	2.58	0.70	1.29	4.57	4.24	1.08
8	302	234	2.58	0.75	0.74	4.07	4.39	0.93
9	260	292	1.64	0.44	0.26	2.34	2.30	1.02
10	290	334	1.45	0.33	0.25	2.03	2.55	0.80
							mean:	0.97
							standard deviation:	0.12

1: $V = 0.75\ V_{if}$
2: V_{cr} obtained from Eq. (F.4)
3: $\Delta_{fl} + \Delta_{ts}$ obtained from Eqs. (F.2 to F.8)
4: Δ_b obtained from Eqs. (F.10 to F.11)
5: Δ_s obtained from Eqs. (F.13 and F.18)
6: $\Delta = \Delta_{fl} + \Delta_{ts} + \Delta_b + \Delta_s$

In general, a reasonable agreement between the predicted and measured values of stiffnesses (columns 6 and 7 of Table F.III) is obtained. It should be realized that in order to arrive at simple equations, a number of simplifying assumptions are necessary, each of which imposes some limitation on the accuracy of prediction of deformations.

For example, the derivation of the deflection due to bar elongation within the foundations involves an assumption of triangular strain distribution of column steel bar over the development (anchorage) length within the foundations. A previous research report [F.3] provided some experimental data on the strain distribution of 12 mm diameter flexural steel bars (HD12) in walls below the base. In these tests of walls, the measured yield strength of HD12 steel bars was 450 MPa, and the average concrete strength, f'_c, of the wall base blocks was 34 MPa. When these bars were stressed to about half of their yield strength, the tensile strain profiles below wall base appeared to be concave. Measurable strain was recorded over an embedment length of 350 mm. At large ductility levels, tensile yield strains were recorded as deep as 250 mm, i.e. 20 bar diameters below the top of the base block. However, tensile strains were negligible at and beyond embedment length of 500 mm.

The development length of a steel bar also depends on bar spacing, enclosing transverse reinforcement, and the confinement condition of concrete around the bar. In the present test series, six turns of spiral steel reinforcement were provided to column vertical steel bars in the column base block. When a test column was subjected to bi-directional loading histories, the lateral compression in two directions (North - South, & East - West) acted on the vertical surfaces of the column base block, as a result of setting up of the steel loading frames. This provided considerable confinement to the concrete of the base block. All these factors, absent in the reported tests [F.3], would lead to more effective bond transfer within the anchorage, or to shorter development length required for the vertical column bars.

In this project, Eq. (F.10) was found to provide a good estimate of development length for the prediction of deformation due to bar elongation within the foundations. In other situations where the conditions of anchorage bond transfer are considerably different from those of the present test series, Eq. (F.10) may need to be modified.

Another uncertain issue is the shear stiffness of the circular column before the formation of diagonal cracks, as expressed by Eq. (F.13). This equation was formulated by assuming the shear stiffness before formation of diagonal cracks to be a certain percentage of the shear stiffness of an uncracked column. Although the shear deformation predicted by Eq. (F.13) is very small, it can affect the accuracy of the predicted end deflection of columns before the formation of diagonal cracks. The under-estimation of end deflections of test Units 2, 3, and 10 may imply over-estimation of the shear stiffness by Eq. (F.13).

F.3 A PROPOSAL FOR SEISMIC SHEAR DESIGN OF REINFORCED CONCRETE CIRCULAR COLUMNS

In Chapter E, the significance of key parameters (axial compression load intensity, spiral steel content, and loading history) of the shear behaviour of the test columns was quantified. The complex overall behaviour does not encourage an attempt to develop a refined technique, such as the diagonal compression field theory or finite element analysis, to simulate the performance of test columns. The main difficulty lies in the lack of reliable or promising constitutive laws for extensively cracked concrete as a material, when it is subjected to multi-directional cyclic inelastic displacements. From this project, it was not possible to extract sufficient information for such formulation. For this reason, it was necessary to resort to the derivation of empirical expressions, based on statistical evaluation of observed and measured performances of test columns, to develop a shear design procedure for reinforced concrete columns under multi-directional cyclic displacement histories.

Based on regression analysis of experimental results of this project, and those reported by Ang [F.4] (summarized in Table F.IV), a proposal for seismic shear design procedure for reinforced concrete circular columns, taking into account of displacement histories, is formulated. This proposal provides design information on:

1) Flexural strength enhancement factor, $m = M^o/M_1$, which was defined in Section B.2.4.1., and was discussed in Section E.3.2.

2) Maximum strength of the column in terms of the maximum lateral applied force, V_{max}.

3) Dependable displacement ductility capacity, μ_o. This is the highest displacement ductility level at which the peak strength is not less than 80% of the column's ideal flexural strength, V_{if} (see Section C.3.1. for the definition of V_{if}).

4) Achievable strength, $V_{\mu o}$, at the dependable displacement ductility capacity, μ_o. This is the greatest strength developed during load cycling to μ_o.

Table F.IV : Properties and experimental findings of Ang's test units

Properties							Observed			
1	2	3	4	5	6	7	8	9	10	11
Unit	$\frac{L}{D}$	$\frac{P_i}{f'_c A_g}$	ρ_s (%)	ρ_l (%)	f'_c (MPa)	V_{if} (kN)	$\frac{V_{max}}{V_{if}}$ at μ		μ_c	μ_o
(1)	2.0	0.00	0.509	3.20	37.5	306	1.05	2.5	2.5	2.5
(2)	2.0	0.00	0.509	3.20	37.2	220	1.03	4	6	4
(3)	2.5	0.00	0.509	3.20	36.0	242	1.23	2	4	2
(4)	2.0	0.00	0.515	3.20	30.6	299	0.99	1.4	1.4	1.4
(5)	2.0	0.00	0.764	3.20	31.1	301	1.12	2	3	2
(6)	1.5	0.00	0.509	3.20	30.1	402	0.97	1	1.3	1
(7)	2.0	0.00	0.382	3.20	29.5	293	0.96	1.5	1.6	1.5
(8)	2.0	0.20	1.019	3.20	28.7	356	1.33	4	6	4
(9)	2.5	0.20	1.019	3.20	29.9	281	1.37	8	8	8
(10)	2.0	0.20	1.019	3.20	31.2	360	1.25	4	6	4
(11)	2.0	0.20	0.509	3.20	29.9	351	1.15	2.5	2.5	2.5
(12)	1.5	0.10	1.019	3.20	28.6	437	1.20	3	3	3
(13)	2.0	0.10	1.019	3.20	36.2	363	1.22	4	6	4
(14)	2.0	0.00	0.509	3.24	33.7	304	1.02	2	3	2
(15)	2.0	0.00	0.509	1.92	34.8	204	1.13	4	6	4
(16)	2.0	0.10	0.509	3.20	33.4	345	1.10	1.5	1.5	1.5
(17)	2.5	0.10	0.509	3.20	34.3	281	1.17	2	2.5	2
(18)	1.5	0.10	0.509	3.20	35.0	462	1.10	2	1.4	1.4
(19)	1.5	0.10	0.382	3.20	34.4	468	0.93	1.5	1.3	<1.5
(20)	1.75	0.175	0.382	3.20	36.7	477	1.02	1.5	1.5	<1.5
(21)	2.0	0.00	0.382	3.20	33.2	313	0.82	1	1.1	<1
(22)	2.0	0.00	0.386	3.20	30.9	294	0.95	1.5	1.5	<1.5
(23)	2.0	0.00	0.764	3.20	32.3	295	1.15	2	4	2
(24)	2.0	0.00	0.772	3.20	33.1	305	1.11	4	4	2

1: 400 mm dia. reinforced concrete circular column units tested by Ang [F.4]
4: Volumetric spiral steel content, $\rho_s = 4\ A_{sp}/(d_s\ s)$
5: Longitudinal steel content, ρ_l = (total area of longit. steel)/A_g
All units have 20 no. 16 mm Grade 380 deformed bars except that
Unit 2 : 20 no. 16 mm Grade 275 deformed bars
Unit 14: 9 no. 24 mm Grade 280 deformed bars
Unit 15: 12 no. 16 mm Grade 380 deformed bars
10: Ductility capacity, μ_c, at onset of observed instability of hysteretic loops
11: Dependable displacement ductility capacity, μ_o.
At μ_o, the greatest strength developed is $V_{\mu o}$. It was found that
$V_{\mu o} = V_{max}$ except for
Unit 18: $V_{\mu o} = 1.09\ V_{if}$
Unit 24: $V_{\mu o} = 1.09\ V_{if}$

F.3.1 Flexural Strength Enhancement Factor, m

It was discussed in Section E.3.2 that the empirical formulae, Eqs. (B.38a to B.38d), derived by Ang [F.4] for the prediction of flexural strength enhancement factor, $m = M^o/M_i$, gave less satisfactory results for short circular columns with either negligible or high axial compression load. Large shear stresses and the severity of displacement patterns appear to lower the value of this factor. Based on the observed maximum strengths of those test units which exhibited ductile flexural response (those marked by asterisk, *, in Tables V and VI), the flexural strength enhancement factor, m, may be evaluated as follows:

Case 1: When $\frac{P_i}{f'_c A_g} \leq 0.1$ (small axial compression)

$$m = [\frac{f_y}{1166} + 0.894]\, r_d \quad \text{when } \frac{M}{VD} > 2 \qquad (F.19a)$$

$$m = [0.768 + 1.262\,\frac{P_i}{f'_c A_g} + \frac{f_y}{1050}(1 - \frac{P_i}{f'_c A_g})]\, r_d \quad \text{when } \frac{M}{VD} \leq 2 \qquad (F.19b)$$

Case 2: When $\frac{P_i}{f'_c A_g} > 0.1$

$$m = [(4.577 - \frac{f_y}{123.5})\,(\frac{P_i}{f'_c A_g} - 0.1)^2 + (\frac{f_y}{116.7} - 2.357)\frac{P_i}{f'_c A_g} + 1.13]\, r_d \qquad (F.19c)$$

where f_y = the specified yield strength (in MPa) of the steel used for flexural reinforcement. In this project, two grades $f_y = 275$ and $f_y = 380$ of the New Zealand manufactured deformed reinforcing steel were used.

$\frac{M}{VD}$ = aspect ratio = $\frac{L}{D}$ for cantilever columns

r_d = strength reduction factor account for loading history. The estimation of which is described in the following for different displacement patterns:

a) For uni-directional 'u' type displacement pattern

$$r_d = 1.0 \qquad (F.20a)$$

b) For bi-directional 'b' type displacement pattern

$$r_d = 0.97 - 0.20\,\frac{P_i}{f'_c A_g} \qquad (F.20b)$$

c) For bi-directional 's' type displacement pattern

$$r_d = 0.92 - 0.13\,\frac{P_i}{f'_c A_g} \qquad (F.20c)$$

Eqs. (F.19 to F.20) are shown in Figs. F.3 and F.4 respectively.

Table F.V : A comparison of predicted strengths and dependable ductilities with corresponding experimentally observed values for test units subjected to uni-directional 'u' type displacement pattern

		Predicted									Observed			Comparisons		
1	2	3	4	5	6	7	8	9	10	11	12	13	14	15	16	17
Unit	$\frac{P_i}{f'_c A_g}$	m	$\frac{V_{si}}{V_{if}}$	$\frac{V_{ci}}{V_{if}}$	$\frac{V_i}{V_{if}}$	$\frac{V_{max}}{V_{if}}$	$\frac{V_{so}}{V_{if}}$	$\frac{V_i - V_{\mu o}}{\sqrt{f'_c}}$	$\frac{V_{max}/r_d - V_{so}}{\sqrt{f'_c}}$	μ_o	μ_o	$\frac{V_{max}}{V_{if}}$	$\frac{V_{\mu o}}{V_{if}}$	$\frac{m}{m_{Ang}}$	$\frac{7}{13}$	$\frac{7}{14}$
(1)	0.00	1.13	0.29	0.77	1.06	1.06	-	-	-	2	2.5	1.05	1.05	0.93	1.01	1.01
(2)*	0.00	1.03	0.40	1.07	1.47	1.03	0.80	0.153	0.080	3.7	4	1.03	1.03	0.91	1.00*	1.00
(3)*	0.00	1.22	0.36	0.97	1.33	1.22	0.78	0.043	0.171	2.3	2	1.23	1.23	1.00	0.99*	0.99
(4)	0.00	1.13	0.28	0.70	0.98	0.98	-	-	-	2	1.4	0.99	0.99	0.93	0.99	0.99
(5)	0.00	1.13	0.44	0.70	1.14	1.14	-	-	-	2	2	1.12	1.12	0.93	1.02	1.02
(6)	0.00	1.13	0.22	0.70	0.92	0.92	-	-	-	≤1	1	0.97	0.97	0.93	0.95	0.95
(7)	0.00	1.13	0.25	0.71	0.96	0.96	-	-	-	≤1	1.5	0.96	0.96	0.93	1.00	1.00
(8)*	0.20	1.33	0.56	0.92	1.48	1.33	0.77	0.096	0.358	4	4	1.33	1.33	1.07	1.00*	1.00
(9)*	0.20	1.33	0.70	1.20	1.90	1.33	1.01	0.281	0.158	7.1	8	1.37	1.37	1.07	0.97*	0.97
(10)*	0.20	1.33	0.49	0.92	1.41	1.33	0.78	0.051	0.352	4	4	1.25	1.25	1.07	1.06*	1.06
(11)	0.20	1.33	0.28	0.96	1.24	1.24	-	-	-	2	2.5	1.15	1.15	1.07	1.08	1.08
(12)	0.10	1.22	0.40	0.81	1.21	1.21	-	-	-	2	3	1.20	1.20	1.00	1.01	1.01
(13)*	0.10	1.22	0.48	0.82	1.30	1.22	0.86	0.046	0.209	3.9	4	1.22	1.22	1.00	1.00*	1.00
(14)	0.00	1.03	0.28	0.74	1.02	1.02	-	-	-	2	2	1.02	1.02	0.91	1.00	1.00
(15)*	0.00	1.13	0.42	1.08	1.50	1.13	0.84	0.123	0.096	3.4	4	1.13	1.13	0.93	1.00*	1.00
(16)	0.10	1.22	0.25	0.84	1.09	1.09	-	-	-	2	1.5	1.10	1.10	1.00	0.99	0.99
(17)*	0.10	1.22	0.30	1.05	1.35	1.22	0.65	0.060	0.263	3.1	2	1.17	1.17	1.00	1.04*	1.04
(18)	0.10	1.22	0.19	0.85	1.04	1.04	-	-	-	2	1.4	1.10	1.09	1.00	0.95	0.95
(19)	0.10	1.22	0.14	0.84	0.98	0.98	-	-	-	≤1	<1.5	0.93	0.93	1.00	1.05	1.05
(20)	0.175	1.30	0.14	0.85	0.99	0.99	-	-	-	≤1	<1.5	1.02	1.02	1.06	0.97	0.97
(21)	0.00	1.13	0.21	0.71	0.92	0.92	-	-	-	≤1	<1	0.82	0.82	0.93	1.12	1.12
(22)	0.00	1.13	0.21	0.71	0.92	0.92	-	-	-	≤1	<1.5	0.95	0.95	0.93	0.97	0.97
(23)	0.00	1.13	0.42	0.72	1.14	1.14	-	-	-	2	2	1.15	1.15	0.93	0.99	0.99
(24)	0.00	1.13	0.41	0.71	1.12	1.12	-	-	-	2	2	1.11	1.09	0.93	1.01	1.03
1 *	0.19	1.31	0.60	0.97	1.57	1.31	0.92	0.155	0.232	5.6	6	1.30	1.30	1.06	1.01*	1.01
2	0.39	1.61	0.22	1.30	1.52	1.52	-	-	-	2	2	1.31	1.18	1.13	1.16	1.29
3 *	0.39	1.61	0.57	1.28	1.85	1.61	0.86	0.150	0.469	6.5	6	1.63	1.63	1.13	0.99*	0.99
[16]*	0.19	1.31	0.46	0.94	1.40	1.31	0.83	0.056	0.299	4.6	≥4	1.30	-	1.06	1.01*	-
													mean:	1.01	1.02	
													standard deviation:	0.05	0.06	

1: Units in ( ) were tested by Ang, others are specimens of the current test series
Units marked by asterisk, *, are controlled by $V_{max} = V^o_{if}$
Unit [16] was subjected to bi-directional 'r' type displacement pattern
3: m obtained from Eqs. (F.19 to F.20)
4: V_{si} obtained from Eq. (B.33b)
5: V_{ci} obtained from Eqs. (B.33c to B.33e)
6: $V_i = V_{si} + V_{ci}$
7: V_{max} obtained from Eqs. (F.21a to F.21b)
8: V_{so} obtained from Eqs. (F.24 and F.26)
9: $V_{\mu o}$ obtained from Eq. (F.22)
11: μ_o obtained from Eqs. (F.28a to F.28c)
15: m_{Ang} is the flexural strength enhancement factor obtained from Eqs. (B.38a to B.38d)

Table F. VI : A comparison of predicted strengths and dependable ductilities with corresponding experimentally observed values for test units subjected to bi-directional displacement patterns

		Predicted											Observed			Comparisons		
1	2	3	4	5	6	7	8	9	10	11	12	13	14	15	16	17	18	19
Unit	$\frac{P_1}{f'_c A_g}$	m	$\frac{V_{s1}}{V_{1f}}$	$\frac{V_{c1}}{V_{1f}}$	$\frac{V_1}{V_{1f}}$	$\frac{V_{max}}{V_{1f}}$	$\frac{V_{so}}{V_{1f}}$	$\frac{V_{co}}{V_{1f}}$	$\frac{V_{\mu o}}{V_{1f}}$	$\frac{V_1 - V_{\mu o}}{\sqrt{f'_c}}$	$\frac{V_{max}/r_d - V_{so}}{\sqrt{f'_c}}$	μ_o	μ_o	$\frac{V_{max}}{V_{1f}}$	$\frac{V_{\mu o}}{V_{1f}}$	$\frac{m}{m_{Ang}}$	$\frac{7}{15}$	$\frac{10}{16}$
4	0.00	1.10	0.21	0.76	0.97	0.97	-	-	0.97	-	-	≤1	<1.25	0.97	0.97	0.90	1.00	1.00
5	0.00	1.10	0.33	0.75	1.08	1.08	-	-	1.08	-	-	2	2	1.06	1.06	0.90	1.02	1.02
6 *	0.00	1.10	0.56	0.76	1.32	1.10	0.96	0.10	1.06	0.127	0.083	3.6	4	1.09	1.06	0.90	1.01*	1.00
7	0.19	1.22	0.23	0.93	1.16	1.16	-	-	1.16	-	-	2	2	1.14	1.14	0.98	1.02	1.02
8 *	0.19	1.22	0.46	0.93	1.39	1.22	0.74	0.37	1.11	0.173	0.353	3.9	4	1.24	1.23	0.98	0.98*	0.90
9 *	0.39	1.44	0.40	1.25	1.65	1.44	0.62	0.56	1.18	0.301	0.634	4.4	4	1.23	1.16	1.01	1.17*	1.02
10 *	0.39	1.44	0.53	1.28	1.81	1.44	0.76	0.57	1.33	0.300	0.531	5.8	5	1.41	1.27	1.01	1.02*	1.05
16 *	0.19	1.22	0.46	0.93	1.39	1.22	0.74	0.37	1.11	0.174	0.355	3.9	≥4	1.30	-	0.98	0.94*	-
11 *	0.00	1.04	0.56	0.76	1.32	1.04	0.90	0.10	1.00	0.157	0.112	3.2	3	1.03	1.00	0.85	1.01*	1.00
12 *	0.00	1.04	1.24	0.64	1.88	1.04	1.24	0.09	1.04	0.489	-0.064	6.1	5	1.05	0.99	0.85	0.99*	1.05
13 *	0.19	1.17	0.46	0.93	1.39	1.17	0.70	0.37	1.07	0.198	0.377	3.6	4	1.19	1.13	0.94	0.98*	0.95
14 *	0.19	1.17	0.60	0.97	1.57	1.17	0.76	0.39	1.15	0.250	0.327	4.4	5	1.16	1.15	0.94	1.01*	1.00
15 *	0.39	1.40	0.66	1.28	1.94	1.40	0.66	0.57	1.23	0.445	0.595	5.1	6	1.40	1.23	0.99	1.00*	1.00
															mean:	1.01	1.00	
															standard deviation:	0.05	0.04	

1: Units 1 to 10 tested under 'b' type displacement pattern
Units 11 to 15 tested under 's' type displacement pattern
Unit 16 tested under 'r' type displacement pattern
Units marked by asterisk, *, are controlled by $V_{max} = V^o_{1f}$

3: m obtained from Eqs. (F.19 to F.20)

4: V_{s1} obtained from Eq. (B.33b)

5: V_{c1} obtained from Eqs. (B.33c to B.33e)

6: $V_1 = V_{s1} + V_{c1}$

7: V_{max} obtained from Eqs. (F.21a to 21b)

8: V_{so} obtained from Eqs. (F.24 and F.26)

9: V_{co} obtained from Eqs. (F.27a and F.27b)

10: $V_{\mu o}$ obtained from Eqs. (F.23a and F.23b)

13: μ_o obtained from Eqs. (F.28a to F.28c)

17: m_{Ang} is the flexural strength enhancement factor obtained from Eqs. (B.38a to B.38d)

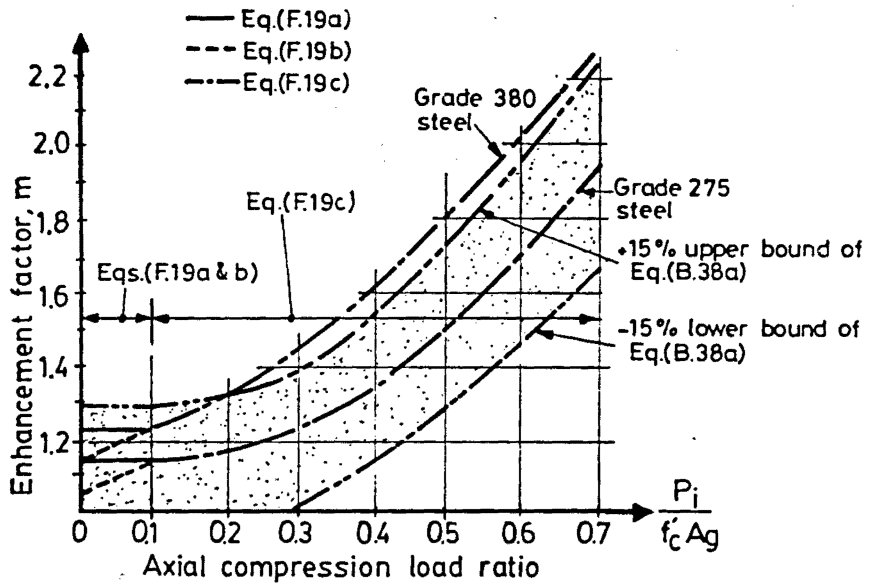

Fig. F.3 : Variation of flexural strength enhancement factor with axial compression load level (r_d = 1)

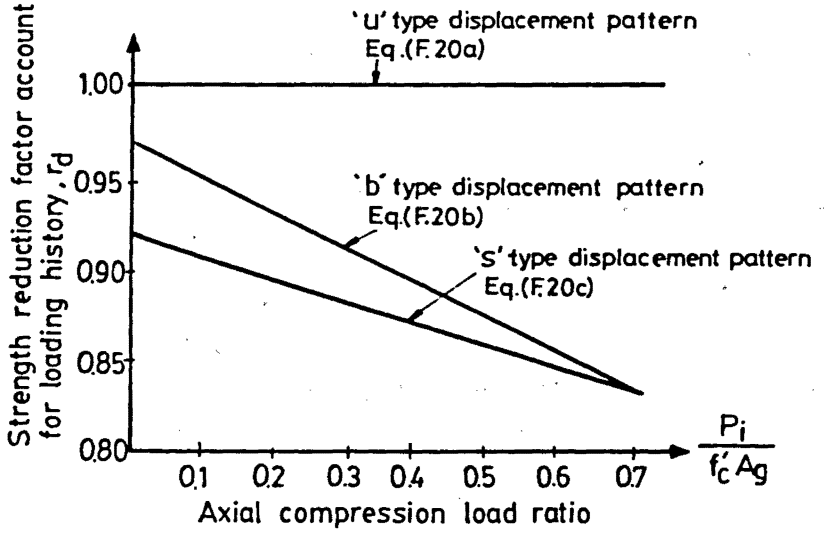

Fig. F.4 : Variation of strength reduction factor r_d with axial compression load level

Eq. (F.19c) is a modification of Eq. (B.38a). These two equations become identical for columns reinforced with Grade 275 steel and subjected to uni-directional 'u' type displacement pattern with $P_i/(f'_c A_g) > 0.1$.

Comparisons of the m factors, obtained from Eqs. (F.19 to F.20), and the flexural strength enhancement factors suggested by Ang, m_{Ang}, calculated from Eqs. (B.38a to B.38d), of test units are shown in columns 15 and 17 of Tables F.V and F.VI respectively. The maximum differences are 13% for test columns subjected to uni-directional displacement pattern, and 15% for test columns subjected to bi-directional displacement patterns.

In the absence of any experimental data, it was assumed that the expressions for r_d, which were derived by regression analysis from the test units reinforced with Grade 380 flexural reinforcement, are also applicable to columns reinforced with Grade 275 flexural reinforcement.

It should be noted that measured material strength properties and a strength reduction factor of unity were used to calculate both the ideal flexural capacity, M_i, of the test columns in this section, and their shear strengths and the dependable displacement ductility capacity presented later in Sections F.3.2 to F.3.4. In design situations where only specified material properties are available, it is proposed that probable yield strengths of reinforcing steel, listed in Table VII (suitable for New Zealand manufactured reinforcing steel), and probable concrete strengths, listed in Table VIII, should be used for the seismic shear design for circular columns, as well as the evaluation of their elastic deformations, recommended in this Chapter.

The values of probable yield strengths of reinforcing steel were taken to be the mean yield strengths of New Zealand manufactured steel reinforcing bars reported by Andriono and Park [F.5] in their statistical study of the properties of New Zealand manufactured Grades 275 and 380 steel reinforcing bars. The probable concrete strengths was taken as the minimum target mean strengths of concrete listed in Table 7 of Specification for Concrete Construction, NZS 3109: 1987 [F.6]. The definitions of the technical terms: High Grade, Special Grade, and Performance Record, used in Table F.VIII, are identical to those defined in that Specification (NZS 3109: 1987).

Table F.VII : Probable yield strengths of New Zealand manufactured reinforcing steel bars

	Grade 275 deformed bar	Grade 380 deformed bar	Grade 275 plain round bar
specified yield strength (MPa)	275	380	275
probable yield strength (MPa)	321	458	331

Table F.VIII : Probable strengths of concrete

	No performance record					With performance record									
	High Grade					High Grade					Special Grade				
specified strength (MPa)	20	25	30	35	40	20	25	30	35	40	20	25	30	35	40
Probable strength (MPa)	30.5	36.5	43.0	49.5	55.0	27.5	33.5	40.0	45.5	51.0	24.5	30.5	36.5	42.5	48.5

F.3.2 Maximum Strength, V_{max}

The maximum strength, V_{max}, of a column defined here is the smaller of its flexural overstrength, V^{o}_{if}, or the shear strength provided before degradation, V_i. i.e.

$$V_{max} = \text{smaller of } V^{o}_{if} \text{ or } V_i \quad \text{(F.21a)}$$

where $$V^{o}_{if} = m\, V_{if} \quad \text{(F.21b)}$$

m = flexural strength enhancement factor, obtained from Eqs. (F.19 to F.20)

V_{if} = ideal flexural strength as defined in Section C.3.1.

V_i is obtained from Eqs. (B.33a to B.33e) with the effective shear stress area, $A_e = (\pi\, d_s^2)/4$

Shear strength before degradation, V_i, is considered to be the sum of the shear force carried by spirals, V_{si}, and that by "concrete mechanism", V_{ci}. With regards quantifying V_i, Ang's equations, Eqs. (B.33a to B.33e), were found to be valid also for units of the current test series. Although the effective shear area, A_e, is defined here to be $(\pi\, d_s^2)/4$, instead of $0.8A_g$, as assigned by Ang in Eq. (B.33c), the difference involved is small enough to be ignored.

As far as the influence of longitudinal reinforcement content, ρ_l, on shear strength is concerned, Arakawa [F.7] and Shibata [F.8] reported that there was only a slight increase in the shear strength with an increase of longitudinal reinforcement content, ρ_l. For example, Arakawa observed that the shear strength was improved by 7% for the increase of ρ_l from 2.5% to 5.1% in his test units with the volumetric spiral steel content, ρ_s, of 0.86% and the axial compression load intensity, $P_i/(f'_c A_g)$, of 0.11.

Based on limited experimental evidence, the effect of longitudinal reinforcement content, ρ_l, on shear strength was also considered in Eq. (B.33e) by the tensile reinforcement content, ρ_w, in the determination of the basic shear stress, v_b, carried by "concrete mechanism". In the present test series, ρ_l is 3.2%, from which v_b was worked out to be $0.37\sqrt{f'_c}$. If ρ_l is reduced, say by half, to a quantity more commonly used in practice, v_b will become about $0.25\sqrt{f'_c}$. As a result, the shear force assigned to "concrete mechanism", V_{ci}, [determined by Eq. (B.33c)] will reduce by about one third. However, the percentage of reduction of shear strength before degradation, V_i, also depends on the contribution from the shear force assigned to the

spiral reinforcement, $V_{s\,i}$. For instance, if ρ_l of the current test units 4 and 6 (both without axial load) is reduced to 1.6%, then the percentages of reduction of V_i will be 25% and 19% respectively. For columns with larger axial compression, V_i would be less sensitive to ρ_l.

There are differences between the experimental observations reported by Arakawa and the prediction by Eqs. (B.33a to B.33e) for the influence of longitudinal reinforcement content on shear strength. Eq. (B.33e) appears to be conservative.

With the consideration of existing information, it was decided to use Eqs. (B.33a to B.33e) with $A_e = (\pi\, d_s^2)/4$, for the prediction of shear strength before degradation, V_i.

Comparisons of the ratios of predicted maximum strengths and observed maximum strengths to the corresponding ideal flexural strength of test units are shown in column 16 of Table F.V , and column 18 of Table F.VI. The predicted values have a close agreement with the test results.

F.4.3 Achievable Strength, $V_{\mu o}$, at Dependable Ductility Capacity

The achievable strength, $V_{\mu o}$, is the largest strength developed at one of the displacement peaks in the first cycle to the dependable displacement ductility capacity, μ_o.

For the test units subjected to uni-directional displacement patterns (Tables F.IV and D.I), the observed maximum strength, V_{max}, occurred in most cases, at the observed dependable ductility capacity, μ_o. As a result, the observed $V_{\mu o}$ coincided with the observed V_{max}.

Different observations were found, however, in the test units subjected to bi-directional displacement patterns (Table D.I). When the observed μ_o of a test column was more than 2, V_{max} was attained before cycling to this observed dependable displacement ductility capacity, and observed $V_{\mu o}$ was always less than observed V_{max} (Table F.VI). However, V_{max} was achieved at the observed dependable ductility capacity in test columns with flexural overstrength V^o_{if} greater than the shear strength provided before degradation, V_i, and when the observed μ_o was not more than 2 (Table F.VI). In these cases, the observed $V_{\mu o}$ again coincided with the observed V_{max}.

Based on these findings, two cases are considered. To determine the achievable strength of circular columns, in terms of the lateral force, $V_{\mu o}$, at dependable ductility capacity, μ_o, it is proposed that:

Case 1: When subjected to uni-directional 'u' type displacement patterns

$$V_{\mu o} = V_{max} \qquad \text{(F.22)}$$

where V_{max} is obtained from Eq. (F.21a).

Case 2: When subjected to bi-directional displacement patterns

i) When $V_i \leq V^o_{if}$

$$V_{\mu o} = V_{max} \qquad \text{(F.23a)}$$

ii) When $V_i > V^o_{if}$

$$V_{\mu o} = V_{so} + V_{co} \leq V_{max} \qquad \text{(F.23b)}$$

where V_{so} = achievable shear carried by spirals at μ_o, obtained from Eqs. (F.24 and F.26) in Section F.3.3.1.

V_{co} = achievable shear assigned to "concrete mechanism" at μ_o, obtained from Eqs. (F.27a to F.27b) in Section F.3.3.2.

V_{max} is obtained from Eq. (F.21a).

Eqs. (F.22.and F.23a) were based on experimental observations, while Eq. (F.23b) was based on the assumption that at dependable ductility capacity, μ_o, the shear force was carried by both spirals and "concrete mechanism". The estimations of V_{so} and V_{co} will be presented in the following sections. The evaluated $V_{\mu o}$ should not be taken any greater than the predicted maximum strength, V_{max}. This is why the "$\leq$" sign appears in Eq. (F.23b). That is, when the sum of V_{so} and V_{co} are greater than the calculated V_{max}, the $V_{\mu o}$ is assigned to be V_{max}.

F.3.3.1 Achievable shear carried by spirals at dependable ductility capacity

When the test specimens were displaced to the observed dependable displacement ductility capacity, μ_o (Table D.I), the inclinations of major diagonal cracks appeared to be much less than 45° (Figs. E.9 to E.11). Therefore, at this stage, it is more appropriate to calculate the shear carried by spirals using a variable-angle truss model.

In Section B.2.4.1, Eqs. (B.34b and B.34d), originally proposed by Ang to evaluate shear carried by spirals at higher ductility levels, were presented. These two equations were derived from the lower bound solution of limit analyses with a constant web effective strength factor, k_c, equal to 0.193 [F.4]. The k_c factor can be considered to allow for a "softening effect" that reduces the strength of concrete diagonal compression field from the standard strength of f'_c to $k_c(f'_c)$. It was reported in Section B.2.3 that the "softening factor", k_c decreased with an increase of the principal tensile strain. This softening effect is also thought to result from irregularities and misfits along crack interfaces during repeated opening and closure of multi-directional diagonal cracks. The value of k_c is thus a variable which depends on the strains of the longitudinal and transverse reinforcement, and shear distortion of a reinforced concrete member. As axial compression load improves stiffness, or reduces the extent of the lateral deformation of a column, it may increase the k_c factor. The shear resistances of test columns also varied with displacement histories (Section E.3.1). As a result, the concrete diagonal compression field may tend to be more "softened" when subjected to severe multi-directional displacement patterns. A smaller value of k_c factor will then be appropriate.

With all this information, it is proposed that the achievable shear carried by spirals, V_{so}, at μ_o, is expressed by Eqs. (F.24a to F.24c), which takes the form of Eqs. (B.34b and B.34d).

$$V_{so} = 0.5\ k\ \pi\ A_{sp}\ f_{yt}\ d_s/s \qquad \text{(F.24a)}$$

where $k = \cot\theta = \sqrt{(k_c - \Omega)/\Omega} \leq L/D$, with $45° \geq \theta \geq 25°$ (F.24b)

θ = inclination of the potential shear failure plane, measured from the longitudinal axis of the column

$\Omega = \rho_s\ f_{yt}/(2\ f'_c)$ (F.24c)

k_c = web effective strength factor, determined by Eqs. (F.26a to F.26c)

In order to select suitable values of k_c for Eq. (F.24b), the calculated k_c factors of the current test columns, with the observed $\mu_o > 2$, were studied. This can be done by re-arranging Eq. (F.24b) so that k_c is expressed as:

$$k_c = \Omega/\tan^2\theta + \Omega \qquad \text{(F.25)}$$

For each test column listed in Table F.IX, the observed average angle of inclined cracks (Figs. E.10 and E.11), being indicative of the inclination of diagonal compression, and the value of Ω, were substituted into Eq. (F.25). The calculated k_c factors were reported in column 7 of Table F.IX.

It seems that the most influential parameter to determine the values of k_c is the severity of displacement pattern. With the exception of test Unit 15, larger values of k_c were obtained for test units subjected to less severe uni-directional 'u' type displacement patterns, whereas smaller values of k_c were obtained for those subjected to more severe bi-directional 's' type displacement patterns. The calculated k_c factor of Unit 15 was too large and was inconsistent with the general findings. This may be due to either low concrete strength (f'_c = 27 MPa) of the column which causes an increase of Ω, or an inappropriate estimation of the angle θ. Regarding the first possibility, Ang [F.4] found that k_c was 0.193 for his test Unit 9 with f'_c = 29.9 MPa, and subjected to uni-directional 'u' type displacement patterns. On the other hand, when the estimated angle θ was revised, say 42°, the calculated k_c became 0.176, which more or less agreed with the expectation. Since it was very difficult to measure the inclination of major cracks under the bi-directional 's' type displacement patterns, a mis-judgement of the angle θ of Unit 15 was the likely cause of the discrepancy.

Axial compression load intensity appeared to improve the k_c factor but only to a small extent. It should be noted that accurate values of k_c cannot be expected since precise measurements of the inclination of diagonal

compression field were not obtainable. Hence, a complicated equation for k_c is not warranted. In order not to overestimate the achievable shear carried by spirals, V_{so}, at the dependable ductility capacity, μ_o, the recommended estimate of k_c is given for the following displacement patterns:

a) For uni-directional 'u' type displacement pattern

$$k_c = 0.193 \qquad \text{(F.26a)}$$

b) For bi-directional 'b' type displacement pattern

$$k_c = 0.165 \qquad \text{(F.26b)}$$

c) For bi-directional 's' type displacement pattern

$$k_c = 0.149 \qquad \text{(F.26c)}$$

Table F.IX : Calculated web effective strength factors k_c of test columns

1	2	3	4	5	6	7
Unit	disp. pattern	$\frac{P_1}{f'_c A_g}$	θ (deg) at μ_o		Ω	k_c
1	u	0.19	30	6	0.0572	0.229
3	u	0.39	35	6	0.0589	0.179
6	b	0.00	30	4	0.0418	0.167
8	b	0.19	32	4	0.0463	0.165
9	b	0.39	35	4	0.0487	0.173
10	b	0.39	35	5	0.0543	0.165
11	s	0.00	32	3	0.0418	0.149
13	s	0.19	32	4	0.0463	0.165
14	s	0.19	37	5	0.0572	0.158
15	s	0.39	38	6	0.0788	0.208

4: Observed average inclination of major diagonal cracks
6: Ω obtained from Eq. (F.24c)
7: k_c obtained from Eq. (F.25)

F.3.3.2 Achievable shear to be assigned to "concrete mechanisms" at dependable ductility capacity

The characteristics of shear carried by "concrete mechanism" have been discussed in Section E.6. Before reaching the observed dependable displacement ductility capacity, some deterioration of shear carried by "concrete mechanism" has already occurred. The rate of this deterioration appeared to be higher for test columns with low axial compression, or those subjected to more severe displacement patterns. Since test results revealed that under uni-directional 'u' type displacement patterns, the observed maximum strength, V_{max}, generally coincided with the observed achieved strength, $V_{\mu o}$ (Section F.3.3), an expression for achievable shear assigned to "concrete mechanism", V_{co}, at dependable ductility capacity is not required for this case. Therefore, V_{co} was quantified only for test columns subjected to bi-directional displacement patterns.

An estimation of V_{co} could be made by re-arranging Eq. (F.23b), i.e., $V_{co} = V_{\mu o} - V_{so}$, where $V_{\mu o}$ was an experimentally observed data, and V_{so} was determined by Eqs. (F.24 and F.26) for each test column under consideration. Subsequently, V_{co} was divided by the corresponding effective shear area, $A_e = (\pi d_s^2)/4$, and expressed as stress.

v_{co} = achievable shear stress assigned to "concrete mechanism" at μ_o

$$= V_{co}/A_e \qquad \text{(F.27a)}$$

Fig. F.5 shows the relation between $v_{co}/\sqrt{f'_c}$ and axial compression intensity, $P_1/(f'_cA_g)$, of test units with $\mu_o > 2$. Test units with $\mu_o \leq 2$ are not included here because their values of $V_{\mu o}$ can be determined by Eq. (F.23a) where the calculation of V_{so} is not involved.

As Fig. F.5 shows $v_{co}/\sqrt{f'_c}$ tended to zero at $P_1/(f'_cA_g) = 0$, and it increased with applied axial compression. At $P_1/(f'_cA_g) > 0.19$, the rate of increase of $v_{co}/\sqrt{f'_c}$ reduced. Different bi-directional displacement patterns ('b' type and 's' type) had a similar effect on $v_{co}/\sqrt{f'_c}$. By regression analysis, it is suggested that under bi-directional 'b' type and 's' type displacement patterns, $v_{co}/\sqrt{f'_c}$ can be determined by Eq. (F.27b).

$$\frac{v_{co}}{\sqrt{f'_c}} = 0.05 + 1.1\,\frac{P_1}{f'_cA_g} - 0.8\left(\frac{P_1}{f'_cA_g}\right)^2 \qquad \text{(F.27b)}$$

Comparison of the predicted achievable shear strengths, $V_{\mu o}$, to the corresponding experimentally observed values are shown in columns 17 and 19 of Tables F.V and F.VI respectively. The predicted values are in agreement with the experimental findings.

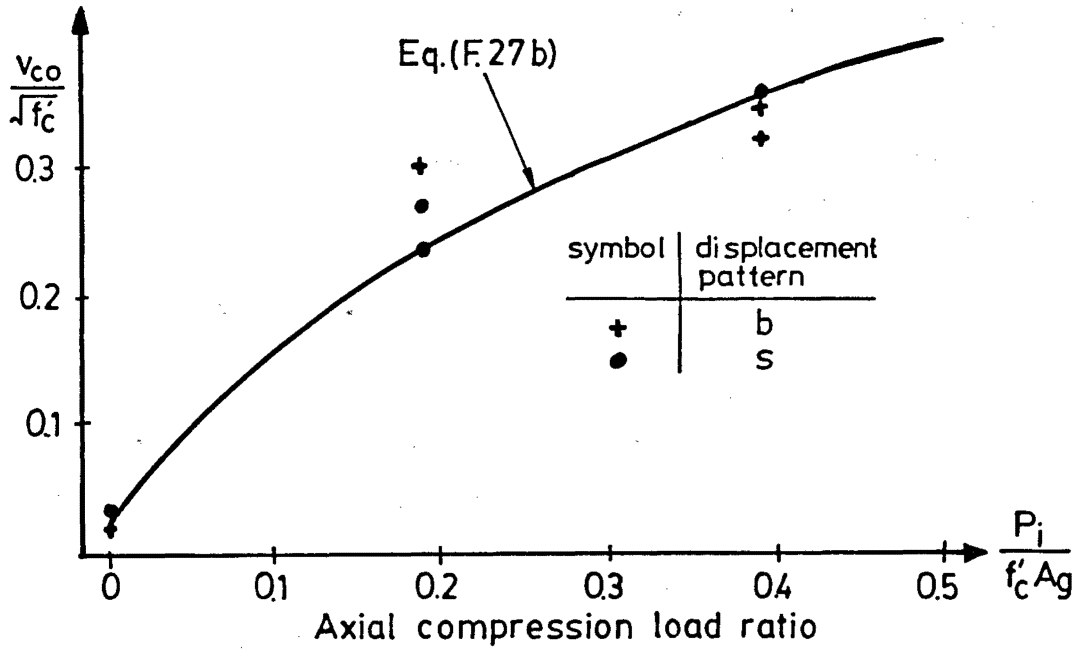

Fig. F.5 : Variation of achievable shear stress, v_{co}, assigned to "concrete mechanism" at dependable ductility capacity, with axial compression load ratio

F.3.4 Dependable Displacement Ductility capacity, μ_o

From the experimental observations of the performance of test columns, summarized in Tables F.V and F.VI, it appeared that the major parameters affecting dependable displacement ductility capacity, μ_o, were available shear strengths, maximum strength developed, types of displacement patterns, and axial compression load intensity. By comparing the initial shear strength provided before degradation, V_i which was obtained from Eqs. (B.33a to B.33e) with $A_e = (\pi\ d_s^2)/4$, and the flexural strengths of test units, the following experimental evidence was obtained:

a) When the initial shear strength provided before degradation, V_i was less than the corresponding ideal flexural strength, V_{if} (see Section C.3.1 for the definition of V_{if}), the observed dependable ductility capacity, μ_o, was generally less than 1.5.

b) When the calculated value of V_i was more than the corresponding V_{if}, but was less than the flexural overstrength, V^o_{if} which was defined by Eq. (F.21b), the observed μ_o was equal to 2.

c) When the calculated value of V_i was more than the corresponding V^o_{if}, the observed μ_o was greater than 2.

Based on this information, empirical expressions to predict μ_o of test columns subjected to the standard displacement histories, namely uni-directional 'u' type displacement patterns, bi-directional 'b' type and 's' type displacement patterns, are formulated as follows:

Case 1 : When $V_i < V_{if}$ then $\mu_o \leq 1$ (F.28a)

Case 2 : When $V_{if} \leq V_i \leq V^o_{if}$ then $\mu_o = 2$ (F.28b)

Case 3 : When $V_i > V^o_{if}$ then μ_o may be calculated as follows:

From the statistical evaluation of predicted strength parameters and the observed performances of test columns, the dependable displacement ductility capacity, μ_o, was found to be best expressed by a function of three parameters. They were: (a) the axial compression load ratio, (b) the difference between the predicted values of V_i and $V_{\mu o}$, and (c) the difference between the predicted values of V_{max} and V_{so}. It should be noted that the

influence of spiral reinforcement content, loading histories, and aspect ratio on μ_o has been taken into account during the evaluation of shear strengths or flexural strengths of the test columns. By regression analysis, μ_o was found to be:

$$\mu_o = 4.67 + 1.12 \frac{v_i - v_{\mu o}}{\sqrt{f'_c}} - 14.30 \frac{v_{max}/r_d - v_{so}}{\sqrt{f'_c}} + 21.65 \frac{P_i}{f'_c A_g} \quad \text{(F.28c)}$$

$$\geq 2$$

where $v_i = V_i / A_e$

$v_{\mu o} = V_{\mu o} / A_e$

$v_{max} = V_{max} / A_e$

$v_{so} = V_{so} / A_e$

r_d = strength reduction factor account for loading history, obtained from Eqs. (F.20a to F.20c)

Comparisons of the predicted dependable ductility capacities with those observed are listed in columns 11 and 12 of Table F.V, and columns 13 and 14 of Table F.VI. The prediction appears to be sufficiently accurate for design purposes. It should be noted that the uncertainty in the estimation of ductility demand μ for any given site is much greater than that relevant to the above prediction of dependable ductility capacity.

The use of Eqs. (F.28) was applied to study the influence of the main parameters, namely, the volumetric spiral steel content, ρ_s, the axial compression load ratio, $P_i/(f'_c A_g)$, and the displacement pattern on the dependable displacement ductility capacity, μ_o, of circular cantilever columns with an aspect ratio of 2.

In this analytical investigation, f'_c = 38 MPa, f_{yl} = 475 MPa, and f_{yt} = 320 MPa were assumed. The overall diameter of columns, D, was 400 mm, and the diameter of concrete core measured to the centres of spirals, d_s, was 362 mm. The longitudinal reinforcement content, ρ_l, was assumed to be 3.2%.

The results of the analyses are shown in Figs. F.6 and F.7. For comparison purposes, the volumetric spiral steel contents for confinement required by NZS 3101 [F.9], ρ_{sNZ}, calculated by Eq. (B.35d) with f'_c = 38 MPa and f_{yt} = 320 MPa, at different axial compression load ratios were shown in Fig. F.6.

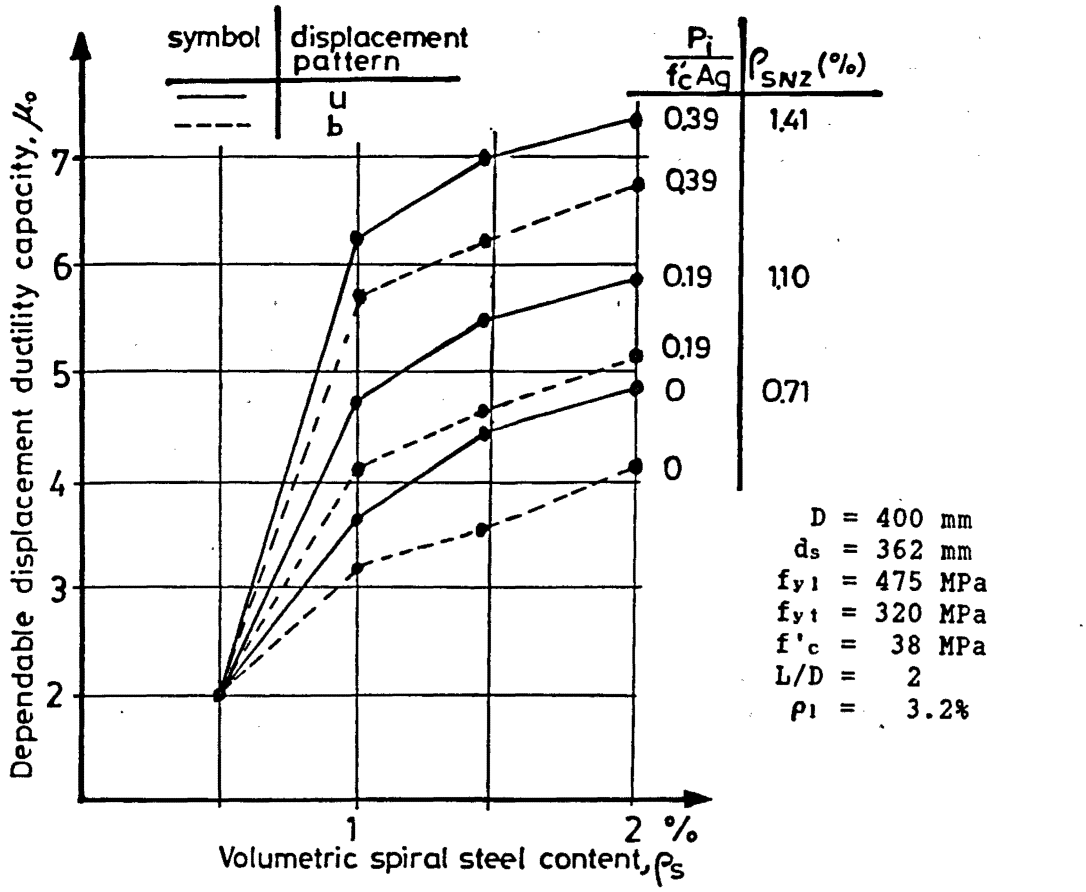

F.6 : Dependable displacement ductility capacity as a function of volumetric spiral steel content and axial compression load ratio

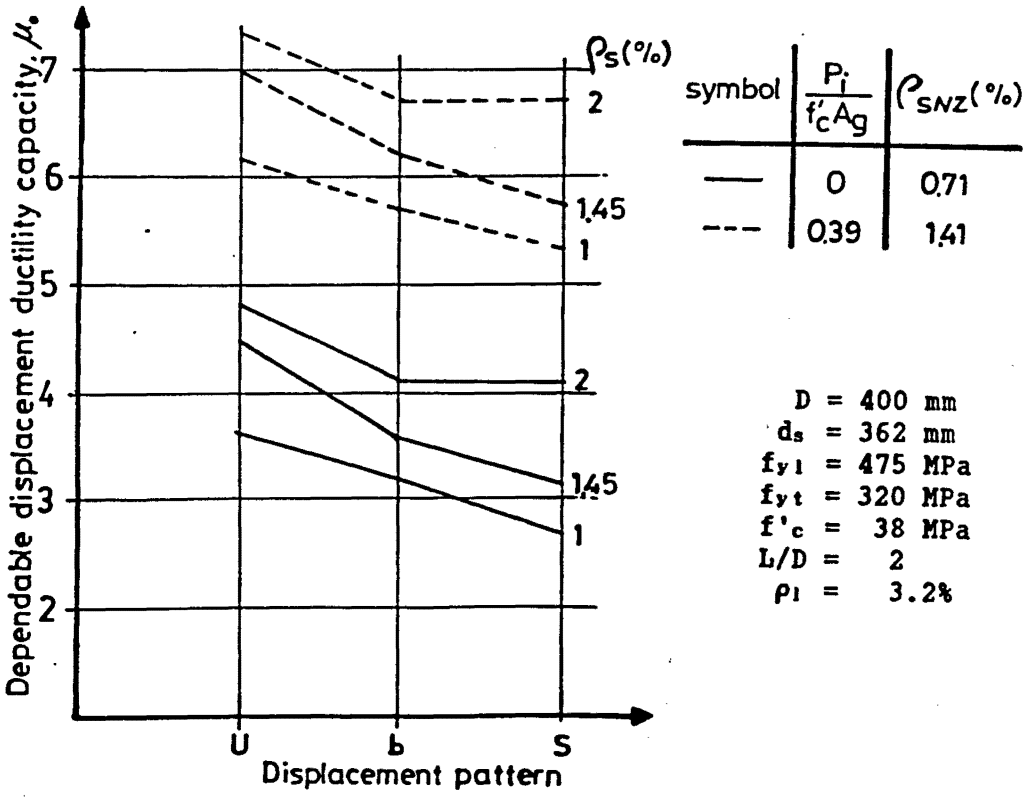

Fig. 7: Dependable displacement ductility capacity as a function of displacement pattern

As is evident from Figs. F.6 and F.7, the dependable displacement ductility capacity, μ_o, distinctively improves with increasing (a) amount of spiral steel provided, and (b) axial compression load ratio. The rate of improving μ_o tends to decrease at excessive provision of spiral reinforcement.

The dependable displacement ductility capacity, μ_o, reduces with increasing severity of displacement pattern. However, using the same reinforcement details and axial compression load ratio, the difference between μ_o attained using the least severe 'u' type displacement pattern and that using the most severe 's' type displacement pattern, is generally less than one.

At higher axial compression load intensity, such as $P_1/(f'_c A_g) > 0.4$, or at aspect ratio greater than 2, the design of spiral steel content is likely to be controlled by the requirements for confinement.

The current New Zealand seismic design provisions for confinement [F.9] are intended to provide for "adequate ductility" of the plastic hinges, which corresponds to curvature ductility factors of typically 15 to 20. Recent researches [F.10, F.11] reported that the New Zealand Code requirements for transverse reinforcement for concrete confinement were conservative for columns with low axial load levels but less conservative for heavily loaded columns. An improved design procedure for determining the amount of confining steel, as a function of the required curvature ductility factor, was proposed by Zahn et. al. [F.11].

In the present test series, the performance of test columns depended on provisions for shear rather than those for concrete confinement. The requirements for the later provision will be critical for the designs of flexural dominated columns. In design practice, the amount of spiral steel provided for columns should satisfy the seismic shear design proposed in this report, and those of the updated design procedure for concrete confinement.

F.3.5 A Prediction on Performance of Unit 16

Unit 16 was the only column of the present test series subjected to irregular bi-directional 'r' type displacement history (Section C.3.1). The experimental observation of this unit is fully documented in Section D.6. It was discussed in Section E.3.1 that the observed performance of Unit 16 was better than its companion unit subjected to 'b' type displacement

history. In this section, the performance of Unit 16 is assessed with the use of the proposed equations for 'u' type and 'b' type displacement patterns. The results are listed in Tables F.V and F.VI respectively.

With regards to the maximum strength of Unit 16, it appears that the expressions for 'u' type displacement pattern (Eqs. (F.21, F.22, and F.28)) give good predictions for both strength and the ductility level at which the maximum strength took place.

The specimen performed exceptionally well during the first and second displacement paths of the displacement history (Fig. C.7). In the first displacement path, the unit developed $1.28V_{if}$ at ductility level of 5, which was only slightly lower than the previously achieved maximum strength ($1.30V_{if}$) at ductility level of 4. In the second displacement path (four cycles to ductility level of 4), the unit still developed a strength of $0.89V_{if}$ at the last displacement peak. This suggests that the dependable ductility capacity, μ_o, of Unit 16 would not be less than 4, but it is not likely to exceed 5. Adequate prediction for μ_o can be obtained using the relevant equations for 'u' type displacement pattern. Accordingly, the predicted μ_o is 4.6. Prediction using equations for 'b' type displacement pattern with μ_o = 3.9 was found to be overly conservative.

The excellent performance of Unit 16 may be explained by comparing the cumulative ductility factors, $\Sigma\mu$, of Unit 16 with those of its companion unit (Unit 8) subjected to 'b' type displacement pattern. The cumulative ductility factor is usually defined as the sum of all previous displacement ductility levels at displacement peaks in each direction achieved up to the stage under consideration. For example, under uni-directional cyclic loading, a structure subjected to 4 cycles of loading to displacement ductility factors of 4 in each direction would undergo a $\Sigma\mu$ = 32.

The cumulative ductility factors of Unit 16 were found to be 27 and 59 after the completion of displacement paths I and II respectively. Similarly, the cumulative ductility factors of Unit 8 were 30 and 86 after the completion of two load cycles to μ of 2 and 4 respectively. Larger values of $\Sigma\mu$ imply more damage to the column concerned. As 'r' type and 'b' type displacements are bi-directional in nature, the values of $\Sigma\mu$ obtained from these displacement patterns are comparable to each other. Thus, it was not surprising to find that the performance of Unit 16, which has undergone the subsequent displacement path III, was much better than that of Unit 8 which was subjected to further load cycling to displacement ductility level of 5.

F.4 SUMMARY OF DESIGN RECOMMENDATIONS

In this section, the design recommendations on the evaluation of (a) elastic deformations in reinforced concrete circular cantilever columns (Section F.2), and (b) the amount of spiral steel reinforcement using seismic shear design requirements for reinforced concrete circular columns (Section F.3), are summarized in form of flow charts for design office use.

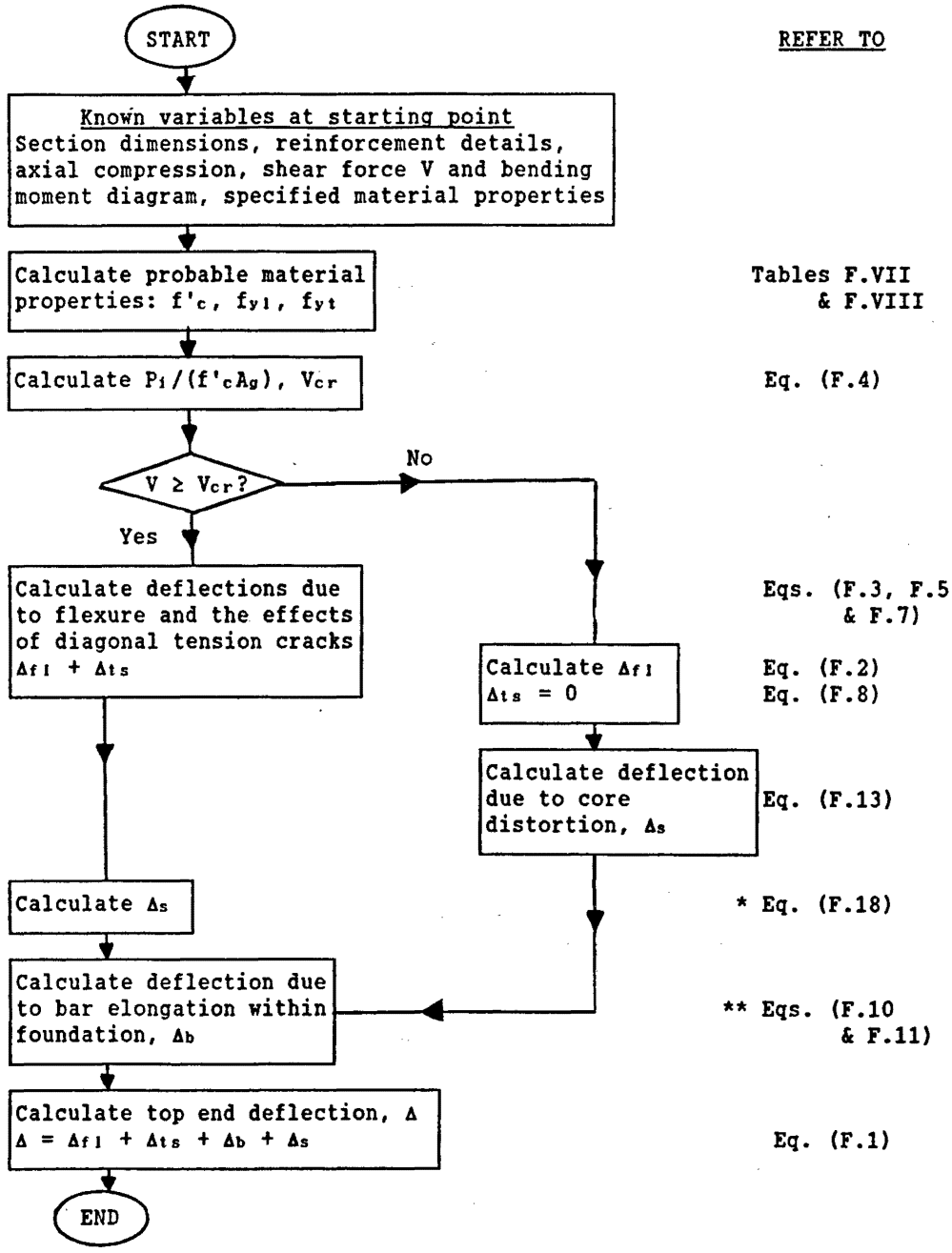

* Applicable only when yielding of spiral steel does not occur.
** If the conditions of anchorage bond transfer are considerably different from those of the present test series, Eq. (F.10) must be modified.

Fig. 8: Flow chart for evaluation of elastic deformations in reinforced concrete circular columns

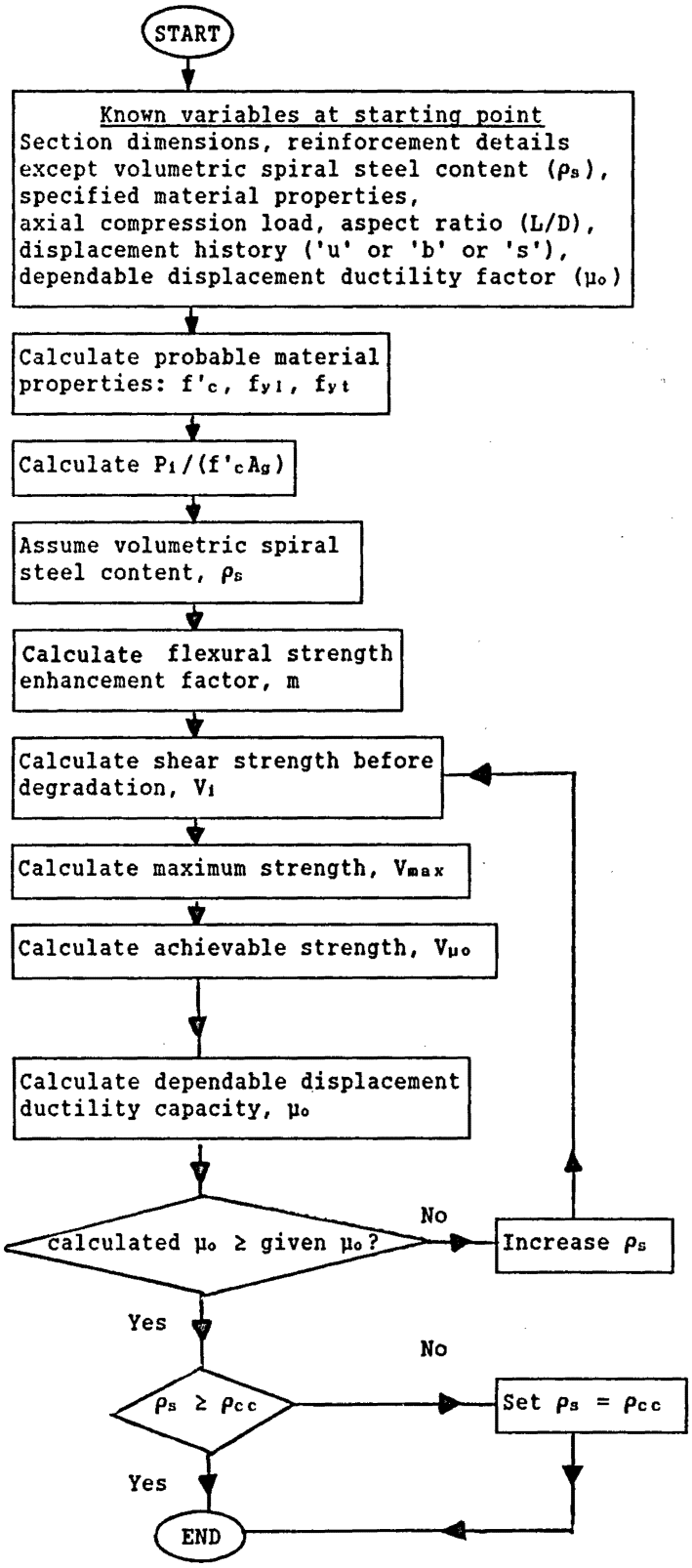

* $A_e = (\pi d_s^2)/4$

** check for volumetric spiral steel content for concrete confinement, ρ_{cc}, based on the updated concrete confinement requirements (see Section F.3.4)

Fig. F.9 Flow chart for evaluation of the amount of spiral steel content using the proposed seismic shear design for reinforced concrete circular columns

CHAPTER G
CONCLUSIONS

G.1 AIMS AND EXTENT OF RESEARCH

The work of numerous analytical and experimental researchers on shear behaviour of reinforced concrete members has been reported. In spite of the identification of the influence on shear performance of key parameters, and the establishment of various shear resisting mechanisms, such understanding has not reached the stage of rational quantitative analysis, particularly, with respect to seismic shear performance of columns with spiral or circular hoop reinforcement.

Experimental research on shear performance of reinforced concrete circular columns subjected to uni-directional cyclic loading histories has been carried out in the Department of Civil Engineering of University of Canterbury since 1978 [G.1, G.2]. This project is the continuation of previous investigations. Sixteen reinforced concrete circular cantilever columns of 400 mm diameter, were constructed and tested under quasi-static multi-directional loading histories. The aspect ratio and longitudinal reinforcement content of test specimens were 2 and 3.2% respectively. The main parameters studied were axial compression load intensity, $P_l/(f'_c A_g)$, ($P_l/f'_c A_g$ = 0, 0.19, 0.39), volumetric spiral steel content, ρ_s, (ρ_s = 0.39% to 2.46%), and displacement history. In this project, four types of displacement patterns, namely 'u', 'b', 's' and 'r', were used. The first one is a uni-directional cyclic displacement pattern which was used in previous research [G.2], whereas the others are bi-directional cyclic displacement patterns. Bi-directional 'r' type displacement pattern, which was derived from dynamic analysis of reinforced concrete circular pier systems subjected to two dimensional earthquake motions, is considered to be a more realistic displacement history that a column would encounter during severe seismic attacks.

In this report, the performance of test columns was discussed and compared. Due to the complexity of the shear behaviour especially after extensive multi-directional cracking, and limited data for the formulation of reliable constitutive laws for concrete subjected to multi-directional cyclic inelastic displacements, an analytical model to simulate the shear performance of test columns could not be developed. Instead, based on statistical evaluation of measured performance of test columns from this project and from the previous research reported by Ang [G.2], a proposal for seismic shear design procedure for reinforced concrete circular columns, taking into account displacement histories, was formulated.

G.2 OVERALL RESPONSE OF TEST COLUMNS

It was evident that the stiffness and hence lateral deformation of test columns depended mainly on axial compression load intensity. The stiffness increased with applied axial compression. Shear deformations represented a considerable fraction of total deflection even at small displacement levels. An increase of spiral steel content reduced shear deformations but only after diagonal cracking. When significant strength degradation occurred, the contribution of shear deformations to total deflection increased considerably. Severity of displacement patterns did not appear to affect the components of deflections.

Within a displacement path, the shear resistances at displacement peaks were of similar magnitude. However, under regular bi-directional displacement patterns 's' and 'b', strengths attained in the first displacement path were higher than those in the second displacement path of the same cycle. Strength loss also took place during repeated cycles to the same ductility level. An increase of axial compression reduced such strength loss. The maximum measured strength appeared to develop at larger ductilities, as axial compression intensity increased. Unless premature shear failure occurred, the ratio of the maximum measured strength of a test column to its ideal flexural strength, computed by the ACI method, was always greater than one. This strength ratio tended to increase with increasing axial compression load intensity, and decreasing severity of displacement patterns. For test units which failed in moderately ductile or ductile manner, the amount of spiral steel content appeared to have no influence on this strength ratio. The drift index at the occurrence of maximum measured strengths varied from 1.5% to 2.5%.

The onset of the strength degradation, as evidenced by strength envelope curves, was delayed as the spiral steel content increased or when the severity of displacement patterns was reduced. However, axial compression increased the rate of strength decay.

The dependable displacement ductility capacity, μ_o, is the highest displacement ductility level at which the peak strength is not less than 80% of the column's ideal flexural strength. The values of μ_o of test columns was distinctly improved with an increase of spiral steel content. Axial compression load also tended to increase the μ_o. On the other hand, severity of regular displacement histories ('u', 'b', 's') appeared to have only a minor adverse effect on the dependable ductility capacity. For

instance, the μ_o of a test specimen subjected to the least severe 'u' type displacement pattern, would not be significantly larger than that of its companion specimen subjected to the most severe 's' type displacement pattern. The difference in the magnitude of the ductility would be typically less than one. With regard to the performance of test columns, 'r' type displacement pattern appeared to be less severe than 'b' type displacement patterns.

As features of failure were concerned, a sudden collapse did not occur for test columns with no axial compression. All specimens subjected to bi-directional 's' type displacement patterns, exhibited large twist at failure. Other features of failure which were common for test units with axial compression and subjected to either 'u' type or 'b' type displacement pattern, were spiral fracture and longitudinal bar buckling. None of the aforesaid features of failure was found in Unit 16 which was the only test unit subjected to bi-directional 'r' type displacement pattern.

Energy dissipation performance of test columns was compared using the relative energy dissipation index, E/E_I (Section E.9). At high ductility levels, E/E_I values noticeably decreased for columns with lower spiral steel content. This was a result of degradation of strength and pinching of hysteresis loops due to shear effects. An increase in spiral steel content improved the energy dissipation performance at all stages of loading history. The influence of axial compression load intensity on the maximum value of E/E_I was not significant. Due to the enhancement of strength with axial compression, there was a trend whereby the E/E_I values for columns with axial compression improved slightly with progressively increasing ductility. Before any significant degradation of strength , the energy dissipation performance was the best with 's' type displacement pattern. At higher ductility levels, good energy dissipation was maintained for columns subjected to the least destructive uni-directional 'u' type displacement.

From the analyses of spiral strain data and crack patterns, the roles of spiral reinforcement were identified. Spiral reinforcement provides some confinement to the core concrete at zero shear condition, irrespective of the magnitude of axial compression. With the application of lateral force, shear transfer by "truss mechanism" develops. The spiral force components in the direction of the external shear and the bond forces along the longitudinal steel bars create a diagonal compression field to resist shear. In the flexural compression zone, spirals will also act as confining reinforcement. Thus, a concrete element in the flexural compression zone is longitudinally subjected to flexural compression, and is also confined by

spirals and diagonal compression field in the transverse direction. Since the forces in diagonal compression field depend on the spiral steel content, spirals will play an important role in confinement mechanisms of the flexural compression zone, even if they perform primarily as shear reinforcement.

The shear carried by spirals, V_s, was evaluated by summing up across the inclined shear failure plane the components of spiral forces in the direction of external force. As expected, this shear V_s was found to be the main contribution to shear strength at higher ductility levels. The difference between the external lateral force, V, and V_s, is regarded as shear carried by "concrete mechanism", V_c. At higher ductility levels, V_c would be small enough to be ignored (Section E.6).

G.3 DESIGN RECOMMENDATIONS

Design recommendations on two topics: (1) an approach to evaluate elastic deformations in reinforced concrete circular cantilever columns, and (2) a proposal of seismic shear design for reinforced concrete circular columns, were derived in Chapter F. Agreement with experimental values was achieved. These recommendations were further summarized in the form of flow charts (Section F.4) ready for design office use.

The first design recommendation offers a simple approach to evaluate different components of the elastic deformations so that the contribution of each component to the total deformation can be assessed. Accordingly, the stiffness of a circular column before the onset of yielding can be estimated with a reasonably degree of accuracy.

The second design recommendation provides information on the flexural strength enhancement factor, the maximum strength, the dependable displacement ductility capacity, and the achievable strength at the dependable displacement ductility capacity, of a detailed circular column subjected to a standard displacement pattern ('u', 'b', 's'). Conversely, the amount of spiral reinforcement required to resist the shear force can be estimated by this design procedure for the expected dependable displacement ductility capacity and the displacement pattern.

Judgement is required with respect to: (a) the standard displacement pattern ('u', 'b', 's') which should be chosen to represent severe seismic attacks, and (b) the value of the dependable displacement ductility capacity to which a column should be relied on to ensure a high chance of survival under severe seismic attacks.

From the parametric studies of the empirical equations for dependable displacement ductility capacity (Section F.3.4), it appeared that the μ_o was primarily a function of volumetric spiral steel content and axial compression load ratio. The chosen displacement patterns ('u', 'b', 's') with different degrees of severity did not appear to cause significant variation of μ_o. Regarding bi-directional displacement patterns, current tests consistently revealed that the overall responses of circular columns tested under more severe and complicated 's' type displacement histories, were not much different from those tested under less severe and relatively simple 'b' type displacement histories. It should be appreciated that a lot of time and effort were required for a test with 's' type displacement pattern. It appears to be unnecessary to design circular columns for, or carry out further tests with, 's' type loading histories.

Unit 16 was the only test column subjected to bi-directional 'r' type displacement pattern which was derived from dynamic time - history analyses of pier systems under severe earthquake attacks. Adequate prediction on the performance of Unit 16 using the relevant equations for 'u' type displacement pattern, was obtained. Prediction using equations for 'b' type displacement pattern was considered to be conservative. However, definite conclusions cannot be made from just one test result. More similar tests would have been desirable. Nevertheless, the chosen 'r' type pattern, i.e. a series of sequential patterns, was considered to be severe enough to test the adequacy of this design procedure.

Since an infinite number of displacement histories, similar to the chosen 'r' type, can be generated from different earthquake records, it will be impossible to verify reliably whether an appropriately designed column can survive any of these random type displacement histories. However, using the proposed shear design procedure, the response of a column under a standard displacement history (uni-directional 'u' or bi-directional 'b') can be predicted. This prediction indicates the expected dependable performance of the column under severe seismic attacks.

It should be appreciated that a chosen displacement history should be consistent with the boundary conditions of the column concerned. For example, when the translational movements of a bridge deck are restrained in its longitudinal direction by an abutment, columns supporting this bridge deck would be required to resist seismic attacks only in the transverse direction. Hence, 'u' type displacement history should be used. Another

example is when the foundation of bridge columns is capable to resist moments in one direction only because of the linear arrangement of piles. Then, the potential plastic hinge of the column at the foundation would be required to be designed for 'u' type displacement history. In building structures, the columns are often designed to resist multi-directional earthquake ground motions. In this situation, 'b' type displacement history would be desirable.

According to NZS 4203 [G.3], a structure defined as fully ductile should undergo four cycles of loading to a displacement ductility factor, μ, of 4 in each direction, before strength reduction at maximum displacement is reduced by more than 20%. This implies a cumulative ductility demand, $\Sigma\mu$, equal to 32. However, a cumulative ductility factor should be used with caution because the application of a larger number of load cycles with ductilities less than that required may well result in a large number for the cumulative ductility. Yet, it may not assure that two or three cycles at the required ductility level could be satisfactorily sustained.

Since 1984, a range of displacement ductilities with the maximum of $\mu = 6$ have been introduced for various types of "fully" ductile structures. Also, fully ductile bridge piers [G.4] are designed to ductilities up to 6. Therefore, the performance criteria suggested by NZS 4203 should be interpreted as $\Sigma\mu$ equal to 48. It was evident that [G.4] this fully ductile performance could be satisfactorily sustained for slender columns, provided that adequate confining steel was present in the plastic hinge. For squat columns, such as the current test units, ductilities up to 6 could be achieved at the expense of very large amounts of transverse reinforcement required to resist shear. Furthermore, columns designed for such large ductility are susceptible to permanent damage already during earthquakes of small intensity. From the practical point of view, it is suggested that the upper design limit of dependable displacement ductility, μ_o, for columns with low aspect ratio (such as $L/D < 3$) should be restricted to 4. At this upper limit, the $\Sigma\mu > 80$ should be developed when a column is designed for the regular 'u' or 'b' type displacement history (Section C.3.1).

G.4 RECOMMENDATIONS FOR FUTURE RESEARCH

The following list of further experimental and theoretical research on seismic shear behaviour of reinforced concrete columns is suggested:

G.4.1 Experimental Investigations

1. Displacement history

Quasi-static tests using regular uni-directional 'u' type and bi-directional 'b' type displacement patterns would provide most of information on seismic performance of reinforced concrete columns. A variety of random displacement patterns, derived from dynamic time-history analyses of pier systems subjected to multi-directional earthquake records (similar to 'r' type), should be used, if at all, for confirmation purposes.

2. Specimen Geometry

The present research is directed only towards circular columns with aspect ratio of 2. The investigation needs to be widened to include other aspect ratios and rectangular sections.

3. Axial load

This study concentrated on bridge piers for which an axial load intensity of $0.4f'_cA_g$ would be exceptional. To extend the applicability of these findings also to columns used in multistorey buildings, higher axial load intensities, such as $0.6f'_cA_g$, should be investigated. Moreover, possibly tension and variable axial load, simulating the effects of horizontal earthquake forces on twin-piers, should also be considered.

4. Reinforcement details

The amount of transverse reinforcement is the main parameter affecting the ductility of a concrete member. Although the influence of longitudinal reinforcement on shear performance is not as critical as transverse reinforcement, it is desirable to check for conditions with low longitudinal reinforcement content, such as half of the quantity of vertical steel used in the present test series, to see to what extent reduced shear would possibly improve the hysteretic performance of short columns.

5. Dynamic testing

Previous dynamic tests on single pier models, and twin-pier models [G.2] indicated an apparent difference in behaviour for columns which were subjected to varying axial load levels. A limited number of data-channels were used and this implied that the observation was only tentative. More testing is needed in this area.

G.4.2 Theoretical Investigations

With more experimental information obtained from future researches, the design recommendations proposed in this report can be verified, and modified to cope with columns of other cross-sectional shapes. In parallel, attempts should be made to formulate a rational analytical model to simulate the seismic shear behaviour of reinforced concrete columns.

REFERENCE

CHAPTER A

A.1 NZS 4203: 1984, "Code of Practice for General Structural Design and Design Loadings for Buildings", Standard Association of New Zealand, Wellington, 1984, 100 pp.

A.2 ANG, B.G., "Seismic Shear Strength of Circular Bridge Piers", Research Report 85-5, Department of Civil Engineering, University of Canterbury, New Zealand, Jul. 1985.

A.3 ANG, B.G., PRIESTLEY, M.J.N, and PAULAY, T.,"Seismic Shear Strength of Circular Concrete Columns", Structural Journal of ACI, Vol. 86 No. 1, Jan. 1989, pp. 45-59.

A.4 SOZEN, M.A. et al, "Engineering Report on the Caracas Earthquake of 29th July 1967", National Research Council, National Academy of Engineering, Washington, D.C., 1968, 84 pp.

A.5 SUZUKI, Z., "General Report on the Tokachi-Oki Earthquake of 1968", Tokyo, 1971, 754 pp.

A.6 JENNINGS, P.C., "Engineering Features of the San Fernando Earthquake", California Institute of Technology, Pasadena, California, 1971, 512 pp.

A.7 SHEPHERD, R., "The October 1, 1987 Whittier Narrows Earthquake", Bulletin of the New Zealand National Society for Earthquake Engineering, Vol. 20, No. 4, Dec., 1987, pp. 255-263.

A.8 MÖRSCH, E., "Die Schubfestigkeit des Betons", Beton und Eisen, Vol. 1, No. 5, Berlin, Oct. 1902, pp. 11-12.

A.9 MÖRSCH, E., "Versuche uber Schubspannungen in Betoneisentragern", Beton und Eisen, Vol. 2, No. 4, Berlin, Oct. 1903, pp. 269-274.

A.10 TALBOT, A.N., " Tests of Reinforced Concrete Beams: Resistance to Web Stresses. Series of 1907 and 1908", University of Illinois Engineering Experiment Station, Bulletin 29, Jan. 1909, 85 pp.

A.11 MÖRSCH, E., "Die Schubfestigkeit des Betons", Report of the 2nd International Congress for Bridge and Structural Engineering, Sept. 1928, Julius Springer, Wien, 1929, pp. 423-451, Discussion pp. 451-461.

A.12 "ACI Standard, 501-36T. Building Regulations for Reinforced Concrete", ACI Journal, Mar.-Apr. 1936, Proceedings, Vol. 32, pp. 407-444.

A.13 MÖRSCH, E., "Der Eisenbetonbau, I. Band, 2. Halfte", 6 Edition, Konrad Wittwer, Stuttgart, Apr. 1929, 541 pp.

A.14 ACI-ASCE COMMITTEE 326, "Shear and Diagonal Tension", ACI Journal Vol. 59, Jan., Feb., Mar., 1962, pp. 1-30, 277-334, 352-396.

A.15 JOINT ASCE-ACI TASK COMMITTEE 426, "The Shear Strength of Reinforced Concrete Members", Journal of the Structural Division, ASCE, Vol. 99, No. ST6, Jun., 1973, pp. 1091-1187.

A.16 BRESLER, B., "Behaviour of Structural Elements, A Review", Proceedings of the Disaster Mitigation Workshop, University of California, Aug., 1972.

A.17 YAMADA, M., and FURUI, S., "Shear Resistance and Explosive Cleavage Failure of Reinforced Concrete Members Subjected to Axial Load", Final Report, Eighth Congress of International Association for Bridge and Structural Engineering, New York, 1968, pp. 1091-1102.

A.18 HIRSOAWA, M., and GOTO, T., "Strength and Ductility of Reinforced Concrete Members Subjected to Axial Load, Part 1 and 2", Summaries of Technical Papers of Annual Meeting, AIJ, Nov., 1971. pp. 817-820.

A.19 BROWN, R.H., and JIRSA, J.O., "Reinforced Concrete Beams under Load Reversals", ACI Journal, Vol. 68, May 1971, pp. 380-390.

A.20 ACI COMMITTEE 318, "Building Code Requirements for Reinforced Concrete ACI 318-63", American Concrete Institute, Detroit, 1963.

A.21 WIGHT, J.K., and SOZEN, M.A., "Strength Decay of R.C. Columns Under Shear Reversals", Journal of the Structural Division, ASCE, Vol. 101, No. ST5, May 1975, pp. 1053-1065.

A.22 ACI COMMITTEE 318, "Building Code Requirements for Reinforced Concrete ACI 318-71", American Concrete Institute, Detroit, 1971.

A.23 GOSAIN, N.K., BROWN, R.H., and JIRSA, J.O., "Shear Requirements for Load Reversals on Reinforced Concrete Members", Journal of the Structural Division, ASCE, Vol. 103, No. ST7, Jul. 1977, pp. 1461-1476.

A.24 HWANG, T.H., and SCRIBNER, C.F., "R.C. Member Cyclic Response During Various Loadings", Journal of Structural Division, ASCE, Vol. 110, No. 3, Mar. 1984, pp. 477-489.

A.25 ATALAY, M.B., and PENZIEN, J., "The Seismic Behaviour of Critical Regions of Reinforced Concrete Components as Influenced by Moment, Shear and Axial Force", Report No. EERC 75-19, University of California, Berkeley, Dec. 1975, 226 pp.

A.26 SAATCIOGLU, M., "Reinforced Concrete Columns Subjected to Uniaxial and Biaxial Load Reversals", Eighth World conference on Earthquake Engineering, Vol. VI, San Francisco, 1984, pp. 585-592.

A.27 ACI COMMITTEE 318, "Building Code Requirements for Reinforced Concrete ACI 318-83", American Concrete Institute, Detroit, 1983.

A.28 ZAGAJASKI, S.W., BETERO, V.V., and BOUWKAMP, J.P., "Hysteretic Behaviour of Reinforced Concrete Columns Subjected to High Axial and Cyclic Shear Forces", Report No. EERC 78-5, University of California, Berkeley, Apr. 1978, 208 pp.

A.29 "Uniform Building Code", International Conference of Building Officials, Whittier, California, 1973.

A.30 MINAMI, K., KURAMOTO, H., and WAKABAYASHI, M., "Shear Design of Reinforced Concrete Members Based on the Plastic Theory", Pacific Concrete Conference, New Zealand, Nov. 1988, pp. 113-124.

A.31 WATANABE, F., and MUGURUMA, H., "Toward the Ductility Design of Concrete Members - Overview of Researches in Kyoto University -", Pacific Concrete Conference, New Zealand, Nov. 1988, pp. 89-100

A.32 PRIESTLEY, M.J.N., and PARK, R., "Strength and Ductility of Bridge Substructures", RRU Bulletin 71, National Roads Board, Wellington, New Zealand, 1984, 120 pp.

A.33 NZS 3101, "New Zealand Code of Practice for the Design of Concrete Structures", Standards Association of New Zealand, Wellington, 1982.

A.34 KARLSSON, B.I., AOYAMA, H., AND SOZEN, M.A., "Spirally Reinforced Concrete Columns Subjected to Loading Reversals Simulating Earthquake Effects", Proceedings of the Fifth World Conference on Earthquake Engineering, Vol. 1, Rome, Italy, 1973, pp. 803-806.

A.35 KHALIFA, J.U., and COLLINS, M.P., "Circular Reinforced Concrete Members Subjected to Shear", Publication No. 81-08, Department of Civil Engineering, University of Toronto, Dec. 1981, 103 pp.

A.36 ACI COMMITTEE 318, "Building Code Requirements for Reinforced Concrete ACI 318-77", American Concrete Institute, Detroit, 1977.

A.37 COLLINS, M.P., and MITCHELL, D., "Shear and Torsion Design of Prestressed and Non-Prestressed Concrete Beams", Journal of the Prestressed Concrete Institute, Vol. 25, No. 5, Sept. 1980, pp. 32-100

A.38 ARAKAWA, T., HE, M.X., ARAI, Y., and MIZOGUCHI, M., "Ultimate Shear Strength of Spirally-Confined Concrete Columns", Transactions of the Japan Concrete Institute, Vol. 9, 1987, pp. 305-312.

A.39 SHIBATA, T., "Ultimate Strength Equations of Reinforced Concrete Members at Brittle Failure", Concrete Journal of JCI, Vol. 18, No. 1, 1980, pp. 26-37.

A.40 POTANGEROA, P.T., PRIESTLEY, M.J.N., and PARK, R., "Ductility of Spirally Reinforced Concrete Columns Under Seismic Loading", Report 79-8, Department of Civil Engineering, University of Canterbury, Feb. 1979, 116 pp.

A.41 "Draft Code of Practice for the Design of Concrete Structures", DZ 3101: Part 1, Standards Association of New Zealand, Wellington, 1978.

A.42 OTANI, S., CHEUNG, V.W.T., and LAI, S.S., "Reinforced Concrete Columns Subjected to Biaxial Lateral Load Reversals", Proceedings of the Seventh World Conference on Earthquake Engineering, Vol. 6, Istanbul, Turkey, 1980, pp. 525-532.

A.43 MARUYAMA, K., and JIRSA, J.O., "Shear Behaviour of Reinforced Concrete Members Under Bi-directional Reversal Lateral Loading", CESRL Report No. 79-1, Department of Civil Engineering, University of Texas, Austin, Aug. 1979, 161 pp.

A.44 RAMIREZ, H., and JIRSA, J.O., "Effects of Axial Load on Shear Behaviour of Short Reinforced Concrete Columns Under Cyclic Lateral Deformations", PMFSEL Report No. 80-1, Department of Civil Engineering, University of Texas, Austin, Jun. 1980, 162 pp.

A.45 WOODWARD, K.A., and JIRSA, J.O., "Behaviour Classification of Short Reinforced Concrete Columns Subjected to Cyclic Deformations", PMFSEL Report No. 80-2, Department of Civil Engineering, University of Texas, Austin, Jul. 1980, 330 pp.

CHAPTER B

B.1 ANG, B.G., "Seismic Shear Strength of Circular Bridge Piers", Ph.D. Report, Department of Civil Engineering, University of Canterbury, Christchurch, July 1985, 407 pp.

B.2 MARUYAMA, K., and JIRSA, J.O., "Shear Behaviour of Reinforced Concrete Members Under Bidirectional Reversed Lateral Loading", CESRL Report No. 79-1, Department of Civil Engineering, University of Texas, Austin, Aug. 1979, 161 pp.

B.3 WOODWARD, K.A., and JIRSA, J.O., "Behaviour Classification of Short Reinforced Concrete Columns Subjected to Cyclic Deformations", PMFSEL Report No. 80-2, Department of Civil Engineering, University of Texas, Austin, July 1980, 339 pp.

B.4 NIELSEN, N.P., BRAESTRUP, M.W., and BACH, F., "Rational Analysis of Shear in Reinforced Concrete Beams", IABSE Proceedings, P-15/78, pp. 1-16.

B.5 "CEB-FIP Model Code for Concrete Structures", (English Translation), Third Edition, April 1978.

B.6 ACI COMMITTEE 318, "Building Code Requirements for Reinforced Concrete", American Concrete Institute, Detroit, Michigan, 1989.

B.7 NZS 3101, "New Zealand Code of Practice for the Design of Concrete Structures", Standards Association of New Zealand, Wellington, 1982.

B.8 CSA COMMITTEE A23.3-M84, "Design of Concrete Structures for Buildings, CAN-A23.3-M84", National Standard of Canada, Canadian Standards Association, Rexdale, 1984.

B.9 VECCHIO, F., "The Response of Reinforced Concrete to In-Plane Shear and Normal Stresses", Ph.D. Thesis, Department of Civil Engineering, University of Toronto, 1981, 332 pp.

B.10 LEONHARDT, F.," Reducing the Shear Reinforcement in Reinforcement in Reinforced Concrete Beams and Slabs", Magazine of Concrete Research, Vol. 17, No. 53, Dec. 1965, pp. 187-198.

B.11 LAMPERT, P., and THURLIMANN, B., "Torsionsversuche an Stahlbetonbalken (Torsion Tests of Reinforced Concrete Beams)", Bericht Nr. 6506-2, Institut fur Baustatik, ETH, Zurich, Jun. 1968.

B.12 CHEN, W.F., "Plasticity in Reinforced Concrete", McGraw-Hill Book Company, New York, 1982, pp. 324-325.

B.13 COLLINS, M.P., "Towards a Rational Theory for Reinforced Concrete Members in Shear", Journal of the Structural Division, ASCE, Vol. 104, No. ST4, April 1978, pp. 649-665.

B.14 VECCHIO, F.J., and COLLINS, M.P., "The Modified Compression Field Theory for Reinforced Concrete Elements Subjected to Shear", ACI Journal, March - April 1986, pp. 219-231.

B.15 PRIESTLEY, M.J.N., and PARK, R., "Strength and ductility of Bridge Substructures", RRU Bulletin 71, National Road Board, Wellington, New Zealand, 1984, 120 pp.

B.16 ANG, B.G., "Ductility of reinforced Concrete bridge piers under Seismic Loading", M.E. Report, Department of Civil Engineering, University of Canterbury, Christchurch, Feb.1981, 109 pp.

B.17 ZAHN, F.A., "Design of Reinforced Concrete Bridge Columns for Strength and Ductility", Research Report 86-7, Department of Civil Engineering, University of Canterbury, Christchurch, Mar. 1986, 330 pp.

CHAPTER C

C.1 ANG, B.G., "Seismic Shear Strength of Circular Bridge Piers", Ph.D. Report, Department of Civil Engineering, University of Canterbury, Christchurch, July 1985, 407 pp.

C.2 NZS 3101, "New Zealand Code of Practice for the Design of Concrete Structures", Standards Association of New Zealand, Wellington, 1982.

C.3 WOODWARD, K.A., and JIRSA, J.O., "Behaviour Classification of Short Reinforced Concrete Columns Subjected to Cyclic Deformations", PMFSEL Report No. 80-2, Department of Civil Engineering, University of Texas, Austin, July 1980, 339 pp.

C.4 MARUYAMA, K., and JIRSA, J.O., "Shear Behaviour of Reinforced Concrete Members Under Bidirectional Reversed Lateral Loading", CESRL Report No. 79-1, Department of Civil Engineering, University of Texas, Austin, Aug. 1979, 161 pp.

C.5 "Methods for Tensile Testing of Metals, BS 18: 1971, Part 2: Steel (General)", British Standards Institution, London, July 1971.

C.6 "Specification for Methods of Test for concrete, NZS 3112: 1986, Part 2: Test Relating to the Determination of strength of Concrete", Standards Association of New Zealand, Wellington, Dec. 1986.

CHAPTER D

D.1 NZS 3101, "New Zealand Code of Practice for the Design of Concrete Structures", Standards Association of New Zealand, Wellington, 1982.

D.2 ACI COMMITTEE 318, "Building Code Requirements for Reinforced Concrete", American Concrete Institute, Detroit, Michigan, 1989.

D.3 HSU, T.T.C., "Torsion of Reinforced Concrete", Van Nostrand Reinhold Company, New York, 1984, pp. 76-83

CHAPTER E

E.1 ANG, B.G., "Seismic Shear Strength of Circular Bridge Piers", Ph.D. Report, Department of Civil Engineering, University of Canterbury, New Zealand, July 1985, 407 pp.

E.2 NZS 3101, "The Design of Concrete Structures", Part I: Code of Practice, Part 2: Commentary, Standards Association of New Zealand, Wellington, 1982.

E.3 ACI COMMITTEE 318, "Building Code Requirements for Reinforced Concrete ACI 318-89", American Concrete Institute, Detroit, 1989.

E.4 KENT, D.C., and PARK, R., "Flexural Members with Confined Concrete", Journal of the Structural Division, Proceedings of American Society of Civil Engineers, Vol. 97, No. ST 7, July 1971, pp. 1969-1990.

E.5 PRIESTLEY, M.J.N, and PARK, R., "Strength and Ductility of Bridge Substructures", RRU Bulletin 71, National Roads Board, New Zealand, 1984, pp. 8-10.

CHAPTER F

F.1 PARK, R., and PAULAY, T., "Reinforced Concrete Structure", A Wiley-Interscience Publication, New York, 1975, 769 pp.

F.2 ACI COMMITTEE 318, "Building Code Requirements for Reinforced Concrete ACI 318-89", American Concrete Institute, Detroit, 1989.

F.3 GOODSIR, W.J., "The Design of Coupled Frame-Wall Structures for Seismic Actions", Report 85-8, Department of Civil Engineering, University of Canterbury, New Zealand, Aug. 1985, 333 pp.

F.4 ANG, B.G., "Seismic Shear Strength of Circular Bridge Piers", Ph.D. Report, Department of Civil Engineering, University of Canterbury, New Zealand, July 1985, 407 pp.

F.5 ANDRIONO, T., and PARK, R., " Seismic Design Considerations of the Properties of New Zealand Manufactured Steel Reinforcing Bars", Bulletin of the New Zealand National Society for Earthquake Engineering, Vol. 19, No. 3, Sept. 1986, pp. 213-246.

F.6 NZS 3109, "Specification for Concrete Construction, NZS 3109: 1987", Standards Association of New Zealand, 1987, pp. 26-31.

F.7 ARAKAWA, T., HE, M.X., ARAI, Y., and MIZOGUCHI, M., "Ultimate Shear Strength of Spirally-Confined Concrete Columns", Transactions of the Japan Concrete Institute, Vol. 9, 1987, pp. 305-312.

F.8 SHIBATA, T., "Ultimate Strength Equations of Reinforced Concrete Members at Brittle Failure", Concrete Journal of JCI, Vol. 18, 1980, pp. 26-37.

F.9 NZS 3101, "The Design of Concrete Structures", Part I: Code of Practice, Part 2: Commentary, Standards Association of New Zealand, Wellington, 1982.

F.10 SOESIANAWATI, M.T., and PARK, R., "Flexural Strength and Ductility of Reinforced Concrete Columns with Various Quantities of Transverse Reinforcement", Pacific Concrete Conference, New Zealand 8-11, Nov., 1988, pp. 65-76.

F.11 ZAHN, F.A., PARK, R., PRIESTLEY, M.J.N., and CHAPMAN, H.E., "Development of Design Procedures for the Flexural Strength and Ductility of Reinforced Concrete Bridge Columns", Bulletin of the New Zealand National Society for Earthquake Engineering, Vol 19, No.3, Sept., 1986, pp. 200-212.

CHAPTER G

G.1 POTANGAROA, R.T., PRIESTLEY, M.J.N, and PARK, R., "Ductility of Spirally Reinforced Concrete Columns Under Seismic Loading", Report 79-8, Department of Civil Engineering, University of Canterbury, Feb., 1979, 116 pp.

G.2 ANG, B.G., "Seismic Shear Strength of Circular Bridge Piers", Ph.D. Report, Department of Civil Engineering, University of Canterbury, New Zealand, July 1985, 407 pp.

G.3 NZS 4203: 1984, "Code of Practice for General Structural Design and Design Loadings for Buildings", Standard Association of New Zealand, Wellington, 1984, 100 pp.

G.4 PRIESTLEY, M.J.N, and PARK, R., "Strength and Ductility of Bridge Substructures", RRU Bulletin 71, National Roads Board, New Zealand, 1984, 120 pp.

APPENDIX I

I.1 ANG, B.G., "Seismic Shear Strength of Circular Bridge Piers", Ph.D. Report, Department of Civil Engineering, University of Canterbury , Christchurch, July 1985, 407 pp.

APPENDIX II

II.1 SHARPE, R.D., "The Seismic Response of Inelastic Structures", Research Report no. 74-13, Department of Civil Engineering, University of Canterbury, 1974.

II.2 CARR, A.J., "Ruaumoko", Computer Program Library, Department of Civil Engineering, University of Canterbury.

II.3 PRIESTLEY, M.J.N, and PARK, R., "Strength and Ductility of Bridge Substructures", RRU Bulletin 71, National Roads Board, Wellington, New Zealand, 1984, pp. 6-7.

APPENDIX IV

IV.1 HSU, T.T.C., "Torsion of Reinforced Concrete", Van Nostrand Reinhold Company, New York, 1984, pp. 76-83.

APPENDIX I

SHEAR FORCE ASSIGNED TO THE SPIRAL REINFORCEMENT, V_s

The following derivation of shear force assigned to the spiral reinforcement is extracted from Ang's Ph.D thesis [I.1]. The notation used is defined in Fig. I.1.

As the potential diagonal failure plane makes an angle θ to the longitudinal Z-axis of a circular reinforced concrete column (Fig. I.1), the summation of spiral forces parallel to the loading direction, crossing this failure plane, is taken to be the shear force carried by spirals, V_s. By assuming that all spirals develop yield strength, f_{yt},

$$V_s = \sum^{n} 2 A_{sp} f_{yt} \cos\beta$$
$$= 2 A_{sp} f_{yt} \sum^{n} \cos\beta$$
$$= 2 A_{sp} f_{yt} n \cos\beta \qquad (I.1)$$

where n = number of spirals or circular hoops crossed by the potential failure plane

$$= d_s \cot\theta / s \qquad (I.2)$$

A_{sp} = area of spiral or circular hoop

d_s = diameter of spiral or circular hoop

s = spacing of spiral or circular hoop

The term $\cos\beta$ in the final expression for Eq. (I.1) is an average value. It can be approximated by

$$\cos\beta \approx \left(\int_0^{r_s} \cos\beta \, dy\right)/r_s \qquad (I.3)$$

where $r_s = d_s/2$, radius of spiral or circular hoop

When considering that

$$y = r_s \sin\beta$$
$$dy = r_s \cos\beta \, d\beta \qquad (I.4)$$

and substituting Eq. (I.4) into Eq. (I.3), it is found that

$$\cos\beta = \pi/4 \qquad (I.5)$$

Substituting Eqs. (I.2 and I.5) into Eq. (I.1)

$$V_s = 0.5 \pi A_{sp} f_{yt} d_s \cot\theta / s \qquad (I.6)$$

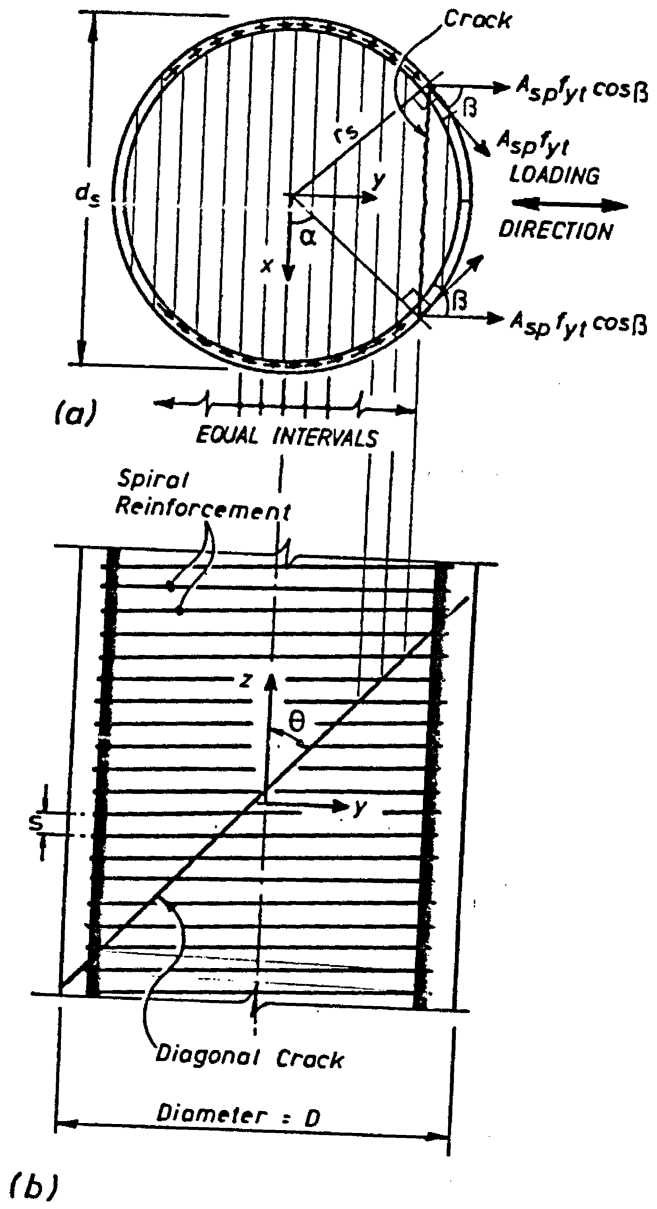

Fig. I.1 : Spiral force component in the loading direction

APPENDIX II
DYNAMIC ANALYSES OF CIRCULAR R.C. PIER SYSTEMS SUBJECTED TO TWO DIMENSIONAL EARTHQUAKE MOTIONS

II.1 INTRODUCTION

The object of this study was to investigate probable displacement patterns of circular reinforced concrete pier systems subjected to simultaneous two dimensional earthquake motions in the horizontal plane. The ultimate goal was to provide information for the selection of representative yet reasonably severe multi-directional 'r' type displacement patterns for this experimental research.

The main parameters studied were periods of piers and various earthquake records. Dynamic time-history analyses were carried using an existing computer program "Ruaumoko" which was written by Sharpe [II.1] and further modified by Carr [II.2]. The equations of motions were solved by step-by-step time-wise integration using the Newmark's constant average acceleration method.

II.2 STRUCTURAL MODELLING

II.2.1 Basic Assumptions

Fig. II.1a shows a typical bridge pier system. The following assumptions were made:

a) Piers were assumed to be restrained against rotations at both ends (Fig. II.1b). Only two translational degrees of freedom in the horizontal X-Y plane were considered.

b) Force - displacement relation in either X or Y directions was represented by tri-linear hysteresis model shown in Fig. II.2a. The interaction of yield surface was circular (Fig. II.2b).

c) Four pier systems, denoted by P_3, P_6, P_8, and P_{12}, having initial periods of 0.3 sec., 0.6 sec., 0.8 sec., and 1.2 sec. respectively, were studied. The stiffness K of pier system P_6, was established from the experimental results of Unit 8 of the present test series. Whereas the stiffnesses K of the other pier systems were derived from that of P_6.

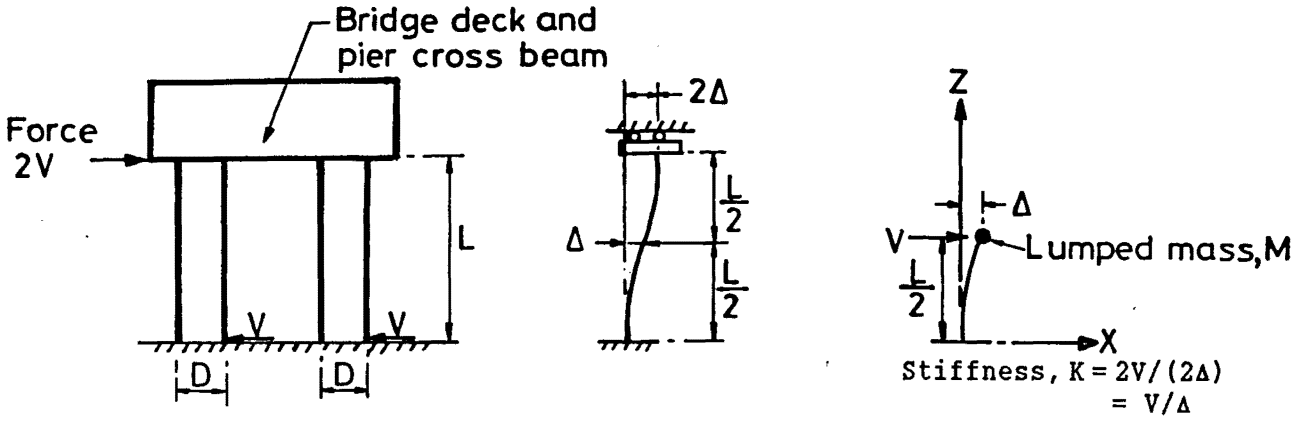

(a) Bridge pier system (b) Deflection profile (c) Analytic model

Fig. II.1 : Bridge pier system subjected to lateral and gravity loads

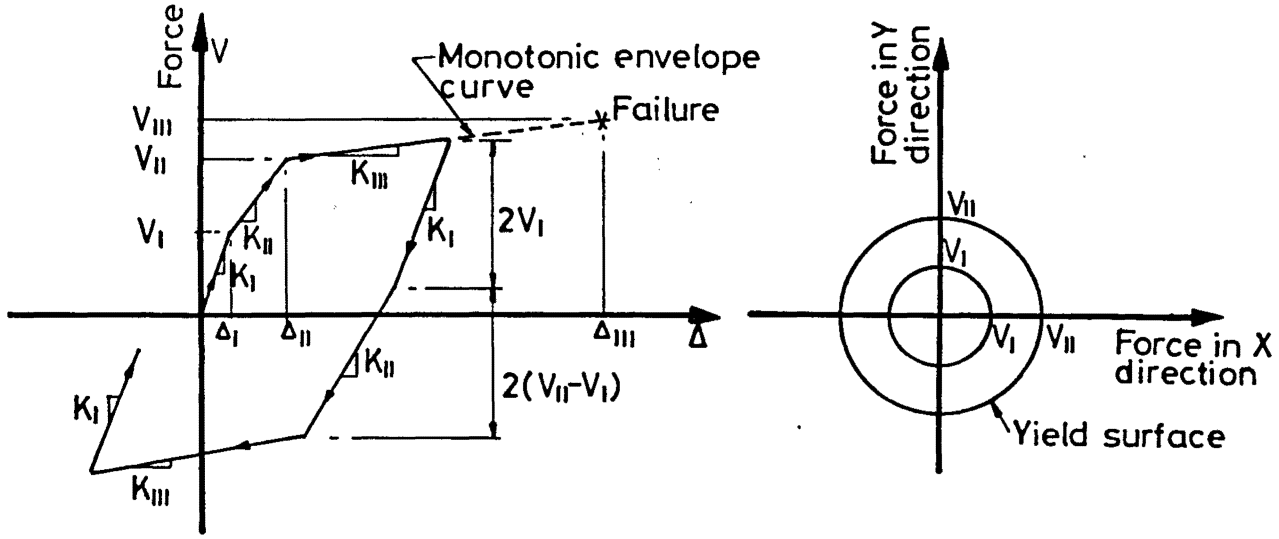

(a) Tri-linear hysteresis model (b) Yield surface

Fig. II.2 : Force - displacement relations used in the analytic model

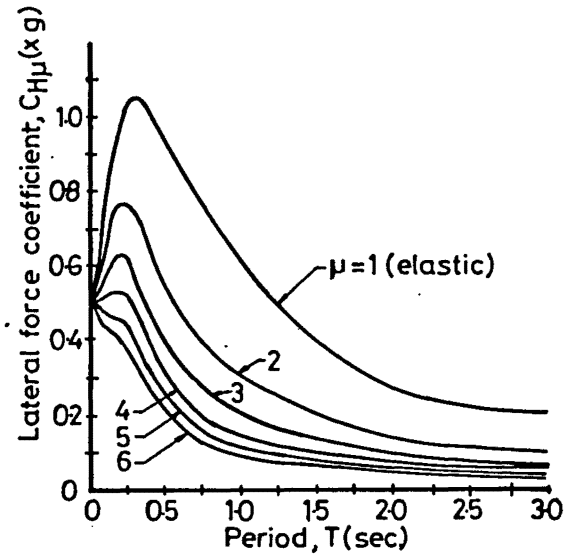

Fig. II.3 : Inelastic design spectra

d) The inertia mass was the same for all pier systems.

e) The lateral force coefficient $C_{H\mu}$, to derive the flexural strength of the pier, was determined from Fig. II.3 : New Zealand Zone A Inelastic Design Spectra [II.3]. The selected return period and displacement ductility were 150 years and 4 respectively.

f) A constant time step of 0.01 second, and viscous damping equal to 5% of critical were used in all calculations.

II.2.2 Pier P_6 (Period, T = 0.6 sec.)

The length of piers, L, was assumed to be four times the pier diameter (4D = 4800 mm). Based on assumption 'a', it was only necessary to analyze the response of half the length of a pier (Fig. II.1c).

Making use of the experimental results for Unit 8 (Table II.I) of this Appendix, the stiffness K_I, K_{II} and K_{III} (Fig. II.2a) of a prototype pier were calculated as below:

By Dimensional Analysis, geometrical scaling factor = 1200/400 = 3

then at 50% of V_{if},	V	$= 3^2(201)$	= 1809 kN
	Δ	$= 3(0.00250)$	= 0.0075 m
at 100% of V_{if},	V	$= 3^2(402)$	= 3618 kN
	Δ	$= 3(0.00585)$	= 0.0176 m
at ultimate,	V	$= 3^2(486)$	= 4374 kN
	Δ	$= 3(0.03500)$	= 0.1050 m

then $K_I = 1809/0.0075$ = 241200 kN/m

$K_{II} = (3618 - 1809)/(0.0176 - 0.0075)$ = 179109 kN/m

$K_{III} = (4374 - 3618)/(0.1050 - 0.0176)$ = 8650 kN/m

and $K_{II}/K_I = 0.74$

$K_{III}/K_I = 0.036$

Since period $T = 2\pi\sqrt{(M/K_I)}$, where M = lumped mass (II.1)

then $M = T^2 K_I/(4\pi^2)$ = 2199470 Kg

= 21577 kN

With a return period of 150 years, $\mu = 4$, and $T = 0.6$ sec.,

$C_{H\mu} = 0.25$ (Fig. II.3)

design yield strengths,	V_{II}	$= 0.25(21577)$	$= 5394$ kN
	V_I	$= 0.5V_{II}$	$= 2697$ kN
corresponding deflections,	Δ_I	$= V_I/K_I$	$= 0.011$ m
	Δ_{II}	$=(V_{II}-V_I)/K_{II} + \Delta_I$	$= 0.026$ m

II.2.3 Piers P_3, P_8 and P_{12}

It is assumed that inertia mass, M, remained constant.

From Eq. (II.1), $K_I T^2 = \text{constant}$ (II.2)

For Pier P3 (Period T = 0.3 sec.),

K_I	$= (0.6/0.3)^2(241200)$	$= 964800$ kN/m
K_{II}	$= (0.6/0.3)^2(179109)$	$= 716436$ kN/m
K_{III}	$= (0.6/0.3)^2(8650)$	$= 34600$ kN/m
$C_{H\mu}$	$= 0.46$ (from Fig. II.3)	

then V_{II}	$= 0.46(21577)$	$= 9925$ kN
V_I	$= 0.5V_{II}$	$= 4963$ kN
Δ_I	$= V_I/K_I$	$= 0.0051$ m
Δ_{II}	$= (V_{II}-V_I)/K_{II} + \Delta_I$	$= 0.0120$ m

The input data for Piers P_8 and P_{12} were obtained in a similar manner. They are listed in Table II.II.

Table II.I : Experimental results of Unit 8

load, V	V/V_{If}	displacement, Δ
kN	-	m
201	0.5	0.00250
402	1.0	0.00585
486	1.2	0.03500 *

* : assumed value

Table II.II : Pier input data for dynamic analyses

1	2	3	4	5	6	7	8	9
pier no.	period	lateral force		displacement		stiffness		
		V_I	V_{II}	Δ_I	Δ_{II}	K_I	K_{II}	K_{III}
-	sec.	kN	kN	m	m	kN/m	kN/m	kN/m
P_3	0.3	4963	9925	0.0051	0.012	964800	716436	34600
P_6	0.6	2697	5394	0.0110	0.026	241200	179109	8650
P_8	0.8	2158	4315	0.0160	0.037	135675	100749	4866
P_{12}	1.2	1402	2805	0.0230	0.054	60300	44777	2163

lumped mass = 21577 kN

K_{III}/K_I = 0.036, K_{II}/K_I = 0.74

Table II.III : Earthquake records used in dynamic analyses

No.	earthquake	date	direction	ground acceleration magnification factor
1	El-Centro	18 May 1940	N-S	1.0
			E-W	1.0
2	El-Centro	18 May 1940	N-S	1.5
			E-W	1.5
3	El-Centro	15 Oct 1979	N-S	1.0
			E-W	1.0
4	El-Centro	15 Oct 1979	N-S	1.5
			E-W	1.5
5	Olympia	13 Apr 1949	N10W	2.0
			N80E	2.0

II.3 EARTHQUAKE FORCES AND COMPUTED DISPLACEMENT PATTERNS

Each pier system was subjected to five earthquake records [II.2] (Table II.III) for a duration of 20 seconds. Some of the computed displacement patterns are shown in Fig. II.4. One set of orthogonal reference axes with centre at zero displacement position is plotted with each displacement pattern so that one of the axes points in the direction of the maximum displacement. Circles representing displacement ductility levels are also marked on the figures.

It appears that in these cases, the patterns of computed displacement paths depend more on the earthquake record than on the periods of the selected pier systems. In general, comparable displacement ductility demands developed along both reference axes. The number of reoccurrence of peak displacements of similar magnitude did not exceed three in each direction. There are only two cases (Figs. II.4c and II.4d) where predicted ductility demands were larger than 4. For these cases, a ground acceleration magnification factor of 1.5 has been applied. The remainder of the results indicated that the ductility demand decreased to much less than 4 with a decrease in the initial period of a system. This implies that in these cases, the lateral force coefficients based on Fig. II.3 are conservative, particularly for piers having short initial periods. However, in order to check the validity of this statement, more refined structural models subjected to a large number of different earthquake excitations should be investigated. This is beyond the scope of the present project.

Finally, having studied the most critical computed displacement patterns (Fig. II.4) for piers under the selected earthquake excitations, the displacement orbits shown in Figs II.4b and II.4d were chosen to form the basis for the construction of 'r' type displacement pattern as described in Section C.3.1.

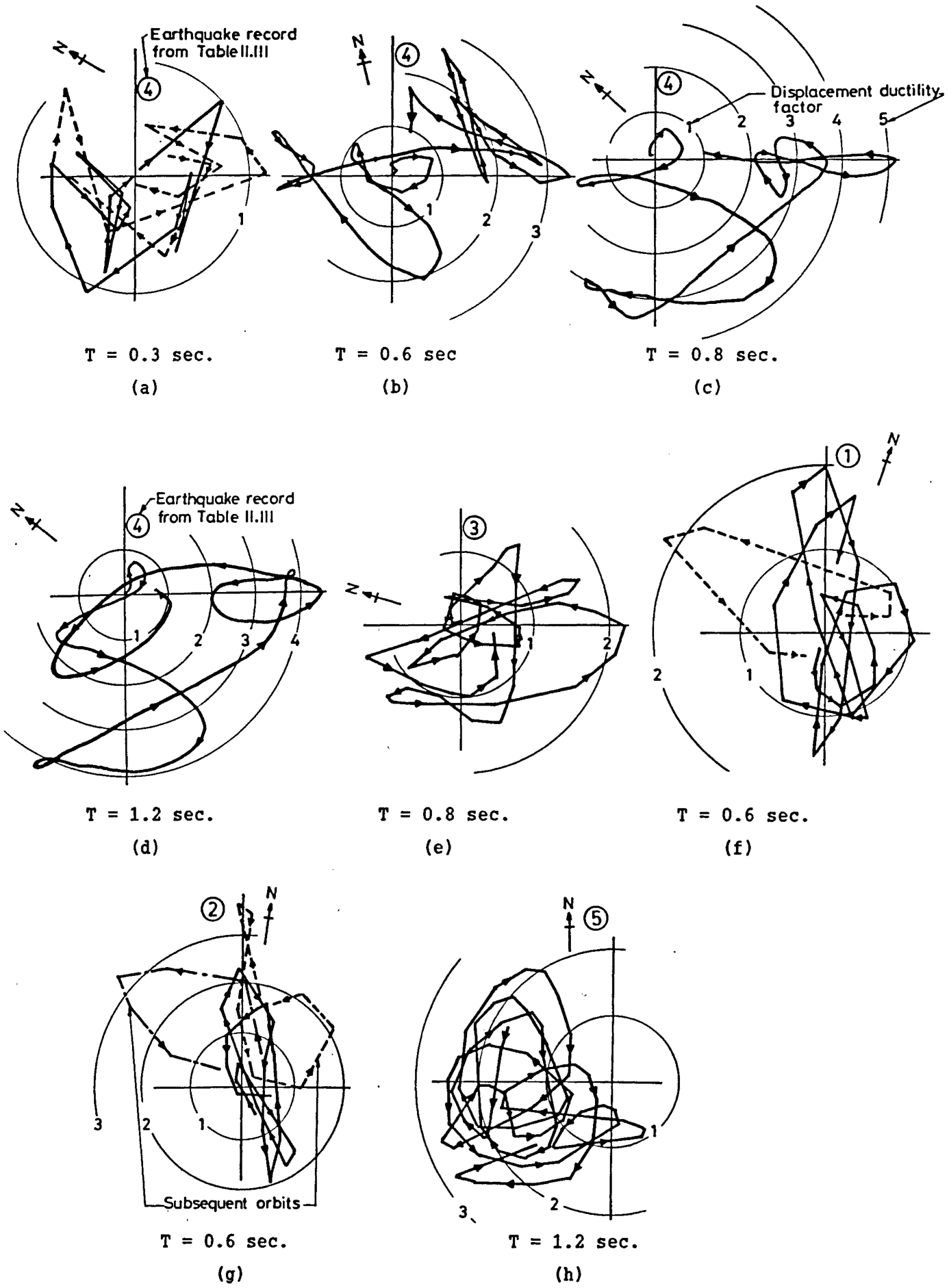

Fig. II.4 : Critical displacement patterns for piers under different earthquake excitations

APPENDIX III

EVALUATION OF LATERAL FORCES ACTING ON A TEST COLUMN

With reference to Fig. III.1, let

1. The coordinates of the centre of the column before applied displacement = (0, 0)
2. The coordinates of the centre of the column after applied displacement = (x_1, y_1)
3. Twist in degrees (measured as shown in Fig. III.1) = θ_t
4. Jack force in E - W direction = V_e
5. Jack force in N - S direction = V_n

Then, the lateral force components (V_x, V_y) acting at the centre of the column and the associated torque T_t can be calculated as below:

$$V_x = V_e \cos\theta_2 + V_n \sin\theta_1 \quad (kN) \qquad (III.1)$$

$$V_y = V_n \cos\theta_1 - V_e \sin\theta_2 \quad (kN) \qquad (III.2)$$

$$T_t = 0.56\,(\sin\theta_t\,(V_n \cos\theta_1 - V_e \cos\theta_2) + \cos\theta_t\,(V_n \sin\theta_1 - V_e \sin\theta_2)) \quad (kNm) \qquad (III.3)$$

where $\theta_1 = (x_1 + 560\,\pi\,\theta_t/180)/1730$ (III.4)

$\theta_2 = (y_2 + 560\,\pi\,\theta_t/180)/1730$ (III.5)

The resultant force is then

$$V = \sqrt{V_x^2 + V_y^2} \qquad (III.6)$$

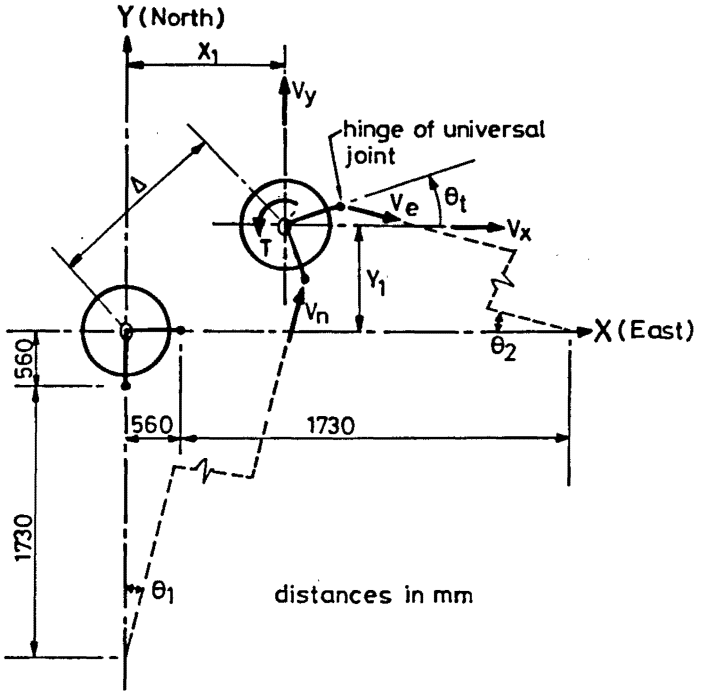

Fig. III.1 : Forces acting on and resulting displacements of test column

APPENDIX IV

THE ESTIMATION OF STRESSES INDUCED IN SPIRALS AND LONGITUDINAL BARS BY TORSION [IV.1]

Method of analysis : The Rausch's space truss analogy is used.

$$\text{Torsion } T_t = 2\,A\,A_{st}\,f_{st}/s \qquad \text{(IV.1a)}$$

$$\text{or } f_{st} = T_t\,s/(2\,A\,A_{st}) \qquad \text{(IV.1b)}$$

where T_t = torsion

A = area within the tube, measured to the inside diameter of spiral

A_{st} = cross - sectional area of spiral reinforcement

f_{st} = stress in spiral due to torsion, T_t

s = spacing of spirals

Also, assuming 45° inclination for the diagonal compression,

$$T_t = 2\,A\,A_{sl}\,f_{sl}/s \qquad \text{(IV.2a)}$$

$$\text{or } f_{sl} = T_t\,s/(2\,A\,A_{sl}) \qquad \text{(IV.2b)}$$

where A_{sl} = cross - sectional area of longitudinal reinforcement

f_{sl} = stress in longitudinal reinforcement due to torsion, T_t

The stresses induced in spirals and longitudinal reinforcement by torsion for test units subjected to 's' type displacement pattern are shown in Table IV.I.

Table IV.I : Stresses induced in spirals and longitudinal reinforcement by torsion

Unit		torsion	μ	f_{st}/f_{yt}	f_{sl}/f_{yl}
no.	notation	kNm	-	-	-
11	0R6 -30s	8.7	4	0.15	0.01
		27.5	5	0.47	0.03
12	0R10-35s	7.0	4	0.06	0.01
		31.6	5	0.27	0.05
13	2R6 -30s	6.1	4	0.11	0.01
		12.7	5	0.23	0.02
14	2R10-60s	4.2	4	0.06	0.02
		12.2	5	0.18	0.05
		33.8	6	0.49	0.14
15	4R10-60s	3.5	4	0.05	0.01
		8.3	5	0.12	0.03
		29.8	6	0.43	0.11

APPENDIX V

MOMENT - CURVATURE RELATIONSHIPS FOR REINFORCED CONCRETE SECTIONS WITH FLEXURE AND AXIAL LOAD

Theoretical moment - curvature relationships for reinforced concrete sections with flexure and axial load are normally based on the assumptions that plane sections before bending remain plane after bending, and the stress-strain curves for concrete and steel are known. For a given axial load level, the curvatures associated with a range of bending moment can be determined using these assumptions, and from the requirements of strain compatibility and equilibrium of forces. A typical calculation procedure for these relationships is outlined as follows:

For each assigned value of concrete strain in the extreme compression fibre, ε_{cm}, the depth of neutral axis, c, is estimated so that the strain profile of the cross-section can then be established (Fig. V.1b).

Since the stress - strain relationships of concrete and steel are known, the internal forces at the section (Fig. V.1c) can be calculated. To compute the internal force from concrete, it is convenient to divide the flexural compression zone into a number of discrete laminae (Fig. V.1a). The concrete strain in the lamina is assumed to be that at the mid-depth of the lamina. In the flexural tension zone, concrete is usually assumed to carry no forces.

Equilibrium of forces requires that these internal forces, from concrete and steel, must balance the applied axial load, P (Fig. V.1d). As a result, an iterative procedure will be needed in determining the depth of neutral axis, c, which satisfies the equilibrium of forces for each value of ε_{cm}.

The corresponding bending moment, M, is then found by taking moment about a reference axis. This reference axis is normally taken as the centre of the section which is the line of application of the axial load, P. The associated curvature, Φ, is given by $\Phi = \varepsilon_{cm}/c$.

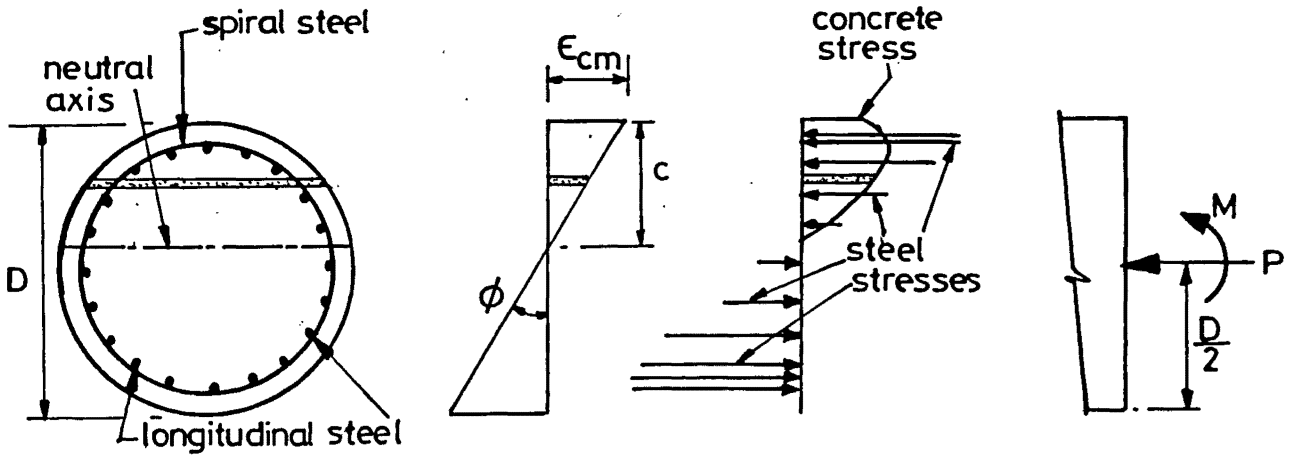

(a) Cross-section (b) Strains (c) Stresses (d) External forces

Fig. V.1 : Column section with strain and stress distributions